Defect of Neurofibromin I (NF1) in Muscle Progenitors Induces Premature Quiescence and Metabolic Myopathy

Inaugural-Dissertation
to obtain the academic degree
Doctor rerum naturalium (Dr. rer. nat.)

Submitted to the Department of Biology, Chemistry and Pharmacy
of Freie Universität Berlin

XIAOYAN WEI

February, 2020

This thesis was carried out during the period of October 2015 and February of 2020 at the Freie Universität Berlin and Max-Planck-Institute for Molecular Genetics under the supervision of Prof. Dr. Sigmar Stricker.

1st Reviewer: Prof. Dr. Sigmar Stricker

2nd Reviewer: Prof. Dr. Simone Spuler

Date of defense: 06.05.2020

Statutory declaration

I hereby declare that the thesis entitled "Defect of Neurofibromin I (NF1) in muscle progenitors induces premature quiescence and metabolic myopathy" has been done only by myself without any aids other than where cited. I confirm for any part of the work presented in this thesis has not previously been submitted for a degree in university or institution.

The results presented here have not yet been published in a publication.

Berlin, Feb 10th 2020

.....

Xiaoyan WEI

Table of contents

1 Introduction

In this project, skeletal muscle tissue-specific functional analysis of neurofibromin I protein associated myopathy in animal models is performed. The overall scientific objective is to elucidate the mechanism of *Nf1* deletion-dependent prenatal muscle development defect as well as the postnatal myopathy seen in the mouse model from a cellular and molecular level. This study will generate first pre-clinical knowledge about the pathomechanism of muscular weakness in NF1 patients, for which scare data are available so far. Furthermore, it will increase our understanding of Nf1 downstream signaling events and the involvement of signaling components in pathological processes, as the results obtained in this project might be transferable to the function of *Nf1* in other cellular contexts. Therapeutic options for skeletal muscle abnormality are still limited currently because of the poor understanding of its pathogenesis. Using the animal model, whether Nf1 muscle defect can be therapeutically prevented or attenuated will be tested. We envision that deciphering the mechanism of the observed NF1 muscle phenotype will yield further advancements in the treatment of musculoskeletal aspects of the Neurofibromatosis type I.

1.1 Skeletal muscle system

1.1.1 Development of Skeletal muscle

Vertebrate limb skeletal muscle derives from progenitors originating in the somites. The earliest myogenic marker in mouse was identified by analyzing the expression pattern of paired domain transcription factors Pax3. Pax3 is initially expressed in the presomitic mesoderm (PSM) during the segmentation process. Followed by newly formed dermomyotome, the committed myotomal cells or muscle progenitors could express Pax3/Pax7, Myod, Myf5, and they migrate into the limb buds at around E9.5, then decreased expression during myogenic differentiation (Fig. 1.1). Besides, not all muscle progenitors go into differentiation fate, there are still some $Pax3^+$ cells in proliferation state and give rise to $Pax7^+$ cells, these cells are the source of the second wave muscle fiber formation apart of which are also maintained for adult muscle stem cell pool[10]. Lineage tracing analysis with a Pax3Cre KI allele reveals that $Pax3^+$ progenitors can give rise to embryonic, fetal as well as adult skeletal muscle tissue, which also strongly indicated that adult limb muscle satellite cells are somitic origin[11]. Gabrielle Kardon's lab using avian somite labeling experiments, and they show that almost all limb satellite cells are derived from the somites[11,12]. Besides, with two Pax3Cre mouse models, they also characterized the genetic origin of these satellite cells[10,11,13,14]. In general, limb myogenesis follows four significant phases. The first step is the embryonic myogenesis stage. It starts at E10.5 and lasts until E13.5. During this stage, the mononuclear myocytes will start to express

differentiation markers such as myogenin, Mrf4, and also start to fuse, give rise to multi-nucleated primary muscle fibers, which is also called the first wave of muscle fiber formation[15]. The second stage is the fetal myogenesis. It is also called the second wave of muscle fiber formation, which occurs between E14.5 and E17.5[16,15]. At this time point, some of the high proliferating muscle progenitors will leave their cell cycle and fuse with the existing primary fibers or form new fibers by themselves (de-novo formation). At the later stage of fetal myogenesis, the basal lamina will be fully formed. Therefore the $Pax7^+$ cells will go out of the cell cycle gradually become quiescent and stay in their stem cell niche underneath the basal lamina. This process is also called neonatal myogenesis. The progenitors are mainly responsible for the repair of adult myofibers which caused by injury or exercise. After stimulation, the progenitors will re-enter the cell cycle to start asymmetric cell division for self-renew and myogenic markers expression for myotube fusion simultaneously. It is the so-called adult muscle myogenesis process[17].

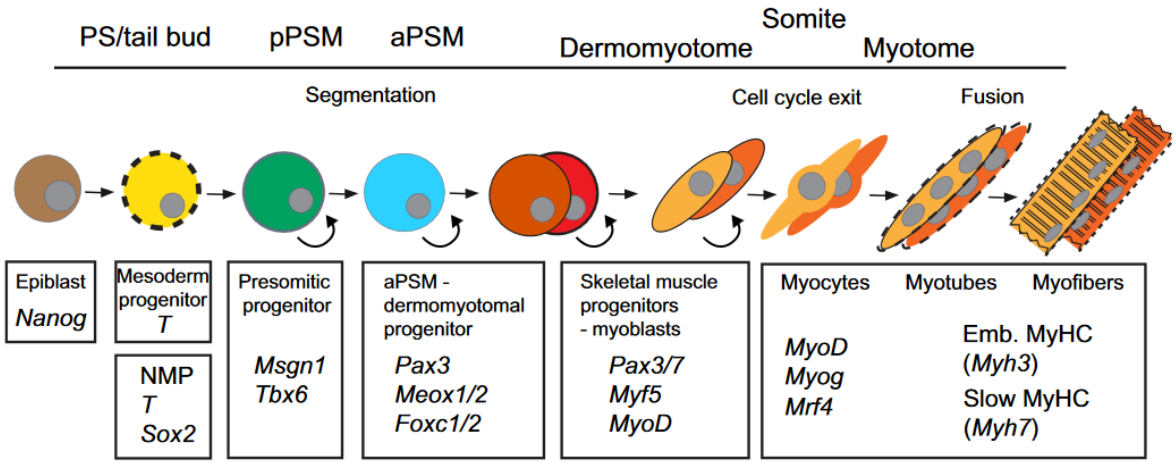

Figure. 1.1. Paraxial mesoderm differentiation towards skeletal muscle.

The diagram outlines the differentiation of paraxial mesoderm gradually to skeletal muscle. From left to right: On top shows the developmental sequence, the middle shows cell types, and the bottom shows gene markers. aPSM, anterior presomitic mesoderm; pPSM, posterior presomitic mesoderm; Emb, embryonic; NMPs, neuromesodermal progenitors[3].

1.1.2 Fiber type formation during skeletal muscle development

Skeletal muscle is composed of different muscle fibers, and its proportion is highly dynamic. One of the reasons that contribute to this diversity might be heterogeneous of the muscle progenitor population[18]; It can also be influenced by the continuous wave of muscle fiber formation during embryonic development and the separation of slow and fast fibers during the perinatal stage and fiber type reprogramming during postnatal development[12]. Under mouse muscle fiber formation context, most of the early muscle progenitors contribute to slow fibers.

This biological process happens between E9.5 and E13.5[19]. Literature shows at around E16, the formation of fast fiber can be first detected from transcripts level, for protein expression as the turn over time is longer than transcripts it is even later[20]. During the first week of postnatal muscle development, these fibers can further give rise to several different fast relative fiber isoforms, including MHC-2A, MHC-2X, MHC-2B[21]. The previous paper shows that isolation and culture of mouse early embryonic myoblast, these cells can only differentiate into slow fibers. However, late embryonic myoblast behaves oppositely. Besides, researchers also show that satellite cells attached with fast fibers can only differentiate into fast fibers during in vitro cell culture, and interestingly satellite cells isolated from slow fibers can differentiate into both fiber types. The exact regulation mechanism of these cells is still a mystery and needs more effort on it. The perinatal period is a critical time point for fiber type diversification featured by the formation of adult fast type myosin heavy chain (MHC) isoforms and its subtypes of MHC. Until now, during development, how these embryonic and fetal fibers get reprogrammed and form different muscle fiber types is still unclear. Anne-Françoise Richard and her colleagues used specific gene knock out mouse model proved that at E18.5, *Sox6/Nfix* and its target genes *Six1/Six4* could regulate glycolysis and oxidative phosphorylation metabolism genes expression thus repress the formation of slow fibers which might be one of the molecular mechanism of muscle fiber type formation at fetal stage[22,23]. *Six1* is mainly expressed in adult fast-twitch fiber nuclei. Interestingly just opposite with fetal stage, at the embryonic stage, Sox6 positively regulated slow fiber formation through Mef2c[24]. At the prenatal stage, the percentage of slow fibers reach their highest level. With time past fiber type reprogramming will happen gradually until the adult stage. Fast fibers play a dominant role for adult mouse, and slow fibers predominantly left in few muscles as the soleus[25,26].

1.1.3 Metabolism of skeletal muscle system

During postnatal development, skeletal muscle is one of the most important organs and accounts for 30 - 50% of human body mass. Most of the glucose that ingested from food will be used by muscle cells and then provide energy for body moving. Different types of muscle fibers within the tissue have been distinguished according to SDH (succinate dehydrogenase) staining assay, the myosin ATPase assay (ATP staining), or α-glycerophosphate dehydrogenase (αGPD) assay. Based on histochemical staining, immunostaining, various myosin heavy chain (MYH) expression pattern, and myosin ATPase activity, skeletal muscle fibers can be separated into several sub-families[27]. Totally speaking, muscle fibers can be divided into slow-twitch fibers, also being called red muscle or Type I (Myh7) muscle, which has a higher content of mitochondrial and smaller cross-section area. More blood vessels to supply oxygen and the increased levels of myoglobin that is also the reason why they have

red color and being called red muscle. They generate ATP through the transfer of electrons to O_2 by a sequential electron carrier located in mitochondrial. High energy molecules, including NADH and $FADH_2$, which are produced by glycolysis, fatty acid oxidation, and citric acid cycle, are the primary source of these electrons. In contrast with slow fiber, fast-twitch fibers, also being called white muscle or type II muscle, just have different properties. This fiber group can also be separated into three subgroups: 2A (Myh2), 2X (Myh1), 2B (Myh4). Despite there are no type 2B fibers in humans, the proportion of slow fibers is much higher in humans than mouse[28]. Take gastrocnemius muscle as an example, the proportion of type I fibers in mouse is around 8% - 10%, but in human, the distribution of fast and slow fibers are almost equal. For fast fibers, they generate energy mainly through glycolytic metabolism[29]. At rest status, glucose from blood will be transferred into muscle cytoplasm through Insulin-dependent Glut4 transporter. After several steps of enzymatic reactions, one molecule of glucose can be transformed into two pyruvates yielding two ATP, two NADH in the process. In slow fibers Pyruvate will be changed into Acetyl–CoA and goes into the citric cycle for two CO_2, three NADH, and one $FADH_2$. After mitochondrial electronic transport chain, in total, one molecule of glucose can generate 30-32 ATP. However, fast fibers mainly rely on glycolysis alone without TCA cycle and electron transport chain. Compared with glycolysis (2 ATP), the TCA cycle is a much more efficient way to generate energy. However, researchers also prove that glycolysis is not mainly for energy production; its primary function is to provide biomaterials for rapid high proliferating cells to sustain their protein and DNA synthesis rate[30], which is also why even with sufficient oxygen, activated cells still prefer to use glycolysis[30]. For different fiber types, their mitochondrial content reduces gradually from type I to type II, and their insulin-stimulated glucose uptake ability is also following this pattern (I > IIA > IIX > IIB/X ≈ IIB)[31-33]. Several research groups used different methods to separate real slow and fast fibers followed by single fiber microarray analysis or proteomics analysis. Gene ontology (GO) analysis of transcriptome data showed GO terms for Mitochondrial, Contractile fiber part, Ribosome are highly enriched in type I fibers. KEGG pathway analysis showed pathways including Ribosome, Cardiac muscle contraction, Oxidative phosphorylation, Fatty acid metabolism are enriched in type I fibers. GO and KEGG pathway enriched in type IIb fibers, including Glycolysis, Proteolysis, Insulin signaling pathway, and Wnt signaling pathway[34]. One of the common diseases related to the muscle fiber is Sarcopenia, especially in aged individuals, the phenomenon of this disease is patients will gradually lose their muscle mass and strength followed by decreased performance as well as self-renew capacity reduction. One character was noticed that this change is fiber type-dependent. It starts with type 2 fast fiber loss, and atrophy leads to a smaller diameter of type 2 fibers, thus influence the quality of people's life[35]. The first identified metabolic myopathy is McArdle Disease, also being called glycogen storage disease type V (GSD-V). This disease was caused by deficiency and activity loss of

myophosphorylase, which impairs glycogen breaks down, thus caused skeletal muscle carbohydrate metabolism disorder. Until now, several animal models have been established, including sheep and mice. Thomas O. Krag et al. used 20 weeks McArdle mice showed comparable muscle physiology with human patients. The muscle contraction ability of mutant mice was affected by the degeneration of structure relative proteins because of glycogen accumulation. Also, mutation mainly influences glycolytic muscles as they mainly rely on glucose metabolism, and these fast fibers are much more resistant to be fatigued. Therapies used to help patients to manage this disease include specifically attention with food rich with carbohydrate more creatine supplement and drink or eat a certain amount of sucrose before taking exercise[36,37].

1.1.4 Hypertrophy and atrophy of skeletal muscle

Skeletal muscle is highly dynamic and heterogeneous. Muscle mass and muscle strength can directly influence its biological functions, thus influence life quality. One of the reasons for muscle dynamic is skeletal muscle mass is regulated by both intrinsic (genetic and sex) and external stimulation (nutrition and training variables). Before the mouse grows into an adult stage, especially at the beginning of the first three postnatal weeks, skeletal muscle weight increased several times, and this is mainly from the muscle hypertrophy[38]. During this period, muscle hypertrophy is mainly induced by myofibril to increase its diameter, thus lead to bigger muscle fiber size. How could myofibril have such a dramatic size increase? One way for skeletal muscle to regulate its muscle mass is by keeping the balance between contractile protein synthesis and degradation[39]. For juvenile individuals, dramatically muscle hypertrophy will sustain until they reach the point of adult time. In this time, the protein synthesis rate is much higher than its degradation rate. Also, a large amount of myoblast generated from activated muscle stem cells will incorporate into existing muscle fibers. In order to maintain the essential nuclear domain size, fibers with more nuclear will stimulate more protein synthesis and make fibers diameter grow fast. In theory, the number of muscle fibers has been predetermined during the embryo development stage. That is to say, only muscle fiber quality can be increased instead of quantity during postnatal skeletal muscle development. For adult animals, endurance exercise has proved to get muscle more stronger by increasing muscle strength, protein synthesis, and the ability of aerobic metabolism through activating muscle mitochondrial enzyme activity[40].

Over the past years, several signaling pathways involved in muscle hypertrophy have been identified. One of them is the pathway induced by insulin-like growth factor I (IGF-1). IGF-1 controls muscle mass by directly activate the phosphatidylinositol-3 kinase (PI3K)/Akt pathway through its downstream targets to control the protein synthesis rate. Overload stimulates

muscle protein synthesis is also in this way[41]. Another critical signal pathway involved in both muscle protein synthesis and muscle metabolism control is mTOR signaling.

Heterodimeric complex composed by tuberous sclerosis complex-1 and -2 proteins (TSC1/2) is an critical regulator of mTOR signaling and it could integrate different growth factors and cell energy status together into mTOR pathway especially for mTORC1[42]. Specific site phosphorylated AKT is a negative regulator of TSC1/2 (tuberous sclerosis complex-1 and -2 proteins); thus, PI3K/AKT works as a positive regulator of the mTOR pathway[43]. Amino acid could activate the mTOR pathway directly by stimulated p70S6K and promote protein synthesis rate[44]. Loss of mTOR function through knock out RAPTOR contributes to sever muscle atrophy，reduction of muscle oxidative capacity and also fiber type shift to type 2 fast fibers[45]. Constitute activation of mTOR lead to a higher glycolysis rate and lower PGC-1a expression, which is a master regulator of mitochondrial genesis[46]. Paul A. Dutchak et al. also showed that knock out NPRL2, which is a component of GATOR1 complex functions as a negative regulator of mTORC1 under the context of amino acid insufficiency could constitutive activate mTORC1 signaling in both fed and fasted states. Muscle fibers from these knockout mice show a fiber type shift from slow oxidative to fast glycolytic composition with enhanced glucose tolerance ability. Furthermore, the depletion of NPRL2 induces aerobic glycolysis and suppresses glucose entry into the TCA cycle[47]. Besides, the mTOR pathway could also be regulated by another master of muscle energy deficiency sensor, namely AMPK[48]. AMPK is a heterotrimeric protein complex consisting of a catalytic α and regulatory β and γ subunits. Two isoforms of α (α1 and α2) and β (β1 and β2) and three isoforms of γ (γ1, γ2, and γ3) subunit have been identified[49]. In skeletal muscle, there are two types of AMPKa (1, 2). Researchers proved that AMPKa1regulate muscle size through the control of mTORC1 signaling activity. AMPKa1 functions as a negative regulator of the mTOR pathway, thus reduce protein synthesis rate leads to smaller muscle size[48]. Instead of being activated by energy deprivation through LKB1 in Ampka2, Ampka1 is mainly activated through low-intensity contraction and also oxidative stress. How AMPK signaling combined with the mTOR pathway to regulate the adult skeletal muscle mass and metabolism is shown in figure.1.2. AMPKa2 plays a predominant role in regulating muscle metabolic adaption[50]. Interestingly AMPK γ3 is mainly expressed in fast glycolytic fibers; the ablation and overexpression of this gene do not influence the content and activity of mitochondrial in resting skeletal muscle. However, overexpression of a single nucleotide mutation of AMPKγ3 can significantly promote the biogenesis of mitochondrial through increasing the expression of PGC-1α in glycolytic skeletal muscle. Activation of AMPK by AICAR in rat glycolytic epitrochlearis muscle promotes translocation of glucose transporter 4 (Glut4), thus increase glucose uptake[51]. The effect is exercise dependent and Insulin-PI3K signaling independent. However, in oxidative soleus muscle, even though

AICAR can still activate AMPK, there is no glucose uptake induced. This phenomenon indicated that AMPK- mediated glucose uptake is likely fiber type dependent[49].

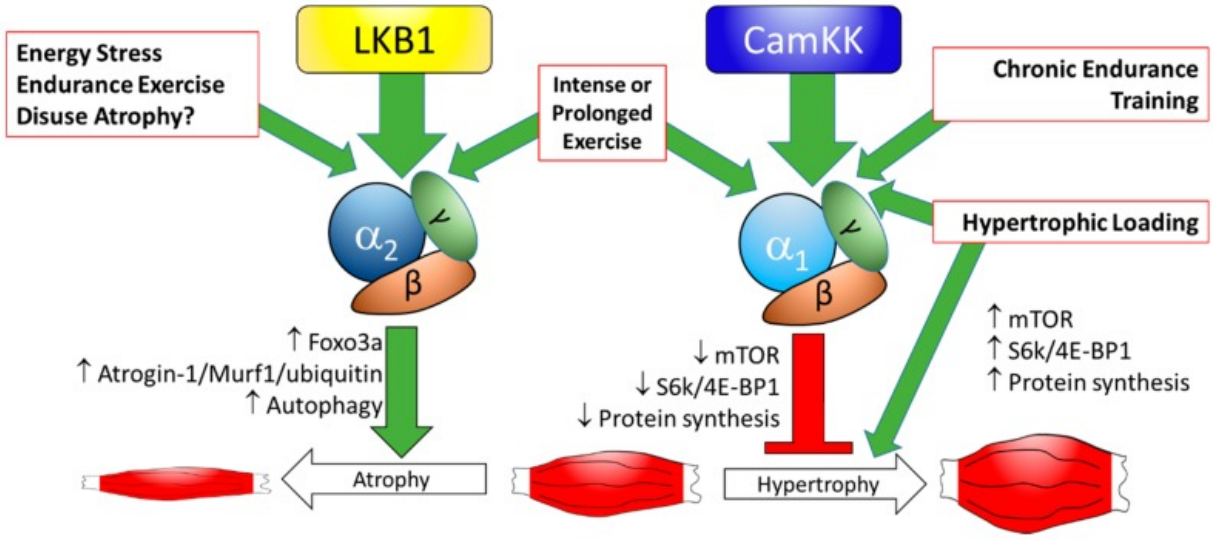

Figure. 1.2. Regulation of muscle mass through signaling pathway/nutrition/exercise regulated muscle hypertrophy and muscle atrophy[1].

Opposite with muscle hypertrophy is muscle atrophy. It is defined as partial or completed loss of muscle weight due to the degeneration of muscle fibers. Muscle atrophy could be divided into different types based on reasons that caused atrophy. Pathology, disuse, and normal aging atrophy are the most common atrophy types. Pathological conditions causing muscle atroph, includ cancer cachexia, sepsis, and AIDS[52]. Even though there is a group of genes that could be inversely regulated by hypertrophy and atrophy, the skeletal muscle atrophy has its unique regulation mechanism, including a higher protein degradation rate, and this was induced at least partly by activation of ubiquitin-proteasome pathway (UPP)[35]. Interestingly muscle atrophy also could activation of the precise transcription process, which is not the converse process of muscle hypertrophy.

The central role of the UPP system for protein degradation and protein turn over has been thoroughly studied in the past two decades. Component of this system includes three enzymes E1 (Ub-activating enzyme), E2 (Ub conjugating proteins), and E3 (Ub-protein ligase). This processing is energy-dependent for ubiquitin activation and removes of ubiquitin chain. Among these three reaction process enzymes, E3 is always being considered as the most important one. This ligase could only recognize specific target protein substrates and catalyzes the reaction. Once the target protein gets labeled with Polyubiquitin chains, this destined degradation protein could be recognized by 26S proteasome, then ubiquitin will be removed, and the target protein will be linearized and digested into small peptides. Finally, these peptides

will be degraded into amino acids in the cytoplasm or being used directly for antigen presentation[53] . In skeletal muscle tissues, two genes encoding E3 ligase have been identified, which are Muscle Ring Finger1 (MuRF1) and Muscle Atrophy F-box (MAFbx), also being called Atrogin-1 respectively[54]. Even though both of them are E3 ligase, how could they recognize their specific target protein is still unclear. Intensive research showed that MAFbx prefers to interact with certain myogenic transcription factors such as MyoD and myogenin, thus implies it might be involved in muscle cells differentiation process. Besides, transcription factor myogenin could also regulate MAFbx expression implies it is a feedback regulation of muscle size control[55-57]. Different from MAFbx, MuRF1 tend to interact with myosin heavy chain (MHC) related proteins and glucose metabolism proteins such as PDH, PDK2, and PDK4[58]. In conclusion, research about the exact roles of *MAFbx* and *MuRF1*, how they chose their substrates and pathways how they get regulated in a particular context is still a mysterious and need a long way to go for research.

1.2 Muscle stem cells

1.2.1 Development of muscle stem cells

Muscle stem cells were identified in 1961 by Mauro A[59]. These somatic stem cells reside beneath the basal lamina of mature muscle fibers; thus, they are also being called muscle satellite cells. Recent research about muscle stem cells and their related diseases are mainly based on gene-modified animal models, among which mice are the most popular ones. E9.5~E10.5, for the dermomyotome cells, they can give rise to myocyte, and $Pax7^+$ specific cells, both of them have the ability of proliferation and differentiation and contribute to the formation of primary myofibers at embryonic stage (E10.5~E13.5). These $Pax7^+$ cells proliferate and fuse with the secondary myofibers at fetal myogenesis stage. During this stage, some of the $Pax7^+$ cells exit from the cell cycle gradually, and only after E17.5, when the basal laminar completely formed, these progenitors found their final anatomical position thus being called satellite cells[60]. At the postnatal stage for the first three weeks, muscle weight increase rapidly through muscle hypertrophy and nuclear muscle addition, then muscle nuclear domain will double, and satellite cell numbers decrease for 2~3 times[61]. Upon injury, adult skeletal muscle has the ability of regeneration through the muscle stem cells. This small collection of mono-nucleated cells located beneath the basal lamina of every myofiber. SCs exist lifelong even though the regenerative ability will decrease with the influence of age and disease[62]. Satellite cells have two different states: quiescent and activated. Most of the time, muscle is a stable tissue, and satellite cells just sit in quiescence state, but after stimulating with the disease, injury, exercise, the regeneration process will be activated. Through proliferation, SCs form a pool of myoblast and then finally differentiate into terminally committed myocytes and

fuse into multinucleate myofibers. For the transition process between quiescent and activated states, it is regulated strictly. Quiescent satellite cells express Pax7 and lack the expression of myogenic determination proteins such as MyoD[63]. Delta/Notch pathway plays a critical role in the stage transition of satellite cells. Its regulation is dosage and context-dependent. During the early embryo myogenesis (E12.5 - E18.5) stage, the Notch pathway maintains muscle progenitors in high proliferation status at the expense of differentiation[64]. At E18.5, activated Notch signaling keeps on blocking differentiation of muscle progenitors. However, unpredictably it has a strong negative influence on their proliferation rate. Consistent with the lower proliferation rate, expression of cell cycle inhibitor p57 kip2 (cdkn1c) is up[65]. At E12.5, most of the muscle progenitors are p57 negative and in the active proliferating state. At E18.5, there is a dramatic increase of p57 and a severe reduction of proliferation. Deletion of Notch ligand Dll1 or RBPJ in muscle cells leads to premature differentiation of muscle progenitors, muscle satellite cell pool depletion, and dramatic muscle hyptrophy[64]. The function of the Notch pathway during puberty muscle development is still needed to be discovered. Young-Yun Kong et al. showed that for pubertal muscle development, sex hormones secreted by testis and Ovary can induce myofibers to express Mib1, which contributes to ubiquitylation and trans-endocytosis of the Notch ligands followed by activation of Notch pathway in cycling juvenile muscle progenitors promote them into adult quiescent satellite cells. This is also the first direct proof that the Notch pathway works to drive juvenile muscle satellite cells to go into quiescent state[66]. Literature showed that freshly isolated satellite cells keep the highest Notch activity, and it declines during myogenic proliferation and differentiation process. It implied the dominant role of the Notch pathway to keep adult muscle satellite cells in quiescent state[67-70]. Forkhead box 3 (Foxo3) as a transcription factor initiates the transcription of Notch receptors (Notch 1-4). When Notch receptors are binding with Notch ligands Delta-like (Dll1, Dll4) / Jagged (Jag 1/ Jag 2), the intracellular domain of Notch (NICD) will be cleaved and migrates to the nucleus. RBP-J, a DNA binding protein, will be released from its corepressor complexes and interacts with NICD and recruits a coactivator complex, including MAML-1, p300/CBP, CSL, et al., resulting in the transcriptional activation of Notch target genes[71]. Three bHLH transcriptional factors Hes1, Hey1, Heyl, are well-known mediators of Notch functions. Interestingly, for *Hey1* or *Heyl* single-gene knockout mice, there is no phenotype gets observed from both satellite cells and the muscle regeneration rate. However, for double knockout mice, a strong phenotype including muscle satellite cell pool exhaustion and regeneration defect are noticed. It suggests that muscle satellite cells require Hey1 and Heyl for entry into and also maintain their quiescence[72,73]. Hes1 is a transcription repressor. It controls postnatal muscle growth by suppressing muscle stem cell differentiation. Ines Lahmann et al. showed that Hes1 drives oscillatory MyoD expression and keeps cells in a proliferative state instead of differenatiation[74].

Besides, recent data from several other groups also showed the function of the Delta-Notch pathway in metabolism regulation. However, it seems like this regulation is highly dynamic under a particular biological context. Notch pathway was found from drosophila, and in drosophila cells, it functions as an activator of the Warburg effect for cells glycolytic shift. Target genes of the Notch pathway include activators of glucose uptake and glycolysis pathway enzymes. Besides, it could also repress the TCA cycle enzymes expression. Conversely, data from mouse macrophages showed hyperactivation of the Notch pathway contributes to mitochondrial oxidative phosphorylation genes expression. Under the context of endothelial cells and mesenchymal progenitors, the Notch pathway could suppress glucose metabolism and oxidative phosphorylation simultaneously by downregulation of glycolysis and mitochondrial complex I relative genes. However, the exact mechanism for different effects of Notch signaling on glucose metabolism is still not known, they likely reflect the variant epigenetic landscape and signaling pathway network in all these cells types[75-77].

Except for the Notch pathway, many other influence factors could also regulate muscle satellite cell activity. Tristertraprolin (TTP) is an RNA binding protein. It binds to the mRNA of MyoD and promotes its degradation[78]. MicroRNA miR31 works with mRNA of Myf5 to form RNA granule and inhibit its translation[79]. $P27^{KIP1}$ functions as a negative regulator of cyclin-dependent kinase[80]. All of these factors work together to stop proliferation and differentiation ability and keep satellite cells in a quiescent state. Influenced by muscle damage or disease, fibroblast growth factor (FGF2) will be secreted, and it works as a positive regulator p38MAPK followed by inhibit TPP activity and increase the translation of MyoD. As a transcription factor, MyoD can regulate the expression of cell division cycle 6 (*Cdc 6*), thus increase cell proliferation[81]. Myf5 is another critical activation regulator, after trauma, expression of miR-31 will decrease, and the RNA granule will also dissociate and increase the expression of Myf5 protein and the transcription of its target genes. In aged mice, FGFR-1-p38MAPK signaling pathway can down-regulate muscle satellite cells self-renew ability[82]. In geriatric muscle stem cells, depression of p16INK4a (Also called *Cdkn2a*) switch reversible quiescence into senescence[83]. CARM1 a histone acetyltransferase, it functions through increase transcription ability of *Pax7* to *Myf5* gene[84]. Sprouty1 (*Spry1*) is a negative regulator of the FGF2 signaling pathway, thus inhibits cell proliferation and helps cell quiescence state maintenance.

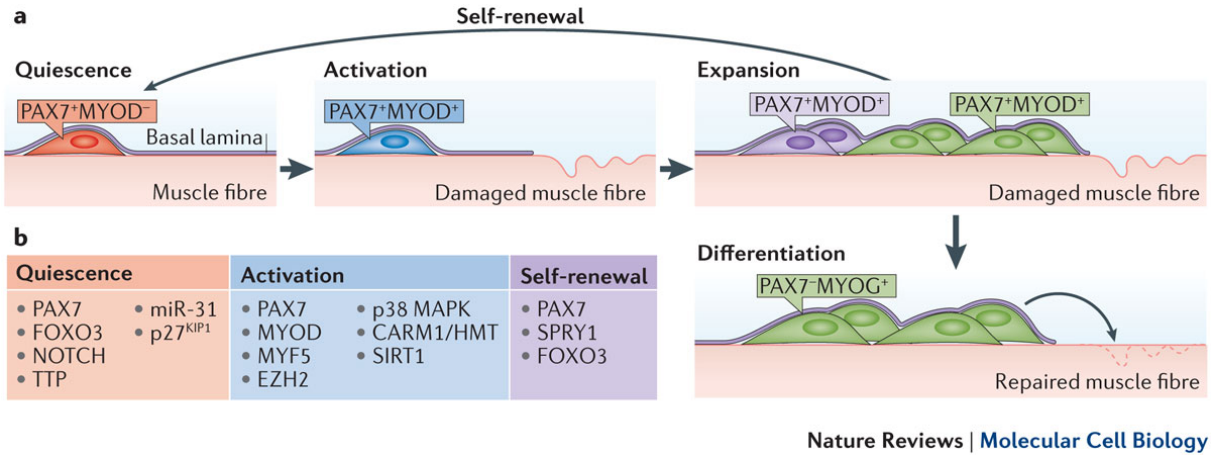

Figure. 1.3. Classical view of muscle myogenesis.
a. For adult healthy muscle fibers, satellite cells are maintained in their stem cell niche in a quiescent state. The quiescent satellite cells are only Pax7 expressed without myogenic determination protein MyoD. Satellite cells get activated by muscle injury and go for proliferation with the expression of both Pax7 and MyoD. A sub-population of activated satellite cells start differentiation by inducing the expression of MyoG and block the expression of Pax7. Ultimately fuse for muscle fiber repairation. Another subpopulation of activated could go back to the quiescent state by inhibiting MyoD expression. They will stay as back up for future muscle repair. **b.** Transcription signature of satellite cells in a different state. *FOXO3*, Forkhead box protein 3; HMT, histone methyltransferase; *MYF5*, Myogenic factor 5 ; *Sirt1*, Sirtuin 1; *Spry1*, Sprouty 1; TTP, Tristetraprolin[8].

In recent years there are several groups proved that imprinted genes like *Peg3, Mest, Cdkn1c, and Dlk1* could also regulate muscle size and weight through muscle stem cells. The constitutive loss function of *Peg3* leads to muscle mass reduction and also reduced muscle fiber numbers. Deletion of *Peg3* in muscle satellite cells resulting in speed up of proliferation and differentiation rate is coupled with increased mitochondrial function[85].

At present, people can isolate SCs based on their biomarkers, the expression of the paired box of transcription factors (*Pax3*, *Pax7*) has been generally accepted as the main feature, but *Pax3* is downregulated after birth in most of the muscles. An experiment of gene knockout in mice proved that *Pax7* is necessary for SCs maintenance and self-renewal[86]. All the SCs can be distinguished by *Pax7*, and it seems they are homogeneous. However, an increasing number of molecules markers of SCs proved that they are a heterogeneous population. With the help of Myf5-Cre: Rosa26-YFP mice, Kuang et al. found that satellite cells division in an asymmetric manner[87]. Myf5 belongs to the family of myogenic regulatory factors, which start express in muscle progenitor cells at E10.5 and reach the peak at E12.5[88]. $Pax7^+$ cells can divide into two groups: $Pax7^+/Myf5^-$ cells, around 10% of total satellite cells; they are mainly responsible for self-renewal. Thus, they are also being called satellite stem cells. For at least 90 % of $Pax7^+/Myf5^+$ cells, they performed their ability of differentiation, and they are also being called satellite myogenic cells[89]. The latest progress from Brack lab demonstrated that a discrete population of $Pax3^+$ satellite cells exist. This population can be used as reserve satellite cells as they have lower reactive oxygen species (ROS) level, which can help for sever

stress[90]. Just followed this paper, Relaix lab also showed in muscle satellite cells Pax3 expression can help satellite cells deal with the environmental stress through mTORC1 dependent G-alert response[91]. Work from these two groups proves the existence of reserve satellite cells in adult skeletal muscle, and these satellite cells have higher stress tolerance. Other critical factors can also regulate the process of muscle regeneration, just like Myf5, MyoD can be expressed in the upstream of myogenic, and they can compensate with each other from the function analysis. In the downstream of myogenesis, Myogenin and MRF4 will be stimulated as a marker for muscle cell terminally differentiation[92]. It has been proved that the combination of $CD45^-$, $Sca1^-$, $Mac1^-$, $CXCR4^+$, $ß1^-integrin^+$ can get both phenotype and functionality appropriate large populations of adult satellite cells[93].

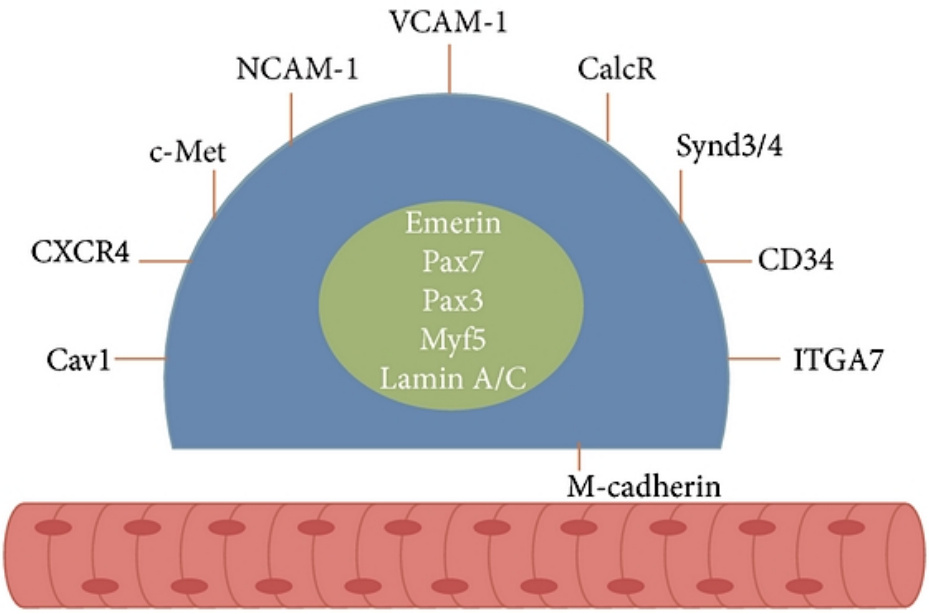

Figure. 1.4. Principal markers are currently used for satellite cell identification[4].

1.2.2 Satellite cell niche

Satellite cell niche consists of ECM, vascular, neural networks, various types of surrounding cells (e.g., fibroblast, immune cells, pericytes, PICs), and various diffusible molecules (e.g., TGFβ1, Wnt, IGF, and FGF). It is defined as anatomic locations that can regulate muscle regeneration, maintenance, and repair after trauma or disease. The dynamic interactions between satellite cells and their niche can specifically protect them from depletion, uncontrolled proliferation, and regulate their homeostasis[94]. Researchers proved that the property of muscle

progenitors and muscle satellite cells is different. Fetal muscle progenitors have a higher proliferation rate with more Pax7 expression, and they have better regeneration efficiency but lower fusion ability. Most of the adult satellite cells are out of the cell cycle and stay in a quiescent state. Data showed the property might be satellite cell niche dependent. During embryo development, tenascin-C is the main component of the extracellular matrix (ECM). The tenascin-c expression will decrease gradually, fibronectin and Col VI will increase over time. For the adult stem cell niche, Col VI becomes the critical ECM component and plays a critical role in muscle stem cell maintenance and muscle regeneration[95]. A recent study through RNA-seq analysis showed the muscle injury response in three distinct phases within 3-24 hours of chemokines for recruiting immune cells to get secreted and reach the peak, which initiated an initial inflammatory phase. Genes involved in satellite cell proliferation and differentiation peak at 72 hours after injury indicated a mitogenic phase. Followed by the myoblast fusion and new muscle fiber regeneration demonstrated a differentiation phase. Even though the exact function of the ECM component in myogenesis is still unclear, component remolding happened during the three phases after injury[96]. Aging-related processes dramaticcally altered the muscle satellite cell nice and can inevitably impair the maintenance and regenerative ability of skeletal muscle tissue. Laura Lukjanenko et al. demonstrated a substantial reduction of fibronectin (FN) in aged stem cell niche lead to a severe reduction of muscle satellite cell number as well as their regeneration capability. Knockout of FN in young mice recapitulate the aging phenotype. Signaling pathway analysis show FN deletion leads to a significantly down-regulated p38 mitogen-activated protein kinase pathway and integrin-mediated signaling through focal adhesion kinase because of inadequate attachment to the niche[97]. Besides, FN can regulate Wnt7 signaling through which influence satellite cell expansion, decrease the differentiation ability of myoblasts in vitro, but laminin functions in the opposite way[98]. Valentina Flamini et al. demonstrated that compared with satellite cells attached with muscle fibers, dispersed cells regulate their cell proliferation and differentiation with a different signaling pathway. Primary myoblasts cultured in vitro without their native stem cell niche regulate the transcriptional activation for cell fate transition through the Erk1/2 pathway. With decreased ERK1/2 activity, primary myoblasts stop proliferation and start differentiation. Myoblasts cultured with fiber regulate the process through increased activity of Trp53. It suggested that the satellite cell niche regulates the balance between self-renew and differentiation might through p53 pathway[99]. Apart from this, research from Meryem B. Baghdadi et al. indicated a new mechanism of the Notch signaling pathway in satellite cells quiescence maintenance in a cell-autonomous manner which involved in the production of ECM molecules. Using antibodies of RBPJ and NICD for chromatin immunoprecipitation sequencing from C2C12 cells showed they bound at the enhancers of *Col5a1*, *Col5a3*, *Col6a1*, and *Col6a2* loci, RBPJ knockout mice show deregulation of these collagen genes. Furthermore, Col V deleted mice show a depletion

of the satellite cell pool because of the cell cycle re-entry, which is a phenotype reminiscent of RBPJ knockout mice. For the downstream signaling, the Calcitonin receptor is identified as the target of Col V as the administration of calcitonin derivative can fully rescue the phenotype of satellite cells caused by Col V deletion. To sum up, a Notch-Col V-Calcitonin receptor signaling cascade that maintains satellite cells in a quiescent state in a cell-autonomous fashion is identified. This is also the first time that illustrates how the Notch pathway regulates satellite cell quiescent state through regulation of ECM component[100]. Besides, there are also enormous quantities of factors from the satellite cell niche that can regulate the activity of satellite cells. What we have known, such as transforming growth factor-ß (TGF-ß) secreted by immune cells, can deplete satellite cells and prevent the regeneration efficiency (Fig. 1.5).

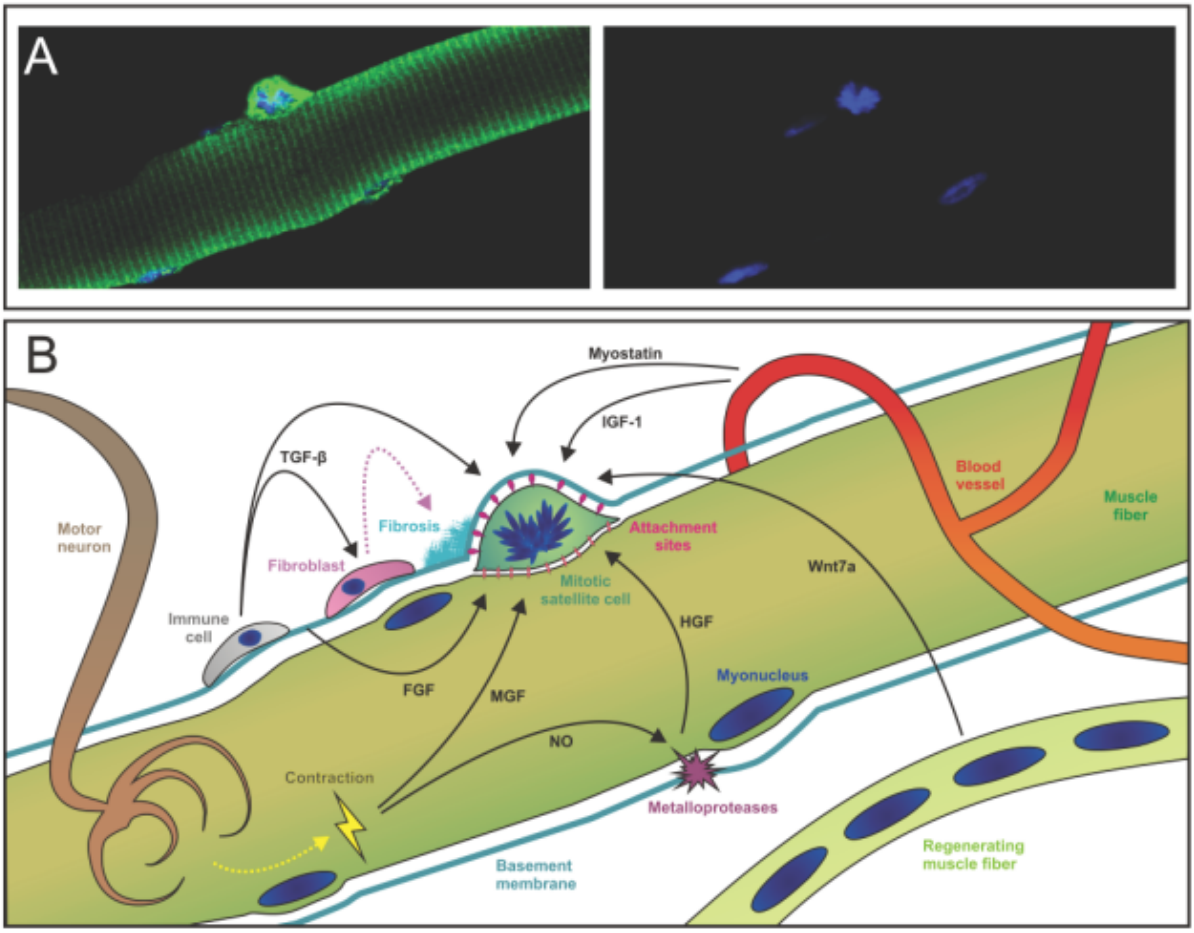

Figure. 1.5. Satellite cell niche and regulatory factors.
A Immuostaining of a mitotic satellite cell. The satellite cell is labeled with a yellow fluoresce and DNA in blue. **B** Schematic of environmental cues influencing a satellite cell in its niche. FGF, fibroblast growth factor; HGF, hepatocyte growth factor; IGF, insulin-like growth factor; MGF, mechano-growth factor; NO, nitric oxide; TGF, transforming growth factor[6].

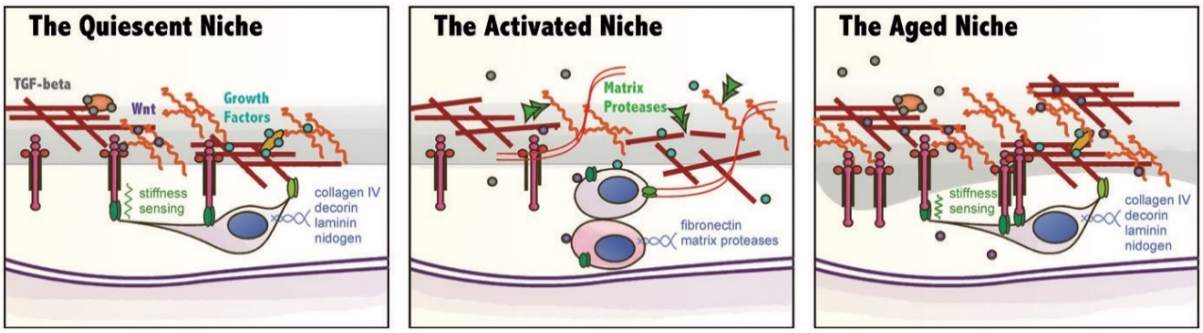

Figure. 1.6. The satellite niche and regulatory factors

Left: The quiescent SC senses the stiffness through integrins and expresses matrix proteins to maintain its extracellular matrix (ECM). Within this matrix, growth factors and signaling molecules are sequestered, maintaining the "quiet" state. **Center:** In response to injury, matrix proteases degrade the components of the basal lamina, which results in the release of signaling molecules to activate the SC. Daughter cells begin to differentiate. **Right:** In the aged niche, matrix components accumulate to form a denser and thicker basal lamina. The stiffness sensing and sequestration of signaling molecules may be affected by this change[7].

1.2.3 Muscle stem cell epigenetic signature

Epigenetics is a term that appeared around the 1990s, which was used to describe a stable inheritable phenotype change without alternation of the DNA sequence[101]. Related epigenetic modification including DNA methylation, histone modification, gene imprinting, X chromosome silencing[102]. DNA epigenetic status change could influence its compaction ability, thus lead to euchromatin and heterochromatin. Euchromatin is less packed chromatin with more DNA expose. During the cell cycle, interphase cells need to growth instead of division; thus, more gene transcription activity will happen and also more protein production. Heterochromatin is tightly packed chromatin. It consists of constitutive heterochromatin and facultative heterochromatin. Constitutive heterochromatin keeps in highly condensed status because of repetitive DNA sequences. It functions in maintaining chromosome structure. Facultative heterochromatin could transit from condensed status to decondensed status, thus regulate gene expression[103]. Histone deacetylation and histone di or tri methylation work in heterochromatin status change. Enhancer of zeste homolog 2 (EZH2) is a histone methyltransferase enzyme. As the catalytic of Polycomb Repressive complex II (PRC2), it represses genes expression through epigenetic modification of H3K27. Research proves that Ezh2 maintains an essential phase of muscle satellite cell expansion but does not regulate terminal differentiation[104]. Immunostaining with specific antibodies showed it expressed in both quiescent muscle stem cells ($Pax7^+/Myf5^-$) and activated muscle progenitor cells ($Pax7^+/Myf5^+$). Co-staining of Pax7 with H3K27me3 also confirmed at p8 more than 80% of $Pax7^+$ cells are

H3K27me3 positive[105]. EZH2 knockout mice showed reduced muscle stem cell numbers, reduced muscle mass, decreased cross-section area. Chip sequencing data from EZH2 knock out and control satellite cells showed p16INK4a, which functions to block cell cycle is the potential target for the activation of satellite cell, and the decreased satellite cell numbers could be rescued by knockdown of p16INK4a in EZH2 null satellite cells. Interestingly EZH2 only regulates activated satellite cell proliferation without any influence for satellite cells self-renew and differentiation[104]. Following this, to get global epigenetics profile of H3K27me3 in satellite cells, Chip sequencing with H3K27me3 antibody showed compared with activated satellite cells (ASC) quiescent satellite cells (QSC) keep in a more permissive chromatin state with fewer genes being epigenetically repressed by H3K27me3. This paper also showed that the H3K27me3 level increased during satellite cells activation[106]. H3K4me3 is stable between quiescent and activated muscle stem cells. However, facultative heterochromatin marker H3K27me3 is much lower in quiescent MuSCs. During activation, its tri-methylation level increases dramatically; however, with differentiated muscle fibers, this tri-methylation pattern decreases again[106]. H4K20me3 marks constitute heterochromatin. Its modification is just on the contrary with H3K27me3[107]. It suggests that activated MuSCs contain a high level of facultative heterochromatin and a low level of constitutive heterochromatin and are primed to undergo a rapid switch to high constitutive heterochromatin following differentiation.

1.2.4 Muscle stem cell metabolism and epigenetic modification

As the primary source of muscle regeneration in adult injured or trauma skeletal muscle systems, muscle stem cells are always out of their cell cycle and stay in a quiescent state once being activated they will go into proliferation state. The function of various transcription factors such as myogenic regulatory factors (MRF) has been extensively studied[88,108]. However, regulators from the microenvironment and how they could interact with each other, especially for metabolism byproduct still need to get more attentation[100]. In the past decade, metabolism was treated as a passive way only for energy production instead of cell state (quiescent activated or differentiated) and cell identity (lineage commitment) regulation. However, recent research showed local nutrition supplement, and central cell metabolism is capable of providing temporal regulation of histone and DNA modifications, thus regulate transcription through the supplement of some histone and DNA key modification metabolites, including acetyl-CoA, nicotinamide adenine dinucleotide, a-ketoglutarate and S-Adenosylmethionine (SAM) among others[2,109,110]. Just like other kinds of somatic stem cells, satellite cells need the energy to sustain life activity. Cells in different statues of their energy-demanding are also different. Different from the quiescent SCs, proliferating and differentiation SCs must get

enough biomass to synthesize new proteins, nucleotides, and phospholipids for rapid cell division and growth. As we know, ATP breaks down is an effective way for cells to get energy and maintain internal homeostasis. ATP can be generated in two different locations inner cells, cytoplasm through glycolysis (2ATP), and mitochondrial via oxidative-phosphorylation (OXPHOS) (32-36ATP). Rely on which way to generate energy mainly determined by substrate, the concentration of oxygen, and the demand for energy. Compared with OXPHOS, glycolysis is a fast but less efficient way for ATP generating; meanwhile, its side pathways such as pentose phosphate pathway and one-carbon cycle can also provide building blocks for nucleotides and SAM as methyl donner for DNA and histone methylation modification. A summary of how metabolic and epigenetic modification of histone markers change during quiescent muscle stem cell activation was shown in the following figure (Fig. 1.6).

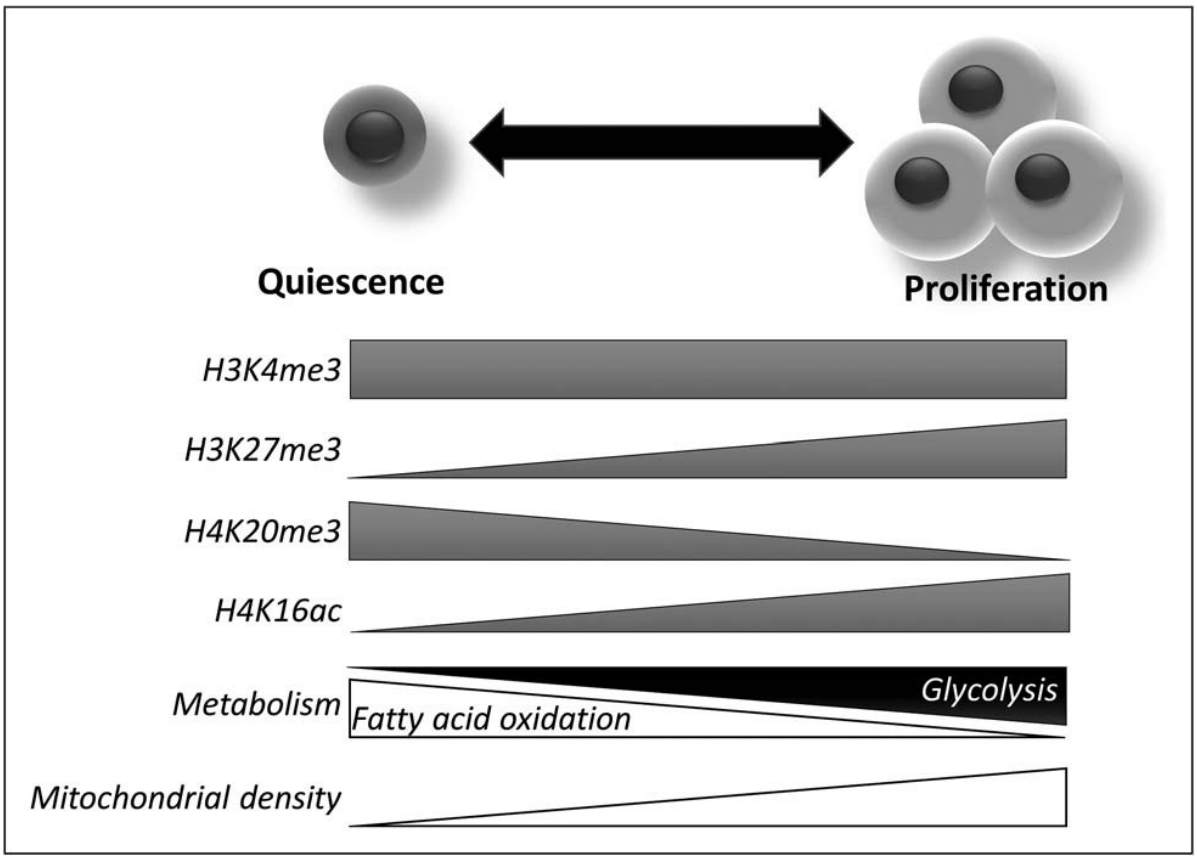

Figure. 1.7. Metabolic and epigenetic transition during satellite cell activation.

From metabolism, compared with proliferating muscle progenitors, quiescent satellite cells have lower mitochondrial density and mainly rely on fatty acid oxidation for energy production. From the epigenetic perspective, the four well-studied histone modification ways including symbolizes of transcription activation: H4K16 ac, H4K20me3, and H3K4me3 and transcription repressive: H3K27me3. H3K4me3 is not influenced affected by cellular status. H3K27me3 and H4K16ac are showing a similarly increased pattern in the process of cell state change. This implies the function of each modification way is highly dependent on cells' transcriptional status. H4K20me3 level decreased during activation. In general, during the process of cell state transition, its chromatin status shift from constitutive heterochromatin to facultative heterochromatin[9].

Stem cells undergo metabolic reprogramming and use different metabolic substrates during differentiation. In recent years research about stem cell metabolism is becoming a central issue, and many important discoveries have been made. Most of the results were achieved in hematopoietic stem cells, which always stayed in a quiescent state in the hypoxic niche. Once the environment is changed, the stem cells will be activated and differentiated into different blood types. Quiescent HCS gets its energy via glycolysis, and this is also necessary for quiescent state maintaining. Through analyzing metabolomics of HCS and the progenitors, it was found the main difference is that HCS can get fructose-1, 6-bisphosphate accumulated, which means a high rate of glycolysis. This way is also HIF1α dependent. HIF1α is a nuclear transcription factor through increasing the transcription of PDK2 and PDK4. It can prevent the pyruvate from go into TCA cycle[111]. Conditional knockout of Ptpmt1(Protein Tyrosine Phosphatase Mitochondrial 1) in HSC showed a metabolism switch from glycolysis to mitochondrial respiration and the metabolism shift is necessary for HSC activation and differentiation[112]. Little is known about how the metabolism will change for different statues of satellite cells. When it is in quiescent, the number of activated mitochondrial is limited, and it generates energy mainly through fatty acid metabolism, the advantage of this metabolism way is it can reduce the production of reactive oxygen species effectively. With the restriction of SCs, previous investigations are mainly performed on C2C12 myoblasts. Data prove that proliferating myoblasts rely on glycolysis, but for differentiating myoblasts, both the density of mitochondrial and OXPHOS activity will increase dramatically. This process is also relying on signal pathways such as AMPK and SIRT1. Nevertheless, for differentiated myotubes, the activities of these two proteins are down-regulated. James G. Ryall et al. show that during satellite cells activation, satellite cells shift energy generation from fatty acid oxidation to glycolysis which leads to a decreased concentration of cytoplasmic NAD^+. This decreases the activity of the NAD^+-dependent histone deacetylase activity of sirtuin1 (Sirt1) thus promoting the acetylation of H4K16 and increase satellite cells differentiation genes expression[113] . Both SIRT1 knockdown and inhibitor treatment can significantly increase H4K16 acetylation and MyoD expression. It suggests that metabolic shift might regulate muscle genes expression through Sirt1 dependent H4K16 acetylation. For double confirmation, skeletal muscle-specific knockout of the Sirt1 mouse model is used, combined using RNA-seq and ChIP-seq to profile gene expression and SIRT1 dependent H4K16 acetylation localization across the genome to determine links between SIRT1-H4K16ac and satellite cell activation genes expression. SIRT1 knockout satellite cells exhibit increased global H4K16ac, precocious activation, and differentiation genes regulated by H4K16ac, including *Mylk2*, *MyoD*, *MyoG*. Besides, defects in skeletal muscle development and regeneration following injury are also noticed. This work connects metabolic cues with satellite cell activation genes expression via epigenetic regulation (Figure 1.7). Machado et al. developed a protocol of in vivo fixation of muscle tissues

before FACS sorting. The advantage of this technique is to permit to analyze truly quiescent satellite cells without considering the cell status change during enzyme digestion and another isolation artefact. It is also confirmed the high enrichment of fatty acid oxidation genes in quiescent satellite cells[114]. However, why quiescent satellite cells prefer to use fatty acid metabolism to generate energy is still needs to be elucidated.

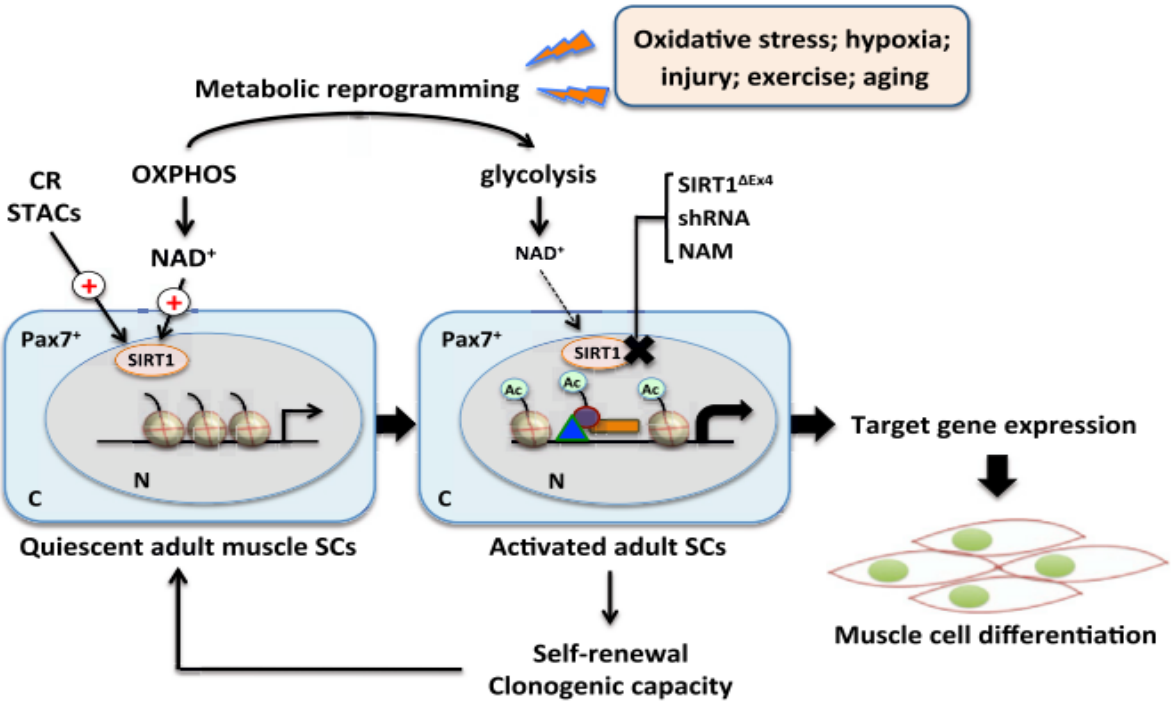

Figure 1.8. In adult skeletal muscle, metabolic reprogramming promotes satellite cell activation. In quiescent satellite cells, the metabolism way of fatty acid oxidation instead of glycolysis leads to an NAD+ concentration increase in the cytoplasm. As a substrate for sirtuins in muscle stem cell context, it could work together with other sirtuins regulators such as calorie restriction and sirtuin-activating compounds to enhance the enzyme activity of Sirt1. Activation of Sirt1 could remove the histone acetylation and make chromatin in a more compact status and prevent transcription initiation. In the case of external stimulation such as injury and aging. Satellite cells will undergo metabolic reprogramming and shift their metabolism way from fatty acid oxidative phosphorylation to glycolysis. Thus contribute to decreased NAD+ and also Sirt1 activity followed by increased histone acetylation level and less compact chromatin status. Then the genes involved in cell proliferation and muscle differentiation will be transcripted, and satellite cells will go for differentiation. STACs = sirtuin-activating compounds; CR = Calorie restriction[2].

.

In addition, another research group, through comparing the epigenetic profiles of quiescent satellite cells from young and old mice observed that epigenetic changes accumulate and may lead to a functional decline in quiescent stem cells. These findings highlight the importance of chromatin mapping in understanding the unique features of stem cell[106]. The latest research

on pig muscle metabolism found the hypomethylation status of PMM (oxidative) and LDM (glycolysis) muscle are different. PMM muscle showed the characteristic of hypo-methylation, the central different methylated regions were mainly responsible for GTPase regulator activity, and the relative signaling pathways that are involved[115]. We know the importance and dramatic epigenetic change during muscle stem cell activation. Varies histone methylation and acetylation modification, DNA methylation, are all enzyme catalase reactions. Then the question will be, where do the substrates for these enzymatic reactions come from? Metabolism intermediate substrate from both glycolysis and TCA cycle could be directly transported to the nucleus as a substrate for DNA modification or after enzymatic reaction being converted into the substrate for DNA methylation (Fig. 1.8). For example, glycolysis product 3-phosphoglycerate could be used as a substrate for enzyme 3-phosphoglycerate dehydrogenase (PHGDH) convert into the serine-glycine synthesis pathway. As a denotation for its side chain to tetrahydrofolate, serine drive one-carbon metabolism and finally provide SAM for DNA methylation. TCA cycle product citrate could be export from the mitochondrial matrix then react with Acyl being converted into Acetyl-CoA and works as a substrate of histone acetylation. aKG could be used directly for DNA demethylation reaction. To sum up, metabolism plays a critical role in DNA and histone modification and also for relative gene transcription.

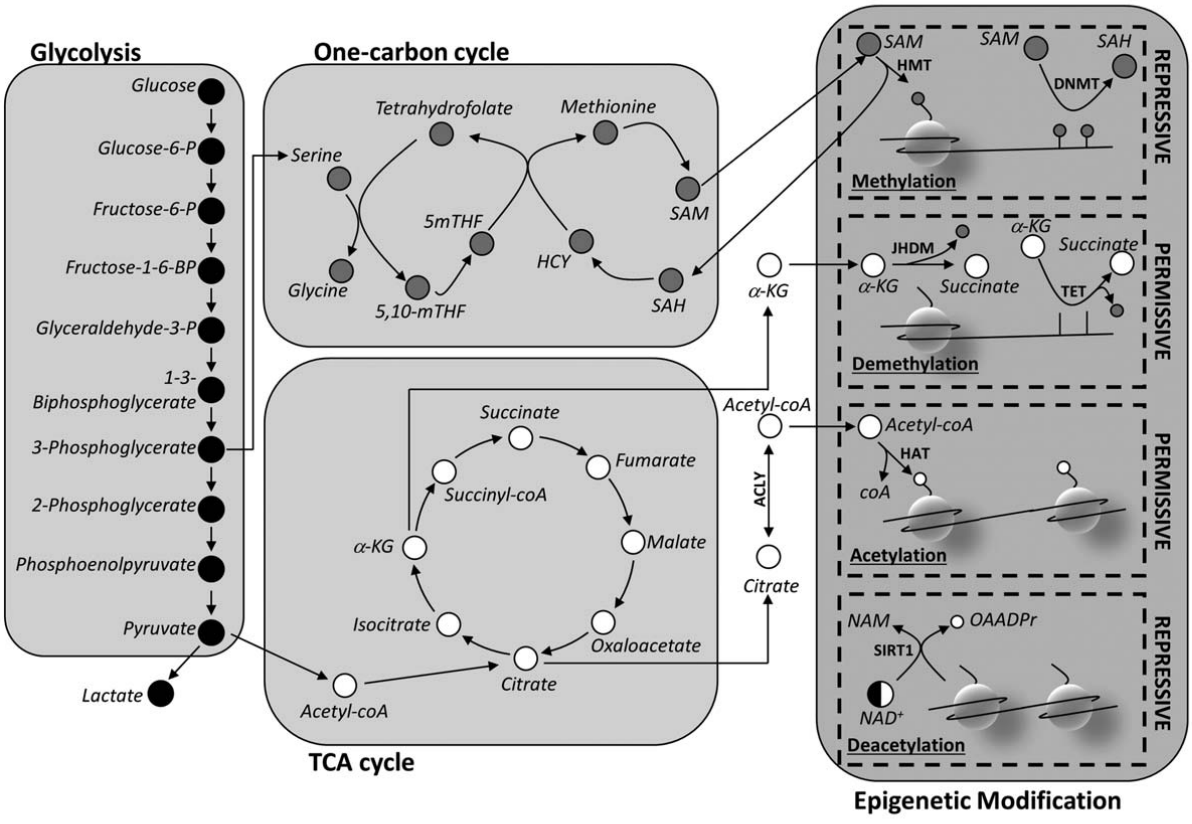

Figure. 1.9. A model for how epigenetic modification being regulated by metabolism.
The substrate of glycolysis 3-Phosphoglycerate could supply serine, which helps to stimulate the one-carbon cycle in the cytoplasm. The product of the one-carbon cycle s-adenosylmethionine is a substrate for both DNA methyltransferase and histone methyltransferase. Glycolysis product pyruvate could be transferred into the mitochondrial matrix and drives the TCA cycle. The product of the TCA cycle citrate could be exported out from mitochondrial and acts as a donor of acyl for histone acetylation reactions. Besides, a-ketoglutarate is an important cofactor for histone and DNA demethylation. The variance between glycolysis and oxidative phosphorylation could influence the cytoplasm NAD^+ concentration, thus change the histone acetylation level through histone deacetylation enzyme Sirt1. ACL = ATP citrate lyase; aKG = a-ketoglutarate; DNMT = DNA methyltransferase; HAT = histone acetyltransferase; HCY = homocysteine; HMT = histone methyltransferase; JHDM = Jumonji domain-containing histone demethylase; NADH = nicotinamide adenine dinucleotide; NAM = nicotinamide; OAADPr = OAcetyl-ADP-ribose; SAH = S-adenosylhomocysteine; SAM = s-adenosylmethionine; TET = ten-eleven translocation methylcytosine dioxygenase[9].

1.3 Neurofibromatosis type 1 (NF1)

Human *NF1* is a potent tumor suppressor gene that lies on chromosome 17q11.2. NF1 encodes a large protein composed of 2818 amino acid named as neurofibromin. Neurofibromatosis type 1 (NF1) is a common multi-system autosomal dominant genetic disorder caused by mutation of the *NF1* gene. It affects one in every 3000 people. Symptoms of NF1 include skin pigmentation spots and tumors growth along nerves. Most adult patients develop neurofibromas, which is a type of commonly noncancerous nerve tumors that form soft bumps on and under the patients skin (Figure. 1.9). But their conditions vary widely among individuals. Neurofibromin is a RAS GTPase-activating protein (GAP). It works as negative regulator of Ras-MAPK signaling. Ras is an activator of mitogen-activated protein kinase (MAPKs). There are at least four different MAPKs in mammals, including extracellular signal-related kinase (ERK1/2), Jun amino-terminal kinase (JNK1/2/3), p38 proteins and ERK5[116]. Among them, Ras could activate ERK1/2, JNK, and p38[117]. Under myogenesis context, research showed in the C2C12 myoblast cell line, the Notch signaling pathway could inhibit p38MAPK activity through induction of MKP-1 (Dusp1), and this induction is RBP-J dependent[118].

Experiments conducted on the function of neurofibromin demonstrated that it could enhance cell motility via regulating actin filament dynamics through the Rho-ROCK-LIMK2-Cofilin signaling pathway. This may partly explain the mechanism of multiple neurofibroma formation[119]. The expression levels of *NF1* in different organs and in different development stages are also different, and neuronal cells are among the highest. Studies have shown that the situation of patients with *NF1* mutation depends on its mutation doses. A mouse model was used for the brain specifically knock out of *Nf1* for one allele, hyperactivated Notch

signaling pathway was detected, and pharmacological inhibition of Notch signaling activity could rescue this mouse phenotype. However, if *Nf1* was knock out for two alleles, inhibitors for MAPK/ MEK, nitric oxide production, and Notch signaling need to be used simultaneously to get the same rescue effect compared with only one allele knock out animals. Notch and Ras pathways are two of the seven highly conserved signaling pathways during embryo development. Widespread research proved the mutual influence between Notch and Ras pathway in particular biological contexts and time points. Overexpression of activated Notch and Ras, respectively, or at the same time during Drosophila development followed by Microarray analysis, compared with the control group, surprisingly, more than 65% of Ras target genes are responsive to Notch activation. The effect of Ras activation on Notch output is obvious but still needs more pronunciation. In addition, they also mentioned a model that for cells receives these two pathways at the same time. The Notch pathway will be more responsive than Ras pathway[120]. In addition, Notch activity on NF1 brain tissue was also being tested, and a similar pattern was observed[121].

Thomas De Raedt et al. used an array comparative genomic hybridization method with 51 malignant peripheral nerve sheath tumors (MPNSTs), which is the most common *NF1* related malignancy. For patients with *Nf1* microdeletion, components of polycomb repressive complex 2 (PRC2) such as SUZ12 and EED were also being deleted, thus lead to lower H3K27me3 level and increase proliferation genes expression and contribute to cancer. 79% *Nf1* microdeletion patients lose SUZ12/EED expression, and 34% none *Nf1* microdeletion patients showed homozygous deletion of SUZ12/EED, 53% of patients without *Nf1* microdeletion possess one or more PRC2 mutations/deletions. These data suggested PRC2 might play a critical role in MPNST pathology. In general, the research revealed an unexpected connection between NF1, PRC2 complex, and Ras. It implied that in the further epigenetics-based therapeutic strategy could be used for *Nf1* relative cancer treatment[122]. In addition, Kelly A. Diggs-Andrews et al. showed neuronal dysfunction can be influenced by sex in NF1 patients. Both patients and genetically modified mice were used for the research. Results showed female patients have more severed visual symptoms and need to be treated for visual decline compared with their male counterparts, and also only female *Nf1* mutation mice exhibited optic glioma relative phenotype. It was also noticed that only male mutated mice showed learning and memory deficits and increased Ras signaling activity. This implies sex is an important prognostic factor for neuron dysfunction in NF1 patients and might be used for interpreting clinical research results[123].

NF1 has variable phenotypes, and several organ systems can be affected, besides central and peripheral nervous system, skeletal muscle system can also be affected[124-126]. Clinical research demonstrating patients with NF1 always show reduced muscle size and muscle weakness. Through conditional gene knock out of *Nf1* in early limb bud mesenchyme using

Prx1-cre ($Nf1^{Prx1}$) mouse model, a muscle development defect was detected including fibrosis, muscle fiber number reduction, muscle force loss and changed muscle patterning.The underlying mechanism is *Nf1* knockout impaired the terminal differentiation ability of myoblast during early embryo development stage (E12.5-E14.5). Our group proved that neurofibromin is necessary for skeletal muscle formation and maintance[125]. Recent studies suggest that $Nf1^{Prx1}$ mouse (limb specific *Nf1* gene conditional knockout mice model), demonstrated an increased SDH activity consistent with increased mitochondrial function, expression of fatty acid synthase and also hormone leptin. On the contrary, a number of fatty acid transporters in this mouse line show the opposite way of expression reduction. These data are the first time to suggest a direct link between NF1 and mitochondrial fatty acid metabolism[126].

Fig. 1.10. Skin manifestations in neurofibromatosis Type 1[5]
Patient with cutaneous neurofibroma and plexiform neurofibroma

1.4 Dissertation Objectives

NF1 patients display muscle phenotype, including muscle mass loss as well as muscle strength reduction. Preliminary work from the function of *Nf1* on early muscle development has shown that *Nf1* plays an indispensable role in embryonic development. Mouse models were generated to investigate the mechanisms of how *Nf1* regulates skeletal muscle development, including $Nf1^{Prx1}$, $Nf1^{Lbx1}$, $Nf1^{MyoD}$, $Nf1^{Pax7creER\text{-}(T2)}$ and $Nf1^{HSA}$ in our laboratory or in other laboratories. However, until now, the pathomechanism behind it is still unclear.

The $Nf1^{Prx1}$ mouse model could recapitulate some of the patients' phenotype, but *Nf1* is not only knocked out in muscle cells but is also knocked out in connective tissue and other cell types. Therefore, it's inaccurate to say this was caused by the function of *Nf1*, specifically in muscle tissue. The $Nf1^{Lbx1}$ mouse model died before birth probably due to the inability of food taking. $Nf1^{MyoD}$ mice could survive the longest for six days after birth. These animal models are not suitable for postnatal muscle development studies. For $Nf1^{Pax7creER\text{-}(T2)}$ mouse model, when Tamoxifen was administrated from 8 weeks on, there was no muscle phenotype being

observed at all, suggesting limitations of this animal model. $Nf1^{HSA}$ mouse model, which deleted *Nf1* in mature muscle fibers with human alpha-skeletal actin cre, also showed no muscle phenotype. Therefore, a suitable mouse model is needed to study the mechanism of how *Nf1* regulates muscle cells in vivo. In this work, the $Nf1^{Myf5}$ mouse model was used in which *Nf1* was knocked out in *Myf5* expressed muscle progenitor cells and their daughter cells. The advantage of this mouse model is that it can survive for about 22 weeks after birth, and it also recapitulated NF1 patients' muscle phenotype. With this mouse model, the following objectives could be achieved:

- Identify the muscle phenotype induced by *Nf1* deletion at different postnatal muscle developmental stages.
- Find out the mechanism of how this muscle phenotype is regulated by *Nf1* deletion. Accumulate more knowledge for its involved signaling pathways.
- With specific signaling pathway inhibitors, attempt treatment to ameliorate the mouse mutant phenotype.
- As preclinical research, provide more useful clinical targets for neurofibromatosis I patients treatment.

Data generated from this project will help reveal the pathogenic mechanisms caused by *Nf1* mutation. Hopefully, in the near future, it could also contribute to improving the life quality and life expectancy of NF1 patients.

2 Materials

2.1 Instruments

Name	Type	Supplier
Sonicator	BioruptorTM NextGen	Diagenode
Fridge	4 °C	Bosch
Freezer	-20°C	Bosch
Freezer	-80°C	Thermo
Thermal PCR cycler	ProFlex PCR System	Thermo
Real time PCR cycler	ABI Prism HT 7900	Applied Biosystems
Microwave	DO2329	DOMO
Shaker	DRS-12	neoLab
Thermomixer	Thermomixer compact 5350	Eppendorf
Water bath	MD	Julabo
Vortex	Microspin FV-2400	Lab4you
Microscope	IX50	Olympus
Fluercence microscope	DMi8	Leica
Confocal laser scanning microscope	LSM 700	Zeiss
FACS	Aria II SORP	BD
Protein electrophoresis equipment	Mini	Bio-Rad
Protein transfer system	Mini Trans-Blot	Bio-Rad
Gel documentation system	Fusion FX Spectra	Vilber
Power supply	EPS301	Amersham Bioscience
Nandrop	2000	Thermo Scientific
Qubit	®Fluorometer	Invitrogen
Bioanalyzer	2100	Agilent
Centrifuge	5424	Eppendorf
Tissuelyser	LT	Qiagen
Single channel Pippte	2,10,20,100,200,1000	Gilson

Cryotome	H560	Microm
Microtome Cool Cut	HM355S	Microm
Embedding station	EC 350-1&2	Microm
Dehydration station	TP 1020	Leica
Plate reader	Spectra Max 250	Molecular Devices
pH meter	HI2211	HANNA instruments
Cell culture incubator		Memmert
Cell culture hood	MSC-ADVANTAGE	Unity Lab
Automated Cell Counter		Luna™
Seahorse	XF96	Aglient
High-Resolution FluoRespirometry	O2k	OROBOROS Instruments
Heating plate	HI1220	Lecia

2.2 Consumables

Materials	Type	Supplier
Cell culture plates	96/48/24/12/6 well	Costar
Cell culture plastic pipettes	5,10,25,50 ml	SARSTEDT
Cell strainer	70	VWR
Cell strainer	40	VWR
Cover slips	10/12/15 mm	DeckGlasser
Cryotome Blades	Disposable	Leica
Glass pipettes	5/10/25/50 ml	ibidi
Glass slides	24 x 60 mm	Roth
Laboratory aluminium foil	30 cm x 150 m	Duni
Laboratory gloves	S/M/L	StarLab
Parafilm	10 cm x 38 m	Roth
Pipette tips	10/200/1000 µl	DeckWorks
Silica beads with indicator	Silica Gel Orange, 2 - 5 mm	Roth

Stainless steel beads	5 mm	Qiagen
Sterile filters	0.2 µm	Sigma
Sterile scalpels	Disposable	BD
Sterile syringes	1/5/10 ml	BD
Transfer membrane	0.45/0.2 µm	GE
8-tube strip and caps	T320	Simport
96-well plate	MicroAmp	Applied Biosystems
384-well plate	AB1384	Thermo
Whatman paper	150 mm	BD

2.3 Chemicals

Unless stated otherwise, chemicals were obtained from Merck, Roth, Sigma-Aldrich and Thermo Fisher.

Buffers and Solutions

Buffers	Component
10x PBS	80g NaCl; 2g KCl; 14.4g Na_2PO_4; 2.4g KH_2PO_4; add bidest and regulate pH to 7.4; Final volume is 1 Litter.
10x TBS	24g Tris-Hcl; 5.6 g Tris base; 88g Nacl, dissolve in 900 ml bidest and regulate pH to 7.6; Final volume is 1 Litter.
PBX	100 ml (10x) PBS stock solution. 1 ml TritonX-100. Bidest to 1 Litter.
PBST	100 ml (10x) PBS stock solution. 1 ml Tween-20. Bidest to 1 Litter.
TBST	100 ml (10x) TBS stock solution. 1 ml Tween-20. Bidest to 1 Litter.
RIPA buffer	50 mM Tris Hcl, pH 8.0; 150 mM Nacl; 1% NP-40; 0.5% Sodium deoxycholate; 0.1% SDS.
Protein Lysis buffer	1 x Complete Protease Inhibitor; 1 x NaF; fill with RIPA.
10x Transfer buffer	30.2 g Tris; 144 g Glycine; Bidest to 1 Liter
10x Running buffer	Tris-base 30 g; Glycine 144 g; SDS 10 g; Bidest to 1 Liter

1x Transfer buffer	100 ml (10x) transfer buffer; 200 ml methanol; 700 ml bidest.
1x Running buffer	100 ml (10x) running buffer; 900 ml bidest.
6 x Protein loading buffer	3.75 ml 1 M Tris pH 6.8; 1.2 g SDS; 6 ml Glycerol; 0.006 g bromophenol blue; 0.462 g DTT; Total volume is 10 ml.
6 x Orange G DNA loading dye	2 ml 50 x TAE buffer; 0.15 g Orange G, 60 ml Glycerol fill up to 100 ml
50 x TAE buffer	242g Tris; 18.61 g EDTA; 57.1 g Glacial acetic acid; Add bidest water to 1 litter.
Sonication buffer	0.1% SDS; 1% Triton X-100; 0.1% Na-deoxycholate; 1 mM EDTA; 140 mM Nacl; 50 mM Hepes pH 7.9; 1 x Roche $_c$omplete Proteinase inhibitor.
Nacl buffer	0.1% SDS; 1% Triton X-100; 0.1% Na-deoxycholate; 1 mM EDTA; 500 mM Nacl; 50 mM Hepes pH 7.9
Licl buffer	350 mM Licl; 1% IPEGAL CA630; 1% Na-deoxycholate 1mM EDTA; 10 mM Tris-Hcl pH 8.0.
TE buffer	1mM EDTA; 10 mM Tris-Hcl pH 8.0
Elution buffer	1% SDS; 100 mM $NaHCO_3$; 250mM Nacl; 0.5 mg/ml Proteinase K.
Staining solution	1 x PBS, 5% BSA, 0.1 % Triton X-100
Growth Medium	DMEM, 20% FBS, 1% Glutamin, 1% Penicillin/streptomycin
Differentiation Medium	DMEM, 2% FBS,1 % Glutamine, 1% Penicillin/streptomycin
10% Matrigel	1 ml Matrigel, 9 ml DMEM, store aliquots in the freezer.
Oil Red O solution	0.5 g Oil Red O in 100 ml isopropanol.

2.4 Enzymes

Name	Company
Collagenase A	Sigma Aldrich
Proteinase K	Boehringer Ingelheim
Reverse Transcriptase Superscript II	Thermo Fisher Scientific
Taq polymerase	Fermentas

Nextra Tn5 transposase enzyme	Agilent
DNase I	Qiagen
RNaseA	Sigma Aldrich

2.5 Reagent Kits

Name	supplier
Seahorse XF Cell Mito Stress Test Kit	Agilent
Seahorse XF Glycolytic Rate Assay Kit	Agilent
AllPrep DNA/RNA/Protein	Qiagen
Pierce BCA Protein Assay Kit	Thermo Fisher Scientific
Reverse Transcription Kit	Invitrogen
Agilent High Sensity DNA kit	Agilent
Nextera XT DNA Library Preparation Kit	Agilent
MinElute PCR Purification Kit	Qiagen
NAD/NADH Quantification Kit	Sigma Aldrich
ATP Determination Kit	Thermo Scientific
Lactate Assay Kit	Sigma Aldrich
SYBR Green qPCR Master Mix	life Technologies
GOTaq qPCR Master Mix	Promega
RNeasy Micro Kit	Qiagen
RNeasy Mini Kit	Qiagen

2.6 Mouse strains

Experimental mice used in this project were bred in the animal facility of Max Plank Institute for Molecular Genetics by Katja Zill. The following mouse lines have been used:

- $Nf1^{flox/flox}$ mouse line

Both exons of 40 and 41 are flanked by LoxP site so that they can be deleted by Cre enzyme-mediated recombination. This mouse line was first generated in the lab of Luis F. Parda to study the function of Nf1 in brain development[127], which was kindly provided by Prof. L. Parada.

- $Myf5^{Cre}$ mouse line

$Myf5^{Cre}$ mouse line was first generated by Tallquist, M.D, to study the function of PDGFA in ribs and vertebrae development[128]. The Cre recombinase DNA sequence was inserted after the Myf5 promoter, thus its expression derived by Myf5 expression. This mouse line was kindly provided by Prof. C. Birchmeyer.

HSA^{Cre} mouse line

To see a target gene's function in skeletal muscle lineage, a transgenic mouse line that could express the Cre recombinase under the control of the human α-skeletal actin promoter was generated[129]. This mouse line was also provided by Prof. C. Birchmeyer.

All animals used in this project were kept with a C57BL6 genetic background. Nf1 knockout mice were generated by crossing of $Nf1^{flox/flox}$ with Myf5Cre or HSA Cre mice. Mice used in the experiment with genotype of $Nf1^{flox/+}$ Myf5 $^{Cre+}$ or $Nf1^{flox/+}$ HSA $^{Cre+}$ were considered as control. $Nf1^{flox/flox}$ Myf5 $^{Cre+}$ or $Nf1^{flox/flox}$ HSA $^{Cre+}$ were treated as knock out animals. Control mouse is always chosen as sex-matched and also the same litter with the knock out animals.

2.7 Software

Function	Name	Supplier
Microscopy imaging	Axio Vission Rel. 4.8	Axio Vision Application
Microscopy imaging	ZEN 2010	ZEISS
Image processing	ImageJ	Wayne Rusband
Image processing	CorelDRAW X7	Corel Corporation
Image processing	Photoshop CS5	Adobe system
Image processing	Illustrator CS5	Adobe system
Data analysis and text processing	Excel/Word/Powerpoint	Microsoft Office

RTqPCR analyses	SDS 2.4	Applied Biosystem
FACS sorting	FACS	DIVATM
FACS analyzing data	FlowJo	BD
Statistical analyses	GraphPad Prism 5	Prism
Wave Desktop	XF96	Agilent
IGV Desktop	2.4.13	Broad Institute
GSEA Desktop	3.0	Broad Institute
R studio	Server	R studio team
Prism	1.0.6	Nuget

2.8 Antibodies

Primary antibodies

Name	Dilution	Species	Supplier
Pax7	1:10	Mouse	DSHB
Pax7	1:100	Guinea pig	*
Ki67	1:500	Mouse	BD Bioscience
Ki67	1:500	Rabbit	Abcam
Col IV	1:500	Goat	Millipore
Laminin	1:1000	Rabbit	Sigma
Myh2	1:50	Mouse	DSHB
Myh4	1:50	Mouse	Sigma
Myh7	1:50	Mouse	DSHB
Desmin	1:1000	Rabbit	Merck-Millipore
MyoD	1:500	Mouse	BD Biosciences
MF20	1:1000	Mouse	DSHB
AMPK	1:1000	Rabbit	CST
p-AMPK(Thr172)	1:1000	Rabbit	CST
Lkb1	1:1000	Rabbit	CST

p-mTOR	1:1000	Rabbit	CST
p-s6	1:1000	Rabbit	CST
β-Tubulin	1:1000	Mouse	CST
Actin	1:1000	Mouse	CST
p-ERK1/2	1:1000	Rabbit	CST
ERK1/2	1:1000	Rabbit	CST
AKT	1:1000	Rabbit	CST
p-AKT	1:1000	Rabbit	CST
NF1	1:100	Rabbit	Bethyl
H4K16ac	2 µg/sample (chipseq)	Rabbit	Merck-Millipore
H3K27ac	1:1000 (western blot)	Rabbit	Merck-Millipore
H3K27me3	2 µg/sample (chipseq)	Rabbit	Merck-Millipore
H3K4me3	2 µg/sample (chipseq)	Rabbit	Merck-Millipore

Antibodies kindly provided by Prof. C. Birchmeier*

FACS antibodies

Name	Dilution	Product information	Supplier
CD31(PECAM1)APC	10 µl /sample	Anti-mouse	Affymetrix
CD45	10 µl /sample	Anti-mouse	BD Bioscience
Ter119	10 µl /sample	Anti-mouse	BD Bioscience
Sca1	5 µl /sample	Anti-mouse	Affymetrix
Integrin alpha 7	5 µl /sample	Anti-mouse	Affymetrix

Secondary Antibodies(Alexa Fluor conjugated)

Name	Host	Product information	Dilution
488,568 and 680	Donkey	Anti-mouse	1:500
488,568 and 680	Donkey	Anti-rabbit	1:500
488,568 and 680	Donkey	Anti-goat	1:500
488 and 568	Goat	Anti-Guinea pig	1:500

All purchased from life technologies TM.

IgG (HRP Conjugated) anti-Rabbit.

IgG (HRP Conjugated) anti-Mouse.

2.9 Internet Source

Name	Website
Primer 3.0	http://primer3.ut.ee
DAVID bioinformatics	https://david.ncifcrf.gov
Ensemble Genome Browser	https://www.ensembl.org/index.html
UCSC Genome Browser	https://genome.ucsc.edu
String	https://string-db.org

2.10 Primers

Primer List for genotyping

Primer name	Primer sequence(5'→ 3')
Lbx1_Cre_fw	CGCCTTCCTCTCGCACCGTC

Lbx1_Cre_rev	GGCAGCCCGGACCGAC
Myf5_Cre_fw	CGTAGACGCCTGAAGAAGGTCAACCA
Myf5_Cre_KO_rev	ACGAAGTTATTAGGTCCCTCGAC
Myf5_Cre_WT_rev	CACATTAGAAAACCTGCCAACACC
Nf1_P1	CTTCAGACTGATTGTTGTACCTGA
Nf1_P2	CATCTGCTGCTCTTAGAGGAACA
Nf1_P3	ACCTCTCTAGCCTCAGGAATGA
Nf1_P4	TGATTCCCACTTTGTGGTTCTAAG
Unspecific_Cre _fw	GAGTGATGAGGTTCGCAAGA
Unspecific_Cre_rev	CTACACCAGAGACGGAAATC

Primer List for qRT-PCR

Primer name	Primer sequence (5'→3')
Lpl_fw	TCATCTCATTCCTGGATTAGCA
Lpl_rev	GGCCCGATACAACCAGTCTA
Fabp3_fw	AGGTGGCTAGCATGACCAAG
Fabp3_rev	CTTGACCTTCCGGTCATCTG
Fabp4_fw	CTTTGCCACAAGGAAAGTGG
Fabp4_rev	GTCGTCTGCGGTGATTTCAT
Il4_fw	CTCGTCTGTAGGGCTTCCAA
Il4_rev	TCTGCAGCTCCATGAGAACA
Il18_fw	GGCTGCCATGTCAGAAGACT
Il18_rev	GTGAAGTCGGCCAAAGTTGT
Fgf21_fw	ACCTGGAGATCAGGGAGGAT
Fgf21_rev	GAGAGCTCCATCTGGCTGTT
Fgf6_fw	AATTGGGAAAGCGGCTATTT
Fgf6_rev	CTCACCACACCCCGTTCTAC
Fgf15_fw	CGCTACTCGGAGGAAGACTG
Fgf15_rev	TTGGCCTGGATGAAGATGAT

Fgf2_fw	TGTTTCTTCTTTGAACGACTGG
Fgf2_rev	AGTATGGCCTTCTGTCCAGGT
Leptin_fw	TGGCTTTGGTCCTATCTGTCTT
Leptin_rev	TGTCATTGATCCTGGTGACAA
Tnfa_fw	GCTGAGCTCAAACCCTGGTA
Tnfa_rev	TCACAGAGCAATGACTCCAAA
Adiponectin_fw	GGAGATGTTGGAATGACAGGA
Adiponectin_rev	CGAATGGGTACATTGGGAAC
Resistin_fw	TGAAGCCATCGACAAGAAGA
Resistin_rev	CTTCCCTCTGGAGGAGACTG
Plin1_fw	TCACAGCTGCCAATGAGTTG
Plin1_rev	CTTCGAAGGCGGGTAGAGAT
Tle3_fw	TTGCGAAGAGACTGAACACAA
Tle3_rev	CAACTCCGTCATGGTGACCT
Rip140_fw	AGAGCTTGGCTCTGATGTGC
Rip140_rev	CACTGCCCGAGAGGTTAAAG
Pparg_fw	CGAGAAGGAGAAGCTGTTGG
Pparg_rev	TCAGCGGGAAGGACTTTATG
Pai-1_fw	CTCTGGAGACTGAAGTGGACCT
Pai-1_rev	CGATCCTGACCTTTTGCAGT
Lpin_fw	CGTGGATTTGCACATGAAGT
Lpin_rev	CATTCTCGCAGCTCCTTCTG
Mgll_fw	CTCACCTGGTCAATGCAGAC
Mgll_rev	TGTCCAGCCCCTTCAACATA
DNMT1_fw	GAACCCCAGATGTTGACCAG
DNMT1_rev	GGTGTCGACAGGACACAGGT
DNMT3a_fw	ACTTGGAGAAGCGGAGTGAA
DNMT3a_rev	TTCTGGTGGGGTCTCAGTTC
Notch1_fw	AGGCAAATGCCTCAACACAC
Notch1_rev	CATTGGAACTCCCCAATCTG

Hey1_fw	CCGACGAGACCGAATCAATA
Hey1_rev	TTTTCAGGTGATCCACAGTCA
Myh3_fw	GGACGCTGGAGGATCAAAT
Myh3_rev	AAAATGGATGCGGATGAACT
Hoxc9_fw	TCGCTCATCTCTCACGACAA
Hoxc9_rev	AGGACGGAAAATCGCTACAG
TCF21_fw	GCTCTCCAAGCTGGACACTC
TCF21_rev	TCACCACTTCCTTCAGGTCA
Rb_fw	TGAAGAACCCGAATTTATTGC
Rb_rev	TGCTGCGATAAAGATGCAGA
C/EBPa_fw	TGCTGGAGTTGACCAGTGAC
C/EBPa_rev	CCTTGACCAAGGAGCTCTCA
Angiotensin_fw	AGCATCCTCCTCGAACTCAA
Angiotensin_rev	GGCTGCTCAGGGTCACAT
Lipe_fw	CCGTTCCTGCAGACTCTCTC
Lipe_rev	ACGCAACTCTGGGTCTATGG
CD36_fw	TCCTTGAAGAAGGAACCACTG
CD36_rev	TGTTCTTTGCCACGTCATCT
Hes1_fw	TCATCAAAGCCTATCATGGAGA
Hes1_rev	AGGTGCTTCACAGTCATTTCC
DNMT3b_fw	GACGTCGAGCATCATCTTCA
DNMT3b_rev	CTGCATCCACCTGTGTGGTA
Notch3_fw	AGGGCCAGAACTGTGAAGTC
Notch3_rev	AGGGCACTGGCAGTTGTAAG
Spry1_fw	TAGGTCAGATCGGGTCATCC
Spry1_rev	TTCGCAGATGAACTTGTGCT
ATP2a1_fw	CTGACCGAAAGTCAGTGCAA
ATP2a1_rev	GGTGGATTTGATGGAGAGGA
Acta1_fw	GATCTGGCACCACACCTTCT
Acta1_rev	ACATACATGGCAGGCACGTT

CPT1b_fw	TCTGTGTCCGTCTCCTGTCC
CPT1b_rev	CCATGCGGTAATATGCTTCA
CPT2_fw	GCTGCCTATCCCTAAACTTGAA
CPT2_rev	CAATGCCGTTCTCAAAATCC
Pfkl_fw	TTCGACCGGAACTATGGGAC
Pfkl_rev	CGATCACACAGGCTGAGTCT
Pfkfb1_fw	TGATGCCACCAACACTACCA
Pfkfb1_rev	CTGCAATGATGTCTGGGTCA
Eno3_fw	AAATCTTCGCCCGGGAAATC
Eno3_rev	TGCTTCATAGATACCCGTGGA
Myh4_fw	CAGAGTCACCTTCCAGCTCA
Myh4_rev	TGATTTCACCTTGACTGACGT
Myh1_fw	CGGGAAGACTGTGAACACGA
Myh1_rev	CGTTCCCAAAGGCCTCCA
Myh2_fw	ACCCTCCCAAGTACGACAAG
Myh2_rev	TACACCGGCAGCCATTTGTA
Myh7_fw	AGCTGGGAAGACTGTCAACA
Myh7_rev	CCAAAGGCCTCCAGAGCA
Camk2a_fw	CAGGGACACCTGGATACCTC
Camk2a_rev	GCTGGTCTTCATCCCAGAAC
Tnc_fw	GCCTGCACCTGAAGGTCTAA
Tnc_rev	GGAGGTCTCTGGTCTCCTCA
Col1a2_fw	CCGTGCTTCTCAGAACATCA
Col1a2_rev	GCCCTCAGCAACAAGTTCA
Col5a3_fw	CCTGGGGTGTGCATAGAGAC
Col5a3_rev	GGACACTGAGAAGGCTGGAC
Col5a1_fw	CACCGAATTGCTCTCAGTGT
Col5a1_rev	CTATTATGGGGTGGTCACTGC
Col6a3_fw	GTGGCTCAGTATGCAGACACT
Col6a3_rev	GTCCAGAGAAGATCCCGTGT

Cfd_fw	CAAGCGATGGTATGATGTGC
Cfd_rev	ATTGCAAGGGTAGGGGTCTC
Fgfr4_fw	CTACTGGACACACCCCCAAC
Fgfr4_rev	CAGTGGATGGTAGGCATGG
Park7_fw	TTGCACTAGCCATTGTGGAG
Park7_rev	CTCCACAATGGCTAGTGCAA
Rcan1_fw	CTGCACAAGACCGAGTTCCT
Rcan1_ rev	GAACTGTTTGTCGGGATTGG
Rcan2_fw	CAGCCATCCCAAATCTGC
Rcan2_rev	GCTGTGGAGGTGCCAAAT
Rcan3_fw	TTTCGCAGAGTGAGGATCAA
Rcan3_rev	GGGTTGTGGTGGCAGTAAGT
Gdf15_fw	GCTTCCAGGACCTGCTGAG
Gdf15_rev	GGTTGACGCGGAGTAGCAG
Myoz1_rw	GGAGCTGTCCCTTCTTACCA
Myoz1_rev	AGCTGTCTCCAGCTGTCCTC
p21_fw	CAGCCTCTCTCGGGGATTC
p21_rev	TTCGACGCCTTGTTCTCCT
Ucp3_fw	GATGCCTACAGAACCATCGC
Ucp3_rev	AGGTCACCATCTCAGCACAG
Gremlin_fw	CATACACTGTGGGAGCGTTG
Gremlin_rev	CTGGACTCAAGCACCTCCTC
p27_fw	GCGGTGCCTTTAATTGGGTC
p27_rev	TCTTCTGTTCTGTTGGCCCT
ucp1_fw	GTCAGAATGCAAGCCCAGAG
ucp1_rev	ACCAGCTCTGTACAATTGATGA
ucp2_fw	GCACTGTCGAAGCCTACAAG
ucp2_rev	TCAGCACAGTTGACAATGGC
Sln_fw	GGTGTGCAATCACAAGTCCT
Sln_rev	ACGAGGAGCCACATAAGGAG

Glut1-fw	GTGGAGCCCTAGGCACACT
Glut1-rev	CAGCAGAGGCCACAAGTCT
Glut4-fw	TGGGAACACTCAACCAACTG
Glut4-rev	GACAGAAGGGCAGCAGAATC
Hk2-fw	GTTTGACCACATTGCCGAAT
Hk2-rev	CACGCCACTGGACTTGAAC
Pfkm-fw	ACGTGACCAAGGCTATGGAT
Pfkm-rev	GACTGGGGGTCTGACATGAG
Ldha-fw	ACTTGGCGGATGAGCTTG
Ldha-rev	GCGGTGATAATGACCAGCTT
Myc-fw	CTCTCCTTCCTCGGACTCG
Myc-rev	GGTTTGCCTCTTCTCCACAG
Gapdh-fw	AAGGTCATCCCAGAGCTGAA
Gapdh-rev	TCAGTGGGCCCTCAGATG
Dll1_fw	GGTGTGATGACCAACATGGA
Dll1-rev	GACAACCTGGGTATCGGATG
Jag1_fw	TGAGCATGCTTGTCTCTCTGA
Jag1_rev	CCCCCATGGGAACAGTTATT
Calcr_fw	AGCCCAACTCCAGTTCTTCA
Calcr_rev	TCCTTCATAAGAGGGCAACTG

2.11 Ladders

Size marker	Company
Page Ruler™ Plus Prestained 10-250kDa Protein Ladder	Thermo Scientific™
1kb DNA ladder	Fermentas
100bp bp DNA ladder	Fermentas

2.12 Medium and supplements for cell culture

Name	Supplier
MEK Inhibitor U0126	Promega
Jagged1 (JAG1)	AdipoGen
DAPT	Sigma-Aldrich
LNAME	Sigma-Aldrich
TSA	*
SAHA	*
DMEM	Gibco
FBS	Gibco
DPBS	Gibco
Glutamin	Gibco
Penicillin/streptomycin	Gibco
Matrigel	Corning
Gelatin	Sigma
Poly-lysine	Millpore
Oligomycin	Roth
FCCP	Roth
Antimycin A	Roth
Rotenone	Roth
2-DG	Sigma Aldrich
Trypsin	Gibco

* Kindly provided by Prof. Dr. med. Britta Siegmund

3 Methods

3.1 Molecular Biological Methods

3.1.1 Genomic DNA isolation

Unless noted otherwise, genomic DNA was isolated from p21 mouse tail tips. p7 mice used for experiment tail tips were cut at p5. Centrifuge at maximum speed for 2 min at room temperature to allow the tips to drop to the bottom of the ep. 50 µl QuickExtract™ genomic DNA isolation solution was used for each sample. All samples were incubated at 65 °C in a Thermomixer and shaken at 350 rpm for 6 minutes, after that the temperature was changed to 98° C and incubated for another 2 minutes. All samples got centrifuged again and let the gDNA solution cooldown on ice, and they were ready as the template for genotyping PCR. Take 2µl as a template and keep the rest in the fridge for back up.

3.1.2 Total RNA isolation from tissue and cells

Total RNA isolation from muscle tissue

For the dissected P21 mice, the entire TA muscle was removed and put into a 1.5 ml tube, followed by liquid nitrogen snap frozen. Put all samples on dry ice then put autoclaved pre-cooled grinding beads inside each tube. 350 µl RLT buffer was added into each tube, TissLyser was used for homogenization. Keep the setting for muscle tissue as 60 Hz, 30sec for twice. Samples were put on ice for 3 min in the middle and then centrifuged at 12000 rpm for 10 min at 4 °C. The supernatant was transferred to a new ep. The following steps were performed based on the underlying RNA isolation protocol from the RNeasy Mini Kit (Qiagen).

Total RNA isolation from cells

For fresh FACS - sorted muscle progenitor cells, cells were centrifuged at 500 g x 5 min after FACS. Remove supernatant immediately and the following steps performed with the protocol provided by RNeasy Micro Kit (Qiagen). For cultured cells, wash cells first before put lysis buffer (RLT). Following steps performed based on protocol provided by RNeasy Mini Kit (Qiagen).

The total mRNA could be stored at -80°C for several months or do the reverse transcription immediately, and the cDNA was stored at -20°C for real-time qPCR.

3.1.3 Polymerase chain reaction for genomic DNA

To investigate the genotype of experimental animals, PCRs were performed using genomic DNA isolated from the tail tip of p21 animals. Different PCR protocols were used for different mouse strains.

$Nf1^{flox/flox}$ PCR

For the genotyping of $Nf1^{flox/flox}$, three independent PCR reactions were performed simultaneously. Their PCR products were P2(280bp), P3(480bp), and P4(350bp), respectively. The PCR product of P2 refers to the Nf1 allele was exercised by Cre recombinase-mediated recombination. The PCR binds of P3 means unexercised by Cre and also unfloxed. The binds of P4 means unexercised by Cre but floxed. These three PCR results were combined to obtain the correct $Nf1^{flox/flox}$ mouse genotype.

PCR mix for one reaction

Amount	Reagent
2 µl	Genomic DNA
2,5 µl	PCR buffer 10x
3.5 µl	dNTPs (1.25 mM)
1 µl	Primer fw (Nf1_P1) 10 mol/µl
1 µl	Primer rev 10 pmol/µl
0,5 µl	Taq polymerase
14.5 µl	A. bidest

PCR cycler Program

Temperature	Time	Cycle
94 °C	5 min	1x
94 °C	30 sec	35x
50 °C	30 sec	
72 °C	1:00 min 10 sec	
72 °C	7 min	1x
4 °C		∞

$Myf5^{Cre}$ PCR

To identify Nf1 knock out mice, $Myf5^{cre}$ PCR was also performed. A product of the size in 603 bp refers to the Myf5 allele without Cre insertion. The target bind size of 400 bp indicates the $Myf5^{cre}$ allele with Cre insertion. $Nf1^{flox/flox}$ $Myf5^{cre+}$ PCR results identified target mutant animals. $Nf1^{flox/+}Myf5^{cre+}$ genotype were used as control animals. $Nf1^{flox/+}$ $Myf5^{cre-}$ were considered as wild type animals.

PCR mix for one reaction

Amount	Reagent
2 µl	Genomic DNA
2,5 µl	PCR buffer 10x
2 µl	dNTPs (1.25 mM)
2 µl	Myf5_Cre_fw 10 pmol/µl
1 µl	Myf5_Cre_WT_rev 10 pmol/µl
1 µl	Myf5_Cre_KO_rev 10 pmol/µl
0,5 µl	Taq polymerase
13 µl	A. bidest
1 µl	Magnesium chloride 25 mM

PCR cycler Program

Temperature	Time	Cycle
95°C	5 min	1x
95 °C	40 sec	
59 °C	1:00 min	35x
72 °C	1:00 min	
72 °C	7 min	1x
4 °C	∞	

HSA^{cre} PCR

To specifically knock out Nf1 in mature muscle tissues, HSA cre mice were used for matting with Nf1 flox/flox mice. The expected genotype PCR bind size for HSA Cre is 650bp. Mutant animals were identified by Nf1$^{flox/flox}$ HAS^{Cre+}.

PCR mix for one reaction

Amount	Reagent
2 µl	Genomic DNA
2,5 µl	PCR buffer 10x
2 µl	dNTPs (1.25 mM)
1 µl	Unspecific_Cre_fw 10 pmol/µl
1 µl	Unspecific_Cre_rev 10 pmol/µl
0,5 µl	Taq polymerase
16 µl	A. bidest

PCR cycler Program

Temperature	Time	Cycle
94°C	5 min	1x
94 °C	30 sec	
55 °C	30 sec	35x
72 °C	1:00 min	
72 °C	7 min	1x
4 °C	∞	

3.1.4 cDNA synthesis

The concentration of total mRNA isolated from myoblasts, muscle tissue, and adipose tissue was measured by Nanodrop2000. 1 µg of mRNA was used for one reverse transcription reaction. For RNA isolated from muscle stem cells, all RNA was used for reverse transcription. The cDNA solution volume for each reaction was maintained at 40.5 µl with Rnase free water and 2 µl of Rnasin.

Master Mix for one reaction

Amount	Reagent
10 µl	10x Buffer
22 µl	25mM $Mgcl_2$
20 µl	dNTPs
5 µl	Random Hexamer /Oligo (dT)
2.5 µl	Reverse Transcriptase

Program for the thermal PCR cycler

Temperature	Time
25°C	10 min
48 °C	30 min
95 °C	5 min
4 °C	∞

The total volume for each reaction was 100 µl. Complementary DNA (cDNA) was stored at -20°C or start with real-time qPCR immediately.

3.1.5 Quantitative polymerase chain reaction (qPCR)

Syber-Green-based method was used for real-time qPCR. Dilute the cDNA with Rnase free water with 1:10 for RNA isolated from muscle tissue, myoblasts, or 1:3 for RNA isolated from muscle stem cells. 6 µl of diluted cDNA was used for each PCR reaction as a template. 5 µl forward primer and 5 µl reverse primers (100 µM stock solution) were diluted with 322.5 µl Rnase free water. 3 µl of the primer mix and 9 µl Syber-Green-Mix were put into each well of the 384 well plates. The total qPCR reaction volume was 18 µl. All reactions were performed in triplicate; wells with 6 µl water instead of template were used as blank control for each gene. All primers used in real-time qPCR were designed using Primer 3.0 online software. The sequence of target genes was found by the ENSEMBL genome browser. β-Actin, Gapdh were used as housekeeping genes for target genes relative expression normalization. Reactions and data collection was performed using the 7900 HT Fast Real-Time PCR Cycler and SDS 2.4 data analysis system, respectively.

3.1.6 Next-Generation Sequencing (RNAseq)

Total RNA was isolated from fresh FACS sorted muscle progenitor cells. Both forelimb and hind limbs of muscle from p7 (7 days postnatal) $Nf1^{flox/flox}Myf5^{cre+}$ (mutant), $Nf1^{flox/+}/Myf5^{cre+}$ (control) animals were taken for digestion and each condition for two animals. After FACS sorting, total RNA was isolated immediately with the Qiagen RNA isolation Micro kit. For RNA isolated from p21 TA muscle, The entire TA muscle was used, and the Qiagen RNA isolation Mini kit was chosen. The quantity and quality of RNA were tested with Nanodrop^{2000} and bioanalyzer, respectively. All samples were sent to the MPIMG sequencing facility for library preparation and next-generation sequencing.

3.2 Cell culture

3.2.1 Muscle stem cell culture

3.2.1.1 Isolation and culture of muscle stem cells

Separation of muscle satellite cells was accomplished by a well-established fluorescence-activated cell sorting (FACS) method[130]. In short, mice were killed with a high concentration of carbon dioxide (CO_2), and skeletal muscle tissue was separated from both hind limbs and forelimbs. The muscle was cut into small pieces followed by 2 mg/ml collagenases A (stock solution 100 mg/ml) digestion for 1.5 hours with 37 °C rotates at 450 rpm. Check the digestion efficiency with a sterile syringe and 20 mm needles in the middle. Homogeneous tissue mixture with a syringe, until no large pieces tissue visible. The enzyme digestion was stopped with PBS, wash cells twice with PBS and centrifuge with 300 g for 5 min at room temperature. Remove tissue aggregate with 70 um cell strainer. Re-suspend cells in HBSS and stain cells underneath the foil paper on ice for 30 min with the following antibodies. For lineage positive sorting, membrane markers CD31, CD45, Ter119 (CD31, a marker for endothelial cells, platelets, macrophages and Kupffer cells, granulocytes, lymphocytes, megakaryocytes, and osteoclasts; CD45, a marker for Leukocytes; Ter119, erythroid cell marker), Sca-1 (stem cell antigen-1) and Integrin-7α (muscle cells marker) were used for staining. The cells were washed twice with HBSS and sorted by FACS Aria II SORP (BD) machine. Integrin-7α $^{+}$/CD31^{-}/CD45^{-}/Sca1^{-} cells were taken as muscle stem cells.

Coverslips were coated in a cell culture plate with 10 % Matrigel for 30 minutes under cell culture incubator. Centrifuge sorted muscle stem cells with 500 g for 5 min and resuspend cells with proliferation medium (DMEM / 20% FBS). Culture cells in proliferation medium and change medium for every 48 h.

3.2.1.2 Immunolabeling of proliferating and differentiating muscle stem cells

Freshly sorted satellite cells were cultured in proliferation medium for 48 h to test proliferation rate. Differentiation medium (DMEM with 2 % horse serum or 2 % FBS) was used for 48 h to test differentiation ability. The proliferating or differentiated cells were washed with PBS and then fixed at 4% PFA for 10 min at room temperature. The cells were washed with PBS for 3 x 5min on a shaker. Permeabilize cells at room temperature with 0.1% Triton X-100 in PBS for 5 min. Rewash cells with PBS for 3 x 5 min. To block non-specific binding of antibodies, cells were incubated with 5% BSA in PBX at RT for 1 h. Primary antibodies (different combination of Pax7, MyoD, Ki67, Desmin, MF20) were diluted with blocking buffer. The dilution rate for each antibody was shown in the material section. Incubate cells in a humidified chamber overnight at 4 °C. The next day decants the staining solution and washes cells with PBS 3 x 10 min. Incubate cells with secondary antibodies, and DAPI diluted with PBS in the black box at RT for 1 h. Wash cells with PBS 3 x 10 min and mounting coverslips with a drop of mounting medium. Store in the dark at RT for 3 h and allow the coverslips to dry. Imaging coverslips under a fluorescence microscope.

3.2.1.3 Immunolabeling of cytospin muscle stem cells

For cytospin, poly-L-lysine was used (1:100 dilution with bidest) to coat the coverslips for 1 hour at room temperature. Rinse coverslips with sterile H2O 3 x 5 min. Let coverslips dry under the cell culture hood. The cells were counted and brought to a concentration of approximately 5 x 10^5 cells/ml. Put 100 ul cell suspension on top of each coverslip. Let cells stand at 4° C for 1 h. Spin at 50 g for 5 min. Followed by the standard ICC staining procedure described above.

3.2.1.4 RNA/protein/genomic DNA isolation from muscle stem cells

All Prep DNA / RNA / Protein Mini Kit from Qiagen was used for simultaneous isolation of genomic DNA, total RNA, and protein from p7 muscle stem cells sorted by FACS. One million cells were used for one sample. Pellet one million cells by centrifuging for 5 min at 500 x g at 4° C, carefully remove all supernatant.

Add 350 µl of Buffer RLT pipet thoroughly to mix, pass the lysate at least 5 times through a blunt 20-gauge needle (0.9 mm diameter) fitted to an RNase-free syringe. Transfer the homogenized lysate to an All Prep DNA spin column placed in a 2 ml collection tube. Close the lid gently centrifuge for 30 s at 8000 g. Place the All Prep DNA spin column in a new 2 ml collection tube, and store on ice for later DNA purification steps.

Use the flow-through for RNA purification. Add 250µl pure ethanol to the flow-through, mix well by pipetting. Transfer up to 700 µl of the sample to an RNeasy spin column placed in a 2 ml

collection tube. Close the lid gently and centrifuge for 15 s at 8000 g. Transfer the flow-through to a 2 ml tube for protein purification.

Add 700 µl Buffer RW1 to the RNeasy spin column. Close the lid gently and centrifuge for 15 s at 8000g to wash the spin column membrane. Discard the flow-through. Add 500 µl Buffer RPE to the RNeasy spin column. Close the lid gently and centrifuge for 15 s at 8000 g to wash the spin column membrane. Discard the flow-through. Add 500 µl Buffer RPE to the RNeasy spin column. Close the lid gently and centrifuge for 2 min at 8000 g to wash the spin column membrane. Place the RNeasy spin column in a new 1.5 ml collection tube. Add 30 µl RNase-free water directly to the spin column membrane. Close the lid gently, centrifuge for 1 min at 8000 x g to elute the RNA.

Add 600 µl of Buffer APP to the flow-through for protein purification, mix vigorously, and incubate at room temperature for 10 min to precipitate protein. Centrifuge at full speed for 10 min, and carefully decant the supernatant. Add 500 µl of 70 % ethanol to the protein pellet. Centrifuge at full speed for 1 min and thoroughly remove the supernatant. Dry the protein pellet for 10 min at room temperature.

Add 30 µl Buffer ALO and mix vigorously to dissolve the protein pellet. Incubate for 5 min at 95°C, then cool the sample to room temperature. Centrifuge for 1 min at full speed and store the protein lysis at –20°C, use the supernatant for SDS-PAGE and western blotting.

Add 500 µl Buffer AW1 to the All Prep DNA spin column. Close the lid gently and centrifuge for 15 s at 8000 x g (10,000 rpm) to wash the spin column membrane. Discard the flow-through. Add 500 µl Buffer AW2 to the All Prep DNA spin column. Close the lid gently and centrifuge for 2 min at full speed to wash the spin column membrane. Place the All Prep DNA spin column in a new 1.5 ml collection tube. Add 40 µl Buffer EB (preheated to 70°C) directly to the spin column membrane and close the lid. Incubate at room temperature for 2 min, and then centrifuge for 1 min at 8000 g (10,000 rpm) to elute the DNA.

The quality and quantity of mRNA and genomic DNA were measured with Nanodrop 2000. For mRNA ratio of OD_{260} / OD_{280} is around 2. For genomic DNA ratio of OD_{260}/OD_{280} is around 1.8. Store total mRNA at -80°C for several months, or do the reverse transcription immediately store the cDNA at -20°C for qPCR. Keep the genomic DNA and protein at -20°C.

3.2.1.5 Muscle stem cell culture with ligand treatment

Freshly FACS sorted muscle stem cells for in vitro cell culture. One day before the experiment, coat 24 well plate with 10% Matrigel at 37 °C for 30 min, remove the supernatant, and put Jag1 ligand on top or PBS only for control leave at room temperature overnight. The next day starts muscle prepping in the early morning as described before, making sure during the experiment keep all cells on ice and avoid any freezing step. Calculate cell numbers for 3 x 10^5 cells/well

and put them in the culture immediately. 4 days later, harvest cells and do RNA isolation followed by real-time qPCR for Notch target genes, myogenesis genes, glycolysis genes, and oxidative phosphorylation genes expression detection.

3.2.1.6 Seahorse real time metabolism test for muscle stem cells

Seahorse XF96 extracellular flux analyzer is used to measure OCAR and ECAR for freshly FACS sorted p7 satellite cells. The protocol was kindly shared by Dr. James G. Ryall before the method paper was published[131]. The essential modification being performed based on our experiment platform.

Generally speaking, on day 1, hydrate the cartridge sensor with 200 µl calibrant solution in each well of cartridge plate, put the plate with the sensor in 37 °C incubator without CO_2, and leave it overnight. To avoid evaporation, wrap the plate with parafilm.

Turn on XF96 Analyzer logged in, design personal assay protocol, and make sure to leave four wells as blank control for background normalization, save the assay protocol. Then run the software, leave it there overnight to make sure the inside temperature is 37°C during the real assay time.

On day 2, dissect p7 mice in the early morning take all muscle from both forelimbs and hind limbs prepare single-cell solution and stain with specific antibodies for FACS. Make sure satellite cells are always in the ice cod medium during the whole process. Meantime coat XF96 cell culture microplate with 10% Matrigel (1mg / ml) for 1h at 37°C, prepare assay medium and adjust pH to 7.4, warm medium, and all the rest solution to 37°C, filter before use. After FACS count, the cell numbers accurately pelleted cells with 500 x g for 5min resuspend with warm assay medium and put cells into XF96 cell culture microplate, $5x10^4$ cells in 180 ul assay medium for each well. Centrifuge the cell culture plate 200x g for 5 minutes, observe cells under a microscope make sure all cells are evenly distributed. Put the microplate into a no-CO_2 incubator for 45 minutes.

Make stock solutions from glycolysis stress test kit, including oligomycin, glucose, and 2-DG with pre-warmed assay medium. The concentration is just following the website protocol provided by the kit. Load compound in sensor cartridge in the following way: port one: glucose 20 µl; port two: oligomycin 22 µl, and port three: 2-DG 25 µl. Open the saved wave software start run. Place the loaded sensor cartridge on top of the utility plate, then click ready after calibration load the cell culture plate and run the assay.

3.2.2 Primary myoblasts culture

3.2.2.1 Primary myoblasts isolation

$Nf1^{Myf5}$ and control mouse (n=3 for each group) were killed by exposure to high concentrations of carbon dioxide gas at postnatal day 21. Spray the whole mouse and autoclaved dissection tools with 70% ethanol. Remove skin with sharp scissors and forceps from both hind-limbs to expose muscle. Take target muscle bundles including tibialis anterior (TA), gastrocnemius, soleus, quadriceps, and extensor digitorum longus (EDL) muscles from one hind-limb and place them into one 3.5 mm cell culture dish with 3 ml PBS. Repeat above operation takes all muscles from the other hind-limb and put them into another 3.5 mm cell culture dish. Transfer washed muscles into 2 ml ep and mince muscles with forceps and scissors. One tube with muscles from one hind-limb. The stock solution of Collagenase A (100 mg/ml) was diluted into a working solution (2 mg/ml) with DMEM. Add 1ml digestion solution into each tube and mix well, then incubate on a Thermomixer at 37 °C and 450 rpm for 1.5 hours. In the middle test, the digestion efficiency with a blunt 20 - gauge needle (0.9 mm diameter) stops digestion with growth medium when a single cell solution can be released by a needle. The transfer sample into 50 ml falcon makes a whole solution volume as 25 ml. Centrifuge at 300 g for 5 min, remove supernatant and resuspend the pellet with 2 ml growth medium, afterward the sample was pipetted through a 70 µm cell strainer into 50 ml falcon followed by another 2 ml growth medium to rinse the strainer. All falcons have centrifuged at room temperature 2000 rpm for 5 min. Remove supernatant and resuspend the cell pellet in standard growth medium and seed the cell mixture onto 0.1% gelatin-coated 10 cm dish. Check cells under a microscope and keep all the dishes in a 37 °C CO_2 incubator for another 72 hours.

3.2.2.2 Primary myoblasts culture

Trash cell culture medium and gently wash attachment cells twice with PBS. Split cells by adding 3 ml of 0.25 % trypsin-EDTA and incubate in a CO_2 incubator for 3min, check under the microscope to make sure all cells have been detached add 7ml growth medium to stop the trypsinization. Transfer all solution into a new none coated dish and place at 37 °C in a CO_2 incubator for 45 min. During this step, larger cells like fibroblast will attach with a cell culture dish, and the target cell population is still suspended in the cell culture medium. In the meantime, coat a new cell culture dish with gelatin and transfer suspend cells into the new dish. Pre-plating should be performed every 36 - 48 h until > 98% myoblast purity is achieved. Purity should be measured with immunostaining for Pax7 and MyoD antibodies. Purity = $Pax7^{+}$% $MyoD^{+}$% + $Pax7^{+}$% $MyoD^{-}$%.

The purified primary myoblast should be cultured in growth medium and change the medium every other day. To avoid premature differentiation and fusion of primary myoblast, make sure

cells are split before they reach 70% confluence. Gelatin coated dishes need to be used during the whole culture process. Just like the regular cell lines, myoblast could be trypsinized and collected in freezing medium then kept in liquid nitrogen or -80 °C for future use. The capacity for proliferation and differentiation should be maintained when thawed and cultured again. For differentiation of primary myoblast, plate cells in the desired confluence, keep in mind the differentiation medium could only being changed until the confluence is between 90%-95%. Wash cells with PBS before the medium were changed because cell size in different cell passages varies, so the number of cells in each cell culture plate should be put based on their own experience. The lower passage, the smaller cell size. The differentiation medium should be changed every 48h. Small myotubes could be observed at 48h. Bigger and mature myotubes will be ready for the following experiment at 72-96h.

3.2.2.3 Immunostaining of primary myoblasts and myotubes

24 well cell culture plate with 12 mm coverslips was used for cell purity and differentiation ability test. Trash cell culture medium and wash with PBS. Fix cells with an appropriate amount of 4% PFA at room temperature for 10 min. Cells should be covered by PFA. Remove PFA and wash cells gently with PBS for three times, followed by cell permeabilization, incubate cells with PBX (0.3% Triton X-100) at room temperature for 10min. Wash cells with PBS for three times and block cells with 5% BSA in PBS at room temperature for 1h. Prepare primary antibody mixture in blocking solution. Pax7 (DSHB) 1:25, MyoD (BD Pharmingen™) 1:100, Desmin (R&D Systems) 1:200, MF20 (DSHB) 1:100, Ki67 (BD Pharmingen™). To save antibodies, drop 30 µl antibody mixture on parafilm membrane invert 12 mm coverslip on top, make sure cells are fully covered with antibody solutions. Incubate primary antibody at 4 °C overnight or room temperature for 2-3 h (put the parafilm into a black box with moisture environment make sure the antibody mixture will not cause evaporation). Take coverslips put back to 24 well plate wash with PBX for three times, 5min for each time at room temperature on a shaker. Prepare Alexa Fluor® fluorescent secondary antibodies to dilute with PBS in 1:500 and DAPI (1:1000). Incubate secondary antibody and DAPI in 24 well plates in a black box or covered with foil paper for one h at room temperature. Remove secondary antibody wash with PBX for three times at room temperature, 10 min for each time on a shaker. Check under the fluorescent microscope if there are still background, wash the cells longer. Mount coverslips with mount solution leave at room temperature let them dry for 3h. Take pictures for the next step.

3.2.2.4 Inhibitors and ligand treatment for primary myoblasts

To establish the in vitro cell culture model and study about the signaling pathways involved in vivo. Primary myoblasts were used combined with different inhibitors and ligand treatment to get a mimic of in vivo environment. Split and culture primary myoblasts in proliferation medium in advance two days. One day before the real experiment, start coat the 24 well cell culture plate with 100 µl Jagged1 ligand. The concentration of the stock solution is 0.5 mg/ml in PBS, and the concentration of a working solution is 5 ng/µl. Dilute the stock solution with 1:100 in PBS. Leave the coated plate at 4°C overnight. Take the plate out and remove the supernatant the next day before culture cells on top. For activating Notch signaling, cells need to be cultured with a ligand for at least 48 hours.

To investigate the underlying mechanism of activation of Ras/ERK and Notch pathway, during the notch activation time add panHADC inhibitor TSA (1 mg/ml) use with 1:1000 dilution; Nitric oxide synthesis inhibitor L-NAME (concentration of stock solution is 50 mg/ml) was used with 1:92 to get the final concentration of 2 mM of working solution. To inhibit the Ras/ERK pathway, the U0126 was used to inhibit MEK activity specifically. The stock concentration is 10 mM, and it was used in 1:1000 during cell culture time. All these inhibitors were treated cells for 24 hours to see the function during myoblasts stage and also put them inside the differentiation medium in order to see their function for myoblasts differentiation. Primary myoblasts form control and mutant mice were cultured without any treatment or only with ligand activator were used a control cell. Once reach a specific treatment time point, isolate total RNA from all these cells and do reverse transcription followed by qPCR to see the expression level of Notch target genes, and also metabolism relative genes expression. To double-check the effect of these signaling on primary myoblast proliferation and differentiation, cells with the same treatment were cultured on coverslips and fix the cells and do immunocytochemistry with specific antibodies like muscle stem cell marker Pax7, proliferation marker Ki67, differentiation marker like myosin heavy chain et al. Imaging the staining with fluorescence microscope and calculate the proliferation rate, differentiation index or fusion index.

3.3 Biochemical Methods

3.3.1 Protein isolation from cells and muscle tissue

Protein isolation from cells

RIPA buffer with freshly added cOmplete Mini Protease Inhibitor Tablets (7x stock solution) and serine/threonine phosphatase inhibitors NaF (1:1000) was used as a protein lysis buffer. Wash cultured cells with PBS and trypsin them with 0.25 % trypsin-EDTA in the cell culture incubator for 3 min stop trypsinization by adding an equal volume of cell culture medium.

Transfer cell solution into 15 ml tube and centrifuge for 5 min at 4°C. Check volume of cell pellet adds protein lysis buffer directly, the volume of lysis buffer is based on experience, vortex dramatically for two times, 5 min for each time. In the middle, put samples on ice for 5 min. Centrifuge with the highest speed at 4°C for 10 min. Supernatant needs to be transferred into a new protein low binding tube.

Protein isolation from tissues

Lysis buffer was prepared as described before. Take samples out from -80°C with dry ice. Put auto calved grinding bead into each tube. From experience 10 mg tissue with 1 ml lysis buffer, the final protein concentration is around 1 mg/ml. Use TissueLyser for homogenization and keep the setting as 60 HZ for 1 min for twice. Stop in the middle and put the samples on ice for 5min. Centrifuge at 4°C with full speed for 20 min. Transfer supernatant to a new tube.

3.3.2 Protein concentration determination

Take 2 µl for total protein concentration measurement. Pierce BCA Protein Assay Kit was used, and protein light absorption at 562 nm was measured with an ELISA reader. Protein concentration was calculated based on the equation generated from the BCA standard curve and the dilution rate of samples. Dilute the samples with 6 x SDS protein loading buffer and make the final protein concentration to 1.5 µg/µl. Incubate the samples at 95°C for 5 min to completely denature the protein. Store samples at -20°C for SDS gel running.

3.3.3 SDS PAGE

Charged proteins in mixtures were separated based on their molecular mass, SDS-PAGE (sodium dodecyl sulfate-polyacrylamide gel electrophoresis) was used. The concentration of separation gel was choose depending on the mass of target proteins. For p-mTOR (289 KD), 7.5 % polyacrylamide gel was used. For protein size between 200 KD and 250 KD, 8% gel was used. For protein mass, less than 200 KD, and more than 40 KD, 10% gel was used. For protein size, smaller than 40 KD 12% separation gel was used. For assembling gel, 4% concentration was used. Gels were prepared according to the following protocols

Stacking Gel (4 gels)	4%
Bidest	9 ml
30 % Acrylamide	1.98 ml
0.5 M Tris (pH 6.8)	3.78 ml

10 % SDS	150 µl
10 % APS	75 µl
TEMED	15 µl

Resolving Gel (4 gels)	7.5 %	10 %	12 %
Bidest	14.56 ml	10 ml	8.38 ml
30 % Acrylamide	7.5 ml	8.3 ml	10 ml
1.5 M Tris (pH 8.8)	7.5 ml	6.25 ml	6.25 ml
10 % SDS	300 µl	250 µl	250 µl
10 % APS	150 µl	125 µl	125 µl
TEMED	15 µl	12.5 µl	12.5 µl

Pour resolving gel and put 100% ethanol on top to make the gel smooth, 30 min later trash ethanol add stacking gel and insert comb in, wait for another 30 min let the gel polymerization. Add running buffer into gel chamber load protein and also protein ladder. The amount of protein depends on target protein abundance. Gel running settlement is 80 v, 30 min for stacking gel and 120 v, 1.5 h for separation gel.

3.3.4 Western blot

During the gel running time, prepare transfer buffer and store at -20°C. There are two methods for transferring: wet transfer and semi-dry transfer. Here wet transfer was used for all western blot experiments. Recipe for 1 L wet transfer buffer is 100 ml 10 x transfer buffer, 700 ml double-distilled (ddH_2O or bidest) water, and 200 ml methanol. Keep the transfer buffer bottle at -20°C until use. Stop gel running when the dye in front runs to the bottom of the gel. Remove the stacking gel and measure the size of separation gel, cut 6 filter sheets, and one PVDF (polyvinylidene fluoride) membrane based on the separation gel size. Activate the PVDF membrane with pure methanol for 30 sec and then equilibrating the membrane in a 1x transfer buffer for 3 minutes. Wet the sponge and filter sheets in a 1x transfer buffer. Make a transfer sandwich in the following order: sponge, three filter sheets, gel, PVDF membrane, and another three filter papers. Make sure that there are no air bubbles between the gel and the PVDF membrane. Remove the bubbles and extra transfer buffer with a glass rod. Put the sandwich into the transfer equipment also with the icebox. For larger size protein, get the whole transfer apparatus on ice to make sure the heat production during transfer will not influence the transfer process. Take the transfer buffer out from -20°C and add transfer buffer to the apparatus, ensure that the sandwich is covered with the buffer. Place electrodes on top of the sandwich,

ensuring that the PVDF membrane is between the gel and a positive electrode. Transmembrane for larger size protein needs to put the whole apparatus into one icebox. For larger size, protein transfer buffer is different from the normal one. Tris (5.8 g/L) and glycine (2 g/L) in distilled water without methanol were used for the transfer process. Run the transmembrane process at 100 V for 1 h. Take the membrane out and stain it with ponceau for 10 min with a shaker wash the membrane with PBST and see the transfer efficiency. Remove all staining bands and block the membrane with 5 % milk powder in TBST (block with 5 % BSA for phosphor site detection) in a shaker for one h at room temperature. At the same time, prepare the primary antibody mix to dilute with a blocking solution. Incubate the primary antibody overnight in the cold room with a shaker. The next day removes the primary antibody wash the membrane with TBST 3 times 10 min for each time. Incubate the secondary antibody for one hour at room temperature wash again three times with TBST with 10 min for each time. Use freshly prepared ECL solution put it on top of the membrane incubate for 1 min, eradicate the solution, and take pictures with the western blot gel document system.

3.3.5 Agarose gel electrophoresis

Prepare agarose gel 30 min before PCR running finish. EtBr was added in 1:10000. The concentration of gel depending on the size of the target binds. Leave the gel under the hood for at least 20 min. After finishing the PCR step, remove 8-strip tubes from PCR cycler. Put 5 µl 6x DNA loading buffer and mix for each sample. Loading samples and put the 100 bp DNA ladder into the well. Run the gel with a 1 x TAE buffer for 120 V 30 min. Detect target binds with UV machine or with the Gel documentation system.

3.3.6 Mass spectrometry

Pre-cool all dissection tools and vials with screw caps on dry ice, weigh empty vials take whole TA muscle from Hind limbs of $Nf1^{flox/flox}/Myf5^{Cre+}$ (Mut), $Nf1^{flox/flox}/Myf5^{Cre-}$ (Het) and $Nf1^{flox/+/Myf5\ Cre-}$ (Wt). Weigh vials again with samples, keep all samples on dry ice with precooled disruption bead. Add lysis buffer containing 3 M GdmCL, 5 mM TCEP, 20 mM 2-Chloracetamide, 50 mM Tris pH 8.5 shortly before Fast Prep. To avoid proteolytic activities, tissues were homogenized with a Fast Prep -24 immediately. Total 2 x for 60 sec 4 M/s, after each 60 sec put samples on the ice, take a rest for 5 min. (Notice that Fast Prep can only work with solution volume more than 1 ml otherwise vials will be broken) ; Shake for 15 min at 95°C with 750 rpm; Sonicate for 15 min in the ultrasonic water bath. Transfer the whole sample lysates to a new 2 ml protein

low binding tube (Eppendorf, Germany). Send all samples to the MPIMG Mass spectrometry facility for further processing.

3.3.7 High-Resolution FluoRespirometry

This experiment has collaborated with Dr. Mario Ost from the German Institute of Human Nutrition. In short, our 5 weeks control and knockout mice were transferred to their lab in advance for one day before the experiment starts. In the early morning dissected the mice took targeted muscle bundles, here we used EDL and Soleus as represent for glycolytic fiber and oxidative fiber. For the rest of the tissue, protein and RNA was taken for other analysis. High-Resolution FluoRespirometry was used for mitochondrial respiration analysis. Briefly, gently dissected muscle EDL and Soleus muscle was put into ice-cold biopsy preservation medium (BIOPS) immediately, followed by permeabilization with saponin (50 µg/ ml) at 4 °C for 30 min. Wash fibers with mitochondrial respiration medium (MiR05, 110 mM sucrose, 60 mM K-lactobionate, 0.5 mM EGTA, 3 mM $MgCl_2$, 20 mM taurine, 10 mM KH_2PO_4, 20 mM HEPES, pH 7.1 and 0.1 % fatty acid-free BSA) at 4 °C for 10 min and keep all samples on ice before analysis.
The basic principle of this method is to analyze the respiratory capacity at 37 °C in a hyper oxygenated environment with multiple substrate uncouplers. The following substrate concentrations: 2 mM Malate + 5 mM Pyruvate (LEAK respiration), 5 mM ADP (N-OXPHOS capacity), 10 µM cytochrome c (integrity of outer mt-membrane), 10 mM glutamate (N-OXPHOS capacity), 10 mM succinate (NS-OXPHOS capacity), 0.5 µM FCCP (NS-ETS capacity, ETSCI&CII), 0.5 µM rotenone (S-ETS capacity, ETSCII), 2.5 µM antimycin A (residual oxygen consumption, ROX). Oxygen flux levels were normalized to wet muscle weight of dry blotted fiber bundles.

3.4 Histology

3.4.1 Sample preparation

Pick up the mice that need to be used with a particular time point based on the requirement of the project. Kill the mice with a high concentration of CO_2. For newborn mice, take a tail tip for genotyping. For p21 and even older mice, also take iBAT, cBAT, psWAT as well. Weigh all these tissues before the next step. For forelimbs and hindlimbs kept for histological staining, dissect mice with sterile tools remove skin and fur carefully. Drop isopentane temperature with liquid nitrogen until half-frozen take the container out and leave it on dry ice. Use forceps put

dissected mouse tissue with Tragacanth matrix and cork plate (labeled probably) directly into cold isopentane for 10 seconds, then transfer samples with dry ice and store at -80°C before sectioning.

3.4.2 Sectioning

Take samples out from -80°C and keep samples on dry ice. Before start sectioning, check cryotome, make sure that the inside and blade temperature is -20°C. The cork plate was attached to the metal plate with the TissueTek medium. Set section thickness at 10 µm. Put super frost slides on to 37 °C heating plate. After collecting sections were kept on a heating plate for another 30 min. Pack up all slides put silica beads to keep slides dry and sealed box with tape. Use slides directly for immunostaining or store them at -80°C.

3.4.3 IHC

Slides fixation

Take slides out from -80 °C leave slides at room temperature for two h or put on a 37°C heating plate for 30 min. Rehydrate slides with PBS for 10 min. Trash PBS put a slides box with pre-cooled methanol into -20°C for 10 min. Then wash slides with PBS to remove methanol residues.

Antigen Retrieval

Sections staining with Pax7 or co-staining with Pax7 need to do antigen retrieval with the following method: use bidest water with 2 mM EDTA as an antigen retrieval solution. Cook the solution to 95°C with a water bath, put slides directly inside wait for 10 min. Take slides box out, leave at room temperature for 30 min. Let sections cool down. After this step, wash slides with PBS to remove EDTA.

Blocking unspecific binding site

Surround samples with DAKO pen and wash with PBS. Add 50 µl TSA or 5 % BSA blocking buffer on top, leave the slides at room temperature for 1h.

Primary antibody incubation

Dilute primary antibody with blocking buffer. Working concentration of primary antibodies depending on the recommendation of the antibody and also previous antibody test experiment.

For antibodies like Lamin, ColIV, Rabbit, ki67 (1:1000 dilution) was used. For antibodies from DSHB like Pax7, 1:10 was used, fiber type relative antibodies 1:100 was used. Remove blocking buffer and wash slides with PBS for one time. Put DAKO pen surrounding samples again and wash them with PBS again. Put 50 ul diluted primary antibody on top of each sample and incubate at the cold room with shaker overnight. For Pax7 staining, take slides out and leave at room temperature for another 2 h before the washing step.

Secondary antibody incubation

The next day, take slides out from the cold room. Remove the primary antibody and wash with PBX for three times 10 min for each time. Dilute secondary antibodies and DAPI with PBS in 1:500. Put the DAKO pen again and wash with PBS. Put 50 ul diluted secondary antibodies on top of each sample and incubate at room temperature with shaker for 1 h.

Imaging

After secondary antibodies and DAPI incubation, remove the solutions, and wash slides with PBX for 3 x 10 min. Mount slides with Fluor mount-G®, and let slides dry at room temperature for at least 2 h. Imaging slides with LSM 700 confocal microscopy and all images processed with ZEN (blue edition) software. For further images cropping and merging Photoshop CS5 were used.

3.4.4 Hematoxylin & Eosin staining

Fix slides with 4 % PFA at RT for 10 min, wash slides with PBS for 10 min. Incubate slides with Hematoxylin for 1 min. Rinse slides for 5 min in running tap water. Eosin staining for 30 sec and washed with H_2O. Dehydrate slides by incubating for 5 min each in 70 % EtOH – 80 % EtOH – 90 % EtOH - 100 % EtOH – Xylene. Dry slides completely. Wet slides with Xylene and mount slides with Permount.

3.4.5 Oil Red O staining

Lipid droplet on frozen muscle tissue sections was detected by Oil Red O staining. Firstly, take frozen sections out and leave them at room temperature for 1 h. Wash slides with PBS for 5 min before staining. Rinse slides with 60% isopropanol for 10 min followed by incubation with Oil Red O staining solution for 15 min. Then rinse slides with 60% isopropanol for 10 min and wash with PBS before mounting and imaging.

3.5 Epigenetic analysis

3.5.1 ChIPmentation

CHIPmentation is a method that combines chromatin immunoprecipitation followed by sequencing with Tn5 transposase ('tagmentation') during library preparation. This method was first published on Nature methods in 2015 by Christoph Bock et al[132]. The following protocol is specifically for muscle progenitors which were modified based on protocols from the lab of Karl Lenard Rudolph (Leibniz Institute for Age Research), Kaestner (University of Pennsylvania), Christoph Bock (Research Center for Molecular Medicine of the Austrian Academy of Sciences) Briefly, 200,000 fresh FACS sorted p7 muscle progenitors were used for each sample. Fixing cells with 1% formaldehyde for 10min at room temperature. Quench formaldehyde by adding Glycine to a 125 mM final concentration at room temperature for 5min. Sonicate cells with Bioraptor in sonication buffer, setting "high," 15x (30 sec on/30 sec off), short spin down, and again 15x (30 sec on/30 sec off). Fragment size is around 250 bp for histones. Add antibody (H3K4me3, H3K27me3, H4K16ac) and incubate on a rotator at 4°C overnight. Blocking Protein A/G beads with 0.1% BSA/RIPA at 4°C overnight. Incubate chromatin and beads at 4°C for 2 h rotating. Wash beads with RIPA-LS (2x), RIPA-HS (2x), RIPA-Licl (2x),10 mM Tris pH8 (1x). 2xTD buffer (12.5 µl), nuclease-free water (11.5 µl), Tn5 enzyme (1 µl) were used as tagmentation buffer for each sample. Incubate 10 minutes at 37°C. Inactivate Tn5 with RIPA-LS on ice for 5min. Wash beads with RIPA-LS (2x) and TE (2x). De-crosslinking with Proteinase K at 65°C overnight. Purify eluate by adding 1.8:1 SPRI cleanup and eluting in 20 µl EB (10 mM Tris pH 8.5).

Library amplification

Set up pre-amplification

20 µL DNA

2.5 µL primer 0 (25 µM stock)

2.5 µL primer X (25 µM stock); this primer is unique for each sample

25 µL NEB Next High-Fidelity 2× PCR Master Mix

Run following program

•	1 cycle	5 min 72 °C
		30 sec 98 °C
•	5 cycles	10 sec 98 °C
		30 sec 63 °C
		60 sec 72 °C

Store reactions on ice

Set up side-reaction to determine correct number of amplification cycles
5 µL of previous reaction mix
0.25 µL primer 0 (25 µM stock)
0.25 µL primer X (25 µM stock); this primer is unique for each sample
3 µL H2O
1.5 µL 10× SYBR Green I
5 µL NEB Next High-Fidelity 2× PCR Master Mix

Run following program on qPCR cycler

1 cycle	30 sec	98 °C
20 cycles	10 sec	98 °C
	30 sec	63 °C
	60 sec	72 °C

Determine the number of additional cycles N needed for library amplification
Select plot that shows fluorescence vs. cycle number
Choose cycle number that corresponds to ≈ 1/3 of maximal fluorescence intensity.(Ct+1~2)

Run following program with the remaining 45 µL of reaction

1 cycle	30 sec	98 °C
18 cycles	10 sec	98 °C
	30 sec	63 °C
	60 sec	72 °C

AMPureXP beads were used to remove primer dimers and size selection.
Determine library concentration using the Qbit (2 µl) and quality control library with a Bio-analyzer (1 µl). The concentration is around 2 ng/ µl, and the chromatin size is around 275 bp. Samples are ready for the sequencing facility. Illumina high output sequencing with Nextera sequencing adapters was used.

3.5.2 MeDIP sequencing

Methylated DNA immunoprecipitation, coupled with next-generation sequencing, was used for genomic DNA methylation identification. 200,000 FACS sorted muscle progenitors were used for each sample, and genomic DNA was isolated with Qiagen AllPrep DNA/RNA/Protein Mini Kit. Chromatin concentration was measured with Qbit. Samples were sent to the sequencing facility for the following steps.

3.6 Statistical analysis

RT-qPCR and immunostaining were performed with at least 3 mice for each genotype. Quantification was generated from at least four sections per animal. Two-tailed Student's t-test was used for p-value calculation. Significance is shown in the diagrams with stars. The standard error was calculated and displayed in the bar chart. The number of animals used in each experiment is indicated in each figure legend. For data from TA muscle, Z-Score was calculated for heatmap visualization. For RNAseq, after sequencing, the fastq raw data were mapped to mouse genome 9 using STAR RNAseq aligner, and gene differential expression analysis was performed with DEseq 2. Genes that were significantly up and down-regulated were submitted to DAVID 6.8 bioinformatics or Gene Set Enrichment Analysis (GSEA) for gene ontology (GO) and KEGG pathway analysis. Heatmap visualization was generated with R ggplot2.

4 Results

4.1 Skeletal muscle-specific *Nf1* knock out mouse model.

4.1.1 The efficiency of *Nf1* deletion on muscle progenitors and their daughter cells.

From clinical studies, one of the common features of individual NF1 patients is the reduction of muscle weight and muscle weakness, which is also consistent with preclinical research studies using mouse models shown the function of *Nf1* in muscle development and muscle metabolism[125,126]. To elucidate the pathogenesis of the *Nf1* deleted skeletal muscle system, a specific Nf1 knock out mouse model with the Cre/LoxP system was used in this project. $Nf1^{flox/flox}$ mice[127] were crossed with $Myf5^{Cre}$ allele to introduce *Nf1* knock out in specific *Myf5* expressing muscle progenitors and their descendants. According to the latest mouse genome annotation system, exons, 40 and 41 of *Nf1* have been flanked by flox site, which is essential for encoding GTPase activator protein associated domain (GRD).

RNA was isolated from tibialis anterior muscle (TA) of p21 mice, and p7 FACS sorted muscle progenitors from control ($Nf1^{flox+Myf5+}$) and $Nf1^{Myf5}$ ($Nf1^{flox/floxMyf5+}$) animals respectively. Whole transcriptome analysis was performed. *Nf1* gene knock out efficiency was evaluated by RNAseq results from both p7 muscle progenitors and p21 muscle tissue, and the sequencing reads number (RPKM) from control, and $Nf1^{Myf5}$ samples were compared. Data confirmed the knockout of flox flanked exons 40 and 41, and the knock out efficiency was 77.7% and 71.5%, respectively (Fig. 4.1A, C). For double confirmation, real-time qPCR was used, the knock out efficiency was also confirmed by qPCR, primers designed on exon 40 and 41 were used (Fig. 4.1B). To see the expression of *Nf1* from the protein level a primary antibody against the C-terminal of Nf1 protein was used for western blot. $Nf1^{Myf5}$ primary myoblasts isolated by preplating showed almost no Nf1 protein expression. Interestingly, once the differentiation medium was changed, and myoblasts started differentiation, expression of Nf1 gradually decreased also in control samples from day 1 to day 3 (Fig. 4.1D). This indicates a function for *Nf1* in early myoblast differentiation. The efficiency of *Nf1* knock out on primary myoblasts was tested with real-time qPCR, and primers target exons 40 and 41 were used. Similar to relative mRNA expression with muscle progenitors and muscle tissue, *Nf1* was also significantly down-regulated in $Nf1^{Myf5}$ primary myoblasts (Fig. 4.1E).

Conclusions:

Transcriptome analysis of p21 muscle tissue and p7 FACS sorted muscle progenitors combined with real-time qPCR double confirmation showed exons 40 and 41 of *Nf1* had been efficiently knocked out in both progenitors and muscle tissue. In vitro culture of primary

myoblasts showed that in Nf1^{Myf5} mice, *Nf1* had been deleted on the protein level. Furthermore, in wild type cells, *Nf1* expression declined during myoblast differentiation. Therefore the Nf1^{Myf5} mouse model is suitable for further *Nf1* function analysis during postnatal muscle development.

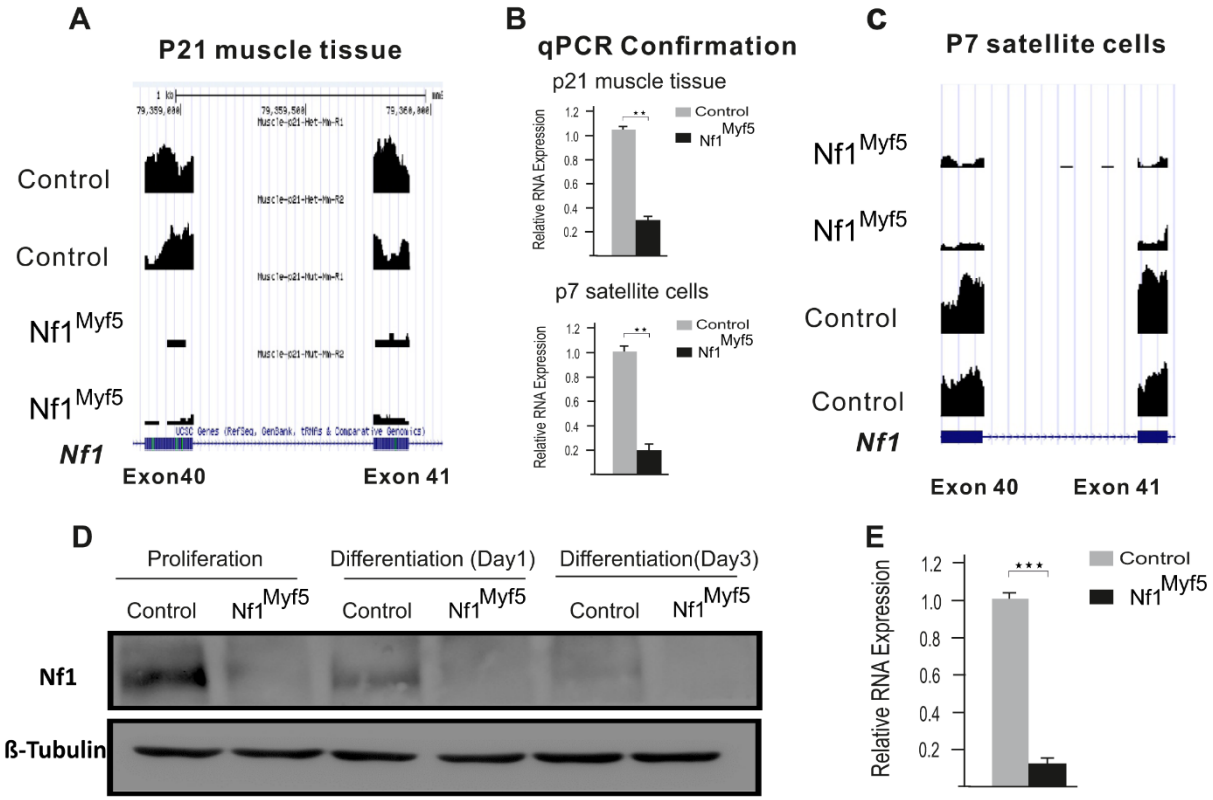

Figure 4.1 *Nf1* was efficiently deleted in Nf1$^{flox/flox}$Myf5 ^{Cre} skeletal muscle.

A Exons of 40 and 41 were deleted in p21 muscle tissue. Total mRNA was isolated from Control (n=2) and Nf1^{Myf5} (n=2) TA muscle, followed by whole transcriptome analysis (RNAseq). RNAseq reads were mapped with mouse genome 9 with STAR RNA-seq aligner. The figure shows *Nf1* expression reads number for exons 40 and 41 in the UCSC genome browser. Scale bar = 1kb. **B** Real-time qPCR confirmation for figure A and C. The top shows RNA expression level of *Nf1* (exons 40 and 41) from TA muscle of p21 Nf1^{Myf5} (n=3) and control (n=3) animals. The bottom shows the RNA expression level of Nf1 (exons 40 and 41) from FACS-isolated muscle progenitors of p7 Nf1^{Myf5} (n=3) and control (n=3) animals. **C** Nf1(exon 40 and 41) was deleted in p7 muscle progenitors. FACS sorted muscle progenitors from Control (n=2), and Nf1^{Myf5} (n=2) animals were used for mRNA isolation immediately followed by whole transcriptome analysis (RNAseq). The figure shows exons 40 and 41 of *Nf1* reads number in the UCSC genome browser. Scale bar = 1kb. **D** Nf1 protein was only detected in primary myoblast. Nf1 protein was isolated from p21 Nf1^{Myf5} (n=3) and control (n=3) primary myoblasts through the preplating method and cultured in proliferation medium. The first day after adding differentiation medium was considered as Day1. **E** Efficiency of *Nf1* knockout in primary myoblasts. Real-time qPCR was performed with mRNA isolated from control (n=3) and Nf1^{Myf5} (n=3) primary myoblasts. Primers designed for exons 40 and 41. ** P ≤ 0.01, *** P ≤ 0.001. p21= postnatal 3 weeks; p7 = postnatal one week.

4.2 Nf1^{Myf5} mice suffered from myopathy.

4.2.1 The phenotype of Nf1^{Myf5} mice.

The weight of the control and Nf1^{Myf5} mice was measured every day from postnatal day five on until 12 weeks old to observe the effects of Nf1 knockout on postnatal muscle development. Interestingly, one phenomenon was noticed that at p0 (the first day of birth), the difference between these two groups was hard to tell, genotype PCR was needed to identify the knockout mice. With time passed, the difference between Nf1^{Myf5} and control animals can be told, in particular, from p6 on. For the mouse body size, the group of Nf1^{Myf5} animals is relatively smaller in both postnatal one week and 12 weeks (Fig. 4.2A). These smaller animals were then labeled, and genotype PCR was performed for double confirmation to make sure these mice were knockout animals from their genetic background. From the overall review, at p6, the average weight of the Nf1^{Myf5} group is 2.235 g, and that is 3.2075 g for the control group. The ratio between control and Nf1^{Myf5} mice is 1.43, and there is a significant difference. As the animal grows, the difference in their body weight is also increased. Under normal skeletal muscle development circumstances, postnatal 21 is considered as the time point that muscle hypertrophy change from mainly depending on nuclear insertion to protein synthesis. At p21, the ratio difference between these two groups reaches 2.03. Typically 12 weeks mice are considered as mature mice; from this time point on, the skeletal muscle system will reach its homeostasis[133]. For mature mice, the average weight of the knockout group is 13.3 g, and that of the control group is 31.7 g. The ration between knockout and control group is 3.6 (Fig. 4.2C). Through comparing the body weight, it suggests that over time, myopathy caused by *Nf1* deficiency appears to get worse and worse, and the longest living knockout mice, in the end, die between 22 and 23 weeks.

Following the bodyweight reduction in Nf1^{Myf5} mice, to see how the skeletal muscle system gets affected, after mouse dissection, all the relative muscle bundles from the hind limbs of the mice were taken separately. Firstly, all of them were weighed, and the weight of Nf1^{Myf5} muscle and control muscle was compared. The muscle mass of Nf1^{Myf5} animals is severely decreased compared with the control group. The muscle mass from Gas (gastrocnemius muscle) and TA (tibialis anterior muscle) are shown here, and the muscle mass of the knockout group is reduced by around 17.7 mg and 14 mg, respectively (Fig. 4.2B). Besides, during the muscle dissection process, the color of these muscle bundles in the knockout group appeared darker red instead of pink-red in the control group. It implied that the composition of the muscle fiber types might be different and also its energy production capability.

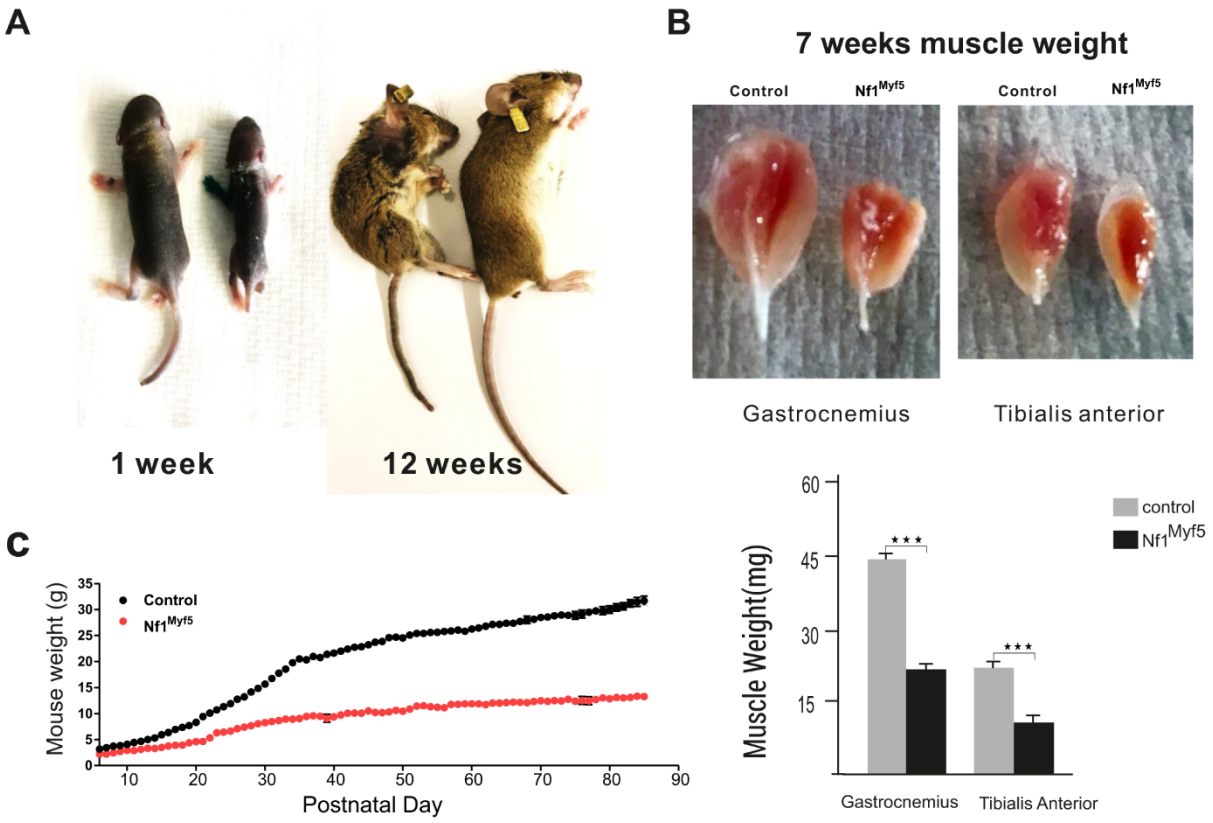

Figure 4.2 Muscle phenotype caused by *Nf1* deletion.

A Photographs show reduced body size of Nf1^{Myf5} mouse. Mouse pictures were taken from postnatal one week and 12 weeks Nf1^{Myf5} and Control mice. **B** Nf1^{Mfy5} mice show reduced muscle mass. The top pictures were taken from Gas and TA muscle of 7 weeks Nf1^{Myf5} and control mice. The bottom column chart shows Gas and TA muscle weight difference between 7 weeks Nf1^{Myf5} (n=3) and Control (n=3) muscle weight. **C** Body weight reduction of Nf1^{Myf5} mice during postnatal development. Bodyweight from p6 to twelve weeks Nf1^{Myf5} (n=4) and control (n=4) mice were measured. Student-t-test was used for statistical analysis. p*<0.05. p**<0.01. P***<0.001; TA= Tibialis anterior. Gas = Gastrocnemius.

Literature showed that during development, brown adipose tissue is also derived from Myf5^{+} progenitors[134]. To check if *Nf1* deletion also affects brown adipose tissue, during muscle dissection, both brown and white adipose tissue were also taken and weighed. 12 weeks Nf1^{Myf5} and control animals were used for white and brown adipose tissue analysis. In addition to the reduction of muscle mass, severely decreased white adipose weight in Nf1^{Myf5} mice during postnatal muscle development is also observed. Specific white and brown adipose weight was normalized with their whole mouse body weight. Interestingly, there was no change in the ratio of interscapular brown adipose tissue (iBAT), constitutive brown adipose tissue (cBAT), and subscapular brown adipose tissue (sBAT). However, the ratio of posterior subcutaneous white adipose tissue (psWAT), anterior subcutaneous white adipose tissue (asWAT), and retroperitoneal white adipose tissue (rWAT) were significantly reduced in the

Nf1^{Myf5} group, especially for psWAT (Fig. 4.4A). As the most critical storage place for lipid droplets, white adipose tissue could provide free fatty acid for muscle metabolism. The weight loss of white adipose tissue indicates that muscle of Nf1^{Myf5} mice might have a higher demand for fatty acid oxidative phosphorylation. Histology of white adipose tissue shows a severe reduction of lipid droplet storage in Nf1^{Myf5} mice; no marked difference is observed for brown adipose tissue (Fig. 4.4C). Intramuscular fat infiltration was analyzed by OilRed O staining, and there is no difference between control and Nf1^{Myf5} mice at both one week as well as 12 weeks mice (Fig. 4.4B). Nf1 deletion therefore only influences skeletal muscle but not brown adipose tissue in the Nf1^{Myf5} mouse model. Possibly, reduction of white adipose tissue is caused by impaired skeletal muscle homeostasis.

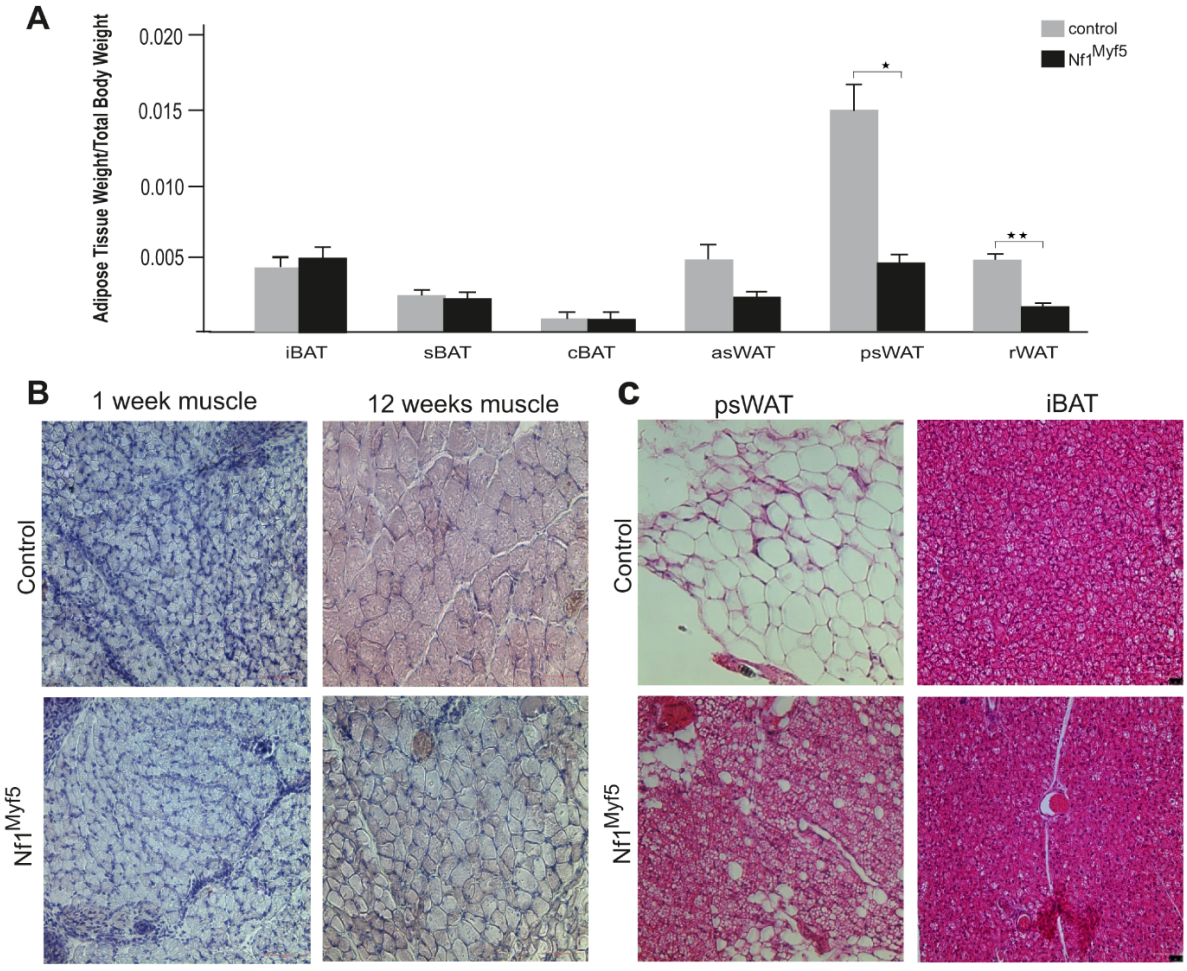

Figure 4.3 Adipose tissue phenotype caused by *Nf1* deletion.

A White adipose tissue weight loss in 12 weeks Nf1^{Myf5} (n=4) and control (n=4) mice animals. **B** No intramuscular fatty infiltration in both groups was observed. OilRed O staining was performed on postnatal one week and 12 weeks control, Nf1^{Myf5} hindlimb cryosections **C,** Nf1 deletion only affects white adipose tissue. Hematoxylin and Eosin staining of 12 weeks Control, and Nf1^{Myf5} psWAT and iBAT cryosections. Student-t-test was used for statistical analysis. p*<0.05. p**<0.01; iBAT= Interscapular brown adipose tissue. sBAT= subscapular brown adipose tissue. cBAT= Cervical brown adipose tissue. asWAT= Anterior subcutaneous white adipose tissue. psWAT= Posterior subcutaneous white adipose tissue. rWAT= Retroperitoneal white adipose tissue.

Conclusions:

In particular, the deletion of *Nf1* in muscle progenitors and their progeny contribute to severe myopathy, which mainly includes a decrease in the mass of skeletal muscle and white adipose tissue, thereby reducing body weight and also body size of $Nf1^{Myf5}$ mice which is a kind of recapitulate the skeletal muscle phenotype that suffered by NF1 patients. It suggests that *Nf1* is critical for postnatal skeletal muscle development and worth for further mechanism studies.

4.3 $Nf1^{Myf5}$ mice showed fiber type shift from fast to intermediate/slow fiber.

4.3.1 Increased intermediate/slow fiber relative genes expression and decreased fast fiber relative genes expression in $Nf1^{Myf5}$ TA muscle.

As $Nf1^{Myf5}$ mice suffer from massive muscle weight loss during the first several weeks postnatal muscle development, to elucidate the underlying mechanism, TA muscles from p21 $Nf1^{Myf5}$ and control animals were used for mRNA isolation followed by whole transcriptome sequencing analysis (RNAseq). Previous literature has shown that during skeletal muscle development, the content of fiber types is in a dynamic state until the animal is adult. The proportion of slow fiber reached a peak during the embryonic period. After birth, the activity of the animal became more and more active, and the content of slow fibers became smaller and smaller until the mouse matured at around 12 weeks and most of the slow fibers are only found in soleus muscle. Thus, three weeks of postnatal mice were used. After sequencing, genes that were significantly up and down-regulated were submitted to DAVID 6.8 bioinformatics and also Gene Set Enrichment Analysis (GSEA) for gene ontology (GO) and KEGG pathway analysis. Downregulated genes were primarily enriched in GO terms such as DNA - template transcription, positive regulation of transcription from RNA polymerase II promoter, and glycogen metabolism process. In contrast, up-regulated genes were mainly belonging to GO terms such as oxidation-reduction process, fatty acid metabolic process, and fatty acid beta-oxidation (Fig.4.8D). Because muscle metabolism is controlled by muscle fiber type, firstly muscle fiber component genes, including different muscle isoforms of myosin heavy chain, were checked. There are two skeletal muscle fiber types, Type I and Type II. Type I fibers are mainly composed of myosin heavy chain 7 (Myh7). Type II fibers can be classified into type II-A and type II B fibers, which are composed of myosin heavy chain 1/2 (Myh1, Myh2) and 4 (Myh4), respectively. RNAseq data showed that the expression of *Myh1* and *Myh2* were upregulated, and the expression of *Myh4* was the downregulated. The average RPKM of *Myh4* in $Nf1^{Myf5}$ samples was only half of that in the control group. On the other hand, the RPKM of

Myh1/2 was doubled in Nf1^{Myf5} samples. Besides, expression changes of genes such as components of the sarcomere and calcium signaling pathway were also being noticed. Fast fiber-related genes such as Actin alpha3 (*Actn3), Atp1b2, Calsequestrin1 (Casq1), Fhl3, Mybpc2, Myl1, Mylpf,* Parvalbumin *(Pvalb), Tpm1* were all went down in Nf1^{Myf5} TA muscle. The exact opposite is the increased expression level of slow fiber-related genes, including Actin alpha 2 (*Actn2)*, Ca^{++} ATPase *(Atp2a2)*, Calsequestrin2 (*Casq2)*, *Mb*, *Mybpc1*, *Myl2*, *Myl12a*, Myomesin3 (*Myom3)*, Myomesin1 (*Myom1)*, Myozenin2 (*Myoz2)*, Troponin, cardiac/slow skeletal (*Tnnc1)*, Troponin I skeletal slow 1 (*Tnni1)*, Troponin1 (*Tnnt1)*. The molecular signature from Nf1^{Myf5} and control TA muscles indicated that the muscle metabolic properties in Nf1^{Myf5} animals might be different from the control muscle[135,34]. It suggests a fiber type transition from fast to slow intermediate fibers in Nf1^{Myf5} mice (Fig. 4.4A). For double confirmation, primers specific for different muscle component isoforms, including *Myh2*, *Myh4*, *Myh7*, and *MyoZ2*, were used for the real-time qPCR test (Fig. 4.4B). This confirmed that Nf1^{Myf5} TA muscle has more intermediate and slow fiber component genes expression, whereas the fast fiber component gene *Myh4* is significantly decreased in Nf1^{Myf5} mice.

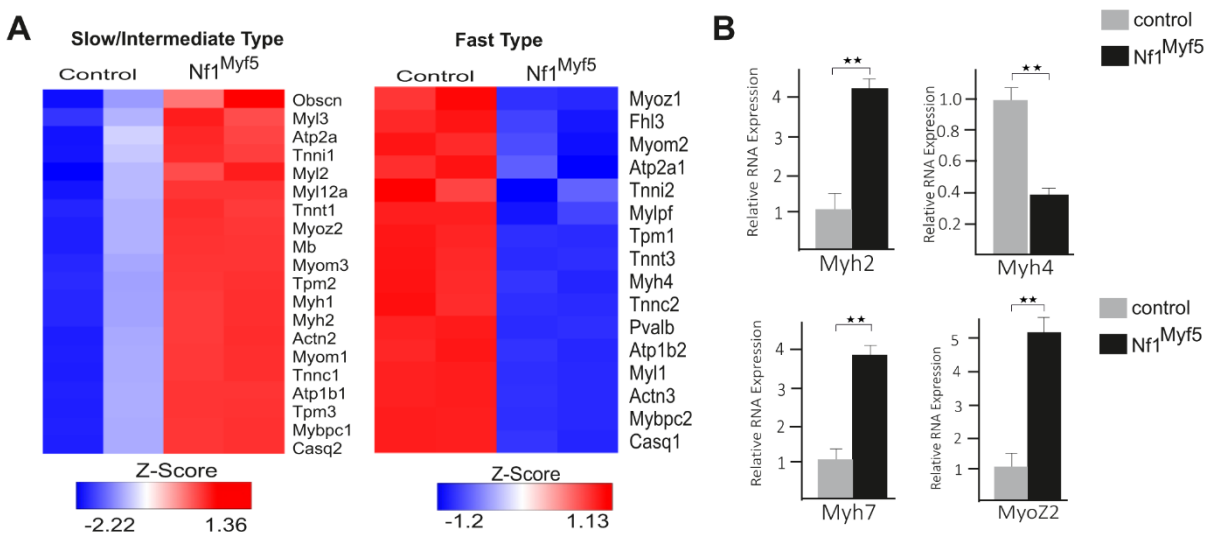

Figure 4.4 *Nf1* deletion leads to muscle fiber type shifted from fast glycolytic fiber to intermediate/slow oxidative fiber.

A Increased slow/intermediate genes expression (left) and decreased fast fiber component genes expression (right) in p21 Nf1^{Myf5} TA muscle. Differential gene expression analysis was performed with DEseq 2, for p_{adj} <0.001 were used as significantly different. Z-score was calculated based on the raw RPKM reads. **B** Real time qPCR confirmation for RNAseq data. Total RNA was isolated from Nf1^{Myf5} (n=3) and control (n=3) p21 TA muscle tissue. *Myh7*, *Myh2*, *Myh4*, and *MyoZ* were chosen as target genes. Student-t-test was used for statistical analysis. p**<0.01

4.3.2 Increased ratio of intermediate/slow fiber in Nf1^{Myf5} TA muscle.

However, except for the transcription level, genes expression from protein level was also checked with specific antibodies for immunostaining. First of all, the whole hindlimb cryosections were taken from a time series postnatal muscle development stages, including one week, two weeks, three weeks. Co-staining for sections with Myh7, lamA primary antibodies, and DAPI were performed, followed by imaging and calculation of slow fiber percentage in each muscle bundle. Immuno-staining shows the underlying trend for fiber type transition during postnatal muscle development is slow to intermediate to fast fibers, which is similar to literature published before (Fig. 4.5). In the first week after birth, there was no significant difference between Nf1^{Myf5} and control animals in the proportion of slow fibers being detected, and slow fibers were evenly distributed in all kinds of muscle bundles. The percentage of slow fibers in control mice is around 13.2%, 21.3%, 60.8% in TA, EDL, and Soleus muscle, respectively (Fig. 4.5A). Interestingly, one week later, a global reduction of slow fibers happened in control mice, and the percentage of slow fibers dropped to 8.7 %, 11.3%, and 38.6% in TA, EDL, and Soleus muscle. Besides, the difference occurred with more slow fibers in Nf1^{Myf5} animals in TA, EDL, and Soleus muscle at p14 (Fig. 4.5B).

This was also confirmed by immunostaining data from three weeks of mice. Compared with control animals, p21 Nf1^{Myf5} mice showed a significantly increased slow fiber component in TA muscle. The proportion of slow fibers in Nf1^{Myf5} TA muscle increased from 4.5% to 5.5%. Interestingly, from the staining except for fibers located within the muscle bundles which are easy to tell. A large proportion of slow fibers were also observed in the periphery of muscle, which was difficult to tell which muscles they belong to (Fig. 4.5C). Since immunostaining only shows the protein expression in the in situ state. Considering staining from different layers of tissue might also influence the analysis. Therefore, the protein was isolated from the whole TA muscle of p21 Nf1^{Myf5} and control animals. Primary antibodies against Myo-slow (Myh7) and Myo-fast (Myh4) were used, respectively. β-actin was used as a housekeeping protein. The gray value of each band was measured with ImageJ. All settings are the same for all the measurements. The ratio of the gray value between the target band with its housekeeping band was used as the relative protein expression level. The relative expression of Myo-slow in Nf1^{Myf5} samples increased from 0.56 to 1.52. For Myofast, the relative expression reduced from 0.98 to 0.45 compared with the control samples (Fig. 4.6A). Therefore, western blot data also supports the fiber type transition from fast fibers to slow fibers in Nf1^{Myf5} mice.

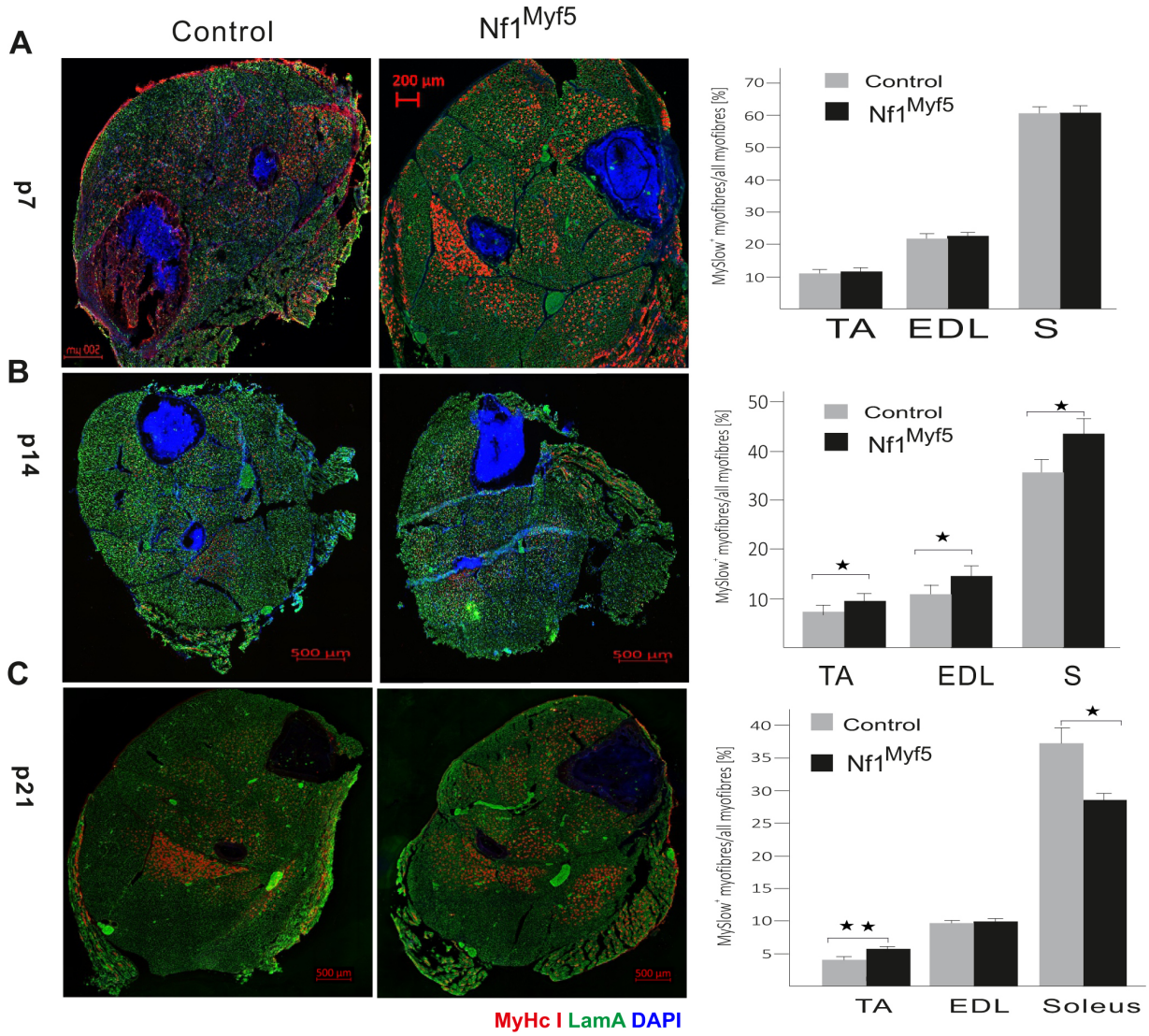

Figure 4.5 Fiber type shift caused by *Nf1* deletion initiate from p14.

A，B, C *Nf1* deletion leads to an increased proportion of slow fiber from p14 on. Immunostaining was performed on hindlimb cryosections of p7, p14 and p21 $Nf1^{Myf5}$ (n=3) and control (n=3) mice. Antibodies against Typ I fiber and basal lamina were used for staining. Quantification was based on the ration between Myo-slow positive and total fiber numbers in each defined muscle bundle. Student-t-test was used for statistical analysis. p*<0.05. Scale bar is 500 µm and 200 µm for p7 staining.

To observe the fiber type composition of adult mice, primary antibodies against real slow fibers, and also type II A fibers were co-stained with LamA and DAPI, and then the ratio of type II A fibers ($Myh2^{+}$) in TA, EDL and Soleus muscle was calculated. Immunostaining data showed that for 12 weeks of adult mice, slow fibers were mainly located in the soleus muscle (Fig. 4.6B). An increase in the proportion of Type II A fibers in 12 weeks $Nf1^{Myf5}$ mice was observed. Compared with the control sections, the proportion of Type IIa fibers in $Nf1^{Myf5}$ TA muscle increased from 5% to 9%. In EDL muscle, it increased from 8% to 16%. In Soleus, it increased

from 30% to 40%. In short, the data showed that the expression level of Myh2 is significantly higher in all of these three muscle bundles (Fig. 4.6B, C). Other than this, the cross-section area (CSA) in the $Nf1^{Myf5}$ group was also more prominent in twelve weeks' soleus muscle, which peaked at 1600 μm^2, and in the control group, it peaked between 1200 and 1400 μm^2 (Fig. 4.6D). It suggested *Nf1* deletion changed the metabolism way, and slow fibers are more functional for energy compensatory. It is in contrast with reduced muscle weight in $Nf1^{Myf5}$ animals, and implicated that myopathy caused by *Nf1* deletion is associated with muscle fiber type.

Conclusions:

Data from this section showed that $Nf1^{Myf5}$ mice have a slower fiber type reprogramming (slow to fast) process during postnatal muscle development, which was confirmed by both transcriptome analysis and immunostaining combined with western blot from protein level. Besides, it was also confirmed at different stages of development (juvenile and adult) the effect from Nf1 deletion was also different. It suggests that a fiber type shift may be involved in myopathy of $Nf1^{Myf5}$ mice.

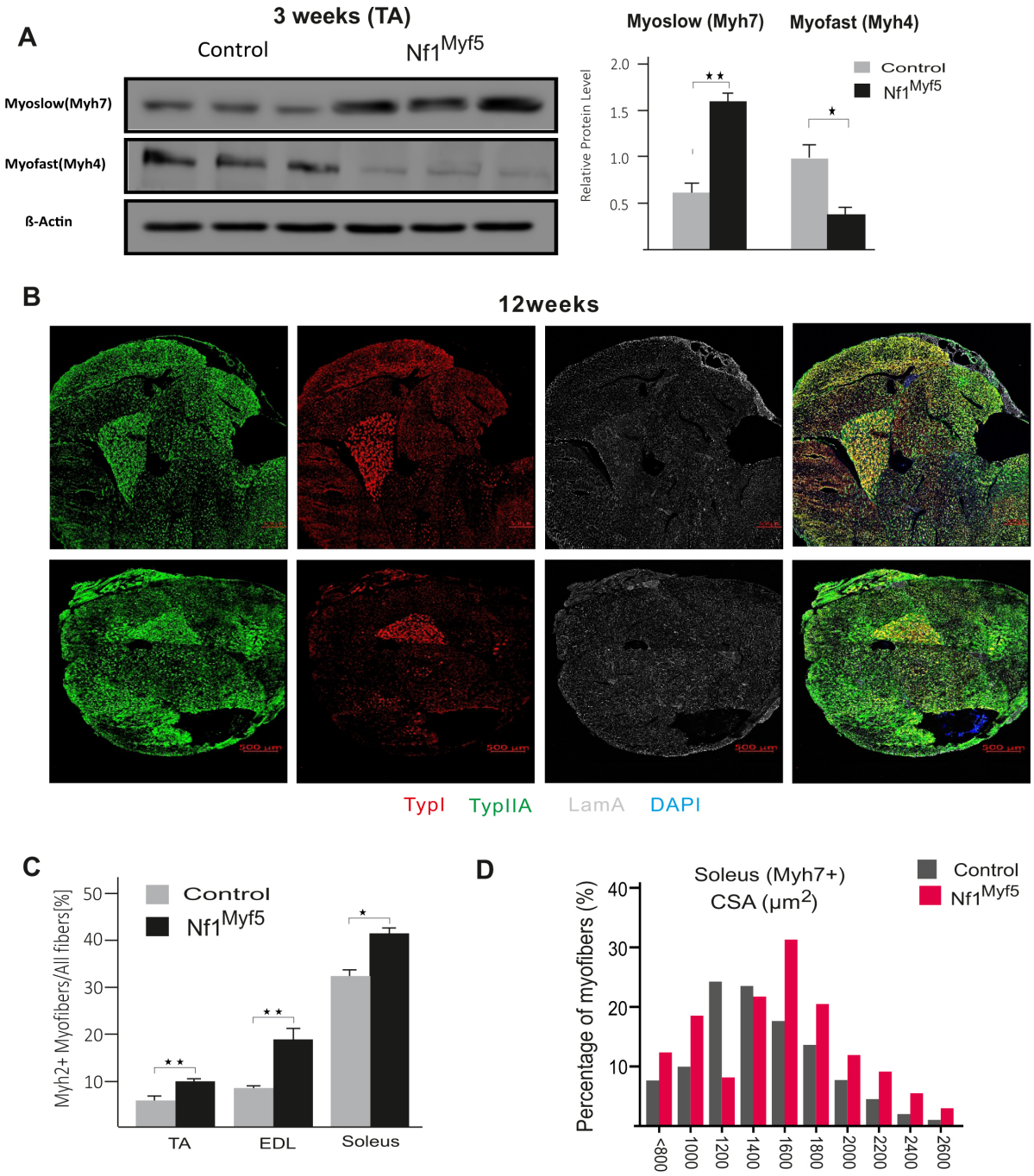

Figure 4.6 Increased intermediate/slow fibers in Nf1^{Myf5} TA muscle from the protein level.

A Increased Myo-slow expression in Nf1^{Myf5} TA muscle. Myoslow and Myofast antibodies were used for western-blot. Image J was used for gray value measurement and relative quantification. β actin was used as a housekeeping protein(n=3). **B,C** Increased type II A fibers in Nf1^{Myf5} adult muscle. Cryosections generated from 12 weeks control (n=3) and Nf1^{Myf5} (n=3) mouse. Antibodies were specific for type I slow fiber, type II-A, and basal lamina was used for labeling. Quantification was based on the ratio between type II-A positive and total fiber number in each defined muscle bundles. **D** The increased cross-section area of type I fibers within Soleus muscle in Nf1^{Myf5} mice. ZEN software was used for CSA measurement. Student-t-test was used for statistical analysis. p*<0.05. p**<0.01. The scale bar is 500 µm.

4.4 Nf1^{Myf5} mice have a metabolism shift from glycolysis to fatty acid oxidative phosphorylation.

4.4.1 Reduced glucose catabolic process in Nf1^{Myf5} TA muscle.

Fiber type is typically determined by fiber contractile and metabolic properties. Therefore, followed by the fiber type shift, metabolic relative genes in Nf1^{Myf5} and control mice were checked. First, in order to avoid the bias from statistical analysis, the entire gene list without DEseq2 analysis was submitted to GSEA (Gene Set Enrichment Analysis). Interestingly, Glucose Catabolic Process was highly enriched in control samples (Fig. 4.7A). After checking the enrichment details, glycolysis relative genes appeared. Since the expression level of genes is highly variable, for better visualization with heatmap, Z-score from these significantly altered expression genes were calculated based on the standard deviation of RPKM and the mean of each gene. The main glycolysis process rate-limiting enzymes and activators were down-regulated in Nf1^{Myf5} samples.

In general, RNAseq data show that glycolysis relative genes expression is much higher than that of fatty acid metabolism genes. It implied that fast glycolytic fibers play a dominant role in p21 TA muscle, and also the higher efficiency of glucose metabolism compared to fatty acid oxidative phosphorylation for energy production. Globally reduction of glycolysis genes in Nf1^{Myf5} TA muscle and these enzymes include Enolase 3 (*Eno3*), a specific skeletal muscle isoform acting as a glycolytic enzyme, which catalyzes the reversible conversion of 2-phosphoglycerate to phosphoenolpyruvate. The expression of Eno3 in the fast fibers was also demonstrated to be higher. 6-phosphofructokinase, muscle type (*Pfkm*) converts phosphofructokinase to phosphorylate fructose-6-phosphate and then cleaves into glyceraldehyde-3-phosphate, which is the rate-limiting step in the glycolysis pathway. Phosphorylase b kinase regulates subunit alpha, skeletal muscle isoform (*Phka1*), a key enzyme in glycogen metabolism. Lactate dehydrogenase (*Ldha*) muscle isoform catalyzes the conversion of lactate to pyruvate and back because it converts NAD^+ to NADH and back. Interestingly, enzymes catalyzing glycolysis final production pyruvate into acetyl-CoA was repressed by upregulation of pyruvate dehydrogenase kinase (*Pdk2/4*) (Fig.4.7B). Considering the reduction of glycolysis in Nf1 deleted muscle fibers then the concentration of blood glucose from the heart of animals was measured. Actually, there is no difference being detected (Fig.4.7C). Besides, insulin signaling pathway related markers were also tested to see the influence of Nf1 knockout on glucose uptake in muscle fibers. Interestingly, there is no difference I IRS1 phosphorylation detected (Fig.4.7D). It suggested that even with a decreased glucose consumption, the boold glucose concentration is still stable and animal body might has compensatory way to regulate the glucose homeostasis.

Conclusions:

Data from this part implied a reduction in the glucose catabolic process in the TA muscle of Nf1^{Myf5} mice, which includes the decomposition of muscle glycogen, the entire glycolysis process, and the conversion of the glycolysis product pyruvate to the TCA cycle for further oxidative phosphorylation. However, no alteration of insulin regulated signaling pathway and blood glucose concentration was detected.

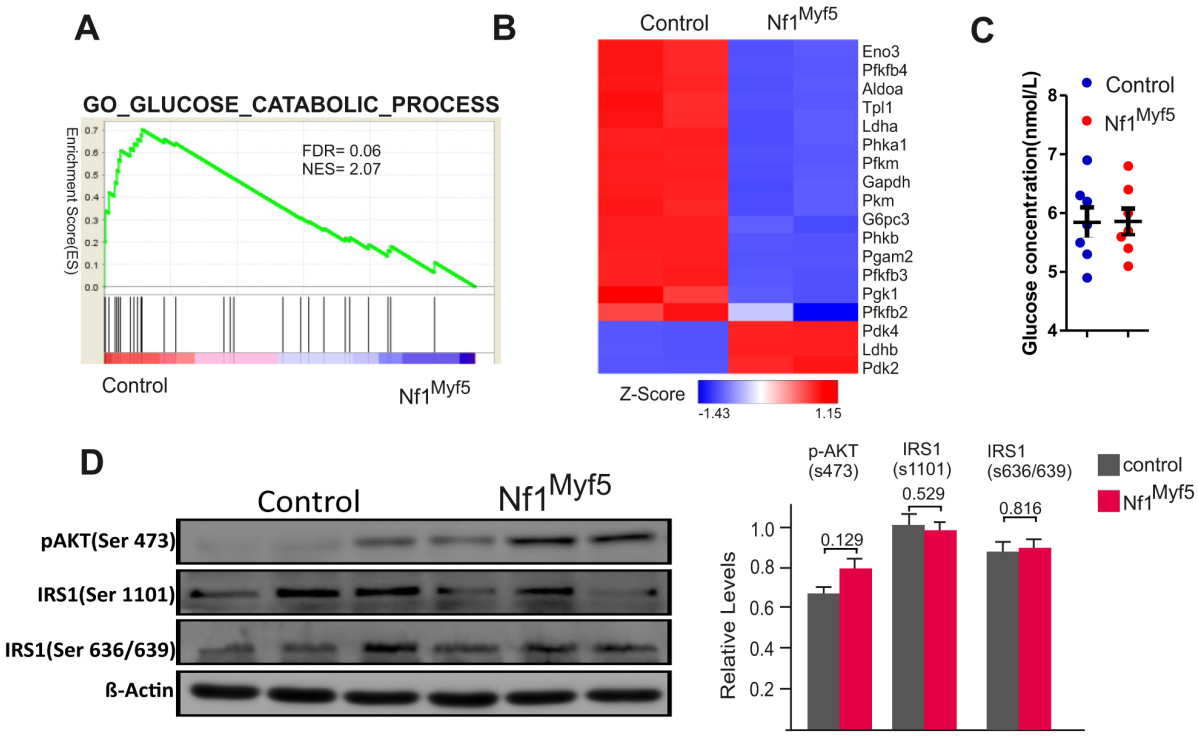

Figure 4.7 Reduced glucose catabolic genes expression in Nf1^{Myf5} TA muscle.

A GSEA analysis shows Gene Ontology enriched for glucose catabolic term in Control TA muscle. GSEA desk was used for enrichment analysis. **B** Decreased glycolytic enzymes expression in Nf1^{Myf5} TA muscle. **C** No difference for blood glucose concentration. **D** No alteration for insulin signaling. A,B Total mRNA was isolated from the p21 TA muscle of Nf1^{Myf5} (n=2) and control (n=2) mice. P adjust value was used to identify the significantly different expression genes. Genes involved in the glucose metabolism process were normalized by Z-score calculation and showed in a heatmap with R studio. For genes, padj <0.001 were treated as significantly changed expression. C: Blood from the heart of mice was take and measured. N=7 mice. D: Protein isolated from p21 TA muscle. Antibodies against IRS1 (ser 636/639), IRS1 (Ser 1101), pAKT (ser 473) and actin were used. N=3 mice. Gray value was measured with ImagJ and Student-t-test was performed.

4.4.2 *Nf1* deletion leads to increased fatty acid metabolism genes expression in TA muscle.

During muscle contraction, skeletal muscle can use both glucose and free fatty acids to generate ATP and maintain energy homeostasis. With decreased glucose metabolism activity, how animals maintain their energy balance is a question popped up. It is well known that fatty acid metabolism is an effective way to produce energy compared to glucose metabolism. In skeletal muscle, 90% of energy production is fatty acid oxidative phosphorylation[136]. Then all fatty acid metabolism relative genes were checked from the RNAseq list to see if $Nf1^{Myf5}$ mice have higher fatty acid metabolism to compensate for the reduction in glucose metabolism. In skeletal muscle, the free fatty acid is transferred to muscle fibers via fatty acid-binding proteins and Cd36. The genes from fatty acid-binding protein (*Fabps*) family and Cd36 were all up-regulated (Fig. 4.8A). These genes work together to transfer long-chain free fatty acid from plasma into muscle fibers, and then the next step free fatty acids are converted into acyl-CoA catalysts by long-chain fatty acyl-CoA synthetase (*Acsl1*), which then is shipped from the cytoplasm into the mitochondria.

For double confirmation, RNA isolated from p21 $Nf1^{Myf5}$ and control muscle tissue was used for real-time qPCR analysis. The significant up-regulated fatty acid metabolism genes showed similar expression patterns, including the free fatty acid transporters *Fabp3*, *Fabp4*, and *Cd36*. Mitochondrial transmembrane transporters *Cpt2* and *Cpt1b* (Fig. 4.8B). Besides, *Il6* was also used for qPCR as literature showed that Il6 could selectively stimulate fatty acid metabolism in human and animal skeletal muscle[137]. Its expression was significantly increased in the $Nf1^{Myf5}$ TA muscle (Fig. 4.8B). Except for RNA expression, protein expression was also checked with proteomics analysis. Protein isolated from the TA muscle of p21 $Nf1^{Myf5}$,heterozygous (Het) and control mice were used for sample preparation. Significantly changed proteins from proteomics analysis were submitted for KEGG pathway analysis, the increased proteins expressed in $Nf1^{Myf5}$ TA muscles were mainly enriched for fat digestion and absorption pathway (Fig. 4.8C top). Also, pathways, including PPAR signaling and oxidative phosphorylation, were enriched in $Nf1^{Myf5}$ TA muscle (Fig. 4.8C bottom).

As mitochondrial have an outer layer membrane and an inner layer membrane, this transmembrane transport requires the support of carnitine palmitoyltransferase (*Cpt1/2*). After these acyl-CoA enters the mitochondrial and find their position, beta-oxidation of the fatty acids will begin. A series of enzymes control the process, the initiation step is the break down of fatty acid into acetyl-CoA. For this process, enzymes involved mainly include dehydrogenase family (*Acads*, *Acadm*, *and Acadl),* enoyl-CoA hydratase (*Echs1*), 3-hydroxy acyl-CoA dehydrogenase (*Hadh*), Acetoacetyl-CoA thiolase (*Acaa*2, *Hadhb*). Finally, the acetyl-CoA produced by the fatty acid beta-oxidation will enter the TCA cycle. After the enrichment analysis,

GO terms for fatty acid catabolic process and fatty acid beta-oxidation using acyl CoA dehydrogenase were highly enriched in Nf1^{Myf5} TA muscle (Fig. 4.8D). The gene details behind these GO terms were checked and shown with Heatmap (Fig. 4.8A). Briefly speaking, *Nf1* deletion contributes to increased fatty acid metabolism genes expression.

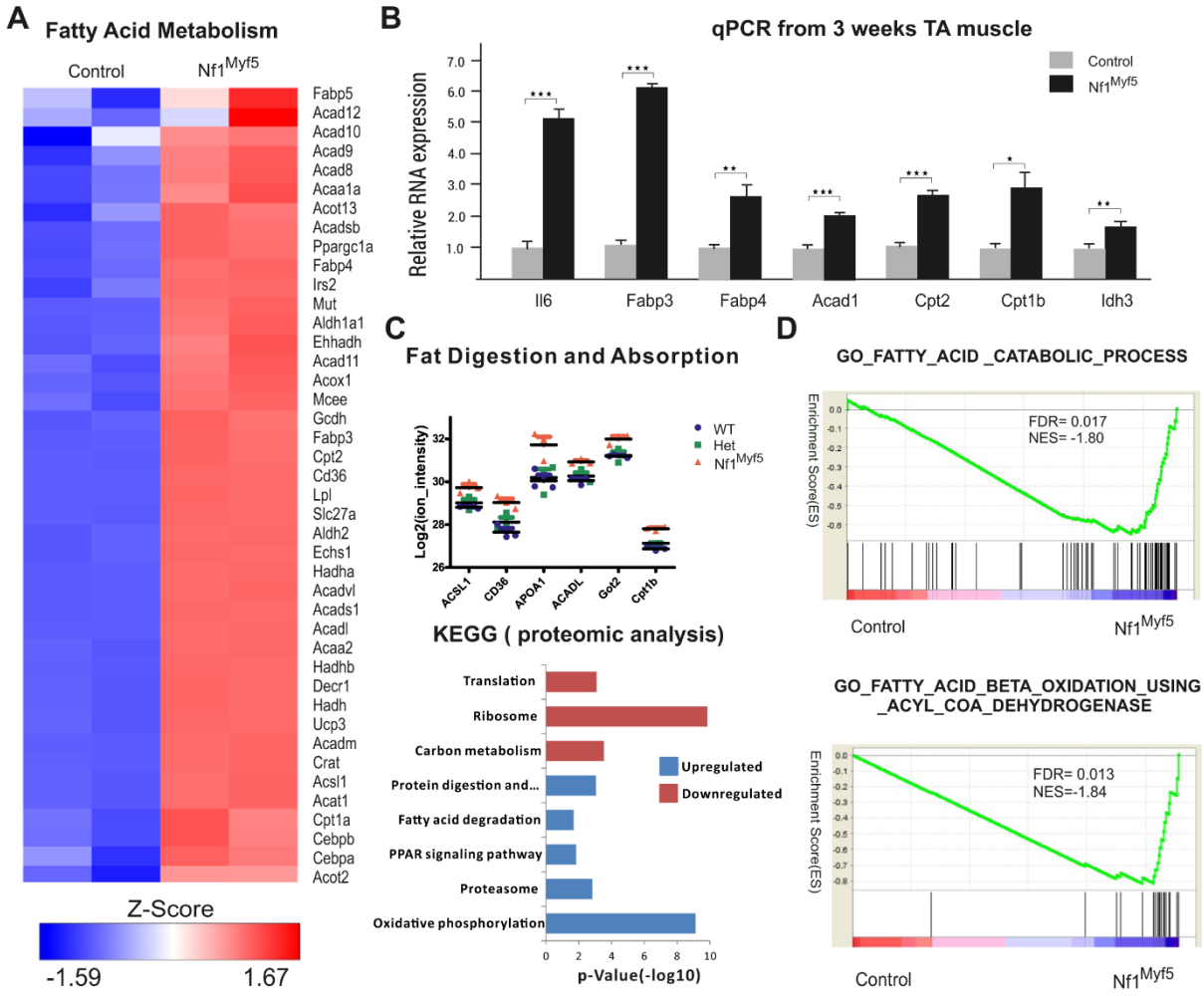

Figure 4.8 Increased fatty acid metabolism genes expression in Nf1^{Myf5} TA muscle.

A Increased fatty acid metabolism genes expression caused by Nf1 knockout in TA muscle. Total mRNA was isolated from the p21 TA muscle of Nf1^{Myf5} (n=2) and control (n=2) animals, respectively. P adjust value was used to identify the significantly differentially expressed genes. Genes involved in fatty acid metabolism process were normalized by Z-score calculation and showed in a heatmap with R studio. **B** A similar expression pattern of selected fatty acid metabolism genes was confirmed by real-time qPCR. Total RNA was isolated from p21 TA muscle tissue of Nf1^{Myf5} (n=3) and Control (n=3) animals. Two tail student-t-test was used for statistical analysis. p*<0.05. p**<0.01. P***<0.001; **C** Proteomics analysis showed increased fatty acid metabolism protein expression. TA muscle of p21 Nf1^{Myf5} (n=3) and control (n=3) animals was used for protein isolation. Two tail student-t-test was performed for statistical analysis. Differently expressed proteins were used for KEGG pathway analysis. Graphpad Prism was used for the graph generation. **D** Fatty acid oxidation was enriched explicitly in the Nf1^{Myf5} TA muscle. The whole RNAseq gene list was submitted to GSEA for enrichment analysis.

4.4.3 Increased Oxidative Phosphorylation ability in Nf1^{Myf5} TA muscle.

With reduced glucose catabolism, including glucose glycolytic and glucose oxidative phosphorylation, the question is, how does the skeletal muscle of Nf1^{Myf5} animals maintain their energy homeostasis? In contrast to glucose metabolism genes expression, GSEA analysis revealed that GO terms such as electron transport chain, a hallmark of oxidative phosphorylation, and mitochondrial protein complex were highly enriched in Nf1^{Myf5} TA muscle (Fig. 4.9C). Once the details of these two GO terms being detected, relative enzymes responsible for the citric acid cycle (TCA cycle) and electron transport chain (ETC) being observed. There are eight enzymes catalyze the TCA cycle: Citrate synthase (*Cs*), Aconitase (*Aco*), Isocitrate dehydrogenase (*Idh*), α-Ketoglutarate dehydrogenase (*Ogdh*), Succinyl-CoA synthetase (*Sucl*), Succinate dehydrogenase (*Sdh*), Fumarase (*Fh*), Malate dehydrogenase (*Mdh*). The expression level of all of these genes was significantly higher in *Nf1* knockout mice. The final step of ATP generation is the transfer of all high energy electrons within NADH and FADH2 produced by the TCA cycle and glycolysis to the electron transport chain (ETC). The components of ETC mainly include five protein complexes located on the inner mitochondrial membrane.

The data also show that the expression of mitochondrial complex component genes was globally increased. It includes mitochondrial complex I, NADH: ubiquinone oxidoreductase (Nduf family); mitochondrial complex II, succinate dehydrogenase (*Sdh* family); mitochondrial complex III, Ubiquinol–cytochrome c oxidoreductase (*Uqcr* family); Complex IV, cytochrome c oxidase (*Cox* family) and complex V, ATP synthase (*Atp5* family) (Fig. 4.9A). From the transcriptome level, a large group of oxidative genes was up-regulated, and some were also confirmed by proteomics analysis from protein level (Fig. 4.9B). Due to the limitations of the method, a total of approximately 3000 proteins were detected in all samples. Since the expression difference from the protein of the entire TA muscle was small, and the variance among samples was significant compared with the difference. Thus not so many proteins were detected as significantly changed. However, proteins responsible for Citrate Cycle and OXPHOS were still enriched from GO analysis. These double confirmed proteins for TCA cycle enzymes and components of the electron transport chain were significantly up-regulated in the Nf1^{Myf5} muscle. In short, the data strongly indicate that skeletal muscle of Nf1^{Myf5} mice show decreased glucose metabolism and require increased fatty acid oxidative phosphorylation for energy compensation. However, a group of proteins termed as Antioxidative stress was noticed as significantly down-regulated in Nf1^{Myf5} TA muscle. It implies that Nf1^{Myf5} mice might

increase the reactive oxygen species (ROS) production, thus suffer from oxidative stress (Fig. 4.9B).

Although all data from RNA and protein expression support the idea of a metabolic shift in $Nf1^{Myf5}$ skeletal muscle, how these muscles work in vivo still needs to be tested. Thus the High-Resolution FluoRespirometry assay was used to test the real-time metabolic rate of muscle bundles. For slow oxidative fibers, soleus muscle was selected, and EDL muscle was selected for glycolytic fast type fibers. The oxygen consumption rate for $Nf1^{Myf5}$ and control tissue was measured simultaneously by coupling with several different kinds of metabolic substrates and specific inhibitors of the electron transport chain. Generally, soleus muscle has a higher oxidative phosphorylation rate than EDL muscle. Both EDL and Soleus muscle from $Nf1^{Myf5}$ mice kept a higher oxygen consumption rate, which also means higher oxidative phosphorylation capacity in $Nf1^{Myf5}$ muscle. Especially for the soleus muscle, because soleus muscle is mainly composed of slow fibers and also mainly rely on oxidative phosphorylation to generate energy, thus its standard deviation is much smaller than EDL muscle. However, glycolytic muscle also has a higher trend for OXPHOS and significantly improved efficiency for mitochondrial complex I and II, at the same time, higher electron transport efficiency (ETS) (Fig. 4.9D). To sum up, $Nf1^{Myf5}$ muscle tissue shifts its metabolic preference from glycolysis to fatty acid oxidative phosphorylation from both the molecular level and also actual function.

Conclusions:

Knock out of *Nf1* increased intermediate/slower fiber type and a decrease in the proportion of fast fibers. The results in this section showed that $Nf1^{Myf5}$ skeletal muscle had reduced the glucose catabolism process while simultaneously increased the digestion/degradation process of fatty acid and also increased the fatty acid oxidative phosphorylation activity. It is not only from transcriptional and protein levels but also from the activity of the real-time metabolic function. It can show the role of *Nf1* in the regulation of muscle metabolism.

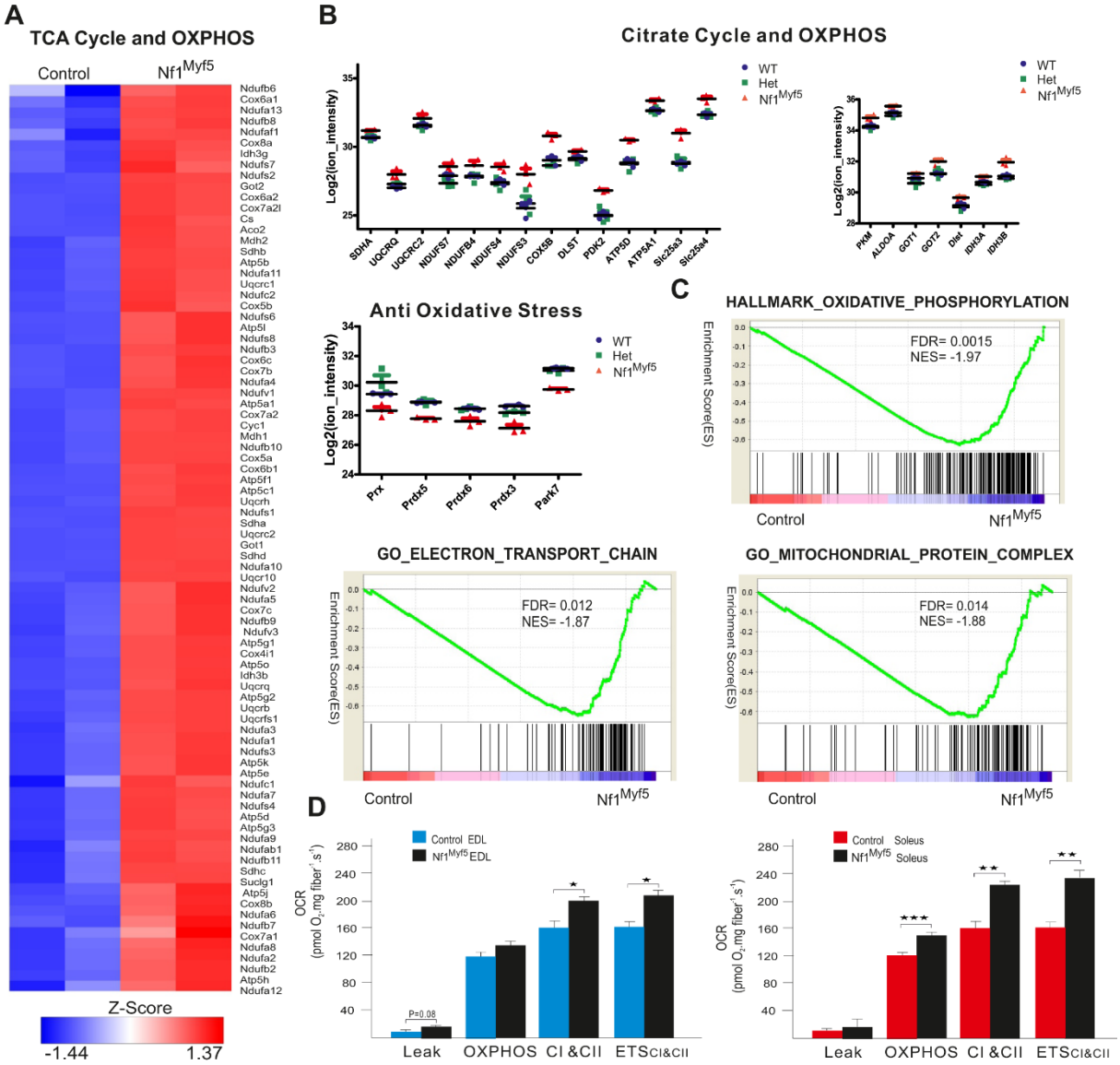

Figure 4.9 Increased Oxidative Phosphorylation ability in Nf1^{Myf5} muscle.

A Increased TCA cycle enzyme and oxidative phosphorylation gene expression in Nf1^{Myf5} mice. Z-Score of significantly differentially expressed genes was calculated. R studio was used for heatmap data visualization. Padj<0.01 genes were considered as significant. **B** Proteomics shows increased TCA cycle and OXPHOS proteins expression in Nf1^{Myf5} TA muscle. Decreased antioxidative stress proteins were also shown. Protein isolated from p21 Nf1^{Myf5} (n=3) and control (n=3) and wild type TA muscle. **C** RNAseq data shows Nf1^{Myf5} TA muscle GSEA analysis enriched for oxidative phosphorylation, electron transport chain, and mitochondrial protein complex. The full gene list was submitted to GSEA enrichment analysis. **D** Nf1^{Myf5} muscle showed increased real-time oxidative phosphorylation ability. Real-time metabolism test (High-Resolution FluoRespirometry assay) for live Soleus and EDL muscle fiber. Oxygen consumption rate was showed in here as an indicator of tissue oxidative phosphorylation ability (n=7 for each group). Student-t-test was used for statistical analysis. p*<0.05. p**<0.01. P***<0.001

4.5 Nf1^{Myf5} mice has energy deficiency and reduced catabolic process.

4.5.1 Increased AMPK/Pparg/Pgc1 α signaling in Nf1^{Myf5} muscle.

Since the efficiency of fatty acid oxidative phosphorylation to generate ATP is much higher, then the question is whether such metabolic compensation is sufficient for *Nf1* knockout mice? The skeletal muscle system is a large organ that consumes ATP during muscle contraction in body rest and activates status. Catalyzed by ATPase, ATP is degraded to ADP and release energy during exercise. Via the adenylate kinase (Adk) reaction, ADP, in turn, is, in part, reconverted to ATP and AMP. Therefore, the ratio between ADP/AMP and ATP is a good indicator of tissue energy balance[138]. In order to sense and regulate the change in energy status, an enzyme called 5' AMP-activated protein kinase (AMPK) would be activated. AMPK consists of three distinct subcomponents: a catalytic α subunit, a regulatory β, and γ subunit. AMPK is activated by phosphorylation of the α subunit at Thr172 site.

Once activated, AMPK functions to regulate mitochondrial biogenesis, increase translocation of Glut4 for glucose metabolism, and also free fatty acid transporters such as Cd36 and Fabps to localize on the plasma membrane, thereby stimulating fatty acid metabolism. Phosphorylated AMPK α (Thr172) in Nf1^{Myf5} and control muscle lysate was then detected by western blot with its antibody. Significantly higher levels of p-AMPK in Nf1^{Myf5} mice indicate that energy deficiency is still present in Nf1^{Myf5} mice (Fig. 4.10A). This may also explain why the phenotype of Nf1^{Myf5} mice is getting worse and worse and dying around 22 weeks. Besides, this metabolic shift can also explain the phenotype that Nf1^{Myf5} mice suffer from a reduction of white adipose tissue weight. The downstream target of AMPK dependent signaling pathway in skeletal muscle system is mainly Pparg/PGC1 α[139], which controls fatty acid metabolism and mitochondrial biogenesis[140]. Peroxisome proliferator-activated receptor gamma (*Pparg*) has been recognized as a positive regulator of free fatty acid and glucose metabolism in both human and mouse skeletal muscle[141,142]. Firstly, real-time qPCR was performed for *Pparg*, *Pgc1α*, and Lipoprotein lipase (*Lpl*). *Lpl* is highly expressed in both skeletal muscle and white adipose tissue. The enzyme acts to hydrolyze plasma triglycerides to free fatty acids. In adipose tissue, it controls the storage of fatty acids in the form of triglycerides[143]. Interestingly, a decrease in the expression of *Lpl* in white adipose tissue was observed in Nf1^{Myf5} animals, which suggests that fewer triglycerides were stored in white adipose tissue, and this might be a reason of white adipose tissue-specific mass loss (Fig. 4.10B). Real-time qPCR also showed that compared with control animals, the expression of *Pparg* and *Pgc1α* increased for more than four and two times, respectively, in TA muscle of Nf1^{Myf5} animals. Besides, the expression

of *Lpl* increased more than two times (Fig. 4.10C). This implied that the triglyceride hydrolysis process in the muscle of Nf1^{Myf5} animals is also increased.

Literature suggests that activation of Pparg in skeletal muscle can induce the production of adiponectin, thus boost muscle cells' insulin sensitivity[144]. The expression of the level of Adiponectin (*Adipoq*) was also detected by real-time PCR, and it was more than two times higher in Nf1^{Myf5} mice (Fig. 4.10C). A primary antibody against Pparg was used to detect the expression of Pparg from the protein level. Due to the presence of two Pparg isoforms, Pparg1 and Pparg2, the molecular weights are 50 KDa and 55 KDa, respectively. Studies have also shown that Pparg1 is the dominant one in skeletal muscle, and Pparg2 is mainly expressed in white and brown adipose[145]. Here, total Pparg protein expression was detected in postnatal young (two weeks) and young adult mice (7 weeks) using Western blot. Pparg1 expression was reduced in adult mice compared to younger mice, suggesting that younger mice require more fatty acids to maintain their energy homeostasis (Fig. 4.10C). It may also be related to the fiber type transition from slow fibers to fast fibers during postnatal skeletal muscle development. In addition, data showed that two isoforms of Pparg being detected, Pparg2 expression was low and could even be ignored in skeletal muscle. Nf1^{Myf5} muscles consistently maintained high Pparg1 expression compared to control mice. This can be used as direct support for increased fatty acid metabolism in Nf1^{Myf5} muscle tissue.

In summary, all of the data in this part implies at the molecular level. The underlying mechanism might be a decrease in glucose metabolism in muscle fibers lead to an energy deficiency of Nf1^{Myf5} muscle. This energy stress activates AMPK signaling lading to up-regulation of Pparg1 and Pgc1α expression and also their target genes such as the oxidative phosphorylation genes to meet the energy compensation and maintains energy homeostasis. This compensation appears not to be enough, thus causing the phenotype to become severe and severe until the animals die around 22 weeks of age.

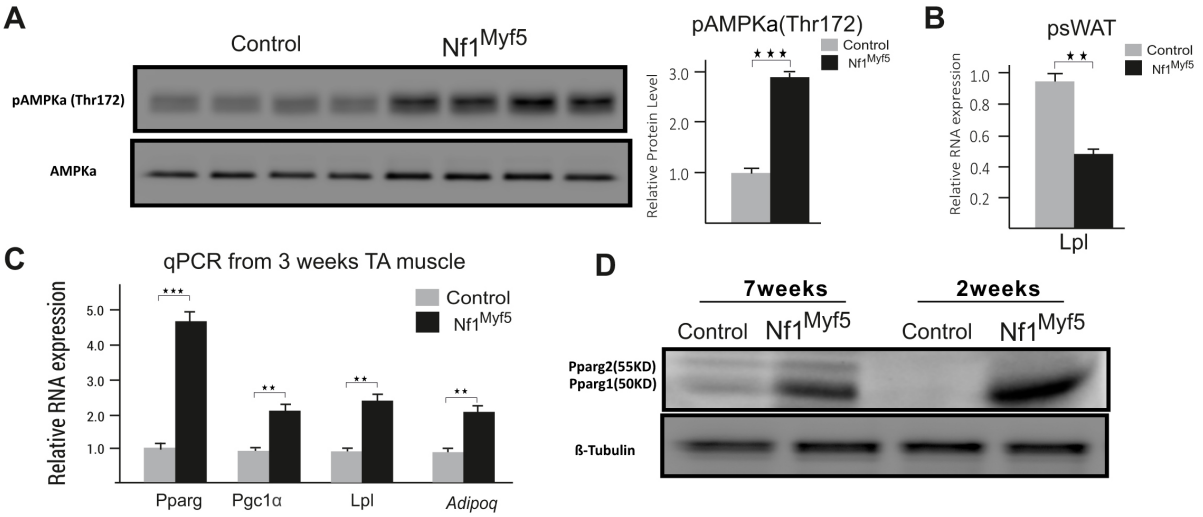

Figure 4.10. Increased fatty acid oxidative phosphorylation in the Nf1^{Myf5} muscle might be AMPK/Pgc1α signaling dependent.

A Hyperactivation of AMPK signaling in Nf1^{Myf5} TA muscle. Protein isolated from p21 Nf1^{Myf5} (n=4) and control (n=4) TA muscle. Primary antibodies against AMPKα and pAMPKα (Thr172) were used. The relative protein level was calculated by western blot bands' gray value normalization. The ratio between the phosphorylated band and its unphosphorylated band was used as a relative protein level. **B,C** Increased *Pparg*, *Pgc1α*,*Lpl* and *Adipoq* expression in Nf1^{Myf5} TA muscle. Total mRNA was isolated from p21 Nf1^{Myf5} (n=3) and control (n=3) TA muscle. ΔΔCt method was used for relative RNA expression calculation. **D** Increased Pparg1 expression in Nf1^{Myf5} TA muscle. Total protein was isolated from two weeks and seven weeks Nf1^{Myf5} and Control mice, respectively. β-tubulin was used as a housekeeping protein. Two isoforms of Pparg were detected at a size of 50 kDa and 55 kDa, respectively. Two-tailed student t-test was performed by GraphPad prism. p**<0.01. P***<0.001;

4.5.2 Decreased protein synthesis and increased protein degradation rate of Nf1^{Myf5} muscle.

As Nf1^{Myf5} animals suffered from energy depletion, theoretically to save energy, animals will reduce all energy-consuming activities, such as anabolic relative processes, and increase catabolic processes through specific signaling pathways. As a primary regulator of metabolic homeostasis, AMPK blocks anabolism by negatively regulating the mTOR pathway and increase fatty acid catabolism[48]. In addition, protein synthesis is also a critical way of postnatal muscle hypertrophy. Since previous data showed that Nf1^{Myf5} mice have a fiber type-specific muscle mass reduction, it is necessary to examine the protein synthesis rate in Nf1^{Myf5} skeletal muscle. Phosphorylated mTOR (ser2448) level is a good indicator of protein synthesis rate, for double check, here its downstream target p-s6 (ser235/ser236) was also detected. The relative protein phosphorylation level of p-mTOR and p-s6 in Nf1^{Myf5} TA muscle reduced from

1.1 to 0.55 and 1.5 to 0.98, respectively, compared to control animals. A significant reduction of both phosphorylated mTOR and p-S6 levels indicated a lower rate of protein synthesis in p21 Nf1^{Myf5} TA muscle (Fig. 4.11A, C). Besides, significantly down-regulated proteins from Nf1^{Myf5} TA muscle proteomics data were also enriched for Translation. These proteins mainly include ribosome component proteins and protein translational regulatory enzymes (Fig. 4.11B).

Interestingly, another enriched term named as the component of proteasome 26s subunit also caught the attention. Since protein synthesis and degradation need to be precisely controlled, and always in a balanced manner, especially for adult skeletal muscle. During muscle development, the rate of protein synthesis is higher than protein degradation, which contributes to postnatal muscle hypertrophy. Increased proteasome 26s subunit proteins expression indicated a higher rate of protein degradation in Nf1^{Myf5} TA muscle (Fig. 4.11B).

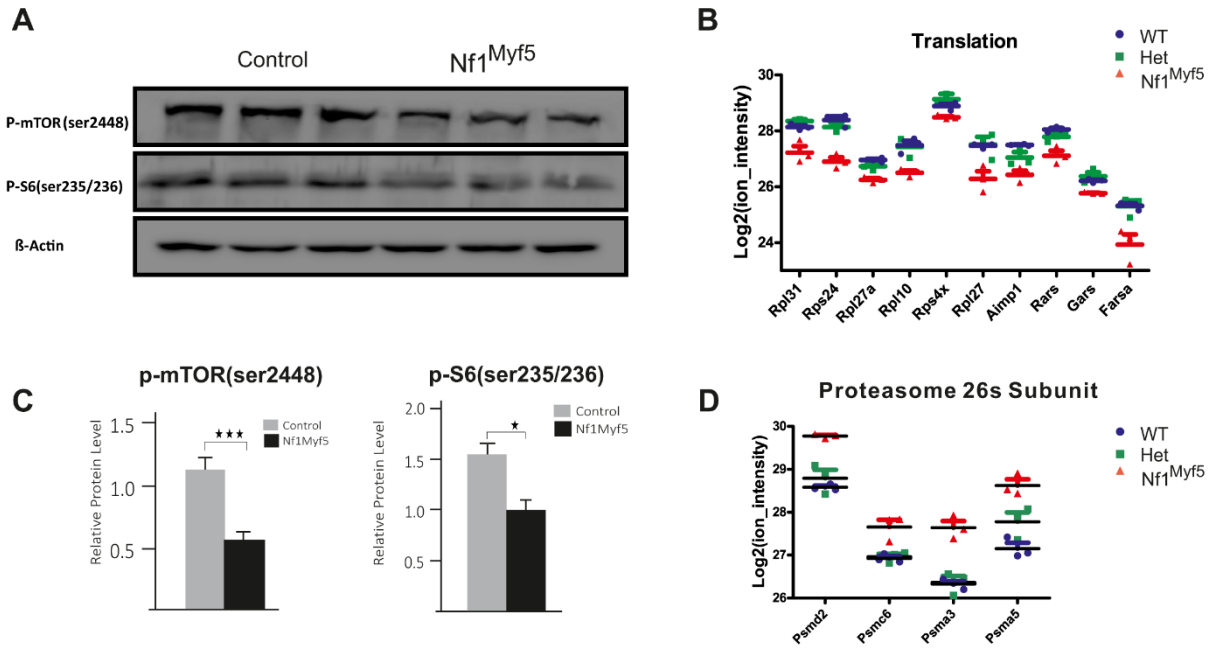

Figure 4.11 Reduced protein synthesis rate of Nf1^{Myf5} mice

A, C Reduced mTOR signaling in Nf1^{Myf5} TA muscle. Protein isolated from p21 Nf1^{Myf5} (n=3) and control (n=3) TA muscle. Primary antibodies against p-mTOR (Ser2448) and p-S6 (ser235/ser236) were used. Western blot bands' gray value was measured with ImageJ; Relative protein expression level was calculated by the gray value ratio between each target band and the housekeeping band. Student-t-test was used for statistical analysis. p*<0.05. P***<0.001; **B, D** Nf1^{Myf5} TA muscle has decreased protein translation and increased protein degradation rate. Proteomics data from p21 Nf1^{Myf5} (n=3) TA muscle and control (n=3) groups. Significant up and down-regulated proteins were enriched mainly for protein translation and proteasome 26s component subunits.

Conclusions:

Even though fatty acid oxidative phosphorylation is an efficient way to generate energy, reduced glucose metabolism still cannot be adequately compensated in $Nf1^{Myf5}$ muscle, and $Nf1^{Myf5}$ mice still suffer from energy deprivation indicated by hyperactivation of AMPK/Pparg/Pgc1α signaling to stimulate mitochondrial biogenesis and oxidative phosphorylation. It results in a reduction in energy expenditure processes, such as protein synthesis (as indicated by decreased mTOR activity) and increased energy production activity, such as protein degradation (represented by increased expression of the proteasome 26s component subunits). This may explain the reduction of muscle and white adipose mass in $Nf1^{Myf5}$ animals. With the ongoing energy deficiency cannot be covered. Thus these knockout mice suffered more and more and finally died around 22 weeks. How *Nf1* regulates fiber type, and metabolic transformation needs to be understood in the following studies.

4.6 $Nf1^{Myf5}$ muscle phenotype was regulated in Nf1/Ras/ERK independent way.

4.6.1 Hyperactivation of Ras-ERK1/2 activity was only detected in $Nf1^{Myf5}$ primary myoblast instead of $Nf1^{Myf5}$ muscle tissue.

Neurofibromin functions as a GTPase activator, which means it is a negative regulator of Ras-ERK signaling. Numerous papers have shown that mutations of *the Nf1* gene will lead to hyperactivation of ERK pathway in different biological contexts[146,147]. Considering all the phenotypes that were obtained from $Nf1^{Myf5}$ skeletal muscle, then the next question is whether this change occurs in the Nf1-Ras-ERK signaling dependent manner in muscle context. Therefore, the pERK1/2 antibody was used to detect p-ERK1/2 activity by Western blot. In general, p-ERK2 was much stronger than pERK1 in skeletal muscle lysate.

Interestingly, for both pERK1 and pERK2, no difference was detected between $Nf1^{Myf5}$ and control TA muscles (Fig. 4.12A). This was unexpected, however *Nf1* expression in muscle progenitors, primary myoblasts and myotubes had indicated that *Nf1* was expressed only before muscle differentiation (Fig. 4.1). For skeletal muscle tissue, the expression level of *Nf1* was very low, so its function on Ras/ERK signaling may be ignored. It can also explain why there was no change in ERK activity. In addition, the $Nf1^{flox}HSA^{cre}$ mouse model that specifically knock out Nf1 in mature muscle tissue also did not show any muscle phenotype[148], indicating that *Nf1* does not play a role in mature muscle tissue. Except for this mouse model, Pax7-creER(T2) induced *Nf1* knockout in adult mouse satellite cells did not result in any muscle phenotype, it also supported the negligible function of *Nf1* in mature skeletal muscle

stem cells, at least in the time frame analyzed in this study[149]. This indicates that *Nf1* may play a role during myogenesis, in myogenic progenitors. ERK1/2 signaling activity was measured on fresh FACS sorted P7 muscle progenitors. The purity of $Pax7^{+}$ cells after FACS was approximately 94% (not shown here); This was consistent with the purity of FACS sorted muscle progenitors from other research groups[130,150]. All positive cells of Pax7, pERK1/2, and DAPI were used for relative fluorescence intensity measurements. A significant increased ERK1/2 phosphorylation was detected in P7 $Nf1^{Myf5}$ muscle progenitors (Fig. 4.12B).

Conclusions:

Data from this section showed that the myopathy caused by fiber type and a metabolic shift was independent of Nf1/Ras/ERK1/2 signaling in muscle fibers. It was confirmed by a mouse model of *Nf1* knockout in mature muscle tissue, and also there was no change in ERK signaling activity in $Nf1^{Myf5}$ muscle tissue. It suggests that *Nf1* can only regulate biological processes before progenitors differentiation. In short, the muscle phenotype suffered by $Nf1^{Mf5}$ mice was derived from undifferentiated muscle progenitors or myoblasts, rather than directly from the function of *Nf1* in mature muscle fibers. Therefore, subsequent regulation ways were focused on muscle progenitors.

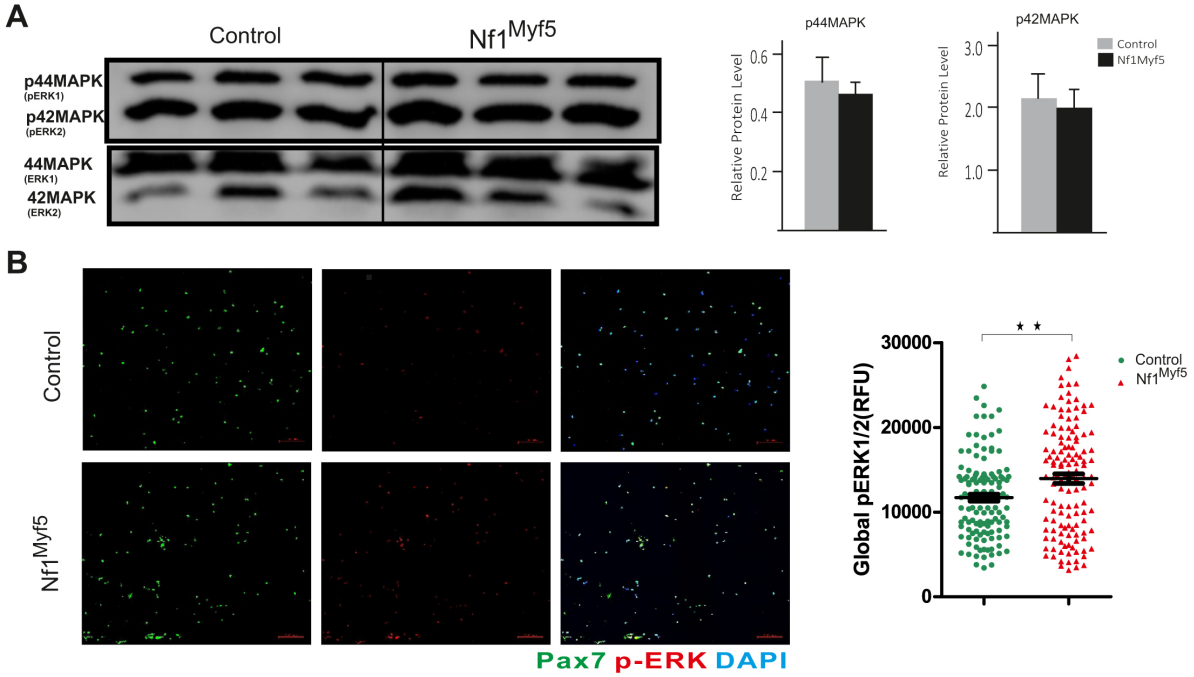

Figure 4.12 Muscle phenotype of $Nf1^{Myf5}$ mice is Ras/ERK1/2 independent.

A No difference for ERK signaling in $Nf1^{Myf5}$ and control TA muscle. Protein isolated from p21 TA muscle was used, primary antibodies against pERK1/2 and ERK1/2 were used. Gray value for each blot bind was measured with ImageJ, and the relative protein level means the ratio between p-ERK and corresponding ERK. N=3; **B** Increased ERK signaling in $Nf1^{Myf5}$ muscle progenitors. Cytospin p7 muscle progenitors co-stained with Pax7 and pERK1/2. Relative fluorescence intensity was measured through ImageJ. N=4. 200 cells from each animal were measured from random pictures. Student-t-test was perfprmed. p**<0.01. Scale bar is 100 μm.

4.7 Nf1^{Myf5} mice have a depletion of muscle stem cell pool during postnatal muscle development.

4.7.1 Muscle progenitors' number decreased dramatically in Nf1^{Myf5} mice.

So far, all previous data still cannot explain the muscle phenotype suffered by Nf1^{Myf5} mice. As we deleted *Nf1* in *Myf5* expressing muscle progenitors, the behavior of these knockout muscle progenitors was checked in vivo. During post-natal muscle development, the number of muscle stem cells gradually decreases. At the first three weeks after birth, only a small population of muscle stem cells remains, which are the genuinely quiescent stem cells that can be retained in their stem cell pool to mediatemuscle damage repair[62].

Since Nf1 is a tumor suppressor gene, a higher proliferation rate and increased, Nf1^{Myf5} muscle progenitors were expected. Initially, only Ki67 with DAPI staining was used on the p21 whole hind limb muscle sections. Surprisingly, there was a dramatic reduction of Ki67 expression on Nf1^{Myf5} sections. For the control sections, approximately 50% of the cells were still in a proliferative state, but on the Nf1^{Myf5} sections, there were almost no proliferating cells left (Fig. 4.13A). A wide variety of cell populations exist in the skeletal muscle system. Then the next question is why these cells leave their cell cycle, and what are these cells?

To see the influence specific for muscle progenitors, cryosections were taken from the hind limbs of Nf1^{Myf5} and control mice. Immunostaining was performed for sections from a time series of whole hindlimb sections from E18.5, one week, two weeks, and three weeks until 12 weeks of adult mice. Specific target protein expression was detected by co-staining of the stem cell marker Pax7 and components of the muscle basement membrane, collagen type IV (ColIV) for stem cell location identification, and DAPI for nuclear detection. Pax7 positive cells combined with their correct location and positive nuclear staining were treated as muscle stem cells. After counting and statistical analysis, at E18.5, a significant increase in the number of muscle progenitors in knockout animals was observed, with an average of 15.3 muscle progenitors per 100 myotubes, compared with that of 10.8 in control animals. Interestingly, the total progenitors' number decreased in both Nf1^{Myf5} and control muscle after birth over time, but for Nf1^{Myf5} muscle, this depletion was faster than the control muscle. At one week after birth (P7), there was no stem cell number difference detected between knockout and control animals. Both have around ten progenitors per 100 myotubes. From two weeks onwards, the number of progenitors in the Nf1^{Myf5} group reduced dramatically, with about six stem cells per 100 myotubes, until at postnatal three weeks when most of the stem cells are in a quiescent state (Fig. 4.13B).

To understand why muscle progenitors number reduced in Nf1^{Myf5} mice, Co-staining of Pax7, Ki67, ColIV, and DAPI was performed, combined the stem cell marker expression with their

cellular location to observe the proliferative capacity of $Nf1^{Myf5}$ $Pax7^{+}$ progenitors. However, co-staining of the proliferation markers Ki67 and Pax7 showed a significant decrease in proliferation rate in $Nf1^{Myf5}$ muscle progenitors compared to control animals (Fig. 4.13C, D). It implied that the properties of progenitors had changed dramatically before and after birth. In addition, MyoD was co-stained with Ki67 and DAPI, but unfortunately, with the limitation of antibody, it never worked. Literature showed that in the embryo stage, muscle progenitors are in a proliferative state to expand the muscle stem cell pool[151]. The muscle stem cell niche formed before birth, and then these muscle progenitors will enter their niche and gradually become quiescent. During this process, the number of muscle stem cells will decrease dramatically until p21[151]. Immunostaining data also showed that even in 12 weeks of adult muscle tissue, there was still a small number of progenitors in a proliferative state. Immuno-staining data suggests that the effect of *Nf1* deletion on muscle progenitors may be due to muscle stem cell niche. Before the formation of muscle stem cell niche, *Nf1* deletion leads to cells in a more activated state, and then they were more difficult to enter their stem cell niche, thus leading to a gradual loss of muscle stem cells during postnatal muscle development.

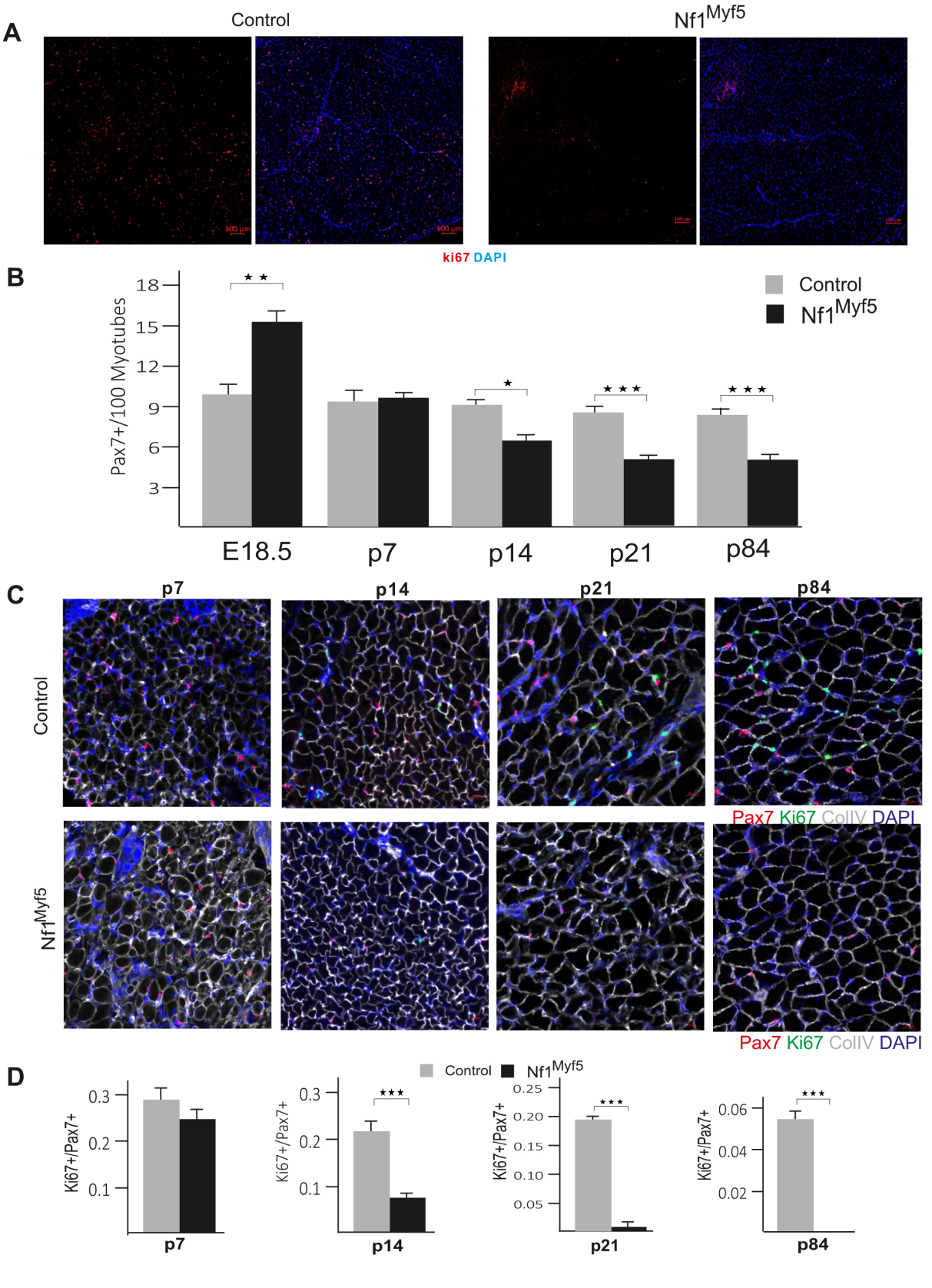
A
Control
Nf1Myf5
ki67 DAPI
B
Pax7+/100 Myotubes
18
15
12
9
6
3
Control
Nf1Myf5
E18.5
p7
p14
p21
p84
C
p7
p14
p21
p84
Control
Nf1Myf5
Pax7 Ki67 ColIV DAPI
Pax7 Ki67 ColIV DAPI
D
Control
Nf1Myf5
Ki67+/Pax7+
p7
p14
p21
p84

Figure 4.13 Nf1^{Myf5} mice suffered from the depletion of muscle stem cells pool during postnatal muscle development.

A Global reduction of proliferation rate in Nf1^{Myf5} muscle tissue. Sections were taken from p21 hind limbs Ki67 was used as a proliferation marker, and DAPI was used to identify nuclear. **B** A stem cell depletion caused by their decreased proliferation rate. Cryosections were taken from the time series development stage. Pax7 was used as a muscle stem cell marker, and Ki67 was used as a proliferation marker, ColIV was used to identify the location of muscle progenitor cells and DAPI for nuclear. Imaging was performed with LSM700 confocal microscope on whole hindlimb sections. The image was processed, and targeted cells were counted with ZEN software. GraphPad was used to generate a graph. N=4 animals. Student-t-test was used for statistical analysis. p*<0.05. p**<0.01. P***<0.001. A, scale bar is 100 µm. C, scale bar is 20 µm.

4.7.2 Nf1^{Myf5} muscle progenitors have a stronger quiescent signature.

Following such dramatic change of Nf1^{Myf5} postnatal muscle stem cell numbers, to elucidate the underlying mechanism, more experiments need to be performed on muscle stem cells. Considering the limitations of antibodies, the number of muscle stem cells and the number of mutant animals, thus further study of muscle stem cell properties, freshly isolated p7 muscle stem cells through FACS sorting were used, followed by cytospin and immunostaining of cells with specific markers to reflect the in vivo state of these cells. First, it is necessary to detect whether this cytospin and in vitro staining can be used to mimic the in vivo state of these cells, co-immunostaining of muscle stem cell marker Pax7, proliferation marker Ki67 and nuclear detector DAPI was performed to observe the expression level of Pax7 and their proliferation rate. FACS sorted cells were mainly composed of Pax7^{+} muscle stem cells (94%). Thus the relative fluorescence units for Pax7 were measured. Nf1^{Myf5} muscle stem cells have significantly higher Pax7 expression compared to control cells (Fig. 4.14A). In combination with published literature, to check whether signaling pathways involved in muscle stem cells quiescent and activation regulation got affected by *Nf1* deletion, with the limitation of the p-mTOR antibody for immunostaining, downstream of the mTOR signaling pathway, p-s6k was used for cytospin immunostaining. A severe reduction of the p-S6k level was detected in Nf1^{Myf5} muscle stem cells (Fig. 4.14B). In addition, the stem cell size of freshly sorted cells was also measured, and it showed a much smaller cell diameter in Nf1^{Myf5} muscle stem cells (Fig. 4.14C). This is supported by the literature that compared with cells inactivation state, quiescent muscle stem cells have lower pS6k/mTOR activity and also smaller cell size[152]. Protein isolated from muscle stem cells was used to test the p-p70s6k (Thr389) level with western blot. It also showed that the phosphorylation level of p70s6k was reduced from 0.8 to 0.38 in Nf1^{Myf5} muscle stem cells (Fig. 4.14D).

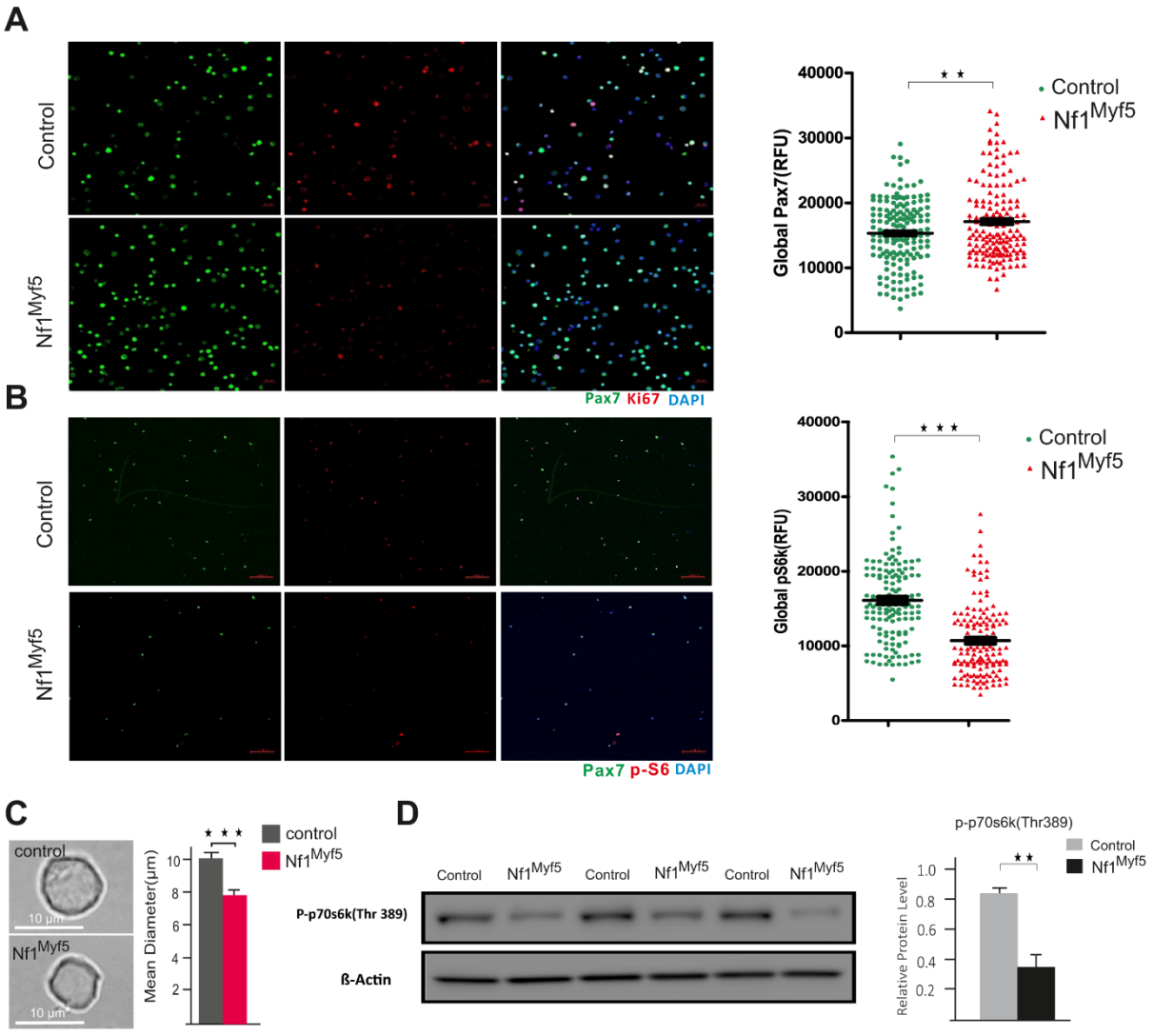

Figure 4.14 Nf1^{Myf5} muscle progenitor cells have a stronger quiescent signature.

A Nf1^{Myf5} progenitors showed increased Pax7 expression and reduced proliferation rate. p7 muscle from both forelimbs and hindlimbs was taken from Nf1^{Myf5} and control animals. After made tissue into single-cell suspension specific markers being used to identify muscle stem cells followed by FACS. Freshly sorted cells were taken for cytospin immediately followed by co-immunostaining for Pax7/Ki67/DAPI. After mounting slides imaging with confocal LSM700. Keep all setting the same between control and Nf1^{Myf5} group. The relative fluorescence unit was measured by Image J with randomly chosen pictures. N=4 animals. **B** Reduced pS6k level in Nf1^{Myf5} muscle progenitors. Co-immunostaining of Pax7/pS6k/DAPI. **C** Cell size reduction of Nf1^{Myf5} progenitors. Freshly FACS sorted progenitors were fixed and imaging with a light microscope. N=3 animals and 200 cells from each animal were measured. **D** Reduced p-p70s6k level in Nf1^{Myf5} muscle progenitors. Protein was isolated from p7 freshly FACS muscle stem cells. The primary antibody against p-p70s6k (Thr389) was used to detect mTOR signaling activity. β-actin was used as a housekeeping protein. The gray value was measured for each target band, and they were normalized with their housekeeping band. N=3 for each animal group. Student-t-test was used for statistical analysis. p**<0.01. P***<0.001. A, scale bar is 20 μm. B, scale bar is 100 μm.

Conclusions:

Nf1^{Myf5} skeletal muscle has more muscle progenitors before birth, but *Nf1* deficiency leads to the depletion of muscle stem cells during postnatal muscle development. The p7 Nf1^{Myf5} muscle stem cells have higher stem cell marker expression and lower mTOR signaling activity. Putting all of these data together, it implied that p7 Nf1^{Myf5} muscle stem cells showed a much stronger shift towards the quiescent state. This may explain why the number of muscle stem cells in Nf1^{Myf5} mice are reduced during postnatal development. More experiments are required to examine this conclusion.

4.8 Nf1^{Myf5} muscle progenitors keep a different property in vivo and in vitro.

4.8.1 Higher proliferation rate and lower differentiation ability of Nf1^{Myf5} muscle progenitors.

Previous data showed that p7 Nf1^{Myf5} muscle progenitors have decreased proliferation rate in vivo and more quiescent signature freshly upon isolation. To observe whether these cells can still retain this property during in vitro cell culture. Fresh FACS-sorted muscle stem cells were immediately cultured with Matrigel-coated coverslips in a 48-well plate with proliferation medium. After 48 hours, the cultured cells were washed with PBS, then fixed and immunostained. Interestingly, even without staining, increased numbers of Nf1^{Myf5} muscle progenitors can be observed. Co-staining of Ki67/MyoD and Pax7/Ki67 have also confirmed this phenotype. For cultured Nf1^{Myf5} muscle progenitors, co-staining of myoblast marker MyoD, and proliferation marker Ki67, the proliferation rate of Nf1^{Myf5} progenitors increased from 0.58 to 0.82 (Fig. 4.15A). Co-staining of stem cell marker Pax7 with Ki67 showed the proliferation rate of these stem cells increased from 0.41 to 0.62 (Fig. 4.15B). Therefore, it was confirmed that Nf1^{Myf5} muscle progenitors lost their in vivo characteristics during the in vitro cell culture, and they turned to a different manner. Followed by an increased proliferation rate in Nf1^{Myf5} progenitors, the differentiation ability of these cells was examined.

Due to the different proliferation rates of muscle progenitors, to avoid the effect of cell number on cell differentiation, the same number of fresh FACS-sorted muscle progenitors were seeded onto Matrigel-coated coverslips in a 48- well plate and allowed them to attach with the coverslips overnight with proliferation medium. The differentiation medium was changed the next day and waiting for another 48 hours for cell differentiation. Primary antibodies against myosin heavy chain (MF20) and myoblast marker MyoD were used for co-immunostaining. It seems that even though the differentiation medium was changed, Nf1^{Myf5} muscle progenitors

were still in proliferation state because it has more DAPI positive nuclei. MF20 staining showed that in control muscle progenitors, after 48 hours differentiation, multinucleated myotubes were observed.

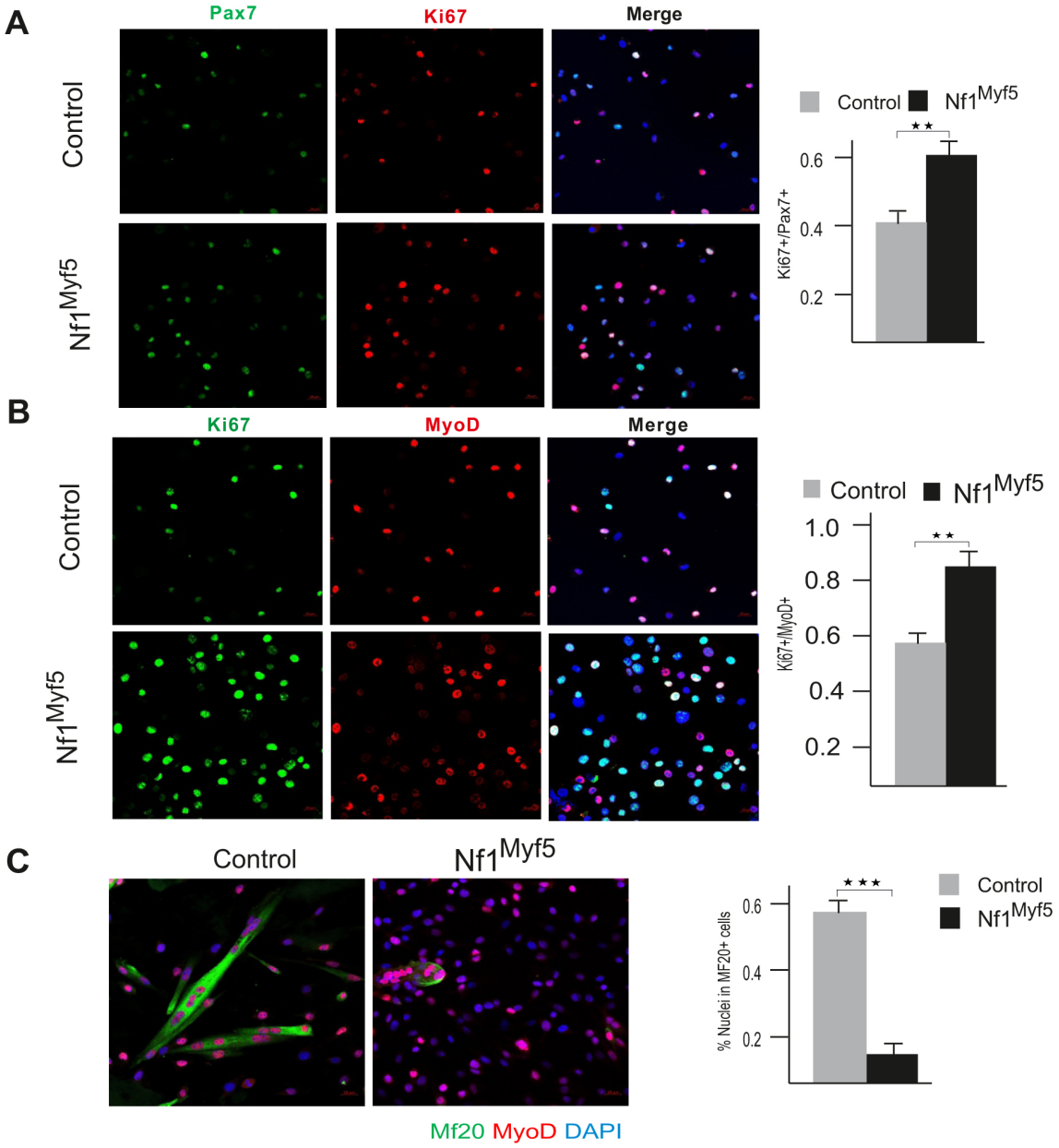

Figure 4.15 Higher proliferation rate and lower differentiation ability of Nf1^{Myf5} muscle progenitors. **A**, **B** Higher proliferation rate of Nf1^{Myf5} FACS-isolated myogenic progenitors. All muscles from both forelimbs and hindlimbs of p7 Nf1^{Myf5} and control animals were used. After 48 hours of culture, cells were fixed, and the primary antibody against Ki67 and MyoD were used to identify the proliferation rate of Nf1^{Myf5} myoblast. After 24 hours of culture, Pax7 and Ki67 co-immunostaining was performed to see the proliferation rate of Nf1^{Myf5} muscle progenitors. **C** Decreased differentiation ability of Nf1^{Myf5} muscle progenitors. N=4 animals, each condition three wells were performed. Cells were counted with Zen software, and GraphPad was used for graph and statistical analysis. Two tailed student-t-test was used for statistical analysis. p**<0.01. P***<0.001. Scale bar is 20 µm

In contrast, the Nf1^{Myf5} muscle progenitors, even with more cells, their differentiation was still in the initial state. Counts for nuclear with myosin heavy chain positive staining showed that a differentiation index of around 0.58 in control muscle progenitors, but for Nf1^{Myf5} muscle progenitor cells, the rate was only around 0.18 (Fig 4.15C). In summary, the data from this section showed that once Nf1^{Myf5} muscle stem cells left their in vivo environment, it was impossible to maintain their in vivo properties. Some influencing factors from their living environment may play a dominant role.

4.8.2 In vitro property of Nf1^{Myf5} muscle progenitors was Nf1 regulated Ras/ERK1/2 signaling dependent.

Due to Nf1^{Myf5} muscle progenitors have different properties in vivo and in vitro, the following experiments were designed to understand how they were regulated. First, signaling involved in promoting the proliferation rate of Nf1^{Myf5} muscle progenitors was identified. Owing to the limitations of Nf1^{Myf5} animals, especially the low number of muscle progenitors obtained by FACS, and high demands of muscle progenitors cultured in vitro, rimary myoblasts isolated by the pre-plating method were used. After several rounds of pre-plating, the purity of primary myoblasts was identified by co-immunostaining of stem cell marker Pax7, myoblast marker MyoD and nuclear detector DAPI, only Pax7 positive, only MyoD positive and Pax7/MyoD double-positive cells were considered as primary myoblasts. The ratio between primary myoblasts and the total number of nuclei was treated as the purity of primary myoblasts. After counting, data showed that the purity of primary myoblasts in the control group was 89%, and that was even higher in the Nf1^{Myf5} group. This was sufficient for the following experiments to demonstrate the molecular mechanism of *Nf1* function in muscle progenitors. Three animals were used for Nf1^{Myf5} and control, respectively. The first experiment with these primary myoblasts was to culture them in proliferation medium and differentiation medium to confirm the effect of *Nf1* on myoblast proliferation and differentiation. Co-staining of MyoD, Ki67, and DAPI was performed to detect the proliferative rate. Each Ki67, MyoD double-positive cells, was regarded as a proliferating myoblast; the proliferation rate of the two groups was calculated. Compared to control cells, the proliferation rate from *Nf1* deleted cells increased from around 60% to more than 80%, which also confirmed a higher proliferation rate of FACS sorting Nf1^{Myf5} muscle progenitors (Fig. 4.16A).

For the underlying signaling mechanism, the first effect caused by *Nf1* deletion was the hyper-activation of ERK1/2 signaling (Fig. 4.12C). Therefore, ERK signaling was blocked by its upstream pMEK1/2 inhibitor U0126. Literature showed that stronger ERK1/2 promotes C2C12

myoblast proliferation and blocks its differenatiation[153]. In differentiation medium, primary myoblasts gradually leave the cell cycle. For vehicle treatment cellsthere was still a significant number of cells (16%) in the proliferative state for $Nf1^{Myf5}$ primary myoblasts after 48 hour culture in differentiation medium. Compared to the control, $Nf1^{Myf5}$ primary myoblasts have a significantly higher proliferation rate, and the loss of *Nf1* leads to an increase in the proliferation rate in the differentiation medium from 3% to 16%. Differentiation staining with Desmin showed that only 5% of the cells in $Nf1^{Myf5}$ myoblasts were Desmin positive, while in control cells, it was about 78%.

Interestingly, when the MEK1/2 inhibitor U0126 was added to the medium, after 48 hours differentiation, the proliferating cells in both groups were reduced to 2%, especially in $Nf1^{Myf5}$ cells that was dropped from 16% to 2%, and the differentiation index increased from 5% to 74%. It implied that U0126 could ultimately rescue the phenotype caused by *Nf1* deletion in primary myoblasts (Fig.4.16B). This indicated that in vitro, Nf1 controls muscle progenitors proliferation and differentiation in a Ras-ERK1/2 signaling dependent way. *Nf1* deletion leads to hyperactivation of ERK1/2, and stronger ERK1/2 signaling maintains primary myoblasts in the cell cycle, thereby blocking its differentiation. However, this still can not explain the phenomenon that in vivo $Nf1^{Myf5}$ progenitor numbers and proliferation rates are decreased, and they show stronger quiescent stem cell signature. The dramatic difference between in vivo and in vitro showed the importance of the environment for cell properties. So far, primary myoblasts are not suitable for in vitro mimic experiments. New signaling pathways from the muscle stem cells niche need to be found and apply for in vitro cell culture.

Conclusions:

$Nf1^{Myf5}$ progenitors show opposite behavior in vivo and in vitro. Earlier quiescence was observed in vivo; conversely, once taken out of their in vivo environment, $Nf1^{Myf5}$ progenitors showed an increased high proliferation rate and a significant reduction of differentiation ability compared to the control cells. This phenomenon is regulated by hyperactivation of Ras/ERK1/2 signaling caused by *Nf1* deletion. It means that the function of *Nf1* in myocyte regulation is the highly dependent on the cellular environment.

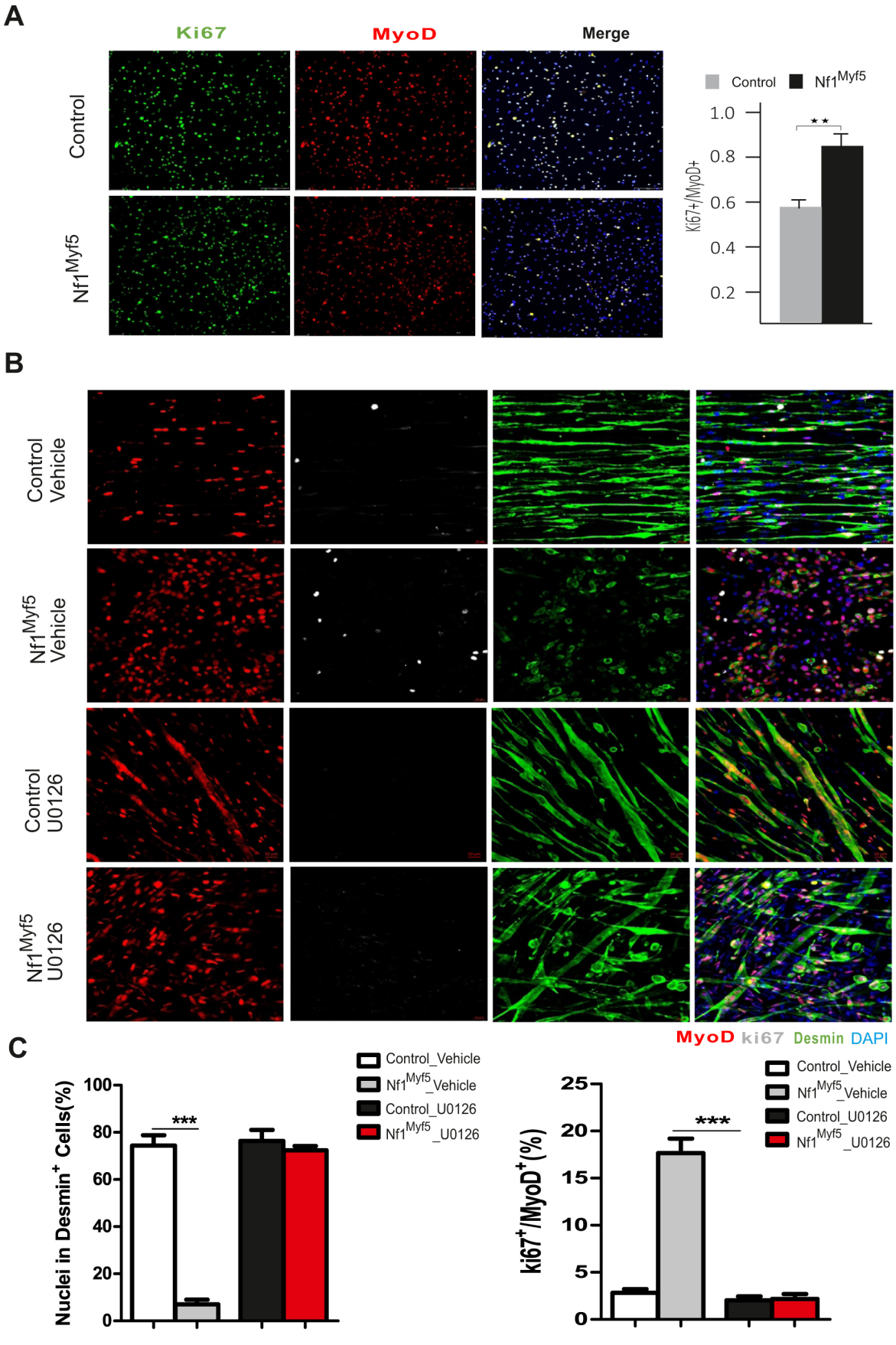
A
Ki67
MyoD
Merge
Control
Nf1Myf5
Control
Nf1Myf5
1.0
0.8
0.6
0.4
0.2
Ki67+/MyoD+
**
B
Control Vehicle
Nf1Myf5 Vehicle
Control U0126
Nf1Myf5 U0126
C
MyoD ki67 Desmin DAPI
Control_Vehicle
Nf1Myf5_Vehicle
Control_U0126
Nf1Myf5_U0126
Nuclei in Desmin+ Cells(%)
100
80
60
40
20
0
***
ki67+/MyoD+(%)
25
20
15
10
5
0
***

Figure 4.16 In vitro property of Nf1^{Myf5} muscle progenitors was Nf1 regulated Ras/ERK1/2 signaling dependent.

A Higher proliferation rate of Nf1^{Myf5} primary myoblast. **B** Increased proliferation rate and decreased differentiation ability was Ras/ERK1/2 signaling dependent. Primary myoblast from hindlimbs of p21 control and Nf1^{Myf5} animals were isolated by pre-platting protocol. Cells were cultured in proliferation and differentiation medium, immunostaining of Ki67/MyoD/DAPI was used for proliferation rate detection. After changed to differentiation medium, MEK1/2 inhibitor U0126 was also added. The same amount of DMSO was used as Vehicle Control. After imaging with confocal LSM700 cells were counted with ZEN software and GraphPad was used for graph and statistical analysis. Two tails student-t-test was used for statistical analysis. p**<0.01. P***<0.001. A, scale bar is 100 μm. B, scale bar is 20 μm.

4.9 P7 Transcriptome analysis indicates that Nf1^{Myf5} muscle progenitors shifted to quiescence earlier.

4.9.1 Increased quiescent and decreased activation relative genes expression in Nf1^{Myf5} muscle progenitors.

Nf1 deletion results in excessive activation of Ras/ERK1/2 signaling, thus helping to increase the rate of proliferation and reduce the ability to differentiate for cells in vitro culture. However, why it works oppositely in vivo still needs to be understood. To answer this question and also have an essential impression of how this regulation works in vivo, transcriptome analysis with fresh FACS sorted p7 muscle progenitors from control and Nf1^{Myf5} mice was performed. Due to the limitation of muscle stem cell numbers, both forelimbs and hind limbs were used. The entire transcriptome gene list from control and Nf1^{Myf5} progenitors was submitted to GSEA (Gene Site Enrichment Analysis) for GO (Gene Ontology) and KEGG pathway analysis to avoid the bias caused by statistical analysis.

All details about these genes were then checked, and a total of 38 activating genes were enriched, including sarcoplasmic/endoplasmic reticulum calcium ATPase (Atp2a1, Atp2a2), Myogenin (Myog), Myosin heavy chain 3 (Myh3) in control muscle progenitors, which showed Nf1^{Myf5} muscle progenitors had reduced activation signature compared to control cells. All RPKM from these genes were obtained, for better visualization, all of these genes were transformed with Log2[RPKM]. After transformation, their expression levels are shown in the heatmap (Fig. 4.17A). Conversely, a large cluster of genes was enriched in Nf1^{Myf5} muscle progenitors were extracellular matrix (ECM) components, which means these muscle progenitors expressed more ECM component genes than control cells. As a major constitutive of the muscle stem cell niche, these ECM components play a critical role in the steady-state maintenance of muscle stem cells. Except for supplying scaffolds and giving biomechanical support, including mechanical transduction and stiffness of muscle stem cells, many critical signaling pathways are also intermediate by the interactions between muscle stem cells and

ECM[154]. The stage-specific role of ECM components has been identified during muscle development[95]. Here, the heatmap showed ECM components, including collagen family such as *ColV*, *ColVI*, and *Tnc* expression is significantly increased in Nf1^{Myf5} muscle progenitors, which implied higher quiescent signature in these cells. Besides, increase expression of stem cell imprinted genes was also observed in Nf1^{Myf5} muscle progenitors (Fig. 4.17B). *Pw1/Peg3* has been shown to keep muscle stem cells in quiescent, and also suppress mitochondrial activity to regulate satellite cell metabolism[85], significantly increased expression of *Peg3* in Nf1^{Myf5} muscle progenitors was observed. Furthermore, increased expression of *Cdkn1c*, a cell cycle negative regulator of suggests a reduction of proliferation rate in Nf1^{Myf5} muscle progenitors (Fig. 4.17B).

Selected genes representative for muscle progenitor quiescence and activation were chosen for qPCR expression confirmation analysis. Nf1^{Myf5} muscle progenitors have higher quiescent genes expression and lower activation genes expression in agreement with RNAseq analysis (Fig. 4.17C). Combined with the recent immunostaining data, Nf1^{Myf5} p7 muscle progenitors showed a quiescent signature compared to control cells. Combined with the recent immunostaining data, Nf1^{Myf5} p7 muscle progenitors showed a quiescent signature compared to control cells. The genes labeled for MyoD target genes were highly enriched in control muscle progenitors (Fig. 4.17D). Putting these transcriptome data together, even though Nf1 regulated cancer signaling was indicated by KEGG analysis, this does not appear to play a dominant role in the biological background of muscle stem cells, at least if these cells are in vivo within their stem cell niche.

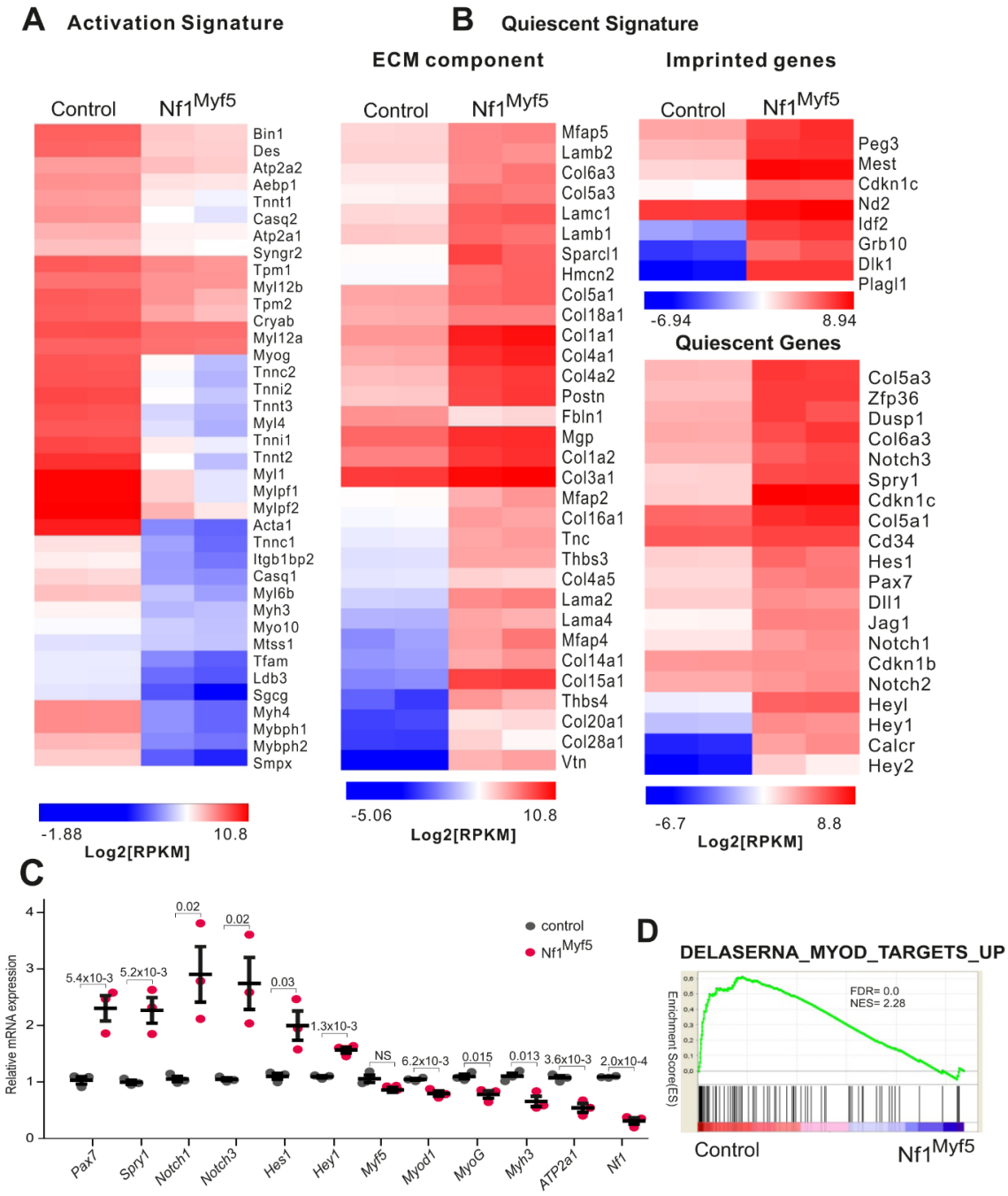

Figure 4.17 Increased quiescent and decreased activation genes expression in Nf1Myf5 muscle progenitors.

A, B Decreased Activation genes, and Increased ECM component, imprinted and quiescent genes expression in Nf1^{Myf5} muscle progenitors. **C** qPCR confirmation of RNAseq analysis. **D** MyoD target genes were enriched in Control muscle progenitors. Muscle progenitors isolated from p7 Nf1^{Myf5} and Control forelimbs and hindlimbs by FACS. N=2 for RNAseq analysis and N=3 for qPCR confirmation. DEseq 2 for differential gene expression analysis. Gene list was submitted to GSEA for GO and KEGG analysis. Log2[RPKM] was used for the heatmap, and a heat map was generated from R studio with the package of ggplot2. Two tails student-t-test was used for statistical analysis. p*<0.05 p**<0.01 P***<0.001

4.9.2 Metabolism shut down of Nf1^{Myf5} muscle progenitors.

Like all other cell types，muscle progenitor cells demand energy expenditure to perform the necessary reactions to maintain cell homeostasis. Different cell states hpwever strongly alter their metabolic requirements. It is clear that for quiescent, proliferating, and differentiating muscle stem cells, their demand for energy production are also very different. Proliferating and differentiating muscle stem cells need to produce a tremendous amount of biomass, such as nucleotides, phospholipids, and proteins, to meet the requirement of rapid cell division and growth[155]. The previous data showed that Nf1^{Myf5} muscle progenitors acquired a much stronger quiescent signature. Thus the metabolism processes of these cells were also examined in the RNAseq data. Subsequently, the enriched KEGG pathway for significantly down-regulated genes was checked. This time, the first one appeared was the metabolic pathway, which has 232 genes involved. Under this KEEG term, the sub-terms include glycolysis/gluconeogenesis and oxidative phosphorylation suggesting a global downregulation of metabolism for *Nf1* knockout cells (Fig. 4.18A). Hereafter, all these single genes expression level was checked, heat map based on original RPKM for each gene with log 2 transformation was used for visualization. There were 20 glycolytic-related genes, and 29 oxidative phosphorylation genes (components of the mitochondrial complex and enzymes for TCA cycle) were enriched, respectively. These Glycolysis/Gluconeogenesis genes include Phosphoglycerate Kinase1 (*Pgk1*), a glycolytic enzyme that catalyzes the conversion of 1,3-diphosphoglycerate to 3-phosphoglycerate. Lactate dehydrogenase A (*Ldha)* is one of the components Lactate dehydrogenase A, which functions to catalyze the inter-conversion of pyruvate and L-lactate accompanied by the mutual conversion of NADH and NAD+. The enolase 3 (*Eno3*) muscle isoenzyme catalyzes the reversible conversion of 2-phosphoglycerate to phosphoenolpyruvate. Triosephosphate isomerase (*Tpi1*) can be used to catalyze the isomerization of glyceraldehyde 3-phosphate (G3P) and dihydroxyacetone phosphate (*Dhap*) in glycolysis and gluconeogenesis. Phosphoglycerate mutase (*Pgam*), which catalyzes the internal transfer of a phosphate group from C-3 to C-2, resulting in the conversion of 3-phosphoglycerate (3PG) to 2-phosphoglycerate (2PG) through a 2,3-bisphosphoglycerate intermediate. Besides, enzymes like Glyceraldehyde 3-phosphate dehydrogenase (*Gapdh*), AldolaseA (*Aldoa*), Dihydrolipoamide S-Acetyltransferase (*Dlat*), 6-phosphofructokinase muscle type (*Pfkm*), Pyruvate dehydrogenase kinase (*Pdk*), Aldehyde Dehydrogenase3 (*Aldh3a*) and Alcohol Dehydrogenase7 (*Adh7*) were also significantly down-regulated in Nf1^{Myf5} muscle progenitors (Fig. 4.18B). It implied that Nf1^{Myf5} muscle progenitors have a stronger quiescent signature and decreased proliferation rate. Therefore they also reduced the supply for biomass with reduced glycolysis process.

It has been documented that quiescent muscle stem cells prefer to use fatty acid to pyruvate oxidation to obtain energy. Therefore, genes involved in fatty acid metabolism were also checked. For instance, fatty acid-binding protein4 (*Fabp4*), cluster of differentiation 36 (*Cd36*), carnitine palmitoyltransferase 1B (*Cpt1b*), Lipase E (*Lipe*), enoyl-CoA Hydratase 1 (Ech1), Acetyl-CoA Acyltransferase 2 (*Acaa2*), acyl-Coenzyme A dehydrogenase (*Acadm*), Hydroxyaryl-CoA Dehydrogenase (*Hadh*) et al. However, for these genes expression， there was no similar pattern such as globally up or down-regulated in $Nf1^{Myf5}$ muscle progenitors, so it was hard to say the impact of *Nf1* deletion on fatty acid metabolism. Contrary to expectations, genes component for the electron transport chain was highly enriched in control muscle progenitors, which revealed an overall reduced oxidative phosphorylation and electron transport chain component genes expression in *Nf1* knockout muscle progenitors. The electron transport chain is primarily a component of five protein complexes located on the inner mitochondrial membrane. The data pointed out that the *Nduf* family genes constitute for mitochondrial complex I, the *Sdh* family component of mitochondrial complex II, the *Uqcr* family for mitochondrial complex III, the *Cox* family for Complex IV were all significantly down-regulated in $Nf1^{Myf5}$ muscle progenitor cells (Fig. 4.18C, D). It implied that these progenitors might also have reduced oxidative phosphorylation activity.

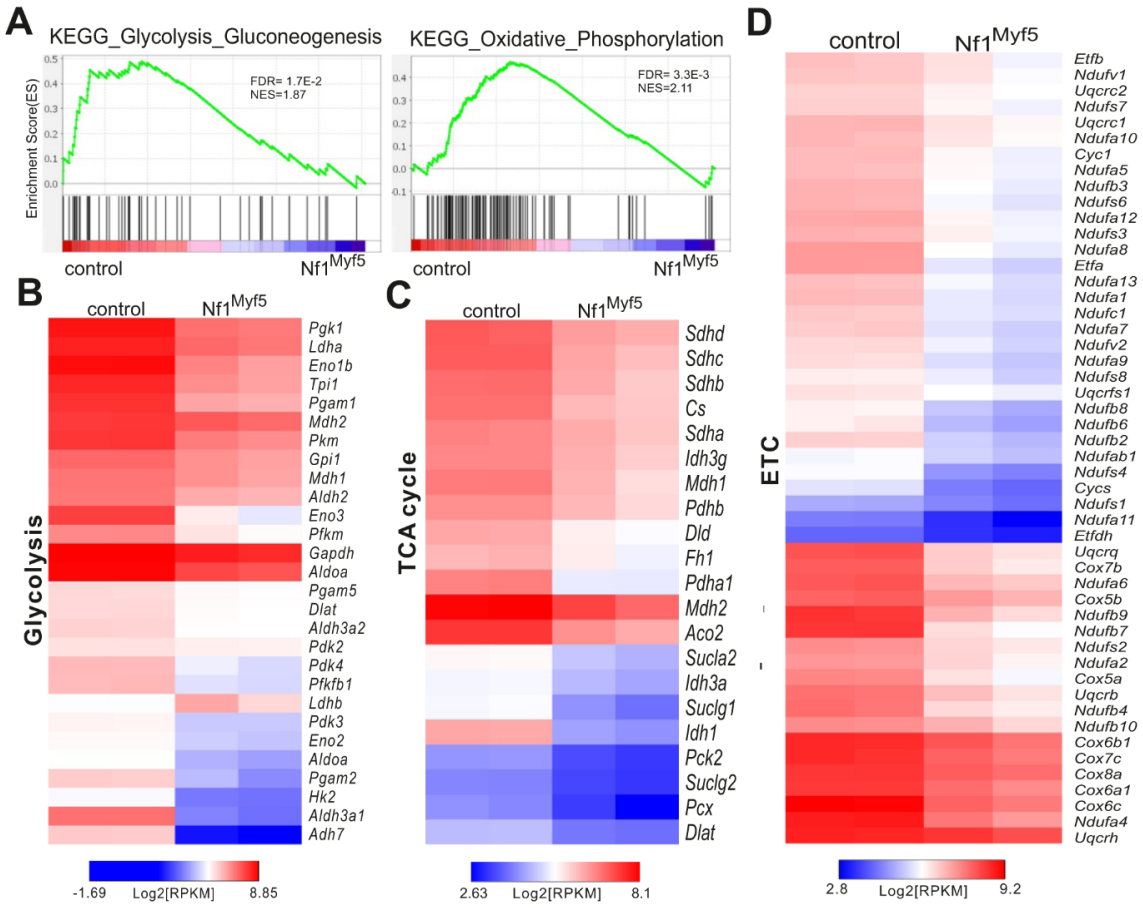

Figure 4.18 Metabolism shut down of Nf1^{Myf5} muscle progenitors.

A Enriched Glycolysis_Gluconeogenesis and Oxidative phosphorylation pathway in control muscle progenitors. **B** Decreased glycolysis genes expression in Nf1^{Myf5} muscle progenitors. **C, D** Reduced TCA cycle and electron transport chain component genes expression in Nf1^{Myf5} muscle progenitors. FACS-isolated muscle progenitors from p7 forelimbs and hindlimbs were used for RNA isolation. Gene list was submitted to GSEA for GO and KEGG analysis. Padj< 0.001 was considered significant. Log2[RPKM] was used for the heatmap, and a heat map was generated from R-studio with the package of ggplot2. N=2 for control and Nf1^{Myf5} animals.

4.9.3 Reduced glycolytic ability and decreased H4K16ac in Nf1^{Myf5} muscle progenitors.

Seahorse XF metabolic analysis method was used to see the real-time metabolic rate of these progenitors. The key parameters used to define glycolytic activity are Glycolysis, Glycolytic Capacity, and Glycolytic Reserve. Glycolysis means the procedure that glucose was converted into pyruvate. During the metabolic test, it refers to the ECAR value after the addition of a full amount of glucose. Glycolytic capacity refers to the maximum ECAR that was measured after oxidative phosphorylation was effectively turned off by the injection of Oligomycin, therefore the capacity of cells to generate energy through glycolysis will reach a maximum. The glycolytic reserve means the capability of cells to react to their energy demand, here it refers to the

stimulated ECAR caused by 2-DG injection. $Nf1^{Myf5}$ muscle progenitors have a significantly lower glycolysis rate, reduced glycolytic capacity, and also glycolytic reserve. Compared with control cells, the glycolysis rate reduced from 12 to 4 mPH/Min, glycolytic capacity reduced from 18 to 7 mPH/Min, and glycolytic reserve dropped from 7 to 2 mPH/Min (Fig. 4.19A). When the glycolysis rate was measured, the basal oxygen consumption rate (OCR) was also measured simultaneously. For $Nf1^{Myf5}$ muscle progenitors, the basal OCR was reduced from 20 to 15 pmol/Min with a p-value of 0.109 (Fig. 4.19B). Thus $Nf1^{Myf5}$ muscle progenitor cells ahow a reduction of glycolysis rate and a slight decrease of oxidative phosphorylation rate. This is in line with a decreased energy demand of quiescent cells.

Literature shows that metabolism reprogramming to glycolysis contributes to the activation of satellite cells, and it mainly depends on the glycolysis substrate NAD^+ level. As the activity of the H4K16 deacetylation enzyme Sirt1 is NAD^+ level regulated, then H4K16ac might be used as an indicator of progenitors status[2] caused by glycolysis rate reduction in $Nf1^{Myf5}$ muscle progenitors. Co-immunostaining was performed to check the in vivo muscle progenitors' H4K16ac modification level for p7 and 12 weeks of muscle tissue. First, Cytospin of P7 FACS sorted muscle progenitors were stained with Pax7 and H4K16ac antibody. A global relative fluorescence unit (RFU) of H4K16ac was measured in both Control and $Nf1^{Myf5}$ muscle progenitors. After statistical analysis, a significant reduction of H4K16ac progenitors was observed in $Nf1^{Myf5}$ mice. The RFU reduced from 16900 to 11000 (Fig. 4.19C). For double check, muscle cryosections from p7 and 12 weeks mice were also used for immunostaining. H4K16ac and Pax7 double-positive cells were counted. It also shows a severe reduction of double-positive cells in the $Nf1^{Myf5}$ muscle. For p7 mice, it was reduced from 38% to 12%, and for 12 weeks mice, it was reduced from 16.5% to 5.5% in $Nf1^{Myf5}$ cryosections (Fig. 4.19D). It suggests that *Nf1* deletion leads to a decreased glycolysis rate; thus, the NAD^+ level likely was increased. This signal was transformed to chromatin by decreased H4K16 acetylation modification, due to increased Sirt1 activity. This in turn likely suppresses satellite cell activation genes expression[2]. To see H4K16 acetylation on a genome-wide level, chipmentation analysis for H4K16ac was performed. After MACS2 peak calling, signals were enriched for 10kb up and downstream of the transcription start site (TSS). The enrichment plot showed $Nf1^{Myf5}$ muscle progenitors has a reduction of signal enrichment suggested a decreased transcription activity in these cells. Data also showed a global reduction of H4K16ac enrichment for myogenesis genes expression, thus promote p7 muscle progenitors into a quiescent state (Fig. 4.19E). Here reduced H4k16ac enrichment around *Myh3* was shown as an example (Fig. 4.19F).

Conclusions:

In this part, transcriptome data illustrated and double confirmed the former immunostaining results that p7 $Nf1^{Myf5}$ muscle progenitors have a stronger quiescent signature. With reduced activation genes expression, and increased quiescent genes expression, including ECM component genes, muscle stem cell imprinted genes, and signaling pathway for quiescence maintenance. The quiescent signature was also supported by the metabolism preference of $Nf1^{Myf5}$ progenitors with a severe reduction of glycolysis and a slightly decreased oxidative phosphorylation ability form both transcription level and real-time metabolism test. Besides, as glycolysis can also regulate gene expression with its substrate NAD^+ concentration, a global reduction of H4K16ac enrichment for up and downstream of transcription start site suggest through metabolism change the muscle progenitors activation genes expression was also down-regulated in $Nf1^{Myf5}$ mice. In summary, *Nf1* deletion drives muscle progenitors into quiescent state earlier during postnatal muscle development.

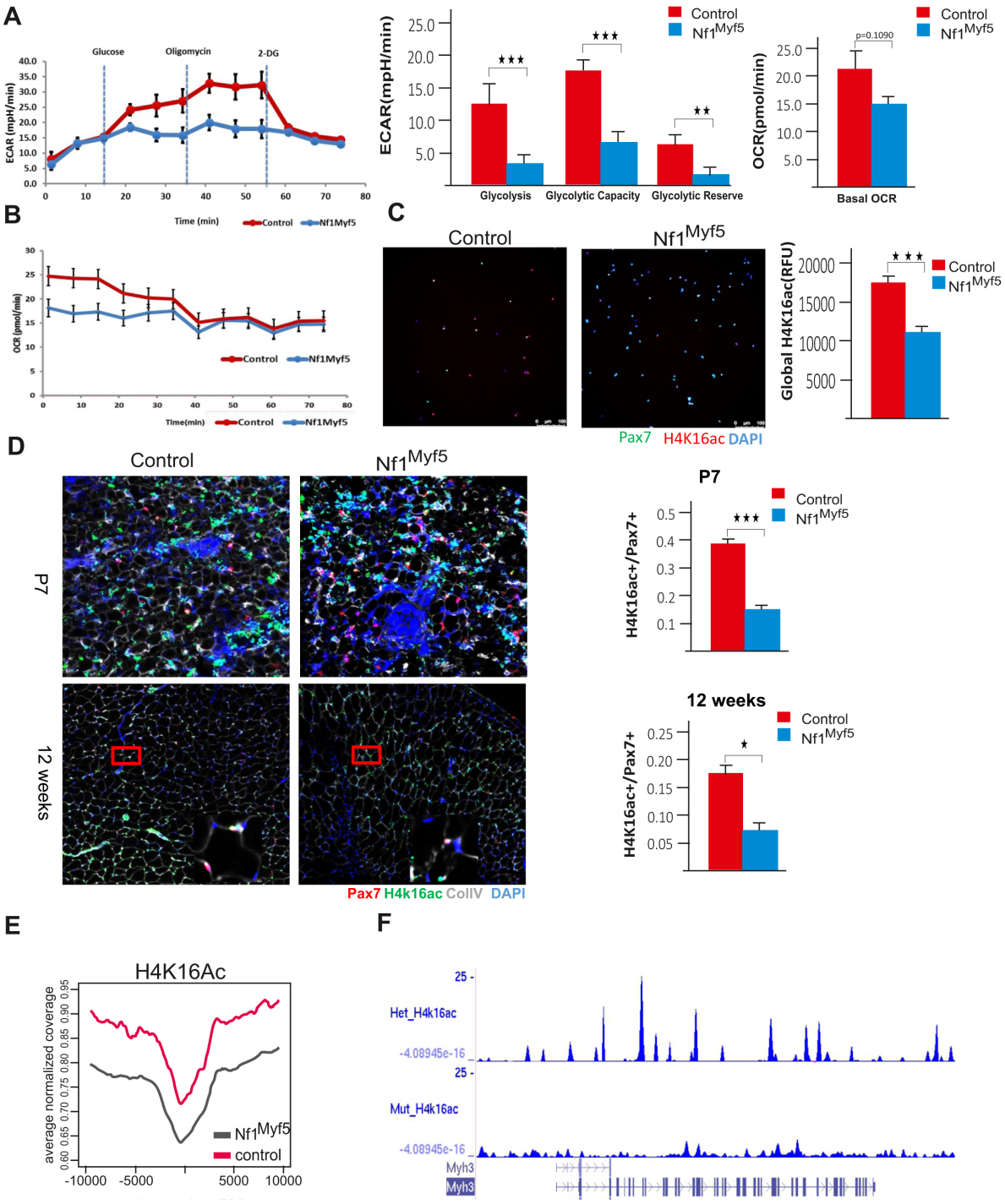

Figure 4.19 *Nf1* deletion leads to a reduction of both glycolysis and oxidative phosphorylation.

A,B Nf1^{Myf5} muscle progenitors decreased the glycolysis and oxidative phosphorylation activity. **C** Reduction of H4K16ac in *Nf1* knockout cells. **D** Decreased H4K16ac positive progenitors during postnatal development. **E, F** Reduced enrichment for DNA bound to H4K16 acetylation around Transcription Start Site (TSS). A, B Muscle progenitors FACS sorted from p7 mice. ECAR and OCR were measured with glycolysis stress kit. N=3 mice and 12 wells for each experiment. C progenitors were cytospin followed by co-immunostaining of H4K16ac and Pax7. N=3 mice and 200 cells/animal. D Sections from p7 and 12 weeks hindlimbs. Antibodies against Pax7, H4K16ac, ColIV were used. N=3 mice. E progenitors were fixed, followed by chipmentation with the H4K16ac antibody. N=2 mice. Student-t-test was used for statistical analysis. p*<0.05 p**<0.01 P***<0.001. C, scale bar is 100 µm. D, scale bar is 20 µm and 100 µm.

4.9.4 *Nf1* deletion lead to muscle progenitors epigenetic modification change to a more quiescent state.

4.9.4.1 Chromatin hypermethylation of Nf1^{Myf5} muscle progenitors.

Nf1^{Myf5} muscle progenitors showed stronger quiescent signature as well as decreased glycolysis rate. Muscle phenotype also showed a fiber type shift from fast glycolytic to slow oxidative fibers, and the decreased hypertrophy rate seems only influenced fast fibers. Besides, the expression of *Nf1* is extremely low on muscle tissue. Thus the curious point is whether muscle progenitors control the muscle phenotype in a certain way that it can be transferred to mature muscle fibers? With this idea, when checking the transcriptome data from muscle progenitors, the expression of a gene family named DNA methyltransferase was significantly increased in Nf1^{Myf5} muscle progenitors attracted the attention (Fig. 4.20A). It implied an increased methylation level of chromatin in Nf1^{Myf5} muscle progenitors. Followed by this, genomic DNA was isolated from Nf1^{Myf5} and Control muscle progenitors, and MeDIP sequencing was performed to check the methylation status in both groups. After analysis, there were 253 hypermethylated DMRs and 35 hypomethylated in Nf1^{Myf5} progenitors. 100 and 11 of them located within CpG islands, respectively (Fig. 4.20B).

Interestingly, for these hypermethylated sites, myosin light chain 1 (*Myl1*) which expressed in fast skeletal muscle and 6-phosphofructo-2-kinase/fructose-2,6-biphosphatase 1 (*Pfkfb1*) an activator of the skeletal muscle glycolysis pathway and an inhibitor of the gluconeogenesis pathway were observed (Fig. 4.20C). It suggested that the expression of these two genes in muscle progenitors might be decreased. Transcriptome data was checked, combined with qPCR analysis. The results showed that the expression of both *Myl1* and *Pfkfb1* dropped significantly in Nf1^{Myf5} muscle progenitors (Fig. 4.20C). DNA methylation is considered as a stable epigenetic modification mark, and it can be maintained for multiple cell divisions. During development and cell differentiation, this modification is relatively dynamic, but methylation patterns can be retained in the form of epigenetic memoryIn the case of Nf1^{Myf5} progenitors, it could be possible that the hypermethylation and decreased expression of *Myl1* and *Pfkfb1* in progenitors, once these cells fused with fibers, may also cause the decreased expression of these genes thus influence the fiber type and metabolism way of mature muscle fibers.

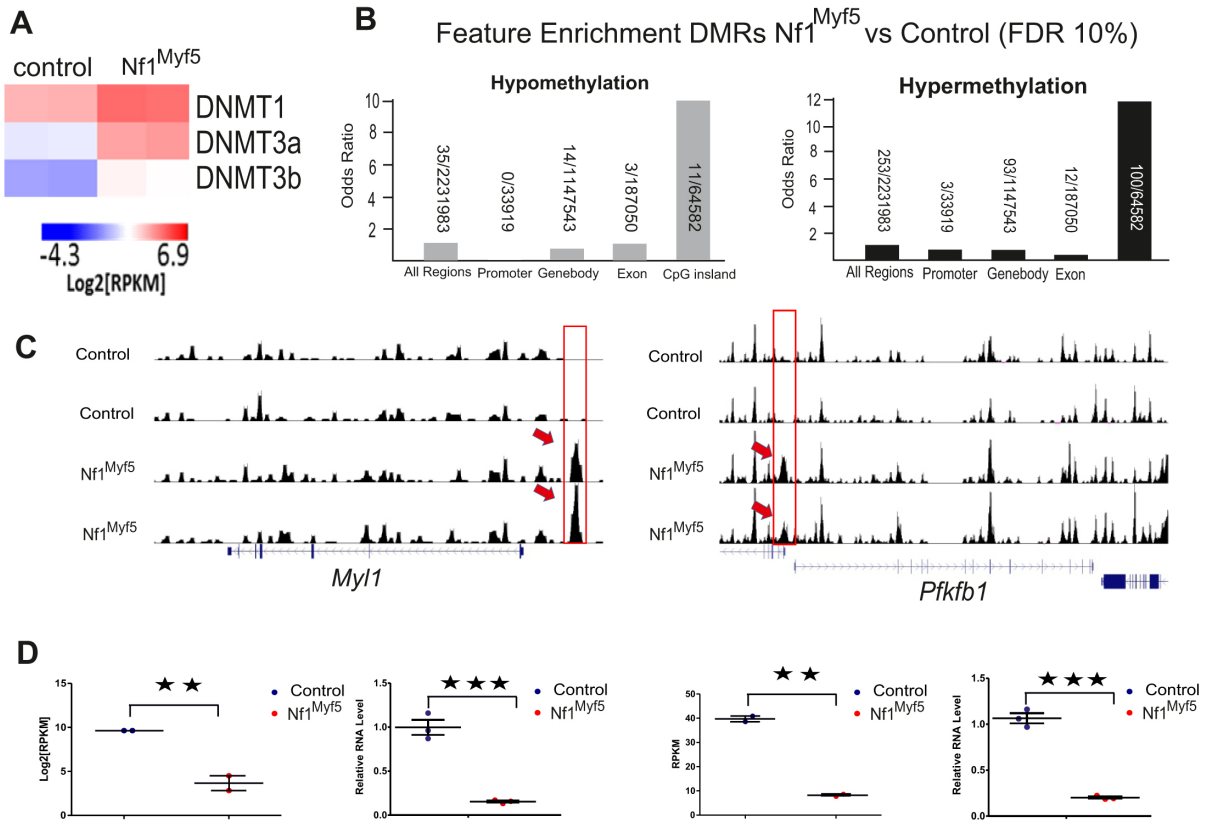

Figure. 4.20 Chromatin Hypermethylation of Nf1^{Myf5} muscle progenitors.

A Increased DNA methyltransferase enzymes expression in Nf1^{Myf5} muscle progenitors. **B** Hypermethylation status of Nf1^{Myf5} progenitors chromatin. **C** Methylation peaks upstream of Myl1 and Pfkfb1 transcription start site in Nf1^{Myf5} progenitors. **D** Decreased expression of *Myl1* and *Pfkfb1* in Nf1^{Myf5} muscle progenitors. A Transcriptome analysis of p7 Nf1^{Myf5} and Control muscle progenitors. N=2 for each group of animals and Padj< 0.001 was considered significant. B, C MeDIP sequencing for Nf1^{Myf5} and Control muscle progenitors. DMRs = differentially methylated regions. N=3 for each group of animals. D Expression of *Myl1* and *Pfkfb1* in p7 muscle progenitors detected by transcriptome analysis (n=2) and double confirmed by qPCR (n=3). Two tails Student-t-test was used for statistical analysis. p**<0.01. P***<0.001.

4.9.4.2 Decreased H3K27me3 in Nf1^{Myf5} muscle progenitors

Except for DNA methylation, histone modification marker H3K27 trimethylation (H3K27me3) was checked in Nf1^{Myf5} muscle progenitors and also muscle tissues. Published literature showed that compared with activated satellite cells, the H3K27me3 modification level is much lower in quiescent state, and the chromatin is mainly in a permissive state[106]. As *Nf1* knockout muscle progenitors shifted to a more quiescent state; thus, the modification status of H3K27me3 was also tested. Firstly, as a convenient and efficient way, immunostaining was performed on FACS sorted muscle progenitors and also TA muscle cryosections with

antibodies against H3K27me3, Pax7, and DAPI. Relative fluorescence units (RFU) analysis showed that for progenitors, the H3K27me3 modification level was significantly decreased(Fig. 4.21A). Besides, both immunostaining and western-blot analysis confirmed the reduction of H3K27me3 also on mature muscle tissues (Fig. 4.21A, B). Chipmentation was performed with an antibody against H3K27me3 to check the precise H3K27me3 level of a specific genetic locus. After mapping the reads with mouse genome nine and MACS2 peak calling, peak signal was enrichment with the length of 10 kb for both up and downstream of transcription start site (TSS). Data showed a severe reduction of H3K27me3 in $Nf1^{Myf5}$ muscle progenitors (Fig. 4.21C). Epigenetic status of Pax7 was shown, and it indicated that increased Pax7 expression in $Nf1^{Myf5}$ muscle progenitors might be caused by decrease of the repressive histone modification marker of H3K27me3 (Fig. 4.21D). With the above experiments, it could be shown that *Nf1* deletion changed the chromatin status of muscle progenitors.

Conclusions

Nf1 knockout in muscle progenitors changed its epigenetic modification status, including increased DNA methylation level and a decreased H3K27me3. This change might regulate the expression of muscle stem cell-related genes such as *Pax7* and also progenitor's differentiation genes expression such as *Myl1*.

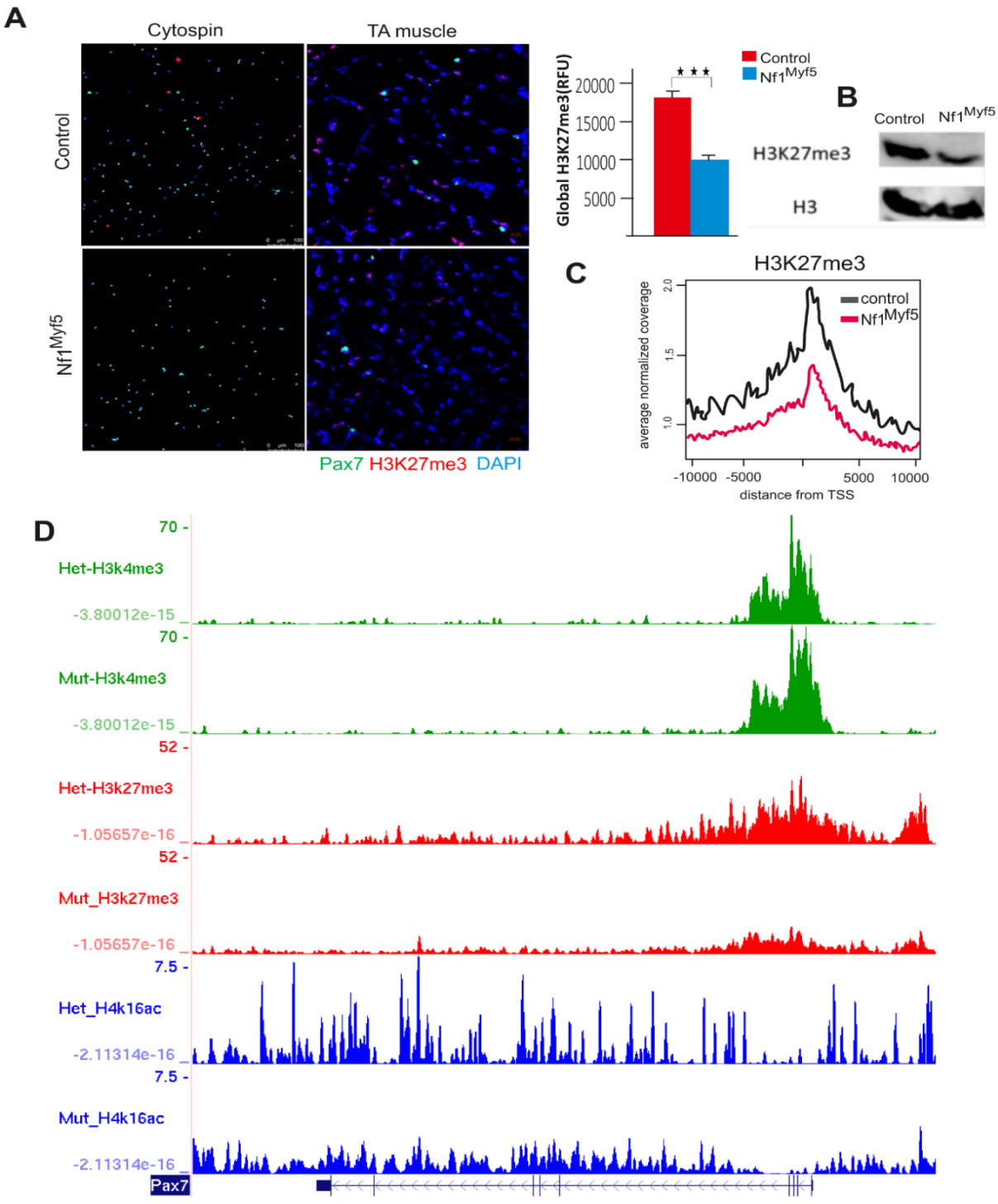

Figure. 4.21 Reduction of H3K27me3 of Nf1^{Myf5} muscle progenitors chromatin.

A, **B** Reduced H3K27me3 in Nf1^{Myf5} progenitors and also muscle tissues. **C** Decreased enrichment of H3K27me signal within 10kb up and dow of transcription start site in Nf1^{Myf5} progenitors. **D** Increased Pax7 expression in Nf1^{Myf5} progenitors might be H3K27me3 dependent. A FACS sorted muscle progenitors were used for cytospin followed by immunostaining with antibodies against Pax7, H3K27me3. Sections from 12 weeks hindlimbs were used for staining. N=3 for each group of animals. RFU was measured for at least 200 cells from each animal. B Western blot was performed with an H3K27me3 antibody on 12 weeks of muscle lysates (N=3). C, D Chipmentation was performed with the H3K27me3 antibody. FACS sorted p7 muscle progenitors were used (N=2). Two tails Student-t-test was used for statistical analysis. P***<0.001. Scale bar 100 µm and 20 µm.

4.10 Stronger quiescent signature of Nf1^{Myf5} muscle progenitors was Delta-Notch signaling pathway dependent.

4.10.1 Nf1^{Myf5} muscle progenitors showed hyper-activation of Delta-Notch signaling.

The entire transcriptome analysis can provide general information about the cell status in the process of checking myogenesis and quiescent related gene expression. An exciting observation was that a group of genes up-regulated in Nf1^{Myf5} muscle progenitors were components of Delta-Notch signaling, and they were enriched for Notch1 target genes during GO and KEGG analysis (Fig. 4.22A). It suggests that Nf1^{Myf5} muscle progenitors have hyperactivation of the Notch signaling pathway. These genes include Notch target genes such as *Pax7*, *Hes1*, *Hey1*, *Heyl*, *Col6a3*, and *Col5a3*, Notch ligand genes *Dll1* and *Jag1*, andexpression of *Notch1*/3. A recent paper showed reciprocal signaling by Notch–Collagen V–Calcr retains muscle stem cells in their niche and keeps them in quiescence[100]. The expression of *Calcr* was also increased in Nf1^{Myf5} muscle progenitors. Since Notch pathway regulates muscle stem cells to enter a quiescent state by modulating the composition of ECM components and its activation also requires ligands from their living environment, then it is a promising pathway to explain why Nf1^{Myf5} progenitors showed a different cellular properties in vivo with the muscle stem cell niche and in vitro with Matrigel culture.

Activation of Notch signaling requires binding of the ligands with the receptors. Typically, Notch ligands are expressed primarily on neighboring cells or muscle fibers, but for the culture of muscle progenitors and primary myoblasts, they cannot attach to each, or they will differentiate, which might be why *Nf1* knockout cells behave entirely in two different directions in vitro and in vivo. To test this, cell culture plates were pre-coated with specific Notch ligand Jag1 before muscle progenitors from FACS sorted Nf1^{Myf5} and Control animals were seeded on top. They were divided into four groups, which were Control, Nf1^{Myf5}, Control_Jag1, Nf1^{Myf5}_Jag1. The Control and Nf1^{Myf5} group were cultured only on Matrigel-coated plates. The Control_Jag1, Nf1^{Myf5}_Jag1 groups were cultured with plates coated with Matrigel and also Notch ligand Jag1. After 48 hours of Notch ligand treatment in proliferation medium, mRNA was isolated, followed by reverse transcription, cDNA was used as the template, and primers were designed based on the Notch pathway target genes for real-time qPCR analysis. $2^{-\Delta\Delta Ct}$ was calculated for target gene relative expression analysis. Data shows that Jag1 treatment stimulated Delta-Notch signaling in both groups. Without Jag1 treatment, no difference was observed for Notch target genes expression between Nf1^{Myf5} and Control cells, indicating that activation of the Notch pathway is highly environment-dependent. With ligand treatment, all related Notch target genes expression increased for approximately two-fold in Control cells, suggesting that ligand treatment was successful. However, in the Nf1^{Myf5}_Jag1 treatment group, it increased by four

to six-fold, which points out that Nf1 deleted muscle progenitors are more sensitive to the activation of the Notch pathway. The qPCR analysis data can nicely mimic the data generated by transcriptome analysis of muscle progenitors. It Indicates that in vitro culture using Notch pathway ligand allows cells to behave more like in vivo status and in vivo, $Nf1^{Myf5}$ muscle progenitors have hyperactivation of Delta-Notch signaling (Fig. 4.22B).

In addition, experiments with Jag1 treatment were also performed for immunostaining to check if the aberrantly increased proliferation rate of $Nf1^{Myf5}$ muscle progenitors in vitro can be rescued. Freshly FACS sorted cells were cultured with both matrigel and Jag1 coated coverslips in Control and $Nf1^{Myf5}$ cells. After cultured in proliferation medium for 48 hours, cells were fixed and co-stained with Pax7/Ki67/desmin and DAPI. Pax7 and DAPI double-positive cells were counted to observe the effect of ligand treatment on the expression of muscle stem cell marker genes. After counting and statistical analysis, the relative fluorescence units of Pax7 increased from 1800 to 2500 compared to control cells (Fig. 4.22C). It indicated that Jag1 treatment increased Pax7 expression, especially in $Nf1^{Myf5}$ muscle progenitors. The proliferation rate of Pax7 positive cells was calculated, both Ki67 and Pax7 positive cells were considered to be proliferating muscle progenitors. Data showed that the proliferation rate of $Nf1^{Myf5}$ cells decreased from 84% to 65% with Jag1 treatment. It indicated that Jag1 treatment could decrease cell proliferation rate, particularly in $Nf1^{Myf5}$ progenitors (Fig. 4.22C). Interestingly, one phenomenon was noticed that without Jag1 treatment, after 48 hours of culture, large amount of progenitors were also Desmin positive, indicating that early differentiation has started, but only a small population of Desmin positive progenitors were detected in $Nf1^{Myf5}$ group in line with the MF20 staining presented earlier (Fig. 4.15C). With Jag1 treatment, there were almost no Desmin positive cells in both groups detected, implying that Notch signaling can promote progenitors to shift into a stem cell-like state and suppress their differentiation (Fig. 4.22C, D).

In summary, it can be concluded that $Nf1^{Myf5}$ muscle progenitors shifted towards quiescent earlier in vivo, concomitant to a hyperactivation of the Delta-Notch signaling pathway.

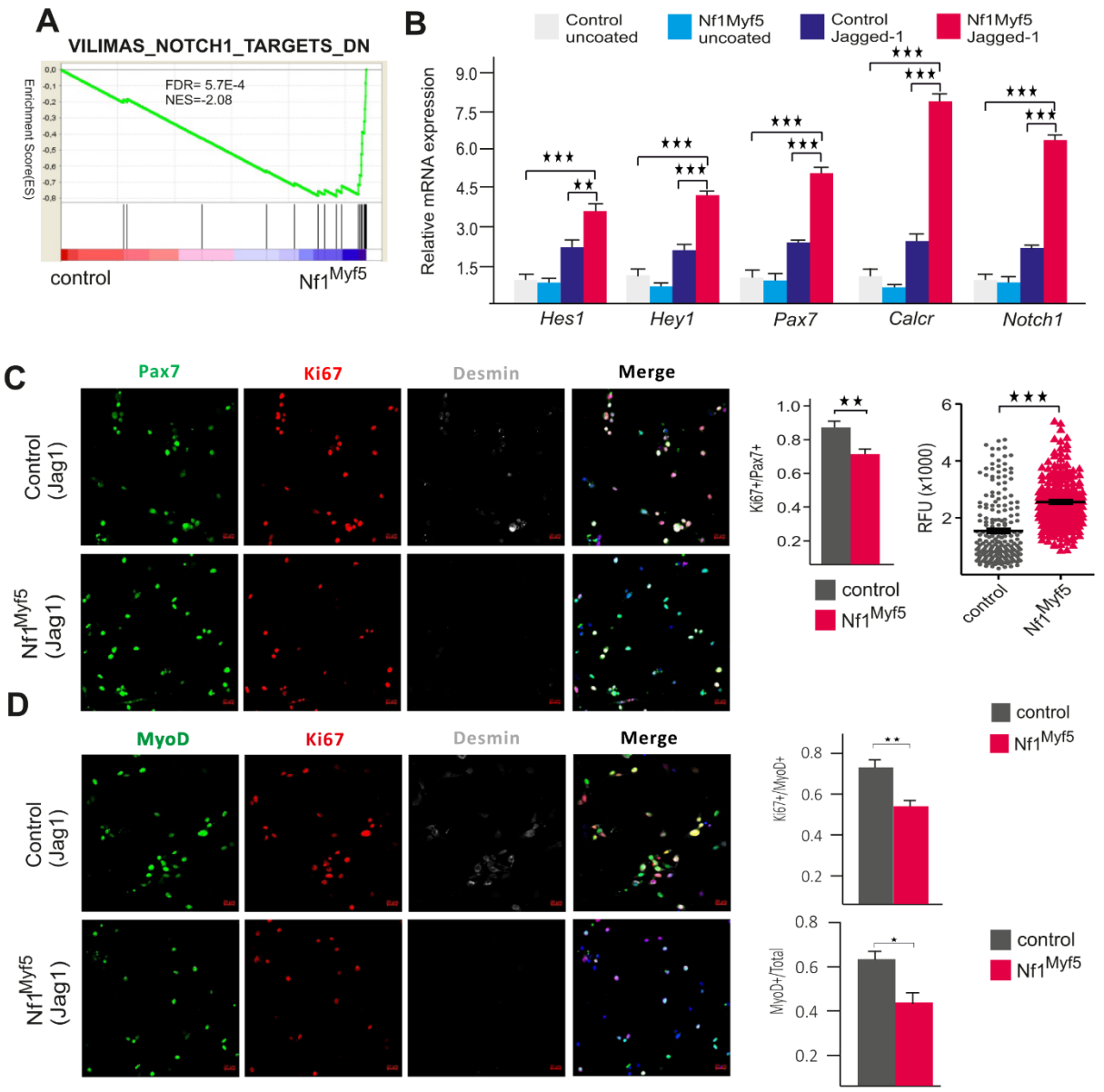

Figure 4.22 Nf1^{Myf5} muscle progenitors showed hyper-activation of Delta-Notch signaling.

A Notch target gene expression is enriched in Nf1^{Myf5} progenitors. Transcriptome analysis for FACS sorted p7 muscle progenitors. GSEA analysis was performed with gene expression list. N=2 animals. **B** Jag1 ligand results in hyperactivation of the Notch pathway in Nf1Myf5 cells, indicated by increased expression of Notch downstream target genes. Freshly FACS sorted muscle progenitors cultured in proliferation medium with/wo Jag1 treated Matrigel-coated plate. Real-time qPCR was performed, and primers were designed for Notch signaling relative genes (N=3 animals). **C** Notch signaling activation increased Pax7 expression and decreased progenitors' proliferation rate. **D** Decreased proliferation rate of Nf1^{Myf5} myoblast. Freshly FACS sorted muscle progenitors were cultured with Jag1 treated Matrigel-coated plate for 48 hours. Primary antibodies against Pax7, Ki67, Desmin and MyoD, Ki67, Desmin were used for staining respectively and DAPI for nuclear identification. Pax7/Ki67 and MyoD/Ki67 double-positive cells were counted for proliferation analysis. B Student-t-test was used for statistical analysis. p*<0.05. p**<0.01. P***<0.001. The scale bar is 20 μm.

4.10.2 Hyper activation of Delta-Notch signaling pathway in Nf1^{Myf5} muscle progenitors is mediated through NO-ERK-Notch Signaling

To elucidate the mechanism how *Nf1* deletion regulates the activation of the Notch pathway, an in vitro experiment was performed. From the literature and our qPCR results, the Notch pathway can be hyperactivated in vitro culture for 48 hours with Jag1 treatment. In oligodendrocyte, the mutation of *Nf1* leads to hyperactivation of the Delta-Notch pathway through ERK regulated nitric oxide production[121]. Nitric oxide is a messenger and functions in most tissues and organs. No-cGMP-PKG signaling is a classical pathway found enriched hereby in diverse backgrounds[121,156-158]. Significantly up-regulated genes from RNAseq were submitted for KEGG analysis. the first pathway with the smallest p-value is Protein digestion and absorption followed by ECM-receptor interaction, focal adhesion, cell adhesion molecules, and PI3K-Akt signaling pathway. Pathways in cancer were also enriched, which means as a tumor suppressor gene, *Nf1* knockout may lead to activation of cancer relative signaling, such as PI3K-Akt signaling (Fig. 4.23A). Interestingly, the cGMP-PKG signaling was also enriched in Nf1^{Myf5} muscle progenitors indicate that activation of ERK/MAPK in Nf1^{Myf5} muscle progenitors might also induce the secretion of nitric oxide thus drive the activation of cGMP-PKG signaling (Fig. 4.23A).

Therefore, an in vitro cell culture model was established with Jag1, ERK/MAPK signaling pathway inhibitor U0126, nitric oxide production inhibitor LNAME treatment. After 48 hours of culture and treatment, mRNA was isolated from the treatment and control group. *Pax7*, *Hes1*, *Hey1* and *Myog* were analyzed by qPCR analysis. Without Jag1 treatment, *Pax7* expression was 1.56 times higher in Nf1^{Myf5} primary myoblasts, and *Hes1* expression was 1.43 times higher, but there was no difference in *Hey1* expression. With Jag1 treatment, the relative expression difference of these genes increased to 2.59, 1.82, and 1.38, respectively. They were all significantly up-regulated compared to the group without Jag1 treatment, which double confirmed that Nf1^{Myf5} primary myoblasts are more sensitive to the Notch pathway.

With nitric oxide synthase inhibitor LNAME treatment, for Nf1^{Myf5} / Jag1 primary myoblasts, the expression of *Pax7*, *Hes1* and *Hey1* were reduced to 0.77, 0.98 and 0.97, respectively, which implies NO inhibitor can eliminate the effect of Notch pathway activation. After treatment with ERK inhibitor U0126, the difference was even reduced to 0.7, 0.35, and 0.52, respectively. The expression of *MyoG* was not different in Nf1^{Myf5} primary myoblasts with or without Jag1 treatment, which was only 0.43 and 0.49 compared to their control cells. With LNAME treatment, *MyoG* expression increased to 2.48 compared to control. By U0126 treatment, the expression of MyoG was even higher, to 4.39 times of the control. In summary, Jag1 treatment increased the expression of *Pax7*, *Hes1*, and *Hey1* in Nf1^{Myf5} primary myoblasts, thus blocking the myogenic process (Fig. 4.23B). Nf1^{Myf5} primary myoblasts were more activated by Notch

ligand compared to control cells. NO inhibitor and ERK1/2 inhibitor block Notch hyperactivation caused by Jag1 treatment in Nf1^{Myf5} primary myoblasts. This suggests that *Nf1* deletion leads to stronger ERK1/2 activity in vivo, and ERK signaling can increase the production of nitric oxide, thereby contributing to activation of the Notch pathway.

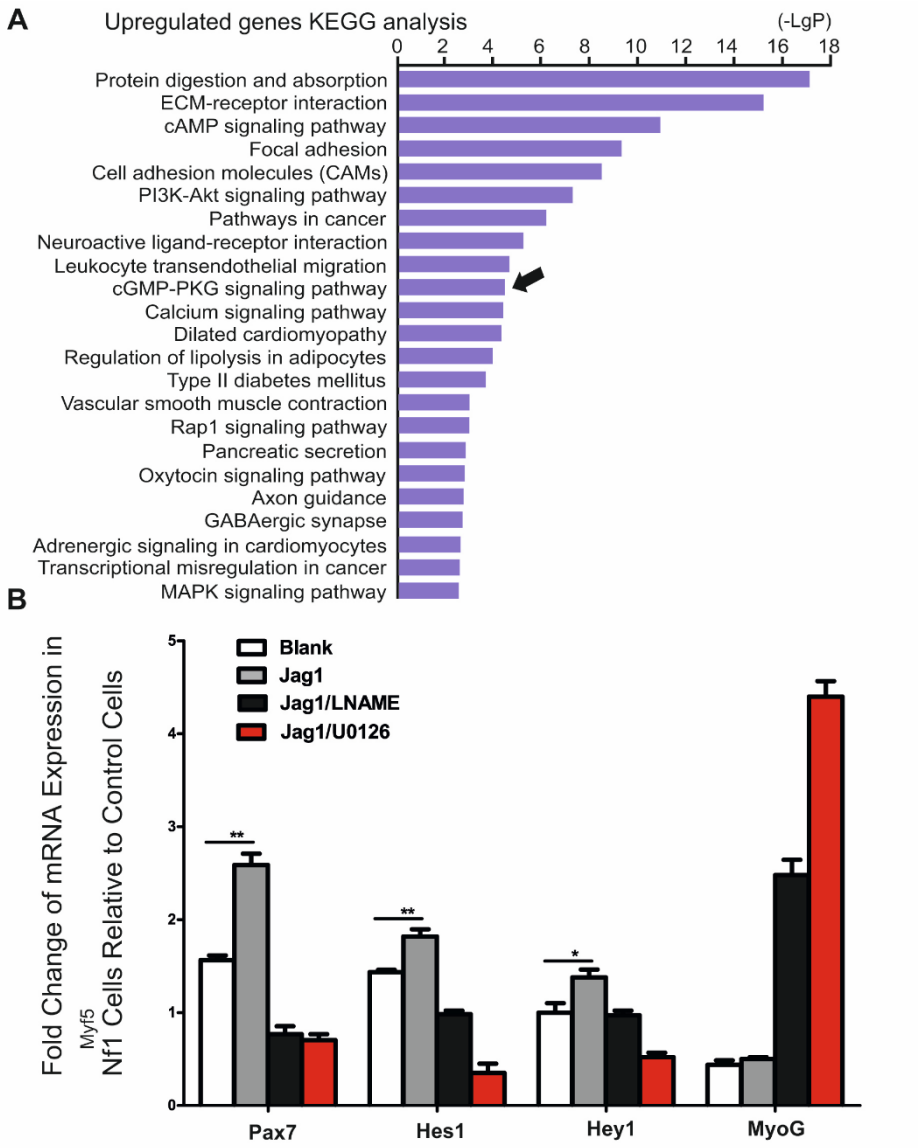

Figure 4.23 Hyperactivation of Delta-Notch signaling pathway in Nf1^{Myf5} muscle progenitors via NO-ERK-Notch Signaling

A Activation of cGMP-PKG in Nf1^{Myf5} muscle progenitors. DAVID bioinformatics was used for KEGG enrichment for significantly up-regulated genes (N=2). **B** Nitric oxide can block Notch signaling activation. A Transcriptome analysis of p7 Nf1^{Myf5} muscle progenitors. Primary myoblast were isolated from Nf1^{Myf5}(n=3) and Control (n=3) animals. Fold change means Nf1^{Myf5} divided by Control. Blank = cultured control and Nf1^{Myf5} primary myoblast without any treatment; Jag1 = Notch ligand Jag1 treatment for both Control and Nf1^{Myf5} cells; Jag1/LNAME = both groups of cells were cultured with Jag1, LNAME was used for Nf1^{Myf5} cells and vehicle was used for control cells; Jag1/U0126 means both groups of cells were cultured with Jag1, U0126 was used for Nf1^{Myf5} cells and vehicle was used for control cells. N=3 for each group of animals. N=3 wells for each treatment condition. Two tail Student-t-test was used for statistical analysis. p*<0.05. p**<0.01. P***<0.001

4.10.3 Notch signaling could repress glycolysis and oxidative phosphorylation genes expression.

My results support the notion that the Notch pathway might drive early postnatal muscle progenitors into a quiescent state, and the metabolism profiling of activated muscle progenitors and quiescent muscle stem cells is also different. For proliferating muscle progenitors, they need to rely on glycolysis to generate biomass for a new synthesis of proteins and DNA, but for quiescent muscle stem cells, they rely primarily on fatty acid metabolism to produce energy[155]. To observe whether the Notch pathway can also block the expression of glycolytic-related genes, FACS isolated wild type p14 muscle progenitors were cultured on Matrigel-coated plates with/without Jag1 treatment. RNA was isolated, followed by reverse transcription and real-time qPCR, specific primers for glycolytic genes, including *Pfkfb1*, *Pfkfb3*, *Ldha*, *Pfkm*, *Eno3*, *Hk2* were selected. Furthermore, the Notch target genes *Pax7*, *Hes1*, and *Hey1* were used as control indicators of in vitro activation of the Notch pathway. Oxidative phosphorylation genes such as *Ndufv1* and *Mtco1* expression were also detected by qPCR. As shown in Figure 4.24. Expression of *Pax7*, *Hes1*, and *Hey1* increased by 2.58, 3.24, and 2.14 fold compared to the Control, confirming efficient activation of Notch signaling. 6-phosphofructo-2-kinase/fructose-2,6-biphosphatase (PFKFBs) could strongly promote glucose utilization by increasing fructose-2,6-bisphosphate levels. It has four tissue type isoforms and *Pfkfb1* and *Pfkfb3* are mainly expressed in muscle tissue. Interestingly, glycolytic and oxidative phosphorylation genes were decreased by Jag1 treatment compared to untreated cells, especially for the expression of *Pfkfb1* and *Pfkfb3* with ratios of 0.41 and 0.51, respectively.

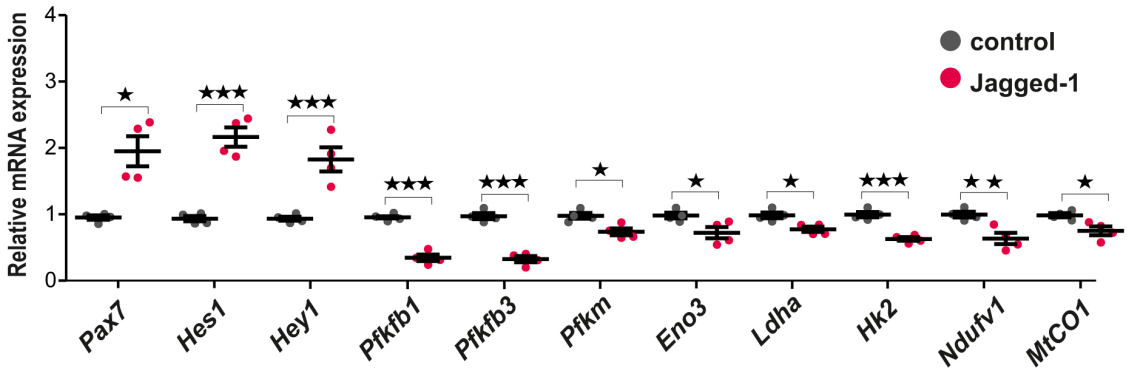

Figure 4.24 Notch pathway represses glycolysis and oxidative phosphorylation genes expression in early postnatal myogenic progenitors.

Significantly down-regulation of glycolysis and oxidative phosphorylation genes expression upon Notch pathway activation. Freshly FACS sorted muscle progenitors cultured with Matrigel-coated plate with/wo Jag1 treatment. Each condition has triplicate, RNA was isolated, followed by reverse transcription and real-time qPCR with primers of Notch target genes, glycolysis, and oxidative phosphorylation genes. Student-t-test was used for statistical analysis. p*<0.05. p**<0.01. P***<0.001

Conclusions:

As a tumor suppressor gene, *Nf1* knockout leads to the activation of cancer-associated pathways, which also include Delta-Notch signaling in different biological backgrounds[121,147]. Under the muscle progenitors biological context, in the embryonic phase, most of these muscle progenitors are proliferating to expand the stem cell pool to support fetal and postnatal muscle growth. A pivotal time point is the formation of muscle stem cells niche at around E17.5[151]. After this time point, activated muscle progenitors consecutively need to enter either into their niche and gradually become quiescent or start to differentiate and incorporate with existing muscle fibers for muscle hypertrophy. The function of the Notch pathway has changed before and after the muscle stem cell niche formation. The Notch pathway promotes muscle progenitor's proliferation before niche formation, but after stem cell niche formation, the function of the Delta-Notch pathway changed from promoting proliferation to inhibit proliferation through Notch-Collagen V-CALCR signaling[100]. Hyperactivation of this pathway in $Nf1^{Myf5}$ animals leads to a gradual decrease in satellite cell numbers, and a reduction of muscle mass Here it was confirmed that *Nf1* deletion leads to hyperactivation of Ras/ERK signaling, which stimulates the Delta-Notch pathway by producing nitric oxide in $Nf1^{Myf5}$ muscle progenitors and a stronger Notch pathway inhibits the expression of glycolytic and oxidative phosphorylation-related genes thus drive cells into a quiescent state.

4.11 $Nf1^{Myf5}$ muscle phenotype could be rescued with Delta-Notch specific inhibitor (DAPT) injection.

4.11.1 Increased progenitor numbers and body weight of DAPT injected $Nf1^{Myf5}$ mice.

As $Nf1^{Myf5}$ progenitors have stronger Notch signaling activity and it might drives muscle progenitors go into a quiescent state, thus causing progenitors depletion, then the next question is if Notch pathway gets suppressed with specific chemical inhibitor, whether the satellite cell pool exhaustion that $Nf1^{Myf5}$ mice suffered can be rescued. Thus, a common γ-secretase inhibitor DAPT was used for subcutaneous injection into $Nf1^{Myf5}$ animals from postnatal day 6. The injection was performed every three days until p21. $Nf1^{Myf5}$ mice with Placebo injection were used as control. Animals were dissected at p21, and hindlimb cryosections were taken, followed by Pax7, Ki67, ColIV, and DAPI co-immunostaining. Whole section tile-scan were taken, and progenitor numbers within each muscle bundles were counted. As data shown in Figure 4.25A. Compared with Placebo injected $Nf1^{Myf5}$ mice, DAPT injection significantly increased progenitor cell numbers within TA, EDL, and Soleus muscle

bundles. Besides, the increased progenitor number might be caused by an increased proliferation rate of these cells, as data showed in the quantification of Ki67 positive Pax7 cells (Figure 4.25A). In addition, expression of Notch pathway-related genes such as *Notch1/3*, *Col5a3*, *Col6a3*, *Hes1*, and *Hey1* was detected by qPCR analysis for double confirmation of DAPT inhibition function for the Notch pathway. Compared with the Control group, the expression of Notch pathway-related genes were all more than 50% down-regulated (Fig. 4.25B). In short, DAPT injection can block the Notch signaling pathway to a physiological level, and satellite cell pool depletion that $Nf1^{Myf5}$ mice suffered can be rescued by DAPT injection.
For postnatal muscle hypertrophy, the insertion of nuclear plays a dominant role, especially when the mice are younger than p21. $Nf1^{Myf5}$ mice showed a severe reduction of muscle cross-section area. The cross-section area was measured in both $Nf1^{Myf5\_Placebo}$ and $Nf1^{Myf5\_DAPT}$ to see the influence of DAPT injection for fiber hypertrophy. Data showed compared with control, DAPT injection significantly increased CSA of muscle fibers (Fig. 4.25C). During muscle dissection, The entire mouse body weight and the weight of psWAT were also measured from both control and DAPT injection groups. Data also showed a significant increase in both body weight and psWAT weight in DAPT injected mice.

Conclusions:

Notch inhibitor DAPT injection could rescue the muscle satellite cell pool depletion that $Nf1^{Myf5}$ suffered. Also, it can improve the life status of $Nf1^{Myf5}$ mice by increasing their muscle mass, white adipose weight, and the whole bodyweight. It double confirmed that the satellite cell pool depletion phenotype of $Nf1^{Myf5}$ mice is dependent on the hyperactivation of Delta-Notch signaling.

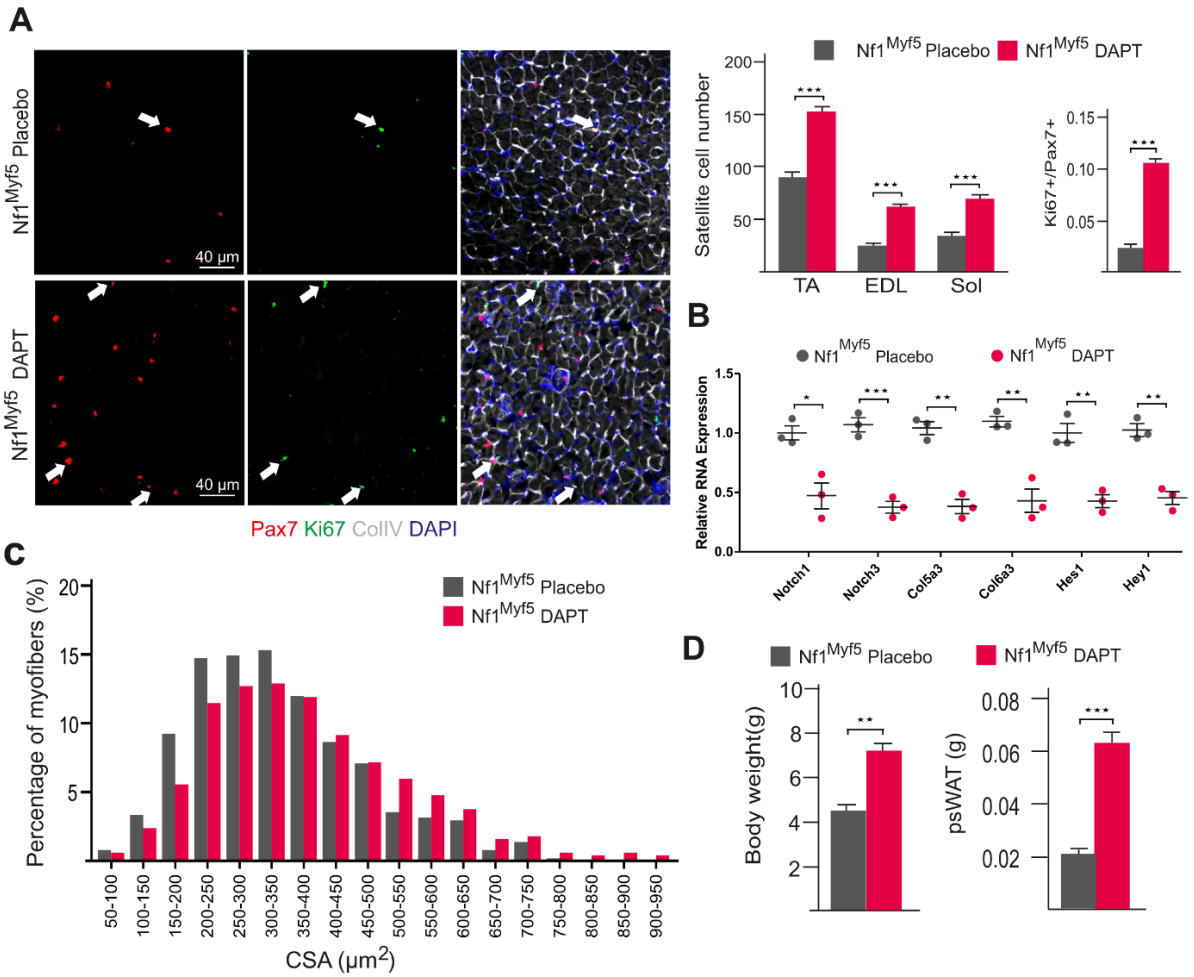

Figure 4.25 DAPT injection partially rescued the phenotype of Nf1^{Myf5} mice.

A DAPT injection increased Nf1^{Myf5} progenitors proliferation rate and numbers. **B** DAPT injection block Notch pathway-related gene expression. **C** Increased cross-section area in DAPT injected Nf1^{Myf5} mice. **D** Body weight and white adipose tissue weight gain by DAPT injection. A p21 hindlimb sections from DAPT and Placebo injected mice. Co-staining with Pax7, Ki67, ColIv, and nuclear. Pax7 positive cells were considered as satellite cells. Ki67/Pax7 double-positive cells were used for proliferation rate measurement. B: mRNA was isolated from Nf1^{Myf5_DAPT} and Nf1^{Myf5_Placebo} TA muscle, respectively, N=4 animals. Two tails Student-t-test was used for statistical analysis. p*<0.05. p**<0.01. P***<0.001. The scale bar is 40 μm.

5 Discussion

Myopathy could severely influence the patient's life quality and lifespan. To better identify whether the Nf1-associated myopathy is generated from the effects of other organs or from the skeletal muscle system itself,tissue-specific gene knock out with the loxP-Cre system is a useful gene-editing tool for this purpose. As a tumor suppressor gene, the mutation of *Nf1* will cause Neurofibromatosis type I, which is characterized by skin coloring and growth of tumors along with the nervous system. Although the symptoms of this disease vary widely, a common phenomenon that NF1 patients suffered is muscle weakness and reduced muscle mass. Several research groups around the world are working on the project of how *Nf1* regulates the development of the skeletal muscle system. So far, people have not clearly understood how this regulation occurs. Therefore, in this work, a skeletal muscle-specific knockout animal model was used to study the behind mechanism of myopathy caused by mutation of *Nf1* in muscle tissue.

5.1 Evaluation of $Nf1^{Myf5}$ mouse model.

Several mouse lines were used in our lab and also other labs to investigate the effect of *Nf1* knock out on skeletal muscle development. Mouse phenotype caused by *Nf1* deletion from different mouse strains can be compared using the published data. Nf1flox/flox mice crossed with Cre recombinase under specific promoters including *Lbx1, Prx1, Pax7, Myf5, MyoD*, and *HSA* have generated different *Nf1* knock out mouse models. Previous literature showed when *Nf1* was knockout in *Prx1* expressing cells, which resulted in severe muscular dystrophy, characterized by increased muscle fibrosis and decreased embryo myoblast differentiation. Besides, since *Prx1* is expressed in early limb bud mesenchyme, the proliferation rate of muscle connective tissue also increased, and an increase of connective tissue can be observed from E16.5. All of these changes are accompanied by hyperactivation of the Nf1-dependent MAPK (mitogen-activated protein kinase) signaling pathway. In summary, this paper showed that *Nf1* is critical for skeletal muscle system development[159]. The disadvantage of this mouse model is that *Nf1* knockout is not specific for muscle tissue, fibroblast, osteocytes, chondrocytes, stromal cells, and tenocytes could also being affected[160].

Lbx1, together with *Pax3* and *c-met*, are co-expressed in embryonic muscle precursors. Our previous work with the $Nf1^{Lbx1}$ mouse model showed no phenotype for embryonic muscle patterning and growth defect, but a reduction in muscle size was observed between E14.5 and E18.5[148]. In addition, the paper also showed that Lbx1 is expressed in both myogenesis and

neurogenesis process[64,161]. Here our Lbx Cre mice used the BAC (bacterial artificial chromosome) method to make the gene Cre activity selective to limb muscle tissue[64]. We visualized the Lbx Cre by crossing the mice with mTmG reporter mouse, and we did not see any Cre activity in neuron cells[148]. $Nf1^{Lbx1}$ mice die after birth likely due to respiratory problems; Thus it is not a good animal model for postnatal research to mimic NF1 children patients.

The $Pax7^{-creERT2}$ transgenic mouse was used to generate the $Nf1^{Pax7\text{-}creERT2}$ animal model and study the function of *Nf1* in adult muscle[149]. Tamoxifen was injected from 8 weeks old mice. Satellite cells give a regular and universal contribution to postnatal muscle hypertrophy even without any injury and damage. Studies have shown that for mice between the ages of 6-12 months, there are still a certain amount of nuclei nserted into existing myofibers[162]. No phenotype was observed in $Nf1^{Pax7\text{-}creERT2}$ mice, including body weight, muscle weight, and also myopathy identified by the histological method. From the muscle function part, there is also no impairment. This might be due to the penetration efficiency of tamoxifen and the activation of Cre activity in the target cell population. Besides, 8 weeks might be too short for satellite cells under homeostatic status and the allele being used could also influence the results. Further protocol modifications for the tamoxifen injection are still under processing[149].

Another group used the $Nf1^{MyoD}$ mouse model to study the function of *Nf1* during postnatal muscle development. For this mouse model, severe muscle phenotypes include the accumulation of lipid droplets intramyocellular and an increase in oxidative metabolic enzyme activity suggesting a function of *Nf1* in mitochondrial fatty acid metabolism[126]. Compared with the OilRed O staining that was performed on $Nf1^{Myf5}$ sections with a tilescan imaging, there was no lipid droplet observed at all in $Nf1^{Myf5}$ muscle. However, some lipid droplet smear was observed in muscle tissue close to muscle-adjacent layer fat tissue, suggesting that that the observation of Sullivan et al may reflect an artefact generated from adipose tissue. In addition, this mouse model also has neonatal lethality[126]. Therefore, a proper mouse model to study the function of *Nf1* in postnatal muscle development is urgent.

Here, $Nf1^{Myf5}$ mouse model was used, the efficiency of *Nf1* knockout is around 80% off specifically for exons 40 and 41 from RNA level for muscle progenitors and also for their offsprings from both RNA and protein level. The Ras/ERK signaling, which can be negatively regulated by Nf1, plays an important role in myoblast proliferation and differentiation. Published literature shows that the proliferating C2C12 myoblasts maintains relatively high Ras signaling activity during proliferation, but for differentiation the signaling need to be repressed[163]. The researchers also showed $NF1^{Prx1}$ satellite cells has differenatiation defect[125]. The critical point for this mouse model is even with strong myopathy, animals can still survive until p160, thus provide the opportunity to study *Nf1* function for postnatal muscle development.

5.2 *Nf1* deletion lead to skeletal muscles development defect

$Nf1^{Myf5}$ mice reduced body weight during postnatal development. Previous studies from clinical research have noted that Neurofibromatosis Type 1 (NF1) patients have an increased chance of developing tumors along human central and peripheral nervous systems[164]. Regarding the function of *Nf1* in muscle development, the first in vivo mouse model was $Nf1^{prx1}$. In this work, *Nf1* was deleted in the mouse embryo mesenchymal cells. The phenotype of the mouse model includes severe myopathy characterized by disruption of muscle pattern and decreased ability of embryonic myoblast differentiation. Besides, muscle fibrosis was also observed. Since mesenchymal cells can give rise to varies cell types, including osteoblasts, chondrocytes, myocytes, and also adipocytes, *Nf1* knock out in different tissue might bring an additive effect on this strong muscle phenotype[159].

For $Nf1^{Myf5}$ mice, the previous data showed there was no influence for muscle patterning and also myoblast differentiation during the embryonic stage, but the growth retardation was observed from E18.5 on and was strengthened over time[148]. In this study, *Nf1* was found to be critical for mouse postnatal muscle development. Reduced mouse body size and weight can be observed from early birth on, and the difference is getting bigger and bigger during postnatal muscle development. As an essential feature of myopathy is a reduction of muscle mass. The muscle mass of $Nf1^{Myf5}$ mice is also significantly decreased. The only mouse model that was reported for the function of *Nf1* in postnatal muscle development is $Nf1^{MyoD}$ mice. Unfortunately, this model showed around 50% body weight reduction and neonatal lethality. Surprisingly, there was no difference detected in the knockout mice, except for lipid droplets were observed in their muscle sections[126]. It implied that the animal's body system is complicated, and further experiments still need to be performed for this mouse model.

Literature showed that $Myf5^{+}$ cells could give rise to brown adipose cells by upregulating expression of *Prdm16* and repressing myogenic genes expression[165]. In $Nf1^{Myf5}$ mice, no difference was detected for iBAT, sBAT, and cBAT for both weight and HE staining. However, a significant reduction of psWAT and rWAT weight was noticed. Skeletal muscle is critical for glucose and fatty acid metabolism and white adipose tissue functions as the energy storage site. Reduced white adipose tissue weight suggests a change of muscle metabolism in $Nf1^{Myf5}$ mice. The acute myopathy suffered by $Nf1^{Myf5}$ mice resulted in a decrease in body size and weight, loss of muscle mass, and also white adipose tissue weight. In short, myopathies of $Nf1^{Myf5}$ mice can recapitulate the muscle phenotype of NF1 patients.

5.3 *Nf1* deletion leads to muscle metabolic defects

5.3.1 Loss of *Nf1* results in fiber type shift towards slow/intermediate fibers

With a strong myopathy that was observed, to get a better understanding of how *Nf1* deletion affects muscle tissues, a whole transcriptome profiling was used for p21 $Nf1^{Myf5}$ and control animals. Since TA muscle consists of both slow and fast fibers at p21, thus p21 TA muscle can was used for fiber type properties and metabolic-related studies[29]. Interestingly, in $Nf1^{Myf5}$ mice, all of the fast fiber component genes expression was reduced, whereas the intermediate slow fiber genes were up-regulated.

With the implication of fiber type conversion from RNAseq analysis, the protein expression level was detected through specific primary antibodies staining. For slow fibers, time-series staining was performed from postnatal 1 week until 12 weeks old mice. A growing number of studies have found that during postnatal development, the composition of fiber type slowly transforms from slow oxidative fibers to fast glycolytic fibers[29]. For 12 weeks old animals, there was almost no slow fiber left in TA and EDL muscle. All the slow fibers only located in the soleus area. For three weeks old animals, data showed a significant increase in type I fiber composition in $Nf1^{Myf5}$ TA muscle. Then it is curious how this transformation happened? Is there any difference at an even earlier stage? Immunostaining from one week and two weeks postnatal sections shows increased type I fiber from two weeks on. For 12 weeks old animals, since there is almost no type I fiber left in TA muscle, more type IIa fibers in $Nf1^{Myf5}$ mice was detected. Besides, western-blot also double confirmed the increased Myoslow and decreased of Myofast expression in $Nf1^{Myf5}$ TA muscle.

A growing body of literature has examined the cause of skeletal muscle fiber shift and the related diseases[135,166,167]. Since 1996, Olanzapine has been administered intramuscularly as an antipsychotic. In recent years, side effects include metabolic inflexibility, hyperglycemia, adiposity, and diabetes have been reported. To observe the effect of this chemical on skeletal muscle, RNAseq was performed with Olanzapine infusion for 24 h in rat gastrocnemius muscle. It showed that Olanzapine could rapidly influence the transcriptome of these animals, causing the composition of muscle fibers shift towards fast fibers, which are more susceptible to atrophy and also chronic metabolism side effects. Type 2 diabetes is a prevalent metabolism associated disease. The research was conducted on patients with type 2 diabetes showed that patients have a 16% reduction for slow fibers and 49% increase of fast fibers as compensation for changes in glucose metabolism in the body[168]. Until now, almost all literature shows slow fibers shift towards fast fibers, such as disuse atrophy, microgravity, and related diseases. In contrast, endurance exercise with oxygen, chronic low-frequency stimulation, and aging usually contribute to fast to slow isoform transition[34]. Proteomics data demonstrated a rapid

fast to slow contractile transformation process during animals and human skeletal muscle aging. This might be caused by muscle wasting, induced by loss of motor neurons, nutritional deficiency, decreased expression of growth hormones, and chronic inflammation, even though precise regulation mechanism is still not clear. Some researchers support idea with selective atrophy of fast fibers during aging[35,34,46].

In summary, different methods were used to examine the fiber type component protein expression in $Nf1^{Myf5}$ and control animals. Although the data shows a trend of fiber type transition from fast to slow/intermediate, the underlying mechanism is still unclear. In addition, some classical histochemical assays such as ATPase and SDH staining could also be used for double confirmation.

5.3.2 Loss of *Nf1* results in metabolism shift towards oxidative phosphorylation

Human skeletal muscle fiber types were identified by biochemical and histology analysis in more than 50 years ago[169]. The definition primarily depends on their combination of morphology, contraction, and metabolic properties. Slow fibers mainly relying on oxidative phosphorylation for energy production. In contrast, fast fibers selectively depending on glucose glycolysis to produce energy[170]. Due to the fiber type switching of $Nf1^{Myf5}$ mice, it also showed a reduction of glycolytic genes expression. There are two predominant substrates for skeletal muscle oxidative phosphorylation metabolism and ATP production, namely glucose and free fatty acids. How to choose which substrate to use is highly flexible in both humans and animals. For the human in a resting state, only 20% of the blood's glucose can enter the skeletal muscle, 60% of which can ultimately be oxidatively phosphorylated by the TCA cycle to produce energy. This process consumes 7% of the body's total intake of oxygen. In short, human in resting state, glucose is not the primary fuel for skeletal muscle metabolism[171]. Compared with humans, mice are much smaller, more activate. It should be more dependent on glucose than humans, which is also a key point when referring to a metabolic-related animal model[172].

$Nf1^{Myf5}$ animals showed significantly decreased glycolytic genes expression. To maintain energy production and homeostasis, free fatty acids consumption should be increased. Since $Nf1^{Myf5}$ mice reduced glucose consumption, then the question is, where does the glucose in the food go? Do $Nf1^{Myf5}$ mice have diabetes? For glucose uptake, there are mainly two regulation ways. One way is insulin-dependent, in a post-meal state, with the increased concentration of glucose in the blood, insulin will be secreted by the β-cells, which promote glucose uptake into skeletal muscle. Upon binding to its receptor, insulin can trigger a cascade of signaling pathways and promote Glut4 translocation from cytoplasm to cell membrane for skeletal muscle glucose uptake. The signaling dependent on insulin is primarily PI3/AKT

cascade, which can act as a regulator of protein translation, stress resistance, and maintenance of systemic stability. The other way of skeletal muscle glucose uptake is muscle contraction dependent. During exercise, muscle contraction contributes to a change of ADP/ATP levels, which in turn activates AMPK signaling. Besides, Calcium, Nitric oxide, and Reactive Oxygen Species (ROS) can also help stimulate glucose uptake[32].

If the reduced glycolysis activity in $Nf1^{Myf5}$ mice is Insulin dependent needs to checked. Modification of insulin receptor substrate (IRS) and p-ATK was detected to observe the activation of the insulin-dependent signaling pathway. However, no difference was detected between $Nf1^{Myf5}$ and control TA muscle. It implied that *Nf1* deletion does not influence the insulin signaling. Besides, NF1 patients and $Nf1^{Myf5}$ mice also do not show any insulin resistance or obesity phenotype. In order to answer the question of glucose fate in $Nf1^{Myf5}$ mice, the glucose concentration of the blood from the animal heart was measured, and also there was no difference. Animals always need to keep blood sugar levels steady, and the mouse liver plays a dominant role in glucose homeostasis maintaining. Glucose uptake in mice can be used for hepatic glycogen synthesis in an insulin-dependent manner[173]. In short, the reduction in skeletal muscle glucose uptake may be balanced by other organs in $Nf1^{Myf5}$ mice. With the reduced glucose metabolism in $Nf1^{Myf5}$ skeletal muscle, how to maintain its energy homeostasis needs to be discussed.

Since the skeletal muscle system can use both glucose and fatty acids to generate ATP, thus $Nf1^{Myf5}$ mice need to have energy compensation for animal survival. As an alternative substrate, using of free fatty acid should be increased in $Nf1^{Myf5}$ mice. The data showed a global increased expression for all free fatty acid metabolism enzymes. Besides, some of these genes expressions were also confirmed by mass spectrometry from the protein level. GSEA analysis indicated that metabolism was converted from glycolysis to oxidative phosphorylation. Based on the enrichment gene sets name, the oxidative phosphorylation genes were highly enriched in $Nf1^{Myf5}$ mice and also fatty acid metabolism genes. As the initiating chemical for the TCA cycle, acetyl-CoA can be produced primarily from carbohydrates, free fatty acids. Between meals, free fatty acids can be released by adipose tissue, which was stored as triglycerides. In the first step, free glycerol needs to be generated with the help of lipases. Then free fatty acids will enter the bloodstream. Different organs have different free fatty acid transporters, in the skeletal muscle system, CD36 plays a leading role in the transfer of free fatty acids. After transferred into cells, the reaction happened to make fatty acyl-adenylate and finally give a fatty acyl-CoA, which was transferred to mitochondrial with the help of CPT1/2, fatty acid beta oxidative phosphorylation will start to generate NADH and $FADH_2$ for the TCA cycle. Interestingly, Lpl, a rate-limiting enzyme for triglyceride hydrolysis, was also observed increased expression in $Nf1^{Myf5}$ skeletal muscle and decreased expression in psWAT. *Lpl* is

expressed in a tissue-type specific manner. The expression on adipose tissue contributes to the storage of triglycerides in adipose tissue. But on skeletal muscle tissue, it stimulates the beta-oxidation of free fatty acids[174]. It also implied a decrease in triglyceride storage from food in white adipose tissue and an increase of fatty acid using in skeletal muscle of $Nf1^{Myf5}$ mice. It is just fit with the white adipose tissue weight loss that $Nf1^{Myf5}$ mouse suffered. In conclusion, $Nf1^{Myf5}$ mice showed a global increased fatty acid metabolism and mitochondrial enzyme genes expression. To make it even more precise, future experiments may focus on real-time metabolic testing with a metabolism chamber, which can efficiently measure animal food intake, energy expenditure, and physical activity simultaneously and non-invasively.

It is well known that oxidative phosphorylation (OXPHOS) is a robust and efficient way to generate energy. High energy compounds (NADH, $FADH_2$) in the redox state produced by glycolysis and TCA cycle can be transferred from the cytoplasmic and mitochondrial matrix to the mitochondrial inner membrane. An electron transport chain consisting of five mitochondrial complexes works to transfer electrons from the donner to the receptor, while at the same time, a proton gradient drives the synthesis of ATP. In theory, with reduced glycolysis ability, the NADH produced by the process, should also be decreased. Then the expression of OXPHOS component genes was checked. Surprisingly, a globally increased expression of these genes was detected, and some of them got even confirmed from the protein level with proteomics analysis.

The increased OXPHOS efficiency can be explained as a compensation for reduced ATP production by glycolysis. It also implied more NADH or $FADH_2$ was generated by the TCA cycle. There are ten steps in the TCA cycle, and the rate-limiting enzymes include citrate synthase, isocitrate dehydrogenase and α-Ketoglutarate dehydrogenase. In theory, glucose metabolism was reduced, the TCA cycle component enzymes expression should be increased, or the enzyme activity should be increased. RNAseq data showed all rate-limiting enzymes expression level increased in $Nf1^{Myf5}$ muscle tissue. Some of these genes expression were also confirmed from the protein level by proteomic analysis. For such complicated series of enzyme-catalyzed reactions, only with enzymes expression was still far away to conclude $Nf1^{Myf5}$ mice have increased TCA cycle activity and also OXPHOS, but data generated from enzymes and component genes expression could at least give some indications. For further confirmation, the TCA cycle metabolism assay kit might be used to see the functions of the enzymes of isolated mitochondria.

All of the above data suggested that $Nf1^{Myf5}$ mice have increased fatty acid oxidative phosphorylation activity. In order to check the real metabolic function of skeletal muscle from $Nf1^{Myf5}$ mice, a real-time metabolic test was performed with EDL and Soleus muscle, which represent glycolytic muscles and oxidative muscles, respectively. The efficiency of

mitochondrial complex I/II and also the efficiency of the entire electron transport chain were significantly increased in Nf1^{Myf5} EDL and Soleus muscle.

In summary, combining the transcriptome analysis, proteomics data, and real-time metabolism test suggested that Nf1^{Myf5} skeletal muscle have a metabolic transformation from glucose metabolism to fatty acid metabolism.

5.3.3 Loss of *Nf1* results in energy deficiency and reduced protein synthesis

Nf1^{Myf5} muscle tissue reduced its glucose catabolic process and increased the ability of fatty acid oxidative phosphorlyation. To check the energy compensation efficiency, one major phosphorylation site within the catalytic subunit of AMP-activated kinase (AMPK α, Thr172) was detected. Nf1^{Myf5} muscle showed an increased phosphorylation level of AMPK, which indicated the energy deficiency is still exist and the internal energy metabolism is still not in a steady-state. A large body of the literature indicated that AMPK has emerged as a master regulator of skeletal muscle metabolism. It acts as an activator for glucose uptake, fatty acid β-oxidation, and mitochondrial biogenesis[1,51,175,176]. Genes expression involved in muscle metabolism is strictly regulated through certain signaling pathways[175]. In addition, former work with human skeletal muscle single fiber analysis showed that the isoform of AMPK also depends on fiber type. For the α1 isoforms, mainly in the type I and type IIa fibers, for isoform α2, is mainly expressed in type IIa and fast fiber[49]. The antibodies used here detect both isoforms simultaneously. For further experiments, new methods such as capillary nanoimmunoassay and mass spectrometry analysis can be used to observe which isoforms are specifically activated, and see if this energy deficiency is fiber type-dependent.

As one of the key energy sensors, AMPK triggers the transcriptional process through its mediator, the peroxisome proliferator-activated receptor-gamma (PPARγ) coactivator-1α (PGC-1α). A mouse model with skeletal muscle-specific overexpression and deletion showed that PGC1α could positively regulate mitochondrial number and function, thereby shifting fast fiber to slow fiber[140,166]. As a transcriptional co-activator, it works directly with different transcription factors, including MEF2, NRF1, NRF2, ERRα, Pparg, to initiate mitochondrial respiratory chain enzymes, mitochondrial fatty acid oxidation pathway enzymes transcription[177]. The data showed that the expression level of *Pparg* and *Pgc1α* increased significantly in Nf1^{Myf5} skeletal muscle. The expression level of Pparg was also confirmed on the protein level. The energy sensor AMPK dependent signaling pathway Pparg/Pgc1α might be involved in the metabolism shift from glycolysis to fatty acid oxidative phosphorylation

Until now，many pieces of evidence have illustrated the direct effects of energy deprivation on skeletal muscle turn over[47,178]. As AMPK is responsible for inner energy homeostasis maintaining[51]. It could repress the ATP consumption anabolic processes (e.g protein and fatty

acid synthesis) and stimulate ATP generation catabolic processes[179]. Thus, with the energy deficiency phenotype that Nf1^{Myf5} skeletal muscle acquired, the protein synthesis and protein degradation signaling pathways were also detected with certain antibodies or primers. Upstream activators of mTOR signaling include mechanical overload and amino acid induction, negative regulators include muscle atrophy inducing pathways, as well as energy deprivation[180]. AMPK is a negative regulator of mTOR signaling which plays a vital role in skeletal muscle mass maintenance[48]. It controls both anabolic and catabolic signaling, thus contribute to the muscle hypertrophy and muscle atrophy[181,182]. Phosphorylated mTOR at ser 2448 was significantly reduced in Nf1^{Myf5} skeletal muscle. Besides, the mTOR target p-s6 kinase at site ser 235/236 was also decreased, indicating that Nf1^{Myf5} mice show reduced mTOR signaling-dependent protein synthesis rate. In fact, more experiments are still need to be performed such as westernblot to detect the phosphorylation level of 4E-BP1 (Thr37/46) another downstream target of mTOR signaling and phosphorylation level of eEF2 (Thr56), one indicator for protein translation enlongation[183,184].

Other than this, proteomics data with gene ontology analysis showed the GO terms enriched for translation in wild type and heterozygous control animals,. This mainly includes the ribosome components and the aminoacyl-tRNA synthetase. In contrast to protein synthesis, the components of the proteasome 26s subunit proteins were significantly increased in Nf1^{Myf5} muscle. The ubiquitin-proteasome system is the major site for protein degradation. Atrogin-1 and MuRF-1 are E3 ubiquitin ligases expressed in skeletal muscle and may alo be involved in the regulation of the protein degradation process, and more qPCR tests still need to be performed.

This part implied that Nf1^{Myf5} muscle mass loss might be caused by energy deficiency induced hyper activation of AMPK pathway and a decrease of protein synthesis regulated by mTOR signaling and also an increase in protein degradation process.

5.4 Muscle phenotype caused by *Nf1* deletion is Nf1/Ras/ERK signaling pathway independent.

Stimulation of the Ras/MAPK/ERK signal pathway can promote anabolism and mitogenic activity[117,185]. It is a key regulator of skeletal muscle growth through transduce growth factor mediated singalings such IGF1-Akt signaling[186]. Besides, genetically modified mice with a consititute activation of ERK signaling in both myoblasts and mature muscle fibers showed an induction of fiber type switch from fast glycolytic type II to slow oxidative type I phenotype and also a protection from muscular dystrophy[187]. Nf1 acts as a negative regulator of MAPK

pathway, theoretically, it's deletion can contribute to hyperactivation of the signaling. Thus $Nf1^{Myf5}$ mice should have healthier state. However, $Nf1^{Myf5}$ mice suffered from the phenotype that is just the opposite. Therefore, the activity of ERK signaling was detected with the phos-ERK1/2 antibody, surprisingly, there was no difference between $Nf1^{Myf5}$ and control muscles. It suggested that *Nf1* deletion does not alter the activity of Ras/MAPK/ERK signaling in skeletal muscle. It is supported by the the $Nf1^{HSA}$ mouse model, which *Nf1* was specifically knockout in mature muscle tissue with human alpha-skeletal actin Cre. This mouse model does not show any overt muscle phenotype[148]. The human protein atlas illustrates that *Nf1* is expressed at a very low protein level in the skeletal muscle system; In addition, the Ras/MAPK/ERK signaling can being influenced by many other factors, such as hormones and energy status. Even though the low expression of *Nf1* could still influence the MAPK signaling, the effect might also be compensated. Thus, the impact caused by *Nf1* deletion may be ignored under this circumstance[188,189]. ERK activity was also tested from muscle progenitors, and immunostaining showed a significant increased ERK1/2 phosphorylation level in $Nf1^{Myf5}$ muscle progenitors. Besides, previous data also showed that Nf1 protein could be detected in primary myoblasts, but after differentiation, its expression level went to even lower. This may be the cause of the phenotype difference between the $Nf1^{Myf5}$ and the $Nf1^{HSA}$ mouse models. In addition, it also implied the muscle phenotype of $Nf1^{Myf5}$ mice might be caused by defects in muscle progenitors, rather than the function of *Nf1* directly in mature muscle tissues. Interestingly, even without alteration of ERK signaling in muscle tissues, a fiber type change from fast to slow still could be observed, which remind that underlying regulators should come from the muscle progenitors.

Thus the following question is, how does the hyperactivation of ERK1/2 signaling affect the development of myogenic progenitors in vivo? ERK1/2 signaling is one of the most intensively studied pathways for both proliferation and differentiation regulation[185,190,191]. In vivo chick embryo development studies indicated that FGF-ERK signaling activity decreased with myogenic differentiation[192], blockage of this signaling pathway with certain inhibitors can accelerate chick myogenic differentiation, and inhibiting MAPK/ERK signaling or ERK nuclear translocation can also induce robust myogenic differentiation[192]. ERK located within nuclear works to promote proliferation and ERK located in the cytoplasmic responsible for differentiation. In addition, the situation is also the same as the in vitro culture of mouse satellite cells[192]. Besides, a mouse model of Ptpn11 (a MAPK/ERK signaling maintenance regulator) knockout in muscle progenitors, showed only in postnatal myogenic stem cells, decreased activity of ERK1/2 activity contribute to reducing proliferation and increasing cell cycle retraction[193]. It also implied the function of ERK1/2 signaling transduction is highly biological

context dependent[193]. Therefore, the next question is, how does the increased ERK1/2 activity affect the muscle progenitors of $Nf1^{Myf5}$ animals?

5.5 *Nf1* deletion leads to muscle progenitors into quiescent through MAPK/ERK/NO/Notch signaling.

5.5.1 Depletion of muscle stem cell pool during postnatal muscle development

As the muscle phenotype caused by *Nf1* deletion might be transmitted from Nf1-deficient muscle progenitors. Therefore, the $Pax7^+$ cells were detected with time series immunostaining. Interestingly, knockout *Nf1* results in a global reduction of proliferating cells in p21 muscle tissues. As muscle tissues are composed of varies cell types, it seems that *Nf1* deletion in muscle cells can also influence other cell types anabolic process. Unexpectedly, for $Pax7^+$ cells, there are still significantly more progenitors in the $Nf1^{Myf5}$ muscle at E18.5, but it changed to the opposite after delivery. The number of $Pax7^+$ cells decreased more rapidly than control, which is caused by a large amount of *Nf1* knockout cells left their cell cycle and behaved more like quiescent stem cells. During postnatal development, most juvenile satellite cells are still in the cell cycle, they are in symmetric or asymmetric cell division, and a cell from asymmetric cell division can exit the cell cycle and become quiescent muscle stem cell[87]. This gradual process starts form the early birth until the mouse matures (around 12 weeks). Muscle stem cells constitute ~30% of the muscle nucleus of neonate mice, and it decreases with age to ~4% for adults and ~2% in the senile (29 – 30 months) mice[92].

Given the function of ERK signaling in the proliferation and differentiation of muscle stem cells after birth, the $Nf1^{Myf5}$ muscle progenitors phenotype was opposed to the expectation. In theory, the $Nf1^{Myf5}$ muscle should have more progenitors instead of the opposite way. Due to the high dynamics and flexibility of the internal muscle system and a large amount of influencing factors may also be involved. In addition, ERK1/2 signaling itself with different dosages and biological background; Its function is also different. $Nf1^{Myf5}$ muscle progenitors showed stronger quiescent characteristics compared with control cells. Immunostaining for cytospin FACS sorted $Pax7^+$ cells suggested *Nf1* deletion increased Pax7 expression and simultaneously decreased their proliferation. Since literature shows that mTORC1 controls the transition of muscle stem cells from a quiescent state to activated state and p-S6 kinase and P-p70s6k are the downstream target of mTORC1[194]. Decreased p-S6 kinase and P-p70s6k levels in *Nf1* knockout $Pax7^+$ cells were observed. Thus mTORC1 signaling pathways might be involved in the regulation of muscle stem cell quiescent induced by *Nf1* deletion. $Nf1^{Myf5}$ muscle progenitors have stronger ERK1/2 activity but reduced mTOR signaling activity. Normally, the

biological functions of these two signaling pathways are similar, namely promoting cell survival, cell proliferation, and cell motility[195,196]. Under certain circumstance, these two pathways can both positively cross talk but also show negative cross inhibition[197-200].

In order to make the activated signaling pathway by *Nf1* knockout more clear, $Nf1^{Myf5}$ progenitors were taken out for in vitro cell culture. Interestingly, *Nf1* deletion caused opposite properties for in vitro cell culture. When in vitro cell culture was performed, even though the differentiation medium has been changed, these cells always maintain a high proliferation rate and delay for differentiation. It might be explained by once cells are taken out, the remaining influencing factors from the in vivo environment will also disappear. Then for $Nf1^{Myf5}$ muscle progenitors, the only difference from control cells is that its ERK1/2 activity leads to an increased rate of proliferation, which is in line with the previously reported functions of ERK/MAPK signaling[153]. Upon inhibition of MEK/ERK1/2 signaling, *Nf1* deleted proliferating myoblasts can be driven out of their cell cycle and start to differentiate like Control cells. The in vitro properties of *Nf1* knockout muscle progenitors and primary muscle myoblasts this clearly are Ras/ERK1/2 signaling dependent.

Muscle satellite cells are heterogeneous populations. At a particular developmental stage, their molecular marker expression and also their cellular properties are also different. During embryonic development, both Pax3 and Pax7 directly bind to the enhancer and promoter of *Myf5* and *MyoD*, respectively, and regulate their expression[201]. Even though Pax3 was only expressed in the early embryonic stage, knockout of Pax3 induced an increase in Pax7 expression as compensation[14]. For double knockout animals, the progenitors will undergo apoptosis without any muscle formation[14]. The function of Pax3 and Pax7 is mainly to maintain the proliferative properties of progenitors and repress their terminal differentiation. Anyone of them is sufficient to induce a myogenic process in mouse embryonic stem cells.

Pax3 is mainly responsible for the embryogenic myogenesis, especially the migration of progenitor cells in the limbs. Pax7 primarily contributes to fetal myoblasts and later muscle satellite cells[14,202]. After birth, Pax3 was sharply downregulated, the muscle progenitors are mainly $Pax7^{+}$ cells, but this population is also not unique. From p1 to p21, a large number of juvenile muscle satellite cells undergo proliferation, differentiation, and fusion with existing muscle fibers for nuclear-inserted muscle hypertrophy. How to maintain the stability of the stem cell pool for further risks such as injury and exercise is a complicated process. Recent studies have shown that for adult satellite cells only about 10% solely $Pax7^{+}$ cells can enter a quiescent state, and this process is regulated by planar cell polarity, which dependent on WNT signaling, allowing cells to be in a planar orientation, thereby enhancing the symmetric division for muscle stem cell pool maintenance[87,203]. Only cells attached with the basal lamina can go into a real quiescent state, which may be related to the stiffness of the basal lamina. That might also

explain specially designed hydrogel could promote the survival of satellite cells during regeneration transplantation[204]. Although satellite cells play a dominant role in muscle regeneration and muscle hypertrophy, the effects of other cell types are also significant in this process. In the early stages of regeneration, macrophages can positively regulate p38MAPK signaling by secreting of growth factors, including TNF, IL-6, and TGF beta, to induce myoblasts to enter a terminally differentiated state[205]. Besides, FAPs can also contribute to the final differentiation of myoblasts[206]. The mechanisms involved in reversible quiescence regulation is also different between MyoD positive and negative cells. For MyoD positive cells, studies showed that the up-regulation of Spry1 could block the ERK signaling and induces cells to return to a quiescent state. However, Spry1 knockout myoblasts can also maintain a stem cell pool homeostatic, implied an alternative way of quiescent reversion exists[207]. For the MyoD negative cell population, most of which are $Pax7^{+}Myf5^{-}$ cells, the return to quiescent is regulated by Tie2 dependent activation of ERK signaling to promote expression of Pax7. It suggests that the role of ERK signaling in modulating satellite cells enter quiescence is time and context dependent[208]. Combined all, it implied a highly complex regulatory network of satellite cells through extrinsic ways.

When culturing cells in vitro, many extrinsic signaling pathways, including Notch, Wnt, and ECM, are mostly abrogated. In addition, the stiffness of the coated cell culture plate is also different from the in vivo status. Only excessive activation of Ras/ERK signaling caused by *Nf1* deletion is left and contribute to different cellular properties. In order to elucidate the in vivo mechanism, more culture conditions need to be used to simulate the in vivo state. Satellite cell culture with their attached fibers combined with signaling pathway inhibitors may be an excellent solution to solve this problem. However, given the limitations of single fiber separation and culture protocol, for example, most protocols use older than 6-week-old mice, which means that almost all satellite cells are in the quiescent state, which is more helpful for quiescent satellite cells activation studies[209,210]. Furthermore, this experiment is intricacy that it works for adult mice, for mice younger than p21, it is almost impossible to obtain intact single fibers, especially from *Nf1* knockout mice with reduced muscle mass. Therefore, the in vitro cell culture model is not sufficient to see the function of *Nf1* on postnatal muscle development, and new methods need to be employed in the future.

5.5.2 Muscle progenitors shift towards quiescent from transcripts level

Previously generated data makes the function of *Nf1* on muscle progenitors a mystery of conflict. Whole transcriptome analysis of *Nf1* deleted muscle progenitors was performed to get a more precise and more basic overview. *Nf1* deletion leads to a global induction of muscle

stem cell quiescent genes expression and downregulation of muscle stem cell activation gene. In total, 38 activation genes were significantly down-regulated in $Nf1^{Myf5}$ muscle progenitors. For the quiescent signature, a large number of genes from the ECM component were detected. The muscle satellite cells are located between the apical sarcolemma and basement membrane (ECM) of the terminally differentiated muscle fibers. The basement membrane is composed of two layers, the internal layer is called the basal lamina, and the external layer is named reticular lamina. Although resident fibroblasts have always been recognized as a significant contributor to the production of ECM components, muscle stem cells can also synthesize and secrete different classes of ECM components, suggesting that they have a direct role in their own niche regulation[211-214]. During myogenesis, to satisfy the functional requirement of muscle progenitors, the ECM component is always in the process of remodeling until muscle stem cells enter a quiescent state[7]. Thus, the stem cell niche composed of ECM components plays a critical role in maintaining a balance between quiescence and activation. In the quiescent state, ECM proteins work to repress mitosis and differentiation of muscle stem cells[95]. Once the muscle is damaged, the components of the basal lamina will be degraded by matrix metalloproteinase, and the activated satellite cells with relative growth factors and signaling molecules will be liberated for damage repair[213]. $Nf1^{Myf5}$ muscle progenitors increased their ECM component genes expression, particularly for *ColIV*, *ColV* , *ColVI*, and *Tnc*, which implied the higher quiescent signature of these progenitors. Except for ECM component genes, another group of genes belonging to the term of imprinted genes also increased their expression in $Nf1^{Myf5}$ muscle progenitors. Previous work has shown that imprinted genes are predominantly expressed in adult somatic stem cells[215,216]. In muscle, the imprinted gene *Pw1*/*Peg3* could regulate skeletal muscle growth, satellite cell metabolic state and self-renewal[85]. Except for *Peg3* and *Dlk1*, the function of another imprinted gene as a critical cell cycle inhibitor, *Cdkn1c*, is in line with a decrease in the proliferation rate of these progenitors. In conclusion, with increased expression of quiescent relative genes and decreased expression of activation related genes, transcriptome analysis demonstrated the quiescent signature of $Nf1^{Myf5}$ progenitors in a more compressed and convincible way.

In hematopoietic stem cells, imprinted genes control their quiescence through a negatively regulated PI3K-mTOR pathway and inhibit their mitochondrial metabolism[217]. Following this point, a global reduction of glycolysis enzymes was observed in $Nf1^{Myf5}$ progenitors, and glycolysis metabolism activity was also significantly reduced. Interestingly, except for glycolytic genes, the expression of mitochondrial metabolic genes in $Nf1^{Myf5}$ muscle progenitors was also slightly lower, indicating that $Nf1^{Myf5}$ progenitors with higher quiescent signature might also need less energy expenditure. Quiescent satellite cells use fatty acid oxidative phosphorylation to generate energy[155], and no difference in these genes expression was detected in $Nf1^{Myf5}$

muscle progenitors. So far, it has been thought that activated satellite cells mainly use glycolysis and quiescent satellite cells mainly dependent on fatty acid oxidative metabolism[218]. However, in vivo, satellite cells are a mixed population that has cells of different statuses: quiescent cells, activating cells, and intermediate cells. For these juvenile progenitors, the intermediate cells are dominant. They can use both ways of energy production. Even though they have reduced rates of glycolysis and oxidative phosphorylation, the energy requirement of these cells with a higher quiescent signature might also be satisfied[219].

Not so many investigations have been performed on juvenile muscle progenitor's metabolism. Thus, it might be an exciting point. A precious method for investigating dynamic metabolic changes is the use of stable isotope-labeled substrates for metabolic flux analysis. It can be used in future experiments. In addition, a paper published by Vittorio Sartorelli's lab showed that cellular metabolism could regulate the expression of myogenic genes through epigenetic modifications of a specific histone marker, which first involves a metabolic process, epigenetic modifications, and myogenesis genes expression. In short, activated satellite cells use glycolysis to maintain their energy stability while simultaneously obtaining the biomass needed for cell division.With an increased glycolysis rate, the NAD^+ will be converted to NADH. During this process, the concentration of NAD^+ in cytoplasm will decrease. Thus the histone deacetylase enzyme Sirt1, whose activity is NAD^+ level-dependent, will also decrease. Then its target H4K16 acetylation will increase. Acetylation of lysine 16 on the tail of histone H4 undermines the interaction of H4 with H2A, which disrupts the higher order of chromatin structure and makes transcription factors more accessibility to DNA and activates myogenesis gene transcription[2,220].

Nf1 deletion leads to progenitors show higher quiescent signature as well as a less energy production. Decreases glycolysis activity very likely caused the reduced the H4K16 acetylation level, thus repressed myogenesis-related genes transcription.

5.5.3 Stronger quiescent signature is MAPK/ERK/NO/Notch signaling dependent.

Apart from the expression difference in stem cell activating genes, ECM component genes, and stem cell imprinted genes. Another set of genes under the GO term of Delta-Notch signaling was also noticed. Since both the Notch receptor and the ligand are transmembrane proteins, this signaling needs to have cell-to-cell interactions. Once this signaling pathway is activated, the intracellular domain of Notch (NICD) will be cleaved and enter the nucleus, as a transcription co-activator combined with RBPJ induces Notch target genes expression[221]. The function of the Notch pathway is profoundly cellular environmental dependent. The literature

showed that during embryonic development, a large number of muscle progenitor cells are still proliferating, and Pax7 is highly expressed, and these cells have high expression of Notch receptors. At this time point, the Notch pathway promotes the proliferation of muscle progenitors[151]. Using the transgenic Notch reporter mouse model RBP-J Pax7CreER^{tm}, Thomas A. Rando's lab showed that Notch signaling was activated and played a critical role in satellite cell quiescent state maintenance[67,68]. In the first few weeks of postnatal muscle development, muscle progenitor cells gradually enter a quiescent state, how does the Notch pathway play a role in this process? Can activated satellite cells drive back into a quiescent state? To answer this question, another paper in 2016 showed that sex hormones could establish a reserve pool of quiescent muscle stem cells by inducing myofibers to express Mind bomb 1 (Mib1) during puberty, which activates the Notch pathway in proliferating juvenile satellite cells and driving them into adult quiescent satellite cells[66].

In this project, for Nf1^{Myf5} animals, an increased number of muscle progenitor cells was observed at E18.5, which can be explained by the activation of the Notch pathway to promote the proliferation rate of Nf1^{Myf5} muscle progenitor cells prenatally. In the first three weeks after birth, Nf1^{Myf5} muscle progenitors gradually decreased, eventually leading to the depletion of adult stem cell pool. This would fit with hyperactivation of the Notch pathway to drive these activated muscle progenitor cells into a quiescent state. Considering the activation of Notch pathway needs cell-cell contact, once the cells being taken out and cultured in vitro the function of this pathway may have been abrogated. Especially for muscle stem cell culture, to avoid differentiation, they cannot attach with each other. Thus the Notch pathway is accidentally completely removed. This is also fit why in vitro cell culture of Nf1^{Myf5} muscle progenitors and Nf1^{Myf5} primary myoblasts, their quiescent signature disappeared, with the only activation of ERK activity, they proliferate much faster and are unable to differentiate even with differentiation medium. In vitro myoblasts culture with MEK inhibitor treatment could block the proliferation and promote the differentiation of Nf1^{Myf5} primary myoblasts. For muscle progenitors cultured with Notch ligand Jag1 could also repress the proliferation rate especially in *Nf1* deleted progenitors. Besides with ligand treatment the expression pattern of Notch target genes and quiescent related genes could also be recapitulated for in the vivo status. Thus hyper activation of Notch pathway regulated by *Nf1* deletion could explain the aberrant behavior of muscle progenitors during development as well as in vitro cell culture.

The effect of *Nf1* deletion is the excessive activation of Delta-Notch signaling. However, the underlying mechanism is still unclear. Previous literature has shown that in pancreatic cancer cells, activation of MEK/ERK signaling can promote the expression of the Notch target gene *Hes1*, and inhibition of the Notch pathway can block MEK/ERK-induced *Hes1* expression. It suggests that the MEK/ERK signaling can positively regulate Notch signaling under this

biological background[222]. In human glioblastomas patients and established mouse models, it was observed that nitric oxide drives the activation of the Notch pathway via the cGMP/PKG signaling pathway. Loss of function experiments also showed that without NO production, Notch signaling was repressed in vivo, and the lifespan of the mouse model was also prolonged. The paper showed that NO/cGMP/PKG signaling promotes tumor cells in the perivascular niche to behave in a stem cell-like character[157]. NF1 patients always suffer from learning deficits because of neurological disabilities. The researchers showed that in *Nf1* mutant oligodendrocytes, excessive activation of MAPK signaling leads to an overproduction of nitric oxide, thus contribute to over activation of Notch signaling. In vivo mouse model, injections were used for pathway rescue experiments with single or combination of inhibitors (including MEKi, L-NAME, and GSI (DAPT)) to confirm the function of MAPK/NO/NOTCH signaling in neuronal cells[121].

GO analysis for RNAseq data from muscle progenitors showed profoundly enriched terms of cGMP/PKG signaling in $Nf1^{Myf5}$ progenitors. As nitric oxide activates NO-guanylyl cyclase, which functions in increase synthesis of cGMP from GTP, thus activate PKG phosphotransferase activity and initiate a cascade of reactions, namely cGMP/PKG signaling[223]. With enriched cGMP/PKG signaling caused by *Nf1* deletion, muscle progenitors might also be affected by nitric oxide. To test it, the in vitro progenitor cell culture model was used with the combination of Notch pathway activation (Jag1 treatment), ERK1/2 signaling repression (U0126 treatment), and nitric oxide production inhibition (LNAME treatment). Under the Notch pathway activation condition, ERK1/2 inhibitor can actively improve the myogenic differentiation of muscle progenitors and reduce their proliferative capacity, while reducing the expression of *Pax7* and Notch target genes such as *Hes1* and *Hey1*, suggesting the cooperative function of ERK signaling in Notch pathway activation in muscle progenitors. Block of nitric oxide production can also repressed the Notch target genes expression and promotes myogenic differentiation indicating nitric oxide also plays a role in Notch pathway activation.

The Notch pathway is one of the fundamental signaling pathways in developmental and cancer research. In recent years, more and more research groups are paying attention to the role of the Notch pathway in metabolic regulation. Since the Notch pathway is always activated in stem cells and cancer cells, it always works with the state transitions of these cells[224-227]. The metabolic shift from oxidative phosphorylation to oxygen-independent glycolysis is a common phenomenon of tumor growth and invasion, known as the Warburg effect[30]. Studies have shown that both the inactivated and activated Notch pathway can induce glycolytic switch through PI3/AKT signaling or a p53 dependent pathway, respectively[228]. This conclusion reveals the role of the Notch pathway in the maintenance of energy homeostasis in breast cancer cells[228]. Also, it has been shown that for pre-T cells, activation of Notch also promotes

glycolysis through the PI3/AKT signaling pathway[77]. For neuronal cells, the literature showed that the Notch pathway might not regulate glycolysis at an early embryonic stage during zebrafish neuron development but positively regulates glucose transporter expression and negatively regulate *Hk2* expression during late developmental stages. It means that the function of the Notch pathway for glycolysis regulation is highly environmentally dependent during development[229]. For mesenchymal progenitor cells, the Notch pathway represses glucose metabolism by down regulating glycolytic related genes, including *Pfkfb 2,3,4, Eno 2,3*, and *Ldha*. It also inhibits the expression of mitochondrial complex I component genes, such as *Ndufaf2*, *Ndufc1*, *Ndufaf4*, *Ndufs5*. Thus Notch pathway block differentiation ability of mesenchymal progenitors by controlling their metabolism[230]. *Nf1* knockout in muscle progenitors leads to excessive activation of the Notch pathway and also at the same time with globally shut down of glucose metabolism, a phenomenon similar to that of mesenchymal progenitor cells[230]. For double-check, in vitro muscle progenitors culture with or without Jag1 was used to detect the role of the Notch pathway for metabolic regulation in myogenesis context. Here, the data showed hyperactivation of the Notch pathway could repress glycolysis and oxidative phosphorylation genes expression also in muscle progenitors.

$Nf1^{Myf5}$ muscle progenitors showed a hyperactivation of the Delta-Notch pathway. The next interesting point is if the Notch pathway gets blocked in vivo with a specific pathway inhibitor, then what will happen for these $Nf1^{Myf5}$ muscle progenitors? To answer this question, firstly, a suitable Notch pathway inhibitor needs to be found. A large amount of Notch pathway inhibitors has been used in recent years, and some of them are just under clinical research[231,232]. The most promising Notch pathway targeted therapies were clinical treatment with γ-secretase inhibitors (GSIs), even though these inhibitors are none-specific and have off-target side effects[233]. Almost all the adverse effects were Notch-mediated, and these could be conquered by dose-limiting and intermittent admiration[234]. Based on the published literature, one member of the GSIs family was chosen here, which was DAPT. DAPT has been widely used in Notch pathway research including for explant culture for presomitic mesoderm/early somite, somite, forelimb bud with DAPT to study the function of the Notch pathway in fate determination during cells migrate from the somite to the limb. It has been proved that the Notch pathway drives dermomyotomal progenitors to vascular instead of skeletal muscle fate in such early embryo development stage[235]. In vitro cell culture for fibro-adipogenic progenitors (FAPs) with DAPT showed that the Notch pathway negatively regulates FAPs differentiation both in vivo and in vitro but for FAPs isolated from MDX mice they are insensitive to Notch pathway[236]. iPSC cells generated from Duchenne muscular dystrophy patient induced into myoblast with DAPT treatment to inhibit the Notch pathway could induce robust and faster myogenic differentiation, which aligns with the function of the Notch pathway for stem cell maintaining[237]. DAPT was

also used for in vivo Notch pathway inhibition in the Duchenne Muscular Dystrophy mouse model, dystrophy/utrophin double knock out mice. With data showed stem cell pool depletion in patients and also mouse model caused by hyperactivation of the Notch pathway. Thus, DAPT was injected as an in vivo Notch inhibitor. Data showed for dKO mice Notch pathway inhibition led to down-regulation of Notch pathway-related genes, including *Notch1/3*, *Hes1*, *Hey1*. On the contrary, myogenesis genes for *Pax7* and *MyoD* expression increased dramatically. Compared with the dKO mouse without DAPT, the satellite cells increased two times[238].

The problem that bothers is how to define the dosage and time point of these injections, as the function of the Delta-Notch pathway is always dosage-dependent. With DAPT injection, Notch pathway-related genes expression was decreased to a medium level, but not abrogated. In line, the data showed that with DAPT injection, a strong increase of muscle progenitors was observed, and muscle progenitors proliferation rate was also increased. DAPT injection resulted in increased muscle fiber size and also mouse body weight and white adipose tissue weight. The quality of DAPT injected $Nf1^{Myf5}$ mouse is much better than control animals. p21 mouse was dissected for relevant analysis. In the future, if more mice could be used, the life span of these animals will be measured. Hopefully, longer survive time for DAPT injected mice could be observed.

5.6 *Nf1* deletion lead to epigenetic modification status change.

Nf1 knockout mice show severe metabolic related myopathy, which might be caused by the reduction of glucose glycolysis in muscle fibers and as compensation AMPK signaling induced fatty acid oxidative phosphorylation genes expression. As the function of *Nf1* in mature muscle tissue appears to be very limited according to its low expression, and no differences in MAPK/ERK signaling in $Nf1^{Myf5}$ muscle. In addition, *Nf1* deletion in muscle fiber with the $Nf1^{HSA}$ mouse model also showed no muscle phenotype[148]. Besides, a decreased glycolysis activity is also observed in *Nf1* knockout muscle progenitors. Thus the myopathy caused by fiber type and metabolism change very likely is already lying down in muscle progenitors and further transmitted to muscle fibers. Thus epigenetic chromatin modification, including DNA and histone modification, as a persistence over cell generations (epigenetic memory) might be a possible mechanism.

Methylation of cytosine bases within CpG dinucleotide pairs is an important epigenetic modification way, which typically reduces gene expression when located within a promoter or enhancer region[239]. DNA methyltransferase (DNMTs) and demethyltransferase (TETs) family

members mediate DNA methylation and demethylation activity. As the substrates of these enzymes are derived from cell metabolism, such as methyl-group is from glycolysis byproduct 3-P-Glycerate initiated one-carbon cycle product SAM. Tet demethylation relies mainly on TCA cycle intermediate α-ketoglutarate[9,240]. Furthermore, DNA methylation is always considered as more stable during cell division[241]. Interestingly, in *Nf1* deleted muscle progenitors, a global significantly increased expression of DNMTs family genes, including *Dnmt1*, *Dnmt3a*, and *Dnmt3b* were observed. It suggested that *Nf1* knockout might drive a DNA methylation status change. To see global DNA methylation changes including myogenesis loci, MeDIP-Seq was performed. Globally increased DNA methylation was detected in $Nf1^{Myf5}$ muscle progenitors. Hypermethylation of fast fiber specific gene Myosin light chain 1 (*Myl1*) and glycolysis activate gene 6-phosphofructo-2-kinase/fructose-2,6-biphosphatase 1 (*Pfkfb1*) in *Nf1* knockout progenitors were noticed. The expression of both genes was commonly decreased in muscle progenitors as well as muscle fibers. $Nf1^{Myf5}$ mice showed reduced fast fiber component genes expression and also glycolysis genes expression in mature muscle fibers, it suggested that these two genes might be the potential targets for further analysis. Previous DNA methylation analysis showed that it functions for the production of specific cell lineages during embryogenesis by downregulation of global gene expression. Demethylation for lineage differentiation genes drives the activation of lineages formation[103,242]. Under myogenesis context, early work has shown that during quiescent muscle stem cell activation, a reduction of TETs and DNMT3a and induction of DNMT1 isoforms was observed implied function of DNA methylation for satellite cells activation[243]. Compared with muscle progenitors, a dramatic decrease in the DNA hypermethylation in mature muscle fibers was noticed[244-246]. For epigenetic memory, researchers for the first time, reported that adult human skeletal muscle keeps an epigenetic memory of earlier muscle hypertrophy induced by acute and chronic anabolic stimulation. Seven weeks loading, seven weeks unloading, and seven weeks reloading was performed, gene expression and methylation profiling were analyzed. This resulted in a doubling of CpGs hypomethylation after reloading compared with earlier loading. *AXIN1*, *GRIK2*, *CAMK4*, *TRAF1* might be the epigenetic memory genes during this process. However, these genes are mostly not well studied for muscle hypertrophy[247].

Except for DNA methylation analysis, as one of the best-studied histone modification markers, H3K27me3 was also analyzed with the chipmentation method. Data showed that *Nf1* knockout leads to decreased H3K27me3 levels from both progenitors and muscle tissue. It was suggested that tumor necrosis factor alpha via P38 alpha activates EZH2, a component of polycomb repressive complex2 (PRC2). PRC2 deposits the repressive marker H3K27me3 on the *Pax7* gene leading to a reduction of *Pax7* expression, which is necessary for satellite cell differentiation and muscle regeneration[205]. Mice with EZH2 specifically knockout in satellite

cells showed a reduction of Pax7+ cells which is associated with the impaired proliferation in satellite cells and a postnatal skeletal muscle defects[105]. Jennifer M. Pell et al. also showed EZH2 is mainly required for the proliferation state of muscle satellite cells and there is no influence for terminal differentiation genes expression[104]. Liu et al. showed that compared with quiescent satellite cells, activated progenitors have a higher H3K27me3 level indicated a role of H3K27me3 on satellite cells activation[106]. A global reduction of H3K27me3 expression in *Nf1* deleted muscle progenitors also includes the decreased H3K27me3 enrichment around the transcription start site of stemness marker *Pax7*, the increased pax7 expression drive these progenitorss into a stronger quiescent status.

In short, an epigenetic status change was detected in *Nf1* deleted muscle progenitors. This change may contribute to decreased fast fiber specific gene (*Myl1)* and glycolysis activator gene (*Pfkfb1*) expression. It might also influence these two gene expressions once progenitors differentiated into myofibers. Besides, a decreased H3K27me3 level also match with the stronger quiescent signature in *Nf1* deleted muscle progenitors.

6 Summary and outlook

Summary

The ultimate purpose of this project was to elucidate the function and underlying mechanism of neurofibromin I during postnatal skeletal muscle development. Neurofibromin I is a tumor suppressor protein that works as a GTPase activator (GAP) through negative regulate the canonical Ras-MAPK-ERK signaling. Mutation of the Nf1 gene leads to a reduction of neurofibromin I, which causes an autochrosomal dominated genetic disorder named neurofibromatosis type I (NF1). Clinical features have been reported in NF1 patients, including pathological changes of the musculoskeletal system, particularly reduction of muscle mass and muscle strength.

In this project, it is the first time that a muscle-specific *Nf1* knock out mouse model was used for functional analysis of *Nf1* during postnatal muscle development. $Nf1^{Myf5}$ mice showed a gradual loss of muscle weight, which recapitulates the patient phenotype. *Nf1* deletion in muscle progenitors leads to muscle stem cell pool depletion. Nf1/ERK/NO/Delta-Notch signaling is involved in the regulation of this phenotype. The results suggest that loss of Nf1 in muscle progenitors results in the hyper activation of Ras/ERK signaling, and ERK signaling via Nitric Oxide leads to a stronger stimulation of the Delta-Notch pathway. During early postnatal muscle development, activation of the Notch pathway drives progenitors out of cell cycle and go gradually to quiescent. For $Nf1^{Myf5}$ muscle progenitors stronger Delta-Notch pathway contribute to the earlier transition of this process and satellite cell pool depletion. The quiescent signature of Nf1 deleted progenitors was identified from transcription of quiescent genes, reduction of glycolysis activity and also epigenetic change.

Nf1 knockout mice showed a metabolism defect of glucose glycolysis and sever energy deficiency. As compensatory, energy sensor AMPK stimulated fatty acid oxidative phorsphorlyation which might through Pparg/Pgc1a signaling, accompanied by suppressed protein synthesis rate and increased the degradation process. In addition, a fiber type transition from fast to intermediate slow fibers was also detected. As *Nf1* functions specifically before myoblasts differentiation. Thus the metabolic myopathy caused by *Nf1* deletion should be generated from muscle progenitors.

One possible explanation might be *Nf1* deletion caused the epigenetic modification status change, in a certain way the change can be remembered by the nucleus of satellite cells even after they differentiated into mature muscle fibers. The reduction of glycolysis genes

expression in both progenitors and mature muscle fibers is a good indicator. However, a further intensive study still needs to be performed to find the potential target mechanism.

Zusammenfassung

Das Ziel dieses Projekts war die Aufklärung der Funktion und des zugrunde liegenden Mechanismus von Neurofibromin I während der postnatalen Skelettmuskelentwicklung. Neurofibromin I ist ein Tumor- Suppressor, der als GTPase-Aktivator (GAP) durch negative Regulierung des kanonischen Ras-MAPK-ERK- Signals wirkt. Eine Mutation des Nf1-Gens führt zu einer Reduktion von Neurofibromin I, was eine autosomal-dominante genetische Erkrankung namens Neurofibromatose Typ I (NF1) verursacht. NF1- Patienten zeigen verschiedene klinische Merkmale, darunter pathologische Veränderungen des Bewegungsapparats, insbesondere eine Verringerung der Muskelmasse und der Muskelkraft.

In diesem Projekt wurde zum ersten Mal ein muskelspezifisches Nf1-Knock-out-Mausmodell für die Funktionsanalyse von Nf1 während der postnatalen Muskelentwicklung verwendet. Nf1Myf5-Mäuse zeigten einen allmählichen Verlust des Muskelgewichts, was den Phänotyp der Patientin rekapituliert. Die Nf1- Deletion in Muskelvorläuferzellen führt zu einer Erschöpfung des Muskelstammzell-Pools, was durch eine Dysregulation des Nf1/ERK/NO/Delta-Notch-Signalwegs verursacht wurde. Die Ergebnisse deuten darauf hin, dass der Verlust von Nf1 in den Muskelvorläuferzellen zu einer Überaktivierung des Ras/ERK-Signals führt, und das ERK-Signal über NO führt zu einer stärkeren Stimulation des Delta-Notch-Signalwegs. Während der frühen postnatalen Muskelentwicklung treibt die Aktivierung des Notch-Signalwegs die Vorläuferzellen aus dem Zellzyklus heraus und in die Quieszenz hinein. Bei den $Nf1^{Myf5}$- Muskelvorläuferzellen zeigt sich eine gesteigerte Induktion dieses Prozesses, gezeigt durch Transkriptomanalyse, epigenetische Analyse und metabolische Flux Analyse, was schließlich zur Erschöpfung des Satellitenzell-Pools führt.

Eine Transkriptomanalyse der Nf1-Knockout-Mäuse deutete einen Defekt der Glykolyse im Muskel an, gleichzeitig zeigten die Tiere Zeichen eines Energiemangels. Demgegenüber war der Fettsäuremetabolismus erhöht, zusammen mit erhöhtem Pparg/Pgc1a-Signaling. Eine Inhibition des mTOR Signalwegs ist der wahrscheinliche Grund für eine verringerte proteinsynthese. Zusätzlich wurde auch ein Fasertyp-Übergang von schnellen glycolytischen zu schnellen oxidativen Fasern festgestellt. Diese Defekte wurden jedoch nicht von einer Funktion von Nf1 im Muskel, sondern von seiner Funktion in Vorläuferzellen ausgelöst. Daher stellt diese Arbeit die Hypothese auf, dass die Nf1-Deletion in Vorläuferzellen eine epigenetische Veränderung verursachte, die nach der Differenzierung zu Muskelfasern

beibehalten wird. Der Mechanismus dieses epigenetischen Gedächtnisses muss in weiteren Studien identifiziert werden.

Outlook

With the energy production change for fatty acid oxidative phosphorylation, feed the $Nf1^{Myf5}$ animals with food rich for fatty acid will be tested to see the influence for life status.

With MEK inhibitor injection there is no phenotype change in the mouse model of other lab. Notch signaling inhibitor might be used for clinical injection in the future.

More stable epigenetic markers will be tested and the potential epigenetic memory target genes will be chosen for function analysis.

The role of *Nf1* in epigenetic modification will be explored.

Inhibitors of epigenetic modification might be used on the $Nf1^{Myf5}$ mouse model.

7 References

1 Thomson, D. M. The Role of AMPK in the Regulation of Skeletal Muscle Size, Hypertrophy, and Regeneration. Int J Mol Sci 19, doi:10.3390/ijms19103125 (2018).

2 Ryall, J. G. et al. The NAD(+)-Dependent SIRT1 Deacetylase Translates a Metabolic Switch into Regulatory Epigenetics in Skeletal Muscle Stem Cells. Cell stem cell 16, 171-183, doi:10.1016/j.stem.2014.12.004 (2015).

3 Chal, J. & Pourquié, O. Making muscle: skeletal myogenesisin vivoandin vitro. Development 144, 2104-2122, doi:10.1242/dev.151035 (2017).

4 Almeida, C. F., Fernandes, S. A., Ribeiro Junior, A. F., Keith Okamoto, O. & Vainzof, M. Muscle Satellite Cells: Exploring the Basic Biology to Rule Them. Stem Cells Int 2016, 1078686, doi:10.1155/2016/1078686 (2016).

5 Dunning-Davies, B. M. & Parker, A. P. Annual review of children with neurofibromatosis type 1. Arch Dis Child Educ Pract Ed 101, 102-111, doi:10.1136/archdischild-2014-308084 (2016).

6 Bentzinger, C. F., von Maltzahn, J. & Rudnicki, M. A. Extrinsic regulation of satellite cell specification. Stem Cell Res Ther 1, 27, doi:10.1186/scrt27 (2010).

7 Thomas, K., Engler, A. J. & Meyer, G. A. Extracellular matrix regulation in the muscle satellite cell niche. Connect Tissue Res 56, 1-8, doi:10.3109/03008207.2014.947369 (2015).

8 Almada, A. E. & Wagers, A. J. Molecular circuitry of stem cell fate in skeletal muscle regeneration, ageing and disease. Nat Rev Mol Cell Biol 17, 267-279, doi:10.1038/nrm.2016.7 (2016).

9 Ryall, J. G. & Lynch, G. S. The molecular signature of muscle stem cells is driven by nutrient availability and innate cell metabolism. Curr Opin Clin Nutr Metab Care 21, 240-245, doi:10.1097/MCO.0000000000000472 (2018).

10 Gros, J., Manceau, M., Thome, V. & Marcelle, C. A common somitic origin for embryonic muscle progenitors and satellite cells. Nature 435, 954-958, doi:10.1038/nature03572 (2005).

11 Schienda, J. et al. Somitic origin of limb muscle satellite and side population cells. Proc Natl Acad Sci U S A 103, 945-950, doi:10.1073/pnas.0510164103 (2006).

12 Hutcheson, D. A., Zhao, J., Merrell, A., Haldar, M. & Kardon, G. Embryonic and fetal limb myogenic cells are derived from developmentally distinct progenitors and have different requirements for beta-catenin. Genes Dev 23, 997-1013, doi:10.1101/gad.1769009 (2009).

13 Murphy, M. & Kardon, G. Origin of vertebrate limb muscle: the role of progenitor and myoblast populations. Curr Top Dev Biol 96, 1-32, doi:10.1016/B978-0-12-385940-2.00001-2 (2011).

14 Relaix, F., Rocancourt, D., Mansouri, A. & Buckingham, M. A Pax3/Pax7-dependent population of skeletal muscle progenitor cells. Nature 435, 948-953, doi:10.1038/nature03594 (2005).

15 Kassar-Duchossoy, L. et al. Mrf4 determines skeletal muscle identity in Myf5:Myod double-mutant mice. Nature 431, 466-471, doi:10.1038/nature02924 (2004).

16 Pownall, M. E., Gustafsson, M. K. & Emerson, C. P., Jr. Myogenic regulatory factors and the specification of muscle progenitors in vertebrate embryos. Annu Rev Cell Dev Biol 18, 747-783, doi:10.1146/annurev.cellbio.18.012502.105758 (2002).

17 Collins, C. A. et al. Stem cell function, self-renewal, and behavioral heterogeneity of cells from the adult muscle satellite cell niche. Cell 122, 289-301, doi:10.1016/j.cell.2005.05.010 (2005).

18 Biressi, S., Molinaro, M. & Cossu, G. Cellular heterogeneity during vertebrate skeletal muscle development. Dev Biol 308, 281-293, doi:10.1016/j.ydbio.2007.06.006 (2007).

19 Sacks, L. D. et al. Regulation of myosin expression during myotome formation. Development 130, 3391-3402, doi:10.1242/dev.00541 (2003).

20 Messina, G. et al. Nfix regulates fetal-specific transcription in developing skeletal muscle. Cell 140, 554-566, doi:10.1016/j.cell.2010.01.027 (2010).

21 Schiaffino, S., Carlo Reggiani. Myosin isoforms in mammalian skeletal muscle. . J Appl Physiol 77(2), 493-501 (1994).

22 Richard, A. F. et al. Genesis of muscle fiber-type diversity during mouse embryogenesis relies on Six1 and Six4 gene expression. Dev Biol 359, 303-320, doi:10.1016/j.ydbio.2011.08.010 (2011).

23 Niro, C. et al. Six1 and Six4 gene expression is necessary to activate the fast-type muscle gene program in the mouse primary myotome. Dev Biol 338, 168-182, doi:10.1016/j.ydbio.2009.11.031 (2010).

24 Taglietti, V. et al. Nfix Induces a Switch in Sox6 Transcriptional Activity to Regulate MyHC-I Expression in Fetal Muscle. Cell reports 17, 2354-2366, doi:10.1016/j.celrep.2016.10.082 (2016).

25 Valéria Augusto, C. R. P. & Campos, G. E. R. Skeletal muscle fiber types in C57BL6J mice. Braz. J. morphol. Sci 21(2), 89-94 (2004).

26 Agbulut, O., Noirez, P., Beaumont, F. & Butler-Browne, G. Myosin heavy chain isoforms in postnatal muscle development of mice. Biology of the Cell 95, 399-406, doi:10.1016/s0248-4900(03)00087-x (2003).

27 Michael H. Brooke, M., Kenneth K. Kaiser, Denver. Muscle Fiber Types: How Many and What Kind? Arch Neurol 23, 369-379 (1970).

28 Talbot, J. & Maves, L. Skeletal muscle fiber type: using insights from muscle developmental biology to dissect targets for susceptibility and resistance to muscle disease. Wiley Interdiscip Rev Dev Biol 5, 518-534, doi:10.1002/wdev.230 (2016).

29 Schiaffino, S. & Reggiani, C. Fiber types in mammalian skeletal muscles. Physiol Rev 91, 1447-1531, doi:10.1152/physrev.00031.2010 (2011).

30 Vander Heiden, M. G., Cantley, L. C. & Thompson, C. B. Understanding the Warburg effect: the metabolic requirements of cell proliferation. Science 324, 1029-1033, doi:10.1126/science.1160809 (2009).

31 Mackrell, J. G., Arias, E. B. & Cartee, G. D. Fiber type-specific differences in glucose uptake by single fibers from skeletal muscles of 9- and 25-month-old rats. J Gerontol A Biol Sci Med Sci 67, 1286-1294, doi:10.1093/gerona/gls194 (2012).

32 Alvim, R. O., Cheuhen, M. R., Machado, S. R., Sousa, A. G. P. & Santos, P. C. J. L. General aspects of muscle glucose uptake. Anais da Academia Brasileira de Ciências 87, 351-368, doi:10.1590/0001-3765201520140225 (2015).

33 Peter H. Albers, A. J. T. P., Jesper B. Birk, Dorte E. Kristensen, Birgitte F. Vind, Otto Baba, Jane Nøhr, Kurt Højlund, and Jørgen F.P. Wojtaszewski. Human Muscle Fiber Type– Specific Insulin Signaling: Impact of Obesity and Type 2 Diabetes. Diabetes 64, 485-497, doi:10.2337/db14-0590/-/DC1 (2015).

34 Ohlendieck, K. Proteomic Profiling of Fast-To-Slow Muscle Transitions during Aging. Front Physiol 2, 105, doi:10.3389/fphys.2011.00105 (2011).

35 Cohen, S., Nathan, J. A. & Goldberg, A. L. Muscle wasting in disease: molecular mechanisms and promising therapies. Nat Rev Drug Discov 14, 58-74, doi:10.1038/nrd4467 (2015).

36 Krag, T. O. et al. Differential Muscle Involvement in Mice and Humans Affected by McArdle Disease. J Neuropathol Exp Neurol 75, 441-454, doi:10.1093/jnen/nlw018 (2016).

37 Real-Martinez, A. et al. Low survival rate and muscle fiber-dependent aging effects in the McArdle disease mouse model. Sci Rep 9, 5116, doi:10.1038/s41598-019-41414-8 (2019).

38 White, R. B., Biérinx, A.-S., Gnocchi, V. F. & Zammit, P. S. Dynamics of muscle fibre growth during postnatal mouse development. BMC Developmental Biology 10, 21, doi:10.1186/1471-213X-10-21 (2010).

39 Schiaffino, S., Dyar, K. A., Ciciliot, S., Blaauw, B. & Sandri, M. Mechanisms regulating skeletal muscle growth and atrophy. FEBS J 280, 4294-4314, doi:10.1111/febs.12253 (2013).

40 Kelly, N. A. et al. Novel, high-intensity exercise prescription improves muscle mass, mitochondrial function, and physical capacity in individuals with Parkinson's disease. J Appl Physiol (1985) 116, 582-592, doi:10.1152/japplphysiol.01277.2013 (2014).

41 Sue C. Bodine, T. N. S., Michael Gonzalez, William O. Kline, Gretchen L. Stover, Roy Bauerlein, Elizabeth Zlotchenko, Angus Scrimgeour, John C. Lawrence†, David J. Glass and George D. Yancopoulos. Akt/mTOR pathway is a crucial regulator of skeletal muscle hypertrophy and can prevent muscle atrophy in vivo. NATURE CELL BIOLOGY 3, 1014-1019 (2001).

42 Huang, J. & Manning, B. D. The TSC1-TSC2 complex: a molecular switchboard controlling cell growth. Biochem J 412, 179-190, doi:10.1042/BJ20080281 (2008).

43 Cai, S. L. et al. Activity of TSC2 is inhibited by AKT-mediated phosphorylation and membrane partitioning. J Cell Biol 173, 279-289, doi:10.1083/jcb.200507119 (2006).

44 Glass, D. J. Skeletal muscle hypertrophy and atrophy signaling pathways. Int J Biochem Cell Biol 37, 1974-1984, doi:10.1016/j.biocel.2005.04.018 (2005).

45 Bentzinger, C. F. et al. Skeletal muscle-specific ablation of raptor, but not of rictor, causes metabolic changes and results in muscle dystrophy. Cell Metab 8, 411-424, doi:10.1016/j.cmet.2008.10.002 (2008).

46 Cunningham, J. T. et al. mTOR controls mitochondrial oxidative function through a YY1–PGC-1α transcriptional complex. Nature 450, 736-740, doi:10.1038/nature06322 (2007).

47 Dutchak, P. A. et al. Loss of a Negative Regulator of mTORC1 Induces Aerobic Glycolysis and Altered Fiber Composition in Skeletal Muscle. Cell Rep 23, 1907-1914, doi:10.1016/j.celrep.2018.04.058 (2018).

48 Mounier, R. et al. Antagonistic control of muscle cell size by AMPK and mTORC1. Cell Cycle 10, 2640-2646, doi:10.4161/cc.10.16.17102 (2011).

49 Tobias, I. S. et al. Fiber type-specific analysis of AMPK isoforms in human skeletal muscle: advancement in methods via capillary nanoimmunoassay. J Appl Physiol (1985) 124, 840-849, doi:10.1152/japplphysiol.00894.2017 (2018).

50 Wim Derave, H. A., Jacob Ihlemann, Lee A. Witters, Søren Kristiansen, Erik A. Richter, and Thorkil Ploug. Dissociation of AMP-Activated Protein Kinase Activation and Glucose Transport in Contracting Slow-Twitch Muscle. DIABETES 49, 1281-1287 (2000).

51 Long, Y. C. & Zierath, J. R. AMP-activated protein kinase signaling in metabolic regulation. J Clin Invest 116, 1776-1783, doi:10.1172/JCI29044 (2006).

52 Bonaldo, P. & Sandri, M. Cellular and molecular mechanisms of muscle atrophy. Dis Model Mech 6, 25-39, doi:10.1242/dmm.010389 (2013).

53 Lecker, S. H., Goldberg, A. L. & Mitch, W. E. Protein degradation by the ubiquitin-proteasome pathway in normal and disease states. J Am Soc Nephrol 17, 1807-1819, doi:10.1681/ASN.2006010083 (2006).

54 Bodine, S. C. & Baehr, L. M. Skeletal muscle atrophy and the E3 ubiquitin ligases MuRF1 and MAFbx/atrogin-1. Am J Physiol Endocrinol Metab 307, E469-484, doi:10.1152/ajpendo.00204.2014 (2014).

55 Tintignac, L. A. et al. Degradation of MyoD mediated by the SCF (MAFbx) ubiquitin ligase. J Biol Chem 280, 2847-2856, doi:10.1074/jbc.M411346200 (2005).

56 Jogo, M., Shiraishi, S. & Tamura, T. A. Identification of MAFbx as a myogenin-engaged F-box protein in SCF ubiquitin ligase. FEBS Lett 583, 2715-2719, doi:10.1016/j.febslet.2009.07.033 (2009).

57 Macpherson, P. C., Wang, X. & Goldman, D. Myogenin regulates denervation-dependent muscle atrophy in mouse soleus muscle. J Cell Biochem 112, 2149-2159, doi:10.1002/jcb.23136 (2011).

58 Foletta, V. C., White, L. J., Larsen, A. E., Leger, B. & Russell, A. P. The role and regulation of MAFbx/atrogin-1 and MuRF1 in skeletal muscle atrophy. Pflugers Arch 461, 325-335, doi:10.1007/s00424-010-0919-9 (2011).

59 Mauro, A. Satellite cells of skeletal muscle fibres. J Biophys Biochem Cyto (1961).

60 Marino, S. & Di Foggia, V. Invited Review: Polycomb group genes in the regeneration of the healthy and pathological skeletal muscle. Neuropathol Appl Neurobiol 42, 407-422, doi:10.1111/nan.12290 (2016).

61 Mclennan, M. Z. a. I. During Secondary Myotube Formation, Primary Myotubes Preferentially Absorb New Nuclei at Their Ends. DEVELOPMENTAL DYNAMICS (1995).

62 Relaix, F. & Zammit, P. S. Satellite cells are essential for skeletal muscle regeneration: the cell on the edge returns centre stage. Development 139, 2845, doi:10.1242/dev.069088 (2012).

63 Kanisicak, O., Mendez, J. J., Yamamoto, S., Yamamoto, M. & Goldhamer, D. J. Progenitors of skeletal muscle satellite cells express the muscle determination gene, MyoD. Dev Biol 332, 131-141, doi:10.1016/j.ydbio.2009.05.554 (2009).

64 Vasyutina, E. et al. RBP-J (Rbpsuh) is essential to maintain muscle progenitor cells and to generate satellite cells. Proc Natl Acad Sci U S A 104, 4443-4448, doi:10.1073/pnas.0610647104 (2007).

65 Zalc, A. et al. Antagonistic regulation of p57(kip2) by Hes/Hey downstream of Notch signaling and muscle regulatory factors regulates skeletal muscle growth arrest. Development (Cambridge, England) 141, 2780-2790, doi:10.1242/dev.110155 (2014).

66 Kim, J. H. et al. Sex hormones establish a reserve pool of adult muscle stem cells. Nat Cell Biol 18, 930-940, doi:10.1038/ncb3401 (2016).

67 Bjornson, C. R. R. et al. Notch Signaling Is Necessary to Maintain Quiescence in Adult Muscle Stem Cells. Stem Cells 30, 232-242, doi:10.1002/stem.773 (2012).

68 Mourikis, P. et al. A critical requirement for notch signaling in maintenance of the quiescent skeletal muscle stem cell state. Stem Cells 30, 243-252, doi:10.1002/stem.775 (2012).

69 Wen, Y. et al. Constitutive Notch Activation Upregulates Pax7 and Promotes the Self-Renewal of Skeletal Muscle Satellite Cells. Molecular and Cellular Biology 32, 2300-2311, doi:10.1128/mcb.06753-11 (2012).

70 Rando, I. M. C. a. T. A. The Regulation of Notch Signaling Controls Satellite Cell Activation and Cell Fate Determination in Postnatal Myogenesis. Developmental Cell 3, 397-409 (2002).

71 Giaimo, B. D., Oswald, F. & Borggrefe, T. Dynamic chromatin regulation at Notch target genes. Transcription 8, 61-66, doi:10.1080/21541264.2016.1265702 (2017).

72 Noguchi, Y. T. et al. Cell-autonomous and redundant roles of Hey1 and HeyL in muscle stem cells: HeyL requires Hes1 to bind diverse DNA sites. Development 146, doi:10.1242/dev.163618 (2019).

73 Fukada, S. et al. Hesr1 and Hesr3 are essential to generate undifferentiated quiescent satellite cells and to maintain satellite cell numbers. Development 138, 4609-4619, doi:10.1242/dev.067165 (2011).

74 Lahmann, I. et al. Oscillations of MyoD and Hes1 proteins regulate the maintenance of activated muscle stem cells. Genes Dev 33, 524-535, doi:10.1101/gad.322818.118 (2019).

75 Slaninova, V. et al. Notch stimulates growth by direct regulation of genes involved in the control of glycolysis and the tricarboxylic acid cycle. Open Biol 6, 150155, doi:10.1098/rsob.150155 (2016).

76 Bi, P. & Kuang, S. Notch signaling as a novel regulator of metabolism. Trends Endocrinol Metab 26, 248-255, doi:10.1016/j.tem.2015.02.006 (2015).

77 Ciofani, M. & Zuniga-Pflucker, J. C. Notch promotes survival of pre-T cells at the beta-selection checkpoint by regulating cellular metabolism. Nat Immunol 6, 881-888, doi:10.1038/ni1234 (2005).

78 Hausburg, M. A. et al. Post-transcriptional regulation of satellite cell quiescence by TTP-mediated mRNA decay. Elife 4, e03390, doi:10.7554/eLife.03390 (2015).

79 Crist, C. G., Montarras, D. & Buckingham, M. Muscle satellite cells are primed for myogenesis but maintain quiescence with sequestration of Myf5 mRNA targeted by microRNA-31 in mRNP granules. Cell Stem Cell 11, 118-126, doi:10.1016/j.stem.2012.03.011 (2012).

80 Chakkalakal, J. V. et al. Early forming label-retaining muscle stem cells require p27kip1 for maintenance of the primitive state. Development 141, 1649-1659, doi:10.1242/dev.100842 (2014).

81 Zhang, K., Sha, J. & Harter, M. L. Activation of Cdc6 by MyoD is associated with the expansion of quiescent myogenic satellite cells. J Cell Biol 188, 39-48, doi:10.1083/jcb.200904144 (2010).

82 Bernet, J. D. et al. p38 MAPK signaling underlies a cell-autonomous loss of stem cell self-renewal in skeletal muscle of aged mice. Nat Med 20, 265-271, doi:10.1038/nm.3465 (2014).

83 Sousa-Victor, P. et al. Geriatric muscle stem cells switch reversible quiescence into senescence. Nature 506, 316-321, doi:10.1038/nature13013 (2014).

84 Kawabe, Y., Wang, Y. X., McKinnell, I. W., Bedford, M. T. & Rudnicki, M. A. Carm1 regulates Pax7 transcriptional activity through MLL1/2 recruitment during asymmetric satellite stem cell divisions. Cell Stem Cell 11, 333-345, doi:10.1016/j.stem.2012.07.001 (2012).

85 Correra, R. M. et al. The imprinted gene Pw1/Peg3 regulates skeletal muscle growth, satellite cell metabolic state, and self-renewal. Sci Rep 8, 14649, doi:10.1038/s41598-018-32941-x (2018).

86 Buckingham, M. Skeletal muscle progenitor cells and the role of Pax genes. C R Biol 330, 530-533, doi:10.1016/j.crvi.2007.03.015 (2007).

87 Kuang, S., Kuroda, K., Le Grand, F. & Rudnicki, M. A. Asymmetric self-renewal and commitment of satellite stem cells in muscle. Cell 129, 999-1010, doi:10.1016/j.cell.2007.03.044 (2007).

88 Biressi, S. et al. Myf5 expression during fetal myogenesis defines the developmental progenitors of adult satellite cells. Dev Biol 379, 195-207, doi:10.1016/j.ydbio.2013.04.021 (2013).

89 Gunther, S. et al. Myf5-positive satellite cells contribute to Pax7-dependent long-term maintenance of adult muscle stem cells. Cell Stem Cell 13, 590-601, doi:10.1016/j.stem.2013.07.016 (2013).

90 Scaramozza, A. et al. Lineage Tracing Reveals a Subset of Reserve Muscle Stem Cells Capable of Clonal Expansion under Stress. Cell Stem Cell 24, 944-957 e945, doi:10.1016/j.stem.2019.03.020 (2019).

91 Der Vartanian, A. et al. PAX3 Confers Functional Heterogeneity in Skeletal Muscle Stem Cell Responses to Environmental Stress. Cell Stem Cell 24, 958-973 e959, doi:10.1016/j.stem.2019.03.019 (2019).

92 Motohashi, N. & Asakura, A. Muscle satellite cell heterogeneity and self-renewal. Front Cell Dev Biol 2, 1, doi:10.3389/fcell.2014.00001 (2014).

93 Cerletti, M., Jang, Y. C., Finley, L. W., Haigis, M. C. & Wagers, A. J. Short-term calorie restriction enhances skeletal muscle stem cell function. Cell Stem Cell 10, 515-519, doi:10.1016/j.stem.2012.04.002 (2012).

94 Scadden, D. T. The stem-cell niche as an entity of action. Nature 441, 1075-1079, doi:10.1038/nature04957 (2006).

95 Tierney, M. T. et al. Autonomous Extracellular Matrix Remodeling Controls a Progressive Adaptation in Muscle Stem Cell Regenerative Capacity during Development. Cell Rep 14, 1940-1952, doi:10.1016/j.celrep.2016.01.072 (2016).

96 Aguilar, C. A. et al. Transcriptional and Chromatin Dynamics of Muscle Regeneration after Severe Trauma. Stem Cell Reports, doi:10.1016/j.stemcr.2016.09.009 (2016).

97 Lukjanenko, L. et al. Loss of fibronectin from the aged stem cell niche affects the regenerative capacity of skeletal muscle in mice. Nat Med 22, 897-905, doi:10.1038/nm.4126 (2016).

98 Bentzinger, C. F. et al. Fibronectin regulates Wnt7a signaling and satellite cell expansion. Cell Stem Cell 12, 75-87, doi:10.1016/j.stem.2012.09.015 (2013).

99 Flamini, V. et al. The Satellite Cell Niche Regulates the Balance between Myoblast Differentiation and Self-Renewal via p53. Stem Cell Reports 10, 970-983, doi:10.1016/j.stemcr.2018.01.007 (2018).

100 Baghdadi, M. B. et al. Reciprocal signalling by Notch-Collagen V-CALCR retains muscle stem cells in their niche. Nature 557, 714-718, doi:10.1038/s41586-018-0144-9 (2018).

101 Berger, S. L., Kouzarides, T., Shiekhattar, R. & Shilatifard, A. An operational definition of epigenetics. Genes Dev 23, 781-783, doi:10.1101/gad.1787609 (2009).

102 Esteller, M. Epigenetics in evolution and disease. Lancet 372, S90-S96 (2008).

103 Grewal, S. I. & Moazed, D. Heterochromatin and epigenetic control of gene expression. Science 301, 798-802, doi:10.1126/science.1086887 (2003).

104 Woodhouse, S., Pugazhendhi, D., Brien, P. & Pell, J. M. Ezh2 maintains a key phase of muscle satellite cell expansion but does not regulate terminal differentiation. J Cell Sci 126, 565-579, doi:10.1242/jcs.114843 (2013).

105 Juan, A. H. et al. Polycomb EZH2 controls self-renewal and safeguards the transcriptional identity of skeletal muscle stem cells. Genes Dev 25, 789-794, doi:10.1101/gad.2027911 (2011).

106 Liu, L. et al. Chromatin modifications as determinants of muscle stem cell quiescence and chronological aging. Cell Rep 4, 189-204, doi:10.1016/j.celrep.2013.05.043 (2013).

107 Boonsanay, V. et al. Regulation of Skeletal Muscle Stem Cell Quiescence by Suv4-20h1-Dependent Facultative Heterochromatin Formation. Cell Stem Cell 18, 229-242, doi:10.1016/j.stem.2015.11.002 (2016).

108 Blum, R., Vethantham, V., Bowman, C., Rudnicki, M. & Dynlacht, B. D. Genome-wide identification of enhancers in skeletal muscle: the role of MyoD1. Genes Dev 26, 2763-2779, doi:10.1101/gad.200113.112 (2012).

109 Shen, H., Xu, W. & Lan, F. Histone lysine demethylases in mammalian embryonic development. Exp Mol Med 49, e325, doi:10.1038/emm.2017.57 (2017).

110 Chatterjee, A. et al. MOF Acetyl Transferase Regulates Transcription and Respiration in Mitochondria. Cell 167, 722-738 e723, doi:10.1016/j.cell.2016.09.052 (2016).

111 Takubo, K. et al. Regulation of glycolysis by Pdk functions as a metabolic checkpoint for cell cycle quiescence in hematopoietic stem cells. Cell Stem Cell 12, 49-61, doi:10.1016/j.stem.2012.10.011 (2013).

112 Yu, W. M. et al. Metabolic regulation by the mitochondrial phosphatase PTPMT1 is required for hematopoietic stem cell differentiation. Cell Stem Cell 12, 62-74, doi:10.1016/j.stem.2012.11.022 (2013).

113 Ryall, James G. et al. The NAD+-Dependent SIRT1 Deacetylase Translates a Metabolic Switch into Regulatory Epigenetics in Skeletal Muscle Stem Cells. Cell Stem Cell 16, 171-183, doi:10.1016/j.stem.2014.12.004 (2015).

114 Machado, L. et al. In Situ Fixation Redefines Quiescence and Early Activation of Skeletal Muscle Stem Cells. Cell Rep 21, 1982-1993, doi:10.1016/j.celrep.2017.10.080 (2017).

115 Shen, L. et al. Genome-wide landscape of DNA methylomes and their relationship with mRNA and miRNA transcriptomes in oxidative and glycolytic skeletal muscles. Sci Rep 6, 32186, doi:10.1038/srep32186 (2016).

116 Lufen Chang, M. K. Mammalian MAP kinase signaling cascades. Nature (2001).

117 Chen, G., Hitomi, M., Han, J. & Stacey, D. W. The p38 pathway provides negative feedback for Ras proliferative signaling. The Journal of biological chemistry 275, 38973-38980, doi:10.1074/jbc.M002856200 (2000).

118 Kondoh, K., Sunadome, K. & Nishida, E. Notch signaling suppresses p38 MAPK activity via induction of MKP-1 in myogenesis. The Journal of biological chemistry 282, 3058-3065, doi:10.1074/jbc.M607630200 (2007).

119 Ozawa, T. et al. The neurofibromatosis type 1 gene product neurofibromin enhances cell motility by regulating actin filament dynamics via the Rho-ROCK-LIMK2-cofilin pathway. J Biol Chem 280, 39524-39533, doi:10.1074/jbc.M503707200 (2005).

120 Hurlbut, G. D., Kankel, M. W. & Artavanis-Tsakonas, S. Nodal points and complexity of Notch-Ras signal integration. Proceedings of the National Academy of Sciences of the United States of America 106, 2218-2223, doi:10.1073/pnas.0812024106 (2009).

121 Lopez-Juarez, A. et al. Oligodendrocyte Nf1 Controls Aberrant Notch Activation and Regulates Myelin Structure and Behavior. Cell reports 19, 545-557, doi:10.1016/j.celrep.2017.03.073 (2017).

122 De Raedt, T. et al. PRC2 loss amplifies Ras-driven transcription and confers sensitivity to BRD4-based therapies. Nature 514, 247-251, doi:10.1038/nature13561 (2014).

123 Diggs-Andrews, K. A. et al. Sex Is a major determinant of neuronal dysfunction in neurofibromatosis type 1. Ann Neurol 75, 309-316, doi:10.1002/ana.24093 (2014).

124 Cornett, K. M., North, K. N., Rose, K. J. & Burns, J. Muscle weakness in children with neurofibromatosis type 1. Dev Med Child Neurol 57, 733-736, doi:10.1111/dmcn.12777 (2015).

125 Kossler, N. et al. Neurofibromin (Nf1) is required for skeletal muscle development. Hum Mol Genet 20, 2697-2709, doi:10.1093/hmg/ddr149 (2011).

126 Sullivan, K. et al. NF1 is a critical regulator of muscle development and metabolism. Hum Mol Genet 23, 1250-1259, doi:10.1093/hmg/ddt515 (2014).

127 Zhu, Y. et al. Ablation of NF1 function in neurons induces abnormal development of cerebral cortex and reactive gliosis in the brain. Genes Dev 15, 859-876, doi:10.1101/gad.862101 (2001).

128 Michelle D, T., Karin E, W., Hellström., M. & Soriano., P. Early myotome specification regulates PDGFA expression and axial skeleton development. Dev.Camb.Engl 127, 5059-5070 (2000).

129 Pierre Miniou, D. T., Tony Frugier, Natacha Roblot, Marianne Le Meur and Judith Melki*. Gene targeting restricted to mouse striated muscle lineage. Oxford University Press 27 (1999).

130 Gromova, A., Tierney, M. T. & Sacco, A. FACS-based Satellite Cell Isolation From Mouse Hind Limb Muscles. Bio-protocol 5, e1558, doi:10.21769/BioProtoc.1558 (2015).

131 Ly, C. H. & Ryall, J. G. in Skeletal Muscle Development (ed James G. Ryall) 61-73 (Springer New York, 2017).

132 Schmidl, C., Rendeiro, A. F., Sheffield, N. C. & Bock, C. ChIPmentation: fast, robust, low-input ChIP-seq for histones and transcription factors. Nat Methods 12, 963-965, doi:10.1038/nmeth.3542 (2015).

133 Pawlikowski, B., Pulliam, C., Betta, N. D., Kardon, G. & Olwin, B. B. Pervasive satellite cell contribution to uninjured adult muscle fibers. Skelet Muscle 5, 42, doi:10.1186/s13395-015-0067-1 (2015).

134 Seale, P. et al. PRDM16 controls a brown fat/skeletal muscle switch. Nature 454, 961-967, doi:10.1038/nature07182 (2008).

135 Lynch, C. J., Xu, Y., Hajnal, A., Salzberg, A. C. & Kawasawa, Y. I. RNA sequencing reveals a slow to fast muscle fiber type transition after olanzapine infusion in rats. PLoS One 10, e0123966, doi:10.1371/journal.pone.0123966 (2015).

136 Francesco Zurlo, K. L., Clifton Bogardus, and Eric Ravussin. Skeletal Muscle Metabolism Is a Major Determinant of Resting Energy Expenditure. Journal of Clinical Investigation 86, 1423-1427 (1990).

137 Munoz-Canoves, P., Scheele, C., Pedersen, B. K. & Serrano, A. L. Interleukin-6 myokine signaling in skeletal muscle: a double-edged sword? FEBS J 280, 4131-4148, doi:10.1111/febs.12338 (2013).

138 Richter, E. A. & Ruderman, N. B. AMPK and the biochemistry of exercise: implications for human health and disease. Biochem J 418, 261-275, doi:10.1042/BJ20082055 (2009).

139 Jiandie Lin, H. W., Paul T. Tarr, Chen-Yu Zhang, Zhidan Wu, Olivier Boss, Laura F. Michael, Pere Puigserver, Eiji Isotani, Eric N. Olson, & Bradford B. Lowell, R. B.-D., Bruce M. Spiegelman. Transcriptional co-activator PGC-1a drives the formation of slow twitch muscle fibres. Nature 418, 797-801, doi:10.1038/nature00936 (2002).

140 Zhang, L. et al. Skeletal Muscle-Specific Overexpression of PGC-1alpha Induces Fiber-Type Conversion through Enhanced Mitochondrial Respiration and Fatty Acid Oxidation in Mice and Pigs. Int J Biol Sci 13, 1152-1162, doi:10.7150/ijbs.20132 (2017).

141 Phua, W. W. T., Wong, M. X. Y., Liao, Z. & Tan, N. S. An aPPARent Functional Consequence in Skeletal Muscle Physiology via Peroxisome Proliferator-Activated Receptors. Int J Mol Sci 19, doi:10.3390/ijms19051425 (2018).

142 Norris, A. W. et al. Muscle-specific PPARγ-deficient mice develop increased adiposity and insulin resistance but respond to thiazolidinediones. Journal of Clinical Investigation 112, 608-618, doi:10.1172/jci17305 (2003).

143 Mary C. SUGDEN, M. J. H., Rachel M. HOWARD. Changes in lipoprotein lipase activities in adipose tisue,heart and skeletal muscle during continuous or interrupted feeding. Biochem. J. 292, 113-119 (1993).

144 Amin, R. H., Mathews, S. T., Camp, H. S., Ding, L. & Leff, T. Selective activation of PPARgamma in skeletal muscle induces endogenous production of adiponectin and protects mice from diet-induced insulin resistance. Am J Physiol Endocrinol Metab 298, E28-37, doi:10.1152/ajpendo.00446.2009 (2010).

145 Medina-Gomez, G. et al. PPAR gamma 2 prevents lipotoxicity by controlling adipose tissue expandability and peripheral lipid metabolism. PLoS Genet 3, e64, doi:10.1371/journal.pgen.0030064 (2007).

146 Sanchez-Ortiz, E. et al. NF1 regulation of RAS/ERK signaling is required for appropriate granule neuron progenitor expansion and migration in cerebellar development. Genes Dev 28, 2407-2420, doi:10.1101/gad.246603.114 (2014).

147 Chen, Y. H., Gianino, S. M. & Gutmann, D. H. Neurofibromatosis-1 regulation of neural stem cell proliferation and multilineage differentiation operates through distinct RAS effector pathways. Genes Dev 29, 1677-1682, doi:10.1101/gad.261677.115 (2015).

148 Grohmann, J. The role of the tumour suppressor Nf1 in growth and metabolism of skeletal muscle cells, Technische Universität Berlin, (2014).

149 Summers, M. A., Mikulec, K., Peacock, L., Little, D. G. & Schindeler, A. Limitations of the Pax7-creER(T2) transgene for driving deletion of Nf1 in adult mouse muscle. Int J Dev Biol 61, 531-536, doi:10.1387/ijdb.170182as (2017).

150 Liu, L., Cheung, T. H., Charville, G. W. & Rando, T. A. Isolation of skeletal muscle stem cells by fluorescence-activated cell sorting. Nat Protoc 10, 1612-1624, doi:10.1038/nprot.2015.110 (2015).

151 Mourikis, P., Gopalakrishnan, S., Sambasivan, R. & Tajbakhsh, S. Cell-autonomous Notch activity maintains the temporal specification potential of skeletal muscle stem cells. Development 139, 4536-4548, doi:10.1242/dev.084756 (2012).

152 Rodgers, J. T. et al. mTORC1 controls the adaptive transition of quiescent stem cells from G0 to GAlert. Nature 510, 393-396, doi:10.1038/nature13255 (2014).

153 Jones NC1, F. Y., Rosenthal RS, Olwin BB. ERK1/2 is required for myoblast proliferation but is dispensable for muscle gene expression and cell fusion. J Cell Physiol 186, 104-115 (2001).

154 Gattazzo, F., Urciuolo, A. & Bonaldo, P. Extracellular matrix: A dynamic microenvironment for stem cell niche. Biochimica et Biophysica Acta (BBA) - General Subjects 1840, 2506-2519, doi:10.1016/j.bbagen.2014.01.010 (2014).

155 Ryall, J. G. Metabolic reprogramming as a novel regulator of skeletal muscle development and regeneration. FEBS J 280, 4004-4013, doi:10.1111/febs.12189 (2013).

156 Carreira, B. P. et al. Differential contribution of the guanylyl cyclase-cyclic GMP-protein kinase G pathway to the proliferation of neural stem cells stimulated by nitric oxide. Neurosignals 21, 1-13, doi:10.1159/000332811 (2013).

157 Charles, N. et al. Perivascular Nitric Oxide Activates Notch Signaling and Promotes Stem-like Character in PDGF-Induced Glioma Cells. Cell Stem Cell 6, 141-152, doi:10.1016/j.stem.2010.01.001 (2010).

158 Wozniak, A. C. & Anderson, J. E. Nitric oxide-dependence of satellite stem cell activation and quiescence on normal skeletal muscle fibers. Dev Dyn 236, 240-250, doi:10.1002/dvdy.21012 (2007).

159 Kossler, N. et al. Neurofibromin (Nf1) is required for skeletal muscle development. Human Molecular Genetics 20, 2697-2709, doi:10.1093/hmg/ddr149 (2011).

160 Logan, M. et al. Expression of Cre Recombinase in the developing mouse limb bud driven by a Prxl enhancer. Genesis 33, 77-80, doi:10.1002/gene.10092 (2002).

161 Sieber, M. A. et al. Lbx1 acts as a selector gene in the fate determination of somatosensory and viscerosensory relay neurons in the hindbrain. J Neurosci 27, 4902-4909, doi:10.1523/JNEUROSCI.0717-07.2007 (2007).

162 Keefe, A. C. et al. Muscle stem cells contribute to myofibres in sedentary adult mice. Nat Commun 6, 7087, doi:10.1038/ncomms8087 (2015).

163 Tonks, A. M. B. a. N. K. Regulation of Distinct Stages of Skeletal Muscle Differentiation by Mitogen-Activated Protein Kinases. Science 278, 4 (1997).

164 Gutmann, D. H., Parada, L. F., Silva, A. J. & Ratner, N. Neurofibromatosis type 1: modeling CNS dysfunction. J Neurosci 32, 14087-14093, doi:10.1523/JNEUROSCI.3242-12.2012 (2012).

165 An, Y. et al. A Molecular Switch Regulating Cell Fate Choice between Muscle Progenitor Cells and Brown Adipocytes. Developmental Cell 41, 382-391.e385, doi:10.1016/j.devcel.2017.04.012 (2017).

166 Handschin, C. et al. Skeletal muscle fiber-type switching, exercise intolerance, and myopathy in PGC-1alpha muscle-specific knock-out animals. J Biol Chem 282, 30014-30021, doi:10.1074/jbc.M704817200 (2007).

167 N., H. Muscle fibre types: their role in health, disease and as therapeutic targets. OA Biology 01, 7 (2013).

168 Oberbach A, B. Y., Lehmann S, Niebauer J, Adams V, Paschke R. Altered fiber distribution and fiber-specific glycolytic and oxidative enzyme activ- ity in skeletal mus. Diabetes Care 29, 5 (2006).

169 BergstrÖM, J. H., Eric. Muscle Glycogen Synthesis after Exercise : an Enhancing Factor localized to the Muscle Cells in Man. Nature 210, 309-310, doi:10.1038/210309a0 (1966).

170 Zierath, J. R. & Hawley, J. A. Skeletal muscle fiber type: influence on contractile and metabolic properties. PLoS Biol 2, e348, doi:10.1371/journal.pbio.0020348 (2004).

171 Reubin Anders, G. C., Kenneth L.Zierler. The quantitatively minor role of carbohydrate in oxidative metabolism by skeletal muscle in intact man in the basal state. Measurment of oxygen and glucose uptake and carbon dioxide and lactate production in the forearm. J Clin Invest. 35, 671-682 (1956).

172 Chandrasekera, P. C. & Pippin, J. J. Of rodents and men: species-specific glucose regulation and type 2 diabetes research. ALTEX 31, 157-176, doi:10.14573/altex.1309231 (2014).

173 Liu, M. et al. Liver Plays a Major Role in FGF-21 Mediated Glucose Homeostasis. Cell Physiol Biochem 45, 1423-1433, doi:10.1159/000487568 (2018).

174 Goldberg, I. J., Eckel, R. H. & Abumrad, N. A. Regulation of fatty acid uptake into tissues: lipoprotein lipase- and CD36-mediated pathways. J Lipid Res 50 Suppl, S86-90, doi:10.1194/jlr.R800085-JLR200 (2009).

175 Jager, S., Handschin, C., St-Pierre, J. & Spiegelman, B. M. AMP-activated protein kinase (AMPK) action in skeletal muscle via direct phosphorylation of PGC-1alpha. Proc Natl Acad Sci U S A 104, 12017-12022, doi:10.1073/pnas.0705070104 (2007).

176 Kishton, R. J. et al. AMPK Is Essential to Balance Glycolysis and Mitochondrial Metabolism to Control T-ALL Cell Stress and Survival. Cell Metab 23, 649-662, doi:10.1016/j.cmet.2016.03.008 (2016).

177 Jung, S. & Kim, K. Exercise-induced PGC-1alpha transcriptional factors in skeletal muscle. Integr Med Res 3, 155-160, doi:10.1016/j.imr.2014.09.004 (2014).

178 Lindqvist, L. M., Tandoc, K., Topisirovic, I. & Furic, L. Cross-talk between protein synthesis, energy metabolism and autophagy in cancer. Curr Opin Genet Dev 48, 104-111, doi:10.1016/j.gde.2017.11.003 (2018).

179 Jorgensen, S. B., Richter, E. A. & Wojtaszewski, J. F. Role of AMPK in skeletal muscle metabolic regulation and adaptation in relation to exercise. J Physiol 574, 17-31, doi:10.1113/jphysiol.2006.109942 (2006).

180 Lin, S. S. & Liu, Y. W. Mechanical Stretch Induces mTOR Recruitment and Activation at the Phosphatidic Acid-Enriched Macropinosome in Muscle Cell. Front Cell Dev Biol 7, 78, doi:10.3389/fcell.2019.00078 (2019).

181 Castets, P. et al. mTORC1 and PKB/Akt control the muscle response to denervation by regulating autophagy and HDAC4. Nat Commun 10, 3187, doi:10.1038/s41467-019-11227-4 (2019).

182 Rion, N. et al. mTOR controls embryonic and adult myogenesis via mTORC1. Development 146, doi:10.1242/dev.172460 (2019).

183 Thomson, D. M., Fick, C. A. & Gordon, S. E. AMPK activation attenuates S6K1, 4E-BP1, and eEF2 signaling responses to high-frequency electrically stimulated skeletal muscle contractions. J Appl Physiol (1985) 104, 625-632, doi:10.1152/japplphysiol.00915.2007 (2008).

184 Bodine, S. C. et al. Akt/mTOR pathway is a crucial regulator of skeletal muscle hypertrophy and can prevent muscle atrophy in vivo. Nature Cell Biology 3, 1014-1019, doi:10.1038/ncb1101-1014 (2001).

185 Haston, S. et al. MAPK pathway control of stem cell proliferation and differentiation in the embryonic pituitary provides insights into the pathogenesis of papillary craniopharyngioma. Development 144, 2141-2152, doi:10.1242/dev.150490 (2017).

186 Schiaffino, S. & Mammucari, C. Regulation of skeletal muscle growth by the IGF1-Akt/PKB pathway: insights from genetic models. Skeletal Muscle 1, 4, doi:10.1186/2044-5040-1-4 (2011).

187 Boyer, J. G. et al. ERK1/2 signaling induces skeletal muscle slow fiber-type switching and reduces muscular dystrophy disease severity. JCI Insight 5, doi:10.1172/jci.insight.127356 (2019).

188 Slack, C. Ras signaling in aging and metabolic regulation. Nutr Healthy Aging 4, 195-205, doi:10.3233/NHA-160021 (2017).

189 Katz, M., Amit, I. & Yarden, Y. Regulation of MAPKs by growth factors and receptor tyrosine kinases. Biochim Biophys Acta 1773, 1161-1176, doi:10.1016/j.bbamcr.2007.01.002 (2007).

190 Elia, D., Madhala, D., Ardon, E., Reshef, R. & Halevy, O. Sonic hedgehog promotes proliferation and differentiation of adult muscle cells: Involvement of MAPK/ERK and PI3K/Akt pathways. Biochim Biophys Acta 1773, 1438-1446, doi:10.1016/j.bbamcr.2007.06.006 (2007).

191 Yang, J., Zhang, X., Wang, W. & Liu, J. Insulin stimulates osteoblast proliferation and differentiation through ERK and PI3K in MG-63 cells. Cell Biochem Funct 28, 334-341, doi:10.1002/cbf.1668 (2010).

192 Michailovici, I. et al. Nuclear to cytoplasmic shuttling of ERK promotes differentiation of muscle stem/progenitor cells. Development 141, 2611-2620, doi:10.1242/dev.107078 (2014).

193 Griger, J. et al. Loss of Ptpn11 (Shp2) drives satellite cells into quiescence. Elife 6, doi:10.7554/eLife.21552 (2017).

194 Zhang, P. et al. mTOR is necessary for proper satellite cell activity and skeletal muscle regeneration. Biochem Biophys Res Commun 463, 102-108, doi:10.1016/j.bbrc.2015.05.032 (2015).

195 Meng, D., Frank, A. R. & Jewell, J. L. mTOR signaling in stem and progenitor cells. Development 145, doi:10.1242/dev.152595 (2018).

196 Ma, X., Chen, H. & Chen, L. A dual role of Erk signaling in embryonic stem cells. Exp Hematol 44, 151-156, doi:10.1016/j.exphem.2015.12.008 (2016).

197 Dai, J., Bercury, K. K. & Macklin, W. B. Interaction of mTOR and Erk1/2 signaling to regulate oligodendrocyte differentiation. Glia 62, 2096-2109, doi:10.1002/glia.22729 (2014).

198 Zhang, W. et al. Aurora-A/ERK1/2/mTOR axis promotes tumor progression in triple-negative breast cancer and dual-targeting Aurora-A/mTOR shows synthetic lethality. Cell Death Dis 10, 606, doi:10.1038/s41419-019-1855-z (2019).

199 Wang, Y., Zhu, L., Kuokkanen, S. & Pollard, J. W. Activation of protein synthesis in mouse uterine epithelial cells by estradiol-17beta is mediated by a PKC-ERK1/2-mTOR signaling pathway. Proc Natl Acad Sci U S A 112, E1382-1391, doi:10.1073/pnas.1418973112 (2015).

200 Sunayama, J. et al. Crosstalk between the PI3K/mTOR and MEK/ERK pathways involved in the maintenance of self-renewal and tumorigenicity of glioblastoma stem-like cells. Stem Cells 28, 1930-1939, doi:10.1002/stem.521 (2010).

201 Bajard, L. A novel genetic hierarchy functions during hypaxial myogenesis: Pax3 directly activates Myf5 in muscle progenitor cells in the limb. Genes & Development 20, 2450-2464, doi:10.1101/gad.382806 (2006).

202 Darabi, R. et al. Assessment of the Myogenic Stem Cell Compartment Following Transplantation ofPax3/Pax7-Induced Embryonic Stem Cell-Derived Progenitors. Stem Cells 29, 777-790, doi:10.1002/stem.625 (2011).

203 Le Grand, F., Jones, A. E., Seale, V., Scime, A. & Rudnicki, M. A. Wnt7a activates the planar cell polarity pathway to drive the symmetric expansion of satellite stem cells. Cell Stem Cell 4, 535-547, doi:10.1016/j.stem.2009.03.013 (2009).

204 Gilbert, P. M. e. a. Substrate Elasticity Regulates Skeletal Muscle Stem Cell Self-Renewal in Culture. Science 329, 1078-1081 (2010).

205 Palacios, D. et al. TNF/p38alpha/polycomb signaling to Pax7 locus in satellite cells links inflammation to the epigenetic control of muscle regeneration. Cell Stem Cell 7, 455-469, doi:10.1016/j.stem.2010.08.013 (2010).

206 Joe, A. W. et al. Muscle injury activates resident fibro/adipogenic progenitors that facilitate myogenesis. Nat Cell Biol 12, 153-163, doi:10.1038/ncb2015 (2010).

207 Shea, K. L. et al. Sprouty1 regulates reversible quiescence of a self-renewing adult muscle stem cell pool during regeneration. Cell Stem Cell 6, 117-129, doi:10.1016/j.stem.2009.12.015 (2010).

208 Abou-Khalil, R. et al. Autocrine and paracrine angiopoietin 1/Tie-2 signaling promotes muscle satellite cell self-renewal. Cell Stem Cell 5, 298-309, doi:10.1016/j.stem.2009.06.001 (2009).

209 Anderson, J. E., Wozniak, A. C. & Mizunoya, W. Single muscle-fiber isolation and culture for cellular, molecular, pharmacological, and evolutionary studies. Methods Mol Biol 798, 85-102, doi:10.1007/978-1-61779-343-1_6 (2012).

210 Lim, C. L., Ling, K.-H. & Cheah, P.-S. Isolation, cultivation and immunostaining of single myofibers: An improved approach to study the behavior of satellite cells. Journal of Biological Methods 5, doi:10.14440/jbm.2018.219 (2018).

211 Light, N. & Champion, A. E. Characterization of muscle epimysium, perimysium and endomysium collagens. Biochemical Journal 219, 1017-1026, doi:10.1042/bj2191017 (1984).

212 Allen J. Bailey, D. J. R., Trevor J. Sims and Victor C. Duance. Meat Tenderness: Immunofluorescent Localisation of the Isomorphic Forms of Collagen in Bovine Muscles of Varying Texture. J. Sci. Food Agric 30, 203-210 (1979).

213 Fry, C. S., Kirby, T. J., Kosmac, K., McCarthy, J. J. & Peterson, C. A. Myogenic Progenitor Cells Control Extracellular Matrix Production by Fibroblasts during Skeletal Muscle Hypertrophy. Cell Stem Cell 20, 56-69, doi:10.1016/j.stem.2016.09.010 (2017).

214 Chapman, M. A., Mukund, K., Subramaniam, S., Brenner, D. & Lieber, R. L. Three distinct cell populations express extracellular matrix proteins and increase in number during skeletal

muscle fibrosis. Am J Physiol Cell Physiol 312, C131-C143, doi:10.1152/ajpcell.00226.2016 (2017).

215 Venkatraman, A. et al. Maternal imprinting at the H19-Igf2 locus maintains adult haematopoietic stem cell quiescence. Nature 500, 345-349, doi:10.1038/nature12303 (2013).

216 Zacharek, S. J. et al. Lung stem cell self-renewal relies on BMI1-dependent control of expression at imprinted loci. Cell Stem Cell 9, 272-281, doi:10.1016/j.stem.2011.07.007 (2011).

217 Qian, P. et al. The Dlk1-Gtl2 Locus Preserves LT-HSC Function by Inhibiting the PI3K-mTOR Pathway to Restrict Mitochondrial Metabolism. Cell Stem Cell 18, 214-228, doi:10.1016/j.stem.2015.11.001 (2016).

218 Andrea Repele, R. L., Simon Eaton, Luca Urbani, Paolo De Coppi and Michelangelo Campanella. Cell metabolism sets the differences between subpopulations of satellite cells (SCs). BMC Cell Biology 14:24, 1-7 (2013).

219 Coller, H. A. The paradox of metabolism in quiescent stem cells. FEBS Lett 593, 2817-2839, doi:10.1002/1873-3468.13608 (2019).

220 Zhang, R., Erler, J. & Langowski, J. Histone Acetylation Regulates Chromatin Accessibility: Role of H4K16 in Inter-nucleosome Interaction. Biophys J 112, 450-459, doi:10.1016/j.bpj.2016.11.015 (2017).

221 Vasyutina, E., Lenhard, D. C. & Birchmeier, C. Notch Function in Myogenesis. Cell Cycle 6, 1450-1453, doi:10.4161/cc.6.12.4372 (2007).

222 Tremblay, I., Pare, E., Arsenault, D., Douziech, M. & Boucher, M. J. The MEK/ERK pathway promotes NOTCH signalling in pancreatic cancer cells. PLoS One 8, e85502, doi:10.1371/journal.pone.0085502 (2013).

223 Clara De Palma, F. M., Sarah Pambianco, Emma Assi, Thierry Touvier, Stefania Russo,, Cristiana Perrotta, V. R., Silvia Carnio, Valentina Cappello, Paolo Pellegrino, Claudia Moscheni, Maria Teresa Bassi, Marco Sandri, Davide Cervia and Emilio Clementi & Deficient nitric oxide signalling impairs skeletal muscle growth and performance: involvement of mitochondrial dysregulation. Skeletal Muscle 4:22, 1-21 (2014).

224 Chiba, S. Notch signaling in stem cell systems. Stem Cells 24, 2437-2447, doi:10.1634/stemcells.2005-0661 (2006).

225 Imayoshi, I., Sakamoto, M., Yamaguchi, M., Mori, K. & Kageyama, R. Essential roles of Notch signaling in maintenance of neural stem cells in developing and adult brains. J Neurosci 30, 3489-3498, doi:10.1523/JNEUROSCI.4987-09.2010 (2010).

226 Pajcini, K. V., Speck, N. A. & Pear, W. S. Notch signaling in mammalian hematopoietic stem cells. Leukemia 25, 1525-1532, doi:10.1038/leu.2011.127 (2011).

227 Xiao, W., Gao, Z., Duan, Y., Yuan, W. & Ke, Y. Notch signaling plays a crucial role in cancer stem-like cells maintaining stemness and mediating chemotaxis in renal cell carcinoma. J Exp Clin Cancer Res 36, 41, doi:10.1186/s13046-017-0507-3 (2017).

228 Landor, S. K. et al. Hypo- and hyperactivated Notch signaling induce a glycolytic switch through distinct mechanisms. Proc Natl Acad Sci U S A 108, 18814-18819, doi:10.1073/pnas.1104943108 (2011).

229 Kuwabara, S., Yamaki, M., Yu, H. & Itoh, M. Notch signaling regulates the expression of glycolysis-related genes in a context-dependent manner during embryonic development. Biochem Biophys Res Commun 503, 803-808, doi:10.1016/j.bbrc.2018.06.079 (2018).

230 Lee, S. Y. & Long, F. Notch signaling suppresses glucose metabolism in mesenchymal progenitors to restrict osteoblast differentiation. J Clin Invest 128, 5573-5586, doi:10.1172/JCI96221 (2018).

231 Massard, C. et al. First-in-human study of LY3039478, an oral Notch signaling inhibitor in advanced or metastatic cancer. Ann Oncol 29, 1911-1917, doi:10.1093/annonc/mdy244 (2018).

232 Ran, Y. et al. gamma-Secretase inhibitors in cancer clinical trials are pharmacologically and functionally distinct. EMBO Mol Med 9, 950-966, doi:10.15252/emmm.201607265 (2017).

233 Espinoza, I. & Miele, L. Notch inhibitors for cancer treatment. Pharmacol Ther 139, 95-110, doi:10.1016/j.pharmthera.2013.02.003 (2013).

234 Al Jaam, B. et al. Reduced Notch signalling leads to postnatal skeletal muscle hypertrophy in Pofut1cax/cax mice. Open Biol 6, doi:10.1098/rsob.160211 (2016).

235 Mayeuf-Louchart, A. et al. Notch regulation of myogenic versus endothelial fates of cells that migrate from the somite to the limb. Proc Natl Acad Sci U S A 111, 8844-8849, doi:10.1073/pnas.1407606111 (2014).

236 Marinkovic, M. et al. Skeletal muscle fibro-adipogenic progenitors of dystrophic mice are insensitive to NOTCH-dependent regulation of adipogenesis. bioRxiv, doi:10.1101/223370 (2017).

237 Choi, I. Y. et al. Concordant but Varied Phenotypes among Duchenne Muscular Dystrophy Patient-Specific Myoblasts Derived using a Human iPSC-Based Model. Cell Rep 15, 2301-2312, doi:10.1016/j.celrep.2016.05.016 (2016).

238 Mu, X. et al. The role of Notch signaling in muscle progenitor cell depletion and the rapid onset of histopathology in muscular dystrophy. Hum Mol Genet 24, 2923-2937, doi:10.1093/hmg/ddv055 (2015).

239 Moore, L. D., Le, T. & Fan, G. DNA methylation and its basic function. Neuropsychopharmacology 38, 23-38, doi:10.1038/npp.2012.112 (2013).

240 Reid, M. A., Dai, Z. & Locasale, J. W. The impact of cellular metabolism on chromatin dynamics and epigenetics. Nat Cell Biol 19, 1298-1306, doi:10.1038/ncb3629 (2017).

241 Li, Q., Eichten, S. R., Hermanson, P. J. & Springer, N. M. Inheritance Patterns and Stability of DNA Methylation Variation in Maize Near-Isogenic Lines. Genetics 196, 667, doi:10.1534/genetics.113.158980 (2014).

242 Jin, W., Peng, J. & Jiang, S. The epigenetic regulation of embryonic myogenesis and adult muscle regeneration by histone methylation modification. Biochem Biophys Rep 6, 209-219, doi:10.1016/j.bbrep.2016.04.009 (2016).

243 Laker, R. C. & Ryall, J. G. DNA Methylation in Skeletal Muscle Stem Cell Specification, Proliferation, and Differentiation. St*em Cells Int* **2016**, 5725927, doi:10.1155/2016/5725927 (2016).

244 Carrio, E. *et al.* Deconstruction of DNA methylation patterns during myogenesis reveals specific epigenetic events in the establishment of the skeletal muscle lineage. *Stem Cells* **33**, 2025-2036, doi:10.1002/stem.1998 (2015).

245 Consalvi, S., Sandona, M. & Saccone, V. Epigenetic Reprogramming of Muscle Progenitors: Inspiration for Clinical Therapies. *Stem Cells Int* **2016**, 6093601, doi:10.1155/2016/6093601 (2016).

246 Davegardh, C. *et al.* Abnormal epigenetic changes during differentiation of human skeletal muscle stem cells from obese subjects. *BMC Med* **15**, 39, doi:10.1186/s12916-017-0792-x (2017).

247 Seaborne, R. A. *et al.* Human Skeletal Muscle Possesses an Epigenetic Memory of Hypertrophy. *Sci Rep* **8**, 1898, doi:10.1038/s41598-018-20287-3 (2018).

8 Abbreviation

A. bidest	Aqua bidest
Acad1	Acyl CoA dehydrogenase
Ampk	AMP-activated protein kinase
ANOVA	Analysis of Variance
asWAT	Anterior subcutaneous white adipose tissue
bp	Base Pairs
BAT	Brown adipose tissue
BSA	Bovine serum albumin
Ca2+	Calcium ion
cBAT	Cervical brown adipose tissue
cDNA	Complementary DNA
Col IV	Collagen type IV
Cpt	Carnitine palmitoyl transferase
Cre	Causes recombination
CSA	Cross sectional area
DAPI	4',6-diamidino-2-phenylindole
DAPT	N-[N-(3,5-Difluorophenacetyl)-L-alanyl]-S-phenylglycine t-butyl ester
DEPC	Diethyl pyrocarbonate
DMEM	Dulbecco's Modified Eagle Medium
DMSO	Dimethyl sulfoxide
DNA	Deoxyribonucleic acid
dNTP	Deoxyribonucleotide
E	Embryo
ECAR	Extracellular acidification rate
ECL	Enhanced chemiluminescence
ECM	Extracellular matrix
EDL	Extensor digitorum longus

EDTA	Ethylene-Diamine-Tetra-Acetic acid
e.g.	For example
Erk	Extracellular signal regulated kinase
EtOH	Ethanol
ETC	Electron transport chain
Fab	Fragment antigen-binding
Fabp	Fatty acid binding protein
FACS	Fluorescence-activated cell sorting
FCS	Fetal calf serum
FBS	Fetal bovine serum
Fgf	Fibroblast growth factor
Fig.	Figure
fw	Forward
g	Gram
GAP	GTPase activating protein
Gas	Gastrocnemius
GDP	Guanosine-5`-diphosphate
GO	Gene Ontology
GSEA	Gene Set Enrichment Analysis
GTP	Guanosine-5`-triphosphate
Het	Heterozygous
HRP	Horse-Radish Peroxidase
HSA	Human alpha-Skeletal Actin
iBAT	Intrascapular brown adipose tissue
Idh	Isocitrate dehydrogenase
IHC	Immunohistochemistry
Il6	Interleukin 6
Jag1	Jagged 1
kb	Kilo-bases
kDA	Kilo-Dalton

KEGG	Kyoto Encyclopedia of genes and genomes
KO	Knock-out
LamA	Laminin type A
loxP	Locus of X-over P1
Lpl	Lipoprotein Lipase
µ	Micro (prefix)
MAPK	Mitogen activated protein kinase
MEK	MAP/ERK kinase
MeOH	Methanol
mol	Moles
MRF	Muscle regulatory factor
mtCO1	Mitochondrially Encoded Cytochrome C Oxidase I
mTOR	Mechanistic Target of Rapamycin Kinase
Mut	Mutant
mRNA	Messenger RNA
MyEmb	Embryonic myosin
Myf	Myogenic factor
MyHc	Myosin heavy chain
MyoD	Myogenic differentiation
Myog	Myogenin
Nf1	Neurofibromin
NF1	Neurofibromatosis I
NS	Not significant
OCR	Oxygen consumption rate
OXPHOS	Oxidative phosphorylation
P	Postnatal day
PAGE	Polyacrylamide gel electrophoresis
Pax	Paired box
PBS	Phosphate-buffered saline
PCR	Polymerase chain reaction

PFA	Paraformaldehyde
PI3K	Phosphatidylinositol-4,5-bisphosphate 3-kinase
Pgc1α	Peroxisome proliferator activated receptor gamma Coactivator 1 alpha
Pparg	Peroxisome proliferator-activated receptor gamma
psWAT	Posterior subcutaneous
qPCR	Quantitative PCR
Ras	Rat sarcoma
Rcf	Relative centrifugal force
Rev	Reverse
RFU	Relative fluorescence units
rpm	Revolutions per minute
RPKM	Reads per kilobase of transcript
rRNA	Ribosomal RNA
RTK	Receptor Tyrosine Kinase
RT-PCR	Reverse transcription PCR
rWAT	Retroperitoneal
S	Soleus
sBAT	subscapular Brown Adipose Tissue
SD	Standard deviation
SDH	Succinate dehydrogenase
SDS	Sodium dodecyl sulfate
SEM	Standard error of the mean
TCA	Tricarboxylic acid cycle
TA	Tibialis anterior
Taq	Thermus aquaticus
TB	Triceps brachii
TEA	Triethanolamine
Tris	Tris-(hydroxymethyl-)aminoethane
TSA	Tyramine signal amplification

UV	Ultraviolet
WAT	White adipose tissue
WB	Western blot
Wnt	Wingless-related MMTV integration site
WT	Wild-type

9 Appendix

9.1 Acknowledgement

Four precious years passed in a foreign country. I would like to sincerely thank all the people who helped and supported me during this critical and challenging life period.

First of all, I would like to thank Prof. Simon Spuler for accepting my work for reviewing and be part of my disputation committee. I want to thank you for guiding the international Ph.D. program in the field of myology and put so much effort into maintaining and promote this international cooperation from which so many people benefited. It is a great honor to be a member of MyoGrad.

Finish this project was only possible with the fantastic opportunity to work at Max Plank Institute for Molecular Genetics. Thanks to Prof. Stefan Mundlos for allowing me to work in your lab in the past years.

With the supervision of Prof. Sigmar Stricker, I learned a lot and got enormous progress. You showed me how to work as a real scientist. Whenever I feel lost for my project after talking and discussing it with you, the direction will be bright again. There are so many different methods need to be used in this project; it is always you who helped me to find the professional people from the field and got suggestions from them. For the tools and machines that we do not have, you could always find the correct group and collaborate with them. These are all super essential capabilities for scientific research. You also put a lot of effort into correcting my thesis and giving me suggestions on how to make it better. At the beginning of my scientific research career, it is lucky to have a supervisor like you. Besides, you always give me enough space to think about the project and simultaneously cares about my ideas on how to develop the project. Working with you always makes me feel equal and get fully respected. It also lights my interests in scientific research.

I want to thank all the collaboration partners and groups:

First, I would like to thank Dr. Mario Ost and also his group leader Prof. Susanne Klaus from the Department of Physiology of Energy Metabolism, German Institute of Human Nutrition. I transferred so many animals to your lab, and we worked together for muscle dissections and metabolism test, and you also give useful suggestions and your precious antibodies to me. I got a lot of encouragement during the process.

Second, I am appreciated for Prof. Britta Siegmund, Dr. Rainer Glauben, and Dr. Wu Hao. They all from the Medical Department. Division of Gastroenterology infectiology and

Rheumatology. Charite. “ Hey! It’s me,” whenever I went to your lab, you are always waiting to open the door for me no matter how late it is. I appreciated Dr. Wu Hao for what he did for me during the experiment time. Also, he has an outstanding personality, always optimistic and good at motivating people around. Thanks to Dr. Rainer Glauben, whenever I need something, you always have it and generously to share with me, and I also like your jokes, make things feel much more comfortable with a happy mood. I also want to thank their group leader Prof. Britta Siegmund to give me this opportunity to use the platform in her lab.

Third, I want to thank my working neighbors — people from Mass Spectrometry Facility MPI-MG. Thanks to Dr. David Meierhofer, Beata Lukaszewsa-McGreal, and Dr. Yang Ni. You showed me how to prepare my precious samples for proteomics analysis. You also kindly shared your chemicals and consumables with me. Besides, you also taught me how to do data analysis and show proteomics data.

Finally, I want to express my gratitude to Dr. Matthias Lienhard from the bioinformatics group of Dr. Ralf Herwig, MPI-MG. You helped a lot with my MeDIP and Chipseq data analysis.

I want to thank the animal caretaker Katja Zill at the MPI-MG for her excellent work for what I have benefited during these years. Furthermore, I would like to thank all members of the service team of Microscopy, Flow Cytometry Facility, and Sequencing Core Facility from MPI-MG.

I want to thank all my colleagues in the AG Mundlos whom I had the pleasure of accompanying during these last years. I am appreciated for Dr. Bjørt Katrinardóttir Kragesteen, who showed me how to do RNAseq analysis. I still remember Norbert Brieske told me a lot of useful information about how-to live-in Berlin, and when I had problems with my landlady, you are the one who supported me in solving the issues. Now I would like to thank all the members of the Stricker group.

Aru, you are the first one who showed me how to work appropriately in MPI-MG. We are always the last ones to leave the institute. I got inspired by your friendly personality, and you are also my first friend in Berlin.

Sophie, you are the queen for preparing delicious cakes, and it's lucky to have a native Berliner friend like you to show me the exciting places and foods. I tried so many new things with you, and at least with you, I am not a lazy cow anymore. You have the magic power to motivate people for sports and also you are an expert for as a trainer.

George, I always have particular fun with you, a cute lovely big boy. You are the source of love. I also enjoyed a lot about the Greek trip that you organized for us. I got a warm welcome from your family, and it will be my best memorize and really to go and visit again.

Pedro, you are the most experienced person with lab skills in our small group. You are always generous to discuss and help to solve the problems that I met for my experiment. You are also expertise for FACS analysis. I am appreciated for what you did for me.

For "external" support, I want to send my biggest thanks to my family, especially my old grandmother and my parents, who have always supported me with your love. I wish I could have more time to stay with you in the future.

Finally, it is you, "my closest and best friend" Jianhui. You always keep me away from loneliness and save me from the difficult times. Without you, life will be a disaster. Thanks for your excellent cooking skills that I got an extra 10 Kilo. Proud of you.